SYNTHESIS OF HIGH PERFORMANCE CERAMIC FIBERS BY CHEMICAL VAPOR DEPOSITION FOR ADVANCED METALLICS REINFORCING

Vithal Revankar and Vladimir Hlavacek

Laboratory for Ceramic and Reaction Engineering
Department of Chemical Engineering
State University of New York at Buffalo
Buffalo,New York 14260

Final Technical Report for the Project Grant No. NAG3-897 submitted to:

NASA Lewis Research Center, Cleveland, OH 44135-3191
for the Period 1988-1991

May 1991

Contents

List of Figures

List of Tables

1 abstract

Some of the potential advantages of fiber reinforced composite materials include: high strength at elevated temperatures, high strength to weight ratio, improved toughness, improved creep and fatigue strength and controlled expansion and conductivity. They also offer the unique advantage to tailor the properties and shape of the high performance material for the application desired.Therefore, there is a critical need of fibers capable of effectively reinforcing these intermetallic matrices at elevated temperature. This research work describes the CVD synthesis of such fibers which can be used for the potential applications in high temperature composite materials. This process was used due to its advantage over other fiber synthesis processes. It is extremely important to produce these fibers with good reproducible and controlled growth rates. However, the complex interplay of mass and energy transfer, blended with the fluid dynamics makes this a formidable task.

The design and development of CVD reactor assembly and system to synthesize TiB_2, CrB_2 , B_4C, TiC fibers was carried out during the course of this research. The thermodynamic and kinetic analysis of TiB_2 and CrB_2, was done to locate the windows for the pure deposit and to scan out different precursors by keeping the emphasis on effect of temperature, concentration of reactants, gas flow rate and morphology.Residual stress analysis for estimating stresses arising from thermal expansion mismatch has been determined. Various techniques to improve the mechanical properties were also carried out. The developed fibers showed extremely good strength. The TiC, B_4C, and B fibers matched the properties of best known results. TiB_2 with the intermediate spongy layer showed the strength up to 250KSI. The exploratory work on CrB_2 gave excellent result with initial strength values varied from 60 to 170 KSI. Various techniques for improving the fiber properties has been elaborated. The crystal structure and its orientation for TiB_2 fiber is discussed in. In short, this report gives an overall view of CVD process to develop CrB_2, TiB_2, and other high performance ceramic fibers.

2 Technical Background

A new generation of composite materials is revolutionizing today's aircraft and automotive industries [Edie, 1987]. In these high technology applications, weight, strength, and stiffness are critical parameters which can be achieved by using high-performance ceramic material composites [Edie and Dunham, 1987]. These ceramic materials offer many outstanding properties for high-temperature applications. This attention led to the discovery of fibers which have excellent high-temperature strength and corrosion resistance, good thermal shock resistance, low density, and low coefficient of thermal expansion. High-performance fibers are available only at high prices and, as a result, tend to serve specialized and restricted markets. Basically, three factors affect this price: raw material, manufacturing, and more important new market development cost. Secondly, the use is partly limited because of their brittle nature and large degree of scatter in strengths which often lead to catastrophic failure. A number of techniques have been considered to lessen or eliminate these problems [Richardson, 1984].

Over the past few years, numerous patents and publications have revealed the use of simple organo-metallic compounds, metal halides, and polymer precursors for routes to ceramics fibers [Campbell et al., 1949]. High Gibb's free energy of formation of organometallic compound frequently allows for lower temperature of formation of ceramics. This fact is utilized in the CVD process. The volatile organometallic precursors allow for simple purification by superfractionalization so that CVD process results in an ultraclean material. Very recent experimental observations predict that traces of impurities in a fiber (e.g., calcium) result in a fast high-temperature degradation (Johnson et al., 1987).

The achievement of consistently high fiber strengths over a long length is important for successful implementation in many composite systems. This requires highly controlled processing operation and conditions [Brenman and Prewo, 1982]. Coating defects may also induce some kind of flaws or microbending losses in the fiber [Glogo, 1975; Gardner, 1975]. Only two ceramic fibers are available commercially (boron, silicon carbide). But these fibers are not matching the properties required for the advanced composite system. For the intermetallic matrix reinforcement we are looking for a special kind of fiber. Because metal matrix composites offer low weight, high strength, high stiffness, and high temperature capabilities to satisfy the performance requirements of future advanced aerospace systems. By choosing a matrix material that bonds well to the fiber, is ductile, and stands up to the environment, properties of the compos-

ite can be tailored to the needs of advanced power and propulsion systems. Titanium diboride, titanium carbide, boron carbide, and chromium diboride fiber compositions were synthesized as reinforcement material for intermetallic matrices in this research.

3 Objective of the Work

Fiber reinforced composites occupy a central role in the development of new materials and has overcome many of the limitations of traditional materials. Some of the potential advantages of fiber reinforced composite materials include: high strength at elevated temperatures, high strength to weight ratio, improved toughness, improved creep and fatigue strength and controlled expansion and conductivity. They also offer the unique advantage to tailor the properties and shape of the high performance material for the application desired.

Therefore, there is a critical need of fibers capable of effectively reinforcing these intermetallic matrices at elevated temperature. This report describes the CVD synthesis of these fibers which can be used for the potential applications in high temperature composite materials. The CVD method has several advantages over other conventional methods; hence, it has been adopted for this research. It is extremely important to produce these fibers with good reproducible and controlled growth rates. Other properties are to be controlled include thickness, composition, purity, crystallinity and surface morphology. These properties are highly dependent on the deposition condition. Hence it is necessary to correlate the fiber properties with temperature of the substrate, system pressure, gas flow rate and concentration of the reactants. However, the complex interplay of mass and energy transfer, blended with the fluid dynamics makes this a formidable task.

Hence, goals were to design and develop the CVD reactor systems which can synthesize TiB_2, CrB_2 , B_4C, TiC fibers. The thermodynamic and kinetic analysis of TiB_2 and CrB_2, with the emphasis on effect of temperature, concentration of reactants, gas flow rate and morphology were carried out. Investigation on the mechanical properties of the developed fiber including strength and modulus were conducted. Residual stress analysis for estimating stresses arising from thermal expansion mismatch has been determined. Various techniques to improve the mechanical properties were also carried out.

4 CVD Synthesis

Broadly defined, chemical vapor deposition, or CVD, is the formation of solid products via chemical reactions of gaseous precursors. A typical CVD process would involve a dynamic flow system in which gaseous reactants pass over a heated substrate. The gases react chemically to produce a condensed coating on the substrate plus product gases, which, together with any remaining reactant gases, dynamically exit from the hot reaction zone.

The application of CVD processes centers around the production of thin films for semi-conductors and other solid state electronic devices (Hess et al., 1985), coating of cutting tools and surfaces needing erosion and/or corrosion protection (Yee, 1978), coating of fibers used in forming composite materials (DiCarlo, 1985 and Guinn and Middleman, 1989), and containment coatings for nuclear fuel and nuclear waste particles (Spear, 1982). CVD processes are also used in the manufacturing of objects with complex shapes (e.g., refractory crucible) out of materials such as tungsten, molybdenum and rhenium which resist conventional machining and fabrication techniques (Iwasa et al., 1987; Shinko and Lennartz, 1987).

A vast number of chemical compounds are considered for these applications (Blocher et al., 1984). Important materials being prepared by CVD for electronic and optic devices include Si, Ge, Si_3N_4, SiO_2, GaAs, CdS, ZnSe and related compounds. Superconducting materials such as Nb_3Sn,Nb_3Ge and NbC_xN_y can be deposited as well (Wahl and Schmanderer, 1989). Erosion and corrosion resistant coatings commonly applied by CVD to tooling materials are TiC, TiN and Al_2O_3. In addition, an appreciable amount of CVD research is being performed on coatings of TaC, TaN, W_2C, TiB_2, SiC, Si_3N_4, B_4C, BN and B for use on cutting tools, tubes, fibers and applications in which the materials are subjected to high temperatures, and corrosive and erosive environments.

4.1 Synthesis of High Performance Ceramic Fibers by CVD

The CVD process involves the formation of solid by decomposition or reduction of one or more gaseous components upon a heated substrate. Typically, a small-diameter substrate wire is run through the glass reaction tube, and suitable gases are introduced. The substrate is resistance heated causing the gas to react and deposit on the heating wire. Uniformity of the coating mainly depends on the uniform surface structure of

the base fiber, temperature and rate of supply of fresh reacting gas to the fiber surface [Pierson et al., 1978]. The non-uniform temperature distribution results in heavier deposits on the hotter region and thereby introduce some flaws in the material. Deposition non- uniformities due to the fluctuations in the concentration of a coating gaseous reaction mixture along the fiber might be overcome by lowering pressure in the system [Sherman, 1987].

The coating adhesion is excellent when some kind of physical/chemical bond is formed by diffusion, or reaction between the coating material and the base. However, this diffusion (or interaction) should be at the "optimum" level to maintain the strength and modulus of the fiber. Cleanliness of the surface of the base material is very important where the surface and base material interaction is necessary to obtain good adhesion. Cleanliness of the matrix is not so important when only physical adhesion of the material is required.

The supersaturation and temperature of the reaction process are important factors affecting the type of deposit. Low temperature or higher supersaturation of gases leads to a gas phase nucleation, thereby decreasing the efficiency of coating and adhesion. Higher temperature or low supersaturation gives epitaxial growth or dendrites kind of growth which is determental for the coating process. Hence, optimum temperature and supersaturation is necessary to obtain the required deposit such as amorphous deposit or fine grain polycrystal [Naslain et al., 1979; Schlichting, 1980].

Deposition rates vary with the material deposited and the process used. Coating efficiency is the measure of material deposited to material supplied as volatilized compound, might vary greatly with the coating process and strongly depends on operating conditions and geometry of a reactor.

Generally, the material necessary for the CVD process can be supplied by a source gas. For the CVD process, two general reaction routes can be followed:

- Reduction of volatile halides
- Pyrolytic methods

The hydrogen reduction of halides process is an effective technique for the synthesis of ceramic fibers by CVD. The principle of this technique is as follows: Hydrogen saturated with metal halides (e.g., $TiCl_4$, $ZrCl_4$, etc.) or nonmetal halides (e.g., CCl_4, BCl_3, etc.) or mixture of these halides is passed into a reactor in which the base filament is

heated (resistively or by any other method). Typically, for example, for a TiB_2 filament synthesis, the following reaction occurs:

$$TiCl_2 + 2BCl_3 + 5H_2 \rightarrow TiB_2 + 10HCl \quad (1)$$

The pyrolytic method represents a thermal decomposition of an appropriate component with low boiling point. For example, silicon carbide fiber can by synthesized from $CH_3.SiCl_3$

$$CH_3SiCl_3 \rightarrow SiC + 3HCl \quad (2)$$

The surface deposition reaction rate varies with the material deposited, the reactant composition and temperature. Usually a material is deposited with the rate of 5 to 100 μm/hr. The important parameters which should be considered in this process are:

- Purity of the deposit and uniformity of coating.
- Coating adhesion.
- The effect of supersaturation and temperature on the structure.
- Efficiency of CVD reactions.
- The reactor geometry and operational arrangement.

5 Experimental Set-up and Operations:

The various applications of CVD have resulted in the development of various kinds of reactors, heating systems and feeding systems. The manner in which the substrate is heated is the primary factor in the design of the deposition chamber. The design will be influenced by the geometry, shape, and the composition of the substrate, the type of deposition process used, the nature of the coating desired and by the economic and personal preference factors. The most important criteria among all these should be the performance and cost. The CVD system used is illustrated in Figure 1. The main components of the system are: the CVD chamber, the vapor precursor feed system, the temperature monitoring unit and the effluent gas handling system. However, the CVD

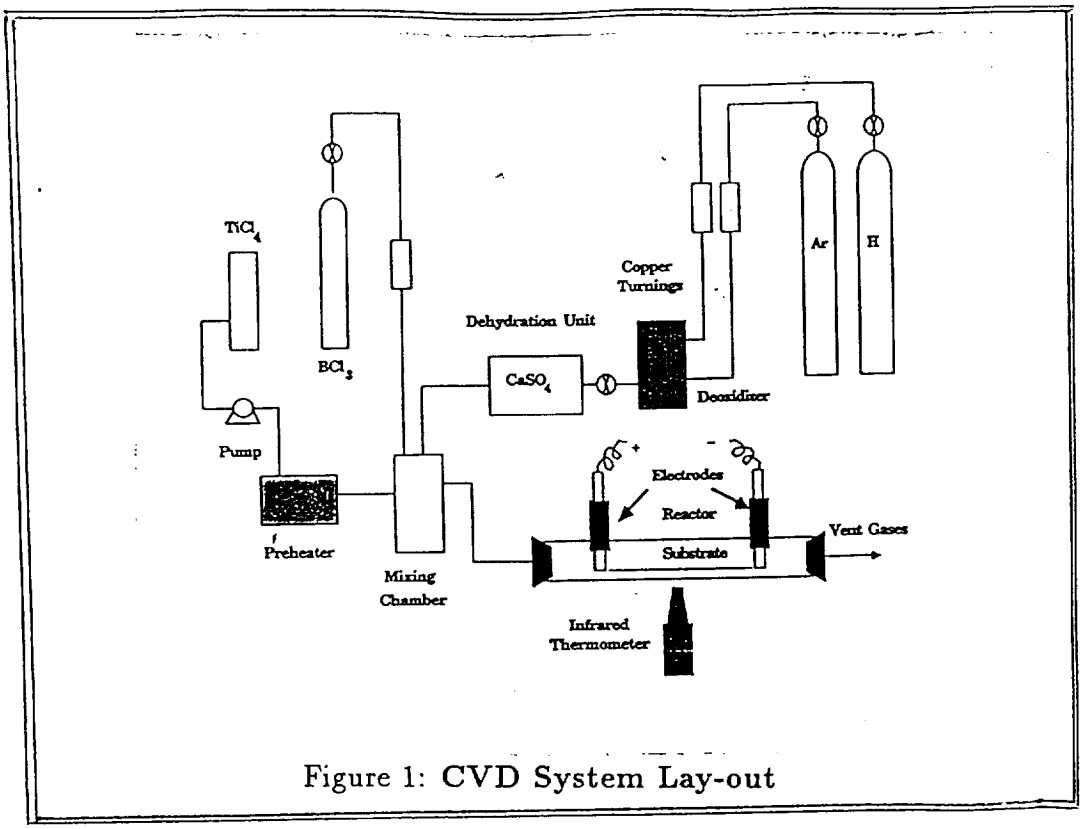

Figure 1: **CVD System Lay-out**

reactor is the most important part of the process. Our batch system basically consists of a quartz reactor of 1.5 inch diameter with projections for electrode insertion. The distance between the electrode is 15 inch (i.e. sample fiber length). The electrodes are of cylindrical shape with a small hole to mount the substrate fiber. The bulkiness of the electrodes was necessary to avoid overheating of the electrodes. The extra heating coil was wound around the reactor to avoid the condensation of sub-metal chlorides on the walls of the reactor. The typical wall temperature was varied from 200-600°C. The reactor is shown in Figure 2.

The vaporizer was maintained at 250°C. This also serves as a mixing chamber for the reactants and the carrier gases, which is critical for uniform deposit. The temperature of the substrate was measured by an optical thermometer ($\pm$5°C accuracy) and controlled by monitoring the applied voltage. The de-oxo system contains activated copper turnings maintained at 500°C to remove traces of oxygen from the carrier gases. The traces of moisture were eliminated by passing through Dehydration unit (anhydrous calcium oxide). The liquid reactants were pumped through a graduated peristatic pump.

In a typical operation, the fiber was mounted between the two electrodes and system was made air-tight. The reactor surface and preheater were brought to the required

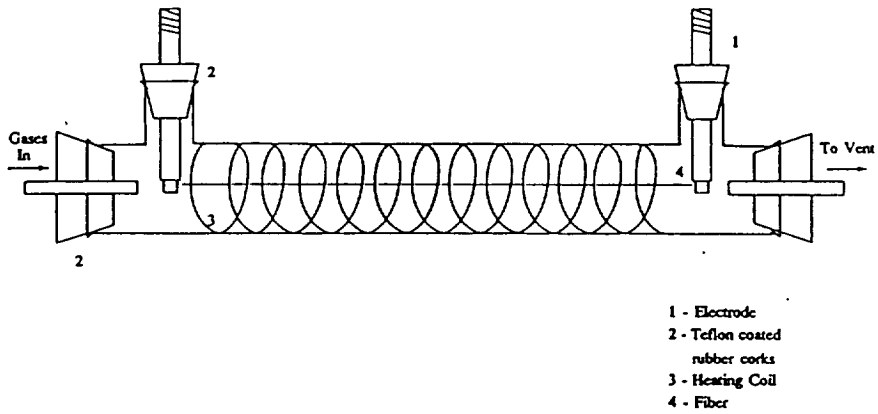

Figure 2: CVD Reactor Lay-out

temperature. Meanwhile, the reactor was continuously flushed with extra pure argon gas which was pre-purified by passing through de-oxo and dehydrating units. After making sure that there is no more oxygen inside, the hydrogen flow was started at 1.5 lit/min., again passing through the pre-purifying unit. The purity of reactants and carrier gases is extremely important because the trace amount of impurities has a deleterious effect on the physico-chemical properties of the fiber [Powell et. al., 1955]. The fiber was brought to required temperature (1000-1300°C) under hydrogen atmosphere. Once the temperature was stabilized, reactants were pumped into the vaporizer/mixing chamber, for a fixed amount of time. Once the deposition was over, the fiber had been cooled to room temperature slowly under hydrogen atmosphere to avoid the thermal stresses.

5.1 CVD - continuous Process

The synthesis of ceramic fibers by CVD technique will be carried out in continuous manner. The set-up is shown in Figure 3.

The metallic or graphite filament to be coated enters the apparatus through a mercury seal and is heated in an inert gas atmosphere in the inlet chamber. The hot fiber enters the main plating chamber through a small hole in the inlet chamber

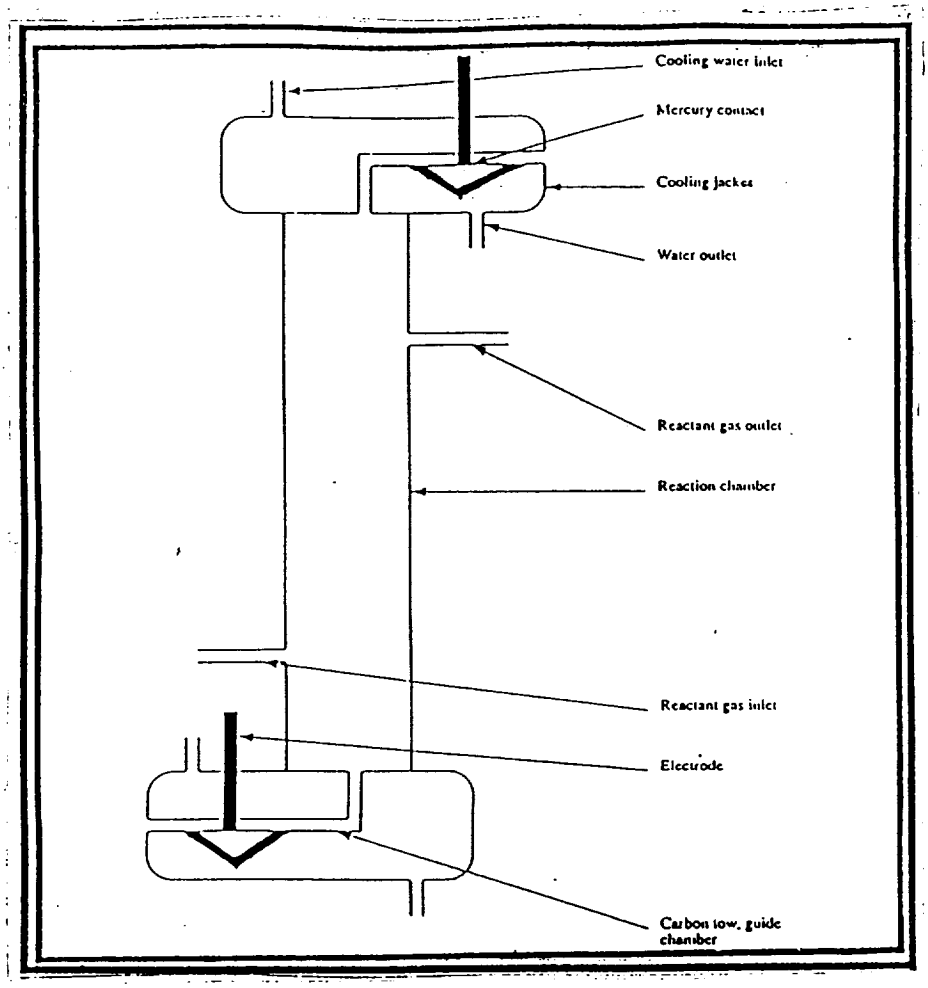

Figure 3: **CVD continuous Reactor**

and finally leaves the apparatus through a similar arrangement at the exit end. The procedure is the same as that of batch operation.

The wire is heated resistively. The reacting gaseous mixture enters the reactor at different axial and angular positions to increase accessibility and uniformity of reactants on the filament surface. A motor- driven reel draws the fiber through the apparatus at a steady, controlled rate.

6 Materials and Chemicals

6.1 Substrate selection:

The final properties of the CVD fiber are dependent on the substrate fiber used. Several substrate uses are reported in the literature [Person and Randich, 1978; Pierson et. al., 1979; Bryant and Meier, 1974]. Basic criteria for a satisfactory substrate selection are as follows:

1. Ability to withstand the temperature of deposition.
2. Chemical inertness to the deposition atmosphere.
3. Thermal expansion is close to that of the deposit.

Several materials were tested for our substrate. Among them Ti, W, Mo, Cu, Ni and C. showed good potential. In all of the experiments, hydrogen is the carrier gas. At the deposition temperature, all the material except W and C, absorbs hydrogen to various degree to form a metal hydride leading to embrittlement. Even though most of the above mentioned material are resistant to HCl, only W and C can withstand prolong attack at deposition temperature. Finally, ductile materials like Ni, Cu are having high thermal expansion mismatches with the ceramic deposit compared to W, Mo and C, creating a larger residual stresses in the deposit. After analyzing all these results, we selected W, C, Mo as the substrate materials for the synthesis of fibers. The properties of the commercial fibers/wires used are given below.

C (Thornel, From AMCO) Fibers:

- - PAN based: Dia.= 5-10 μm, Surface area = 0.5 m^2/g, Strength=100-300 KSI, 2000-5000 filaments in a bundle.
- - Pitch based: Dia.= 6-10 μm, Surface area = 0.3 m^2/g, Strength =300-400 KSI, 2000-5000 filaments in a bundle.

W (wire Johnson Matthey and GE):

- Johnson-Matthey fiber - dia. = 100 μm, tolerance $\pm$8%, Surface area = 0.07 m^2/g

Table 1: Reactant Analysis

Reactants	Impurities in parts per million(PPM)
H_2	O_2= 0.5, Cl_2= 0.1
Ar	H_2= 0.1, O_2=0.1
BCl_3	Si=8, Cl_2=80, $COCl_2$=200, Al=30, Fe=22
$TiCl_4$	Fe <10, Si=50, Sn=100, C=50, V=10
CCl_4	S=10, H_2O=20

- Johnson-Matthey fiber - dia. = 75 μm, tolerance $\pm$8%, Surface area = 0.07 m^2/g.
- GE fiber, Electro polished and Electro etched (customized),
  - Electro etched - Dia. = 40 μm; tolerance $\pm$3%, Surface area = 0.5 m^2/g
  - - Electro etched - Dia. = 100 μm, tolerance $\pm$3%, Surface area = 0.5 m^2/g
  - - Electro polished -Dia.= 70 μm, tolerance $\pm$ 3%, Surface area =0.3 m^2/g
  - - Electro polished - Dia. = 70 μm and 100 μm, tolerance $\pm$ 8%

Ti (Wire, Johnson Matthey): Dia. = 100 μm, tolerance $\pm$ 8%

6.2 Chemicals:

The quality of the film is directly dependent on the purity of the reagents used. It is of utmost importance in CVD to use extra pure material [Powell et al., 1955] to avoid poor physico-chemical properties to the film. Following chemicals are used:

- H_2 and Ar obtained from CS Gas Products, Linde Div. of Union Carbide (electronic grade, extra dry, 99.99% pure). The gases were further purified by passing through de-oxo and dehydration units.
- $TiCl_4$, BCl_3, CH_4, $CrO_2Cl_2$and CCl_4 obtained from Johnson Matthey Co. are of commercial grades. Wherever possible, these materials were redistilled to improve the purity. The typical chemical analysis is given in Table 1.

6.3 Pretreatment of the Substrate

One of the main requirements of the deposited films is that it should adhere to the core at all operating temperatures and capable of withstanding severe deformation without spalling. Hence surface cleanliness of the substrate is of utmost importance. This was done three different ways:

1. treatment with boiling concentrated nitric acid for 10 mins.
2. treatment with steam at 250° for 10 mins.
3. treatment with H_2 at 500°C for 5 mins.

These treatments not only cleans the surface of the substrate material but also increases the surface area. The best results were obtained with hydrogen treatment where surface area of W was increased by 10% and that of carbon was by 25%. This method was used in most of our sample runs; if otherwise, mentioned

7 Titanium Diboride Fiber Synthesis

There is a critical need of fibers capable of effectively reinforcing ceramic and metal matrices at high temperature. The high specific strength and stiffness at elevated temperatures combined with improved toughness, creep and fatigue resistance of these composites, overcome some of the limitations of traditional materials. Titanium diboride (TiB_2) is the most promising candidate for reinforcing the metal matrix. It processes high strength at elevated temperatures, and exhibits high stability and hardness. Its compatibility with Ni-Al and Fe-Al matrix was reported in the recent NASA report [Misra, 1988a, 1988b]. This research gives an overall view of an extensive work carried out in the Laboratory for Ceramic and Reaction Engineering, on the application of Chemical Vapor Deposition technique in the development of TiB_2 fiber. Detailed work on growth and characterization of fiber including simple kinetic expression is discussed. The residual stresses developed due to deposition condition are also explained.

Even though several techniques are available for manufacturing TiB_2 fiber, Chemical Vapor Deposition (CVD) is used because of its flexibility and ability to deposit dense, pure refractory coating. Again, one can obtain the fiber well below the melting

point of the material, with good control over the morphology. Some of the commonly used precursors for the deposition of TiB_2 include Ti + B [Rauch et al., 1968; DiCarlo, 1985; Bunsell, 1988]; $TiCl_4$ + BCl_3 [Lennon, 1965; Anon, 1966, Chernyshova et al., 1985; Hess et al., 1985; Biswas, 1986]; $TiCl_4$ + BBr_3 [Graham, 1971; Chamberlin and Skarman, 1966]; $TiCl_4$ + B_2H_6 [Viguie and Spitz; 1975] and $Ti(BH_4)$, [Monney and Radding, 1982]. In short, one can summarize the precursors to three different categories to produce TiB_2 fibers.

- gas-solid reaction
- bimolecular decomposition and
- decomposition of a organometallic compound.

In gas-solid reaction, boron is directly deposited on titanium metal disc or a wire [Warth, 1923; Thebault et al., 1976] by reducing BCl_3. They have shown the Ti-B reaction to be a diffusion controlled governed by the equation $x = Ct^{\frac{1}{2}}$ where x is the thickness of the boride film and t is the time with C as the rate constant. The deposition of Ti from reduction of $TiCl_4$ on boron was reported by Bouix et al., (1986) and Vincent et al., (1986). This reaction also showed that the thickness of the boride layer is proportional to $t^{\frac{1}{2}}$. The interaction of Ti metal with B powder is discussed by Neronov et al., (1981). The main disadvantage of this process is the formation of multiple borides along with TiB_2. The property of final fiber is very poor with many defects.

Organometallic compounds generally are borohydrides [Campbell, 1956] which are unstable, pyrophoric and can be easily decomposed at a relatively low temperature. The best precursor is $Ti(BH_4)_3$ which is prepared by reacting $TiCl_4$ and $LiBH_3$ [Powell et al., 1955]. Another precursor is titanium monochloro borohydride which is prepared from $TiCl_4$ and $Al(BH_4)_3$ which has the same volatility as $Al(BH_4)_3$. The main disadvantages of this process are:

- purity of the precursor,
- co-deposition of free boron and non stoichiometric deposit ,
- compound instability,
- less control over the morphology of the deposit.

Finally, TiB_2 is deposited on a hot substrate through a bimolecular decomposition of volatile compounds of titanium and boron. This process offers faster deposition rate and greater control on the composition of the deposit. Moers (1931) studied extensively the decomposition of halides of boron and titanium on hot substrate. The titanium precursor is always $TiCl_4$(b.p 136.4°C) whereas boron precursor is either boron halide (BCl_3, BBr_3 or BI_3) or boron hydride (B_2H_6, etc.). Deposition from diborane requires low temperature (600-900°C) [Randich and Gerlach, 1981] but chlorine contamination of the deposit is difficult to avoid. The co- deposition of free boron is also competing. The biggest negative factor is its high toxicity and extreme flammability. Even though BBr_3 or BI_3 decompose at low temperature, it is advantageous to use metal and boron compounds containing a common atom. It is reported that the film deposit from BBr_3 is of poor quality [Zeman et al., 1982].

The most extensively studied reaction for TiB_4 deposition is between $TiCl_4$ and BCl_3 Peshev and Niemyski, 1965]. Their study showed the different morphological forms of TiB_2, depending on the deposition temperature. Gannon et al., [1963] obtained the pure dense deposit of TiB_2 at 1600°C and elaborated the crystal orientation mechanism. The use of different analytic technique was reported by Gebhardt and Gee [1965] and Pierson and Mullendore [1981], along with the optimum deposition conditions. Bessman and Spear [1975, 1977] in a series of three papers published the thermodynamic analysis of $TiCl_4 - BCl_3$ system and also the effect of gas phase composition on the morphology of TiB_2. From our analysis, it was concluded that the best precursors for TiB_2 deposition are BCl_3 and $TiCl_4$. These are available commercially in pure form, and can be handled without any difficulty. The most important factor is the operatability of the system with wide ranging conditions. Most of the experiments were carried out on tungsten substrate because of its resistance to HCl attack and inertness to hydrogen at deposition temperature. Electro polished and electro etched tungsten fibers were supplied by General Electric Co. with tolerance level ±3%. The commercial tungsten filaments of Johnson Mattheys are also tried.

7.1 Results and Discussion on TiB_2 Fibers

7.1.1 Thermodynamic Study

On actual practice, prior to deposition with the various precursors, it is beneficial to conduct a thermodynamic analysis to get an insight of various conditions available for

an experimental operation. This will reduce the amount of experimental data required to optimize the process. As discussed earlier, Bessman and Spear [1977] have analyzed the thermodynamic data of B + Ti system to obtain the window to get the pure TiB_2. Randich and Gerlach [1981] found that the pure TiB_2 phase is possible only at high B to Ti ratio. Our operation is similar to above analysis but covered whole spectrum of parameters. This operation gives the composition of a reaction mixture as a function of operating parameters such as temperature, pressure, and composition assuming equilibrium established in the operating system. Program, NASAF obtained from NASA was used in determining the equilibrium composition of the gas mixture [Gordon and McBride, 1971]. The constants are calculated from thermodynamic data available from JANAF tables [1983].

Temperature, pressure and the concentration of the reactant mixture [$TiCl_4 + BCl_3 + Ar + H_2$] were input to the calculations. The criteria of conservation of each element were imposed in calculating the equilibrium composition that had the minimum Gibbs free energy. The various species considered in the study are B, BCl,BCl_2, BCl_3, BH, BH_2, BCH_3, B_2, Cl,Cl_2, H, H_2, HCl, $TiCl_2$, $TiCl_3$, $TiCl_4$, B(s), Ti(s), TiB(s), $TiB_2(s)$, $Ti_2B_5(s)$ and $Ti_3B_4(s)$.

Figure 4 shows the phase boundary for pure TiB_2. Here $BCl_3/TiCl_4$ ratio is plotted against the operating temperature for various $H_2/TiCl_4$ ratios. Below the plotted line, one can exclusively get pure TiB_2 where as above it is the co-deposition of TiB_2 + B. This region of pure TiB_2 increases with a decrease in H_2 to $TiCl_4$ ratio. Under our operating conditions, only possible solid phases are TiB_2 and B. Multiple borides (Ti_3B_4, Ti_2B_5 and TiB) are observed only at high temperature which is not the scope of this study. This plot gives the thermodynamically required concentration of reactants to get pure condensed TiB_2 phase.

Analysis was carried to find out the effect of $H_2/TiCl_4$ and $BCl_3/TiCl_4$ ratio on the efficiency of deposition at various temperature. Deposition efficiency is defined as the deposition rate of TiB_2 at equilibrium divided by the deposition rate in the absence of any thermodynamic and kinetic limitation. The deposition of TiB_2 efficiency increases with temperature and decreases with $BCl_3/TiCl_4$ ratio. However, for high values of $H_2/TiCl_4$ ratio (>20), the deposition efficiency seems to stabilize. Our analysis concludes that the optimum H_2 to $TiCl_4$ ratio is around 25 and $BCl_3/TiCl_4$ ratio is 2 at operating temperature [1400-1700 K].

The effect of pressure on the deposition efficiency at various temperature for the

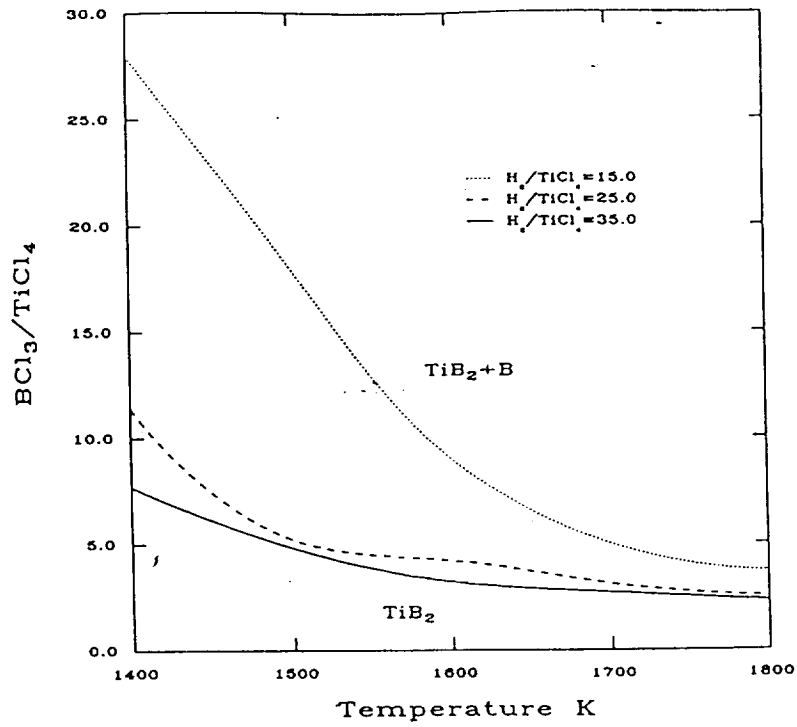

Figure 4: **Phase Boundaries for Pure TiB_2 Deposit**

optimum ratio of reactants is given in Figure 5. It shows that the deposition efficiency increases with decrease in pressure and increase in temperature. This effect is pronounced in the lower temperature range whereas at our operating temperature range [1400-1700 K], it is having negligible effect. We maintained 1 atmosphere because of the difficulty in handling low pressure operations and the marginal effect of pressure on deposition efficiency.

The typical concentration profile of reactants and product gases is given in figure 6. at various temperatures.

At any given temperature H_2, HCl, BCl_3 and $TiCl_4$ make up 95% of the gasphase. Other gases, BCl, BCl_2, BH_2, BH_3, $TiCl_2$, $TiCl_3$. H and Cl are in negligible amount.

This thermodynamic study gave the composition of various compounds and deposition rate at equilibrium, however, their actual use in the experimental operation is limited. In general, CVD systems are often operated far from equilibrium conditions. This leads to a different experimental result than the thermodynamically predicted. So we decided to find out experimentally the kinetics of deposition.

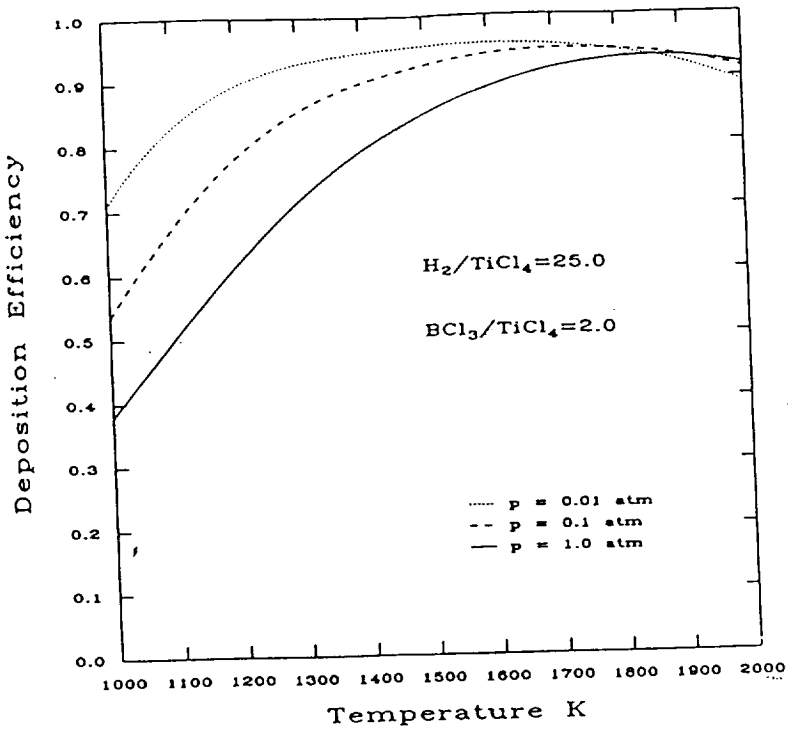

Figure 5: **Effect of Pressure on Deposition Efficiency**

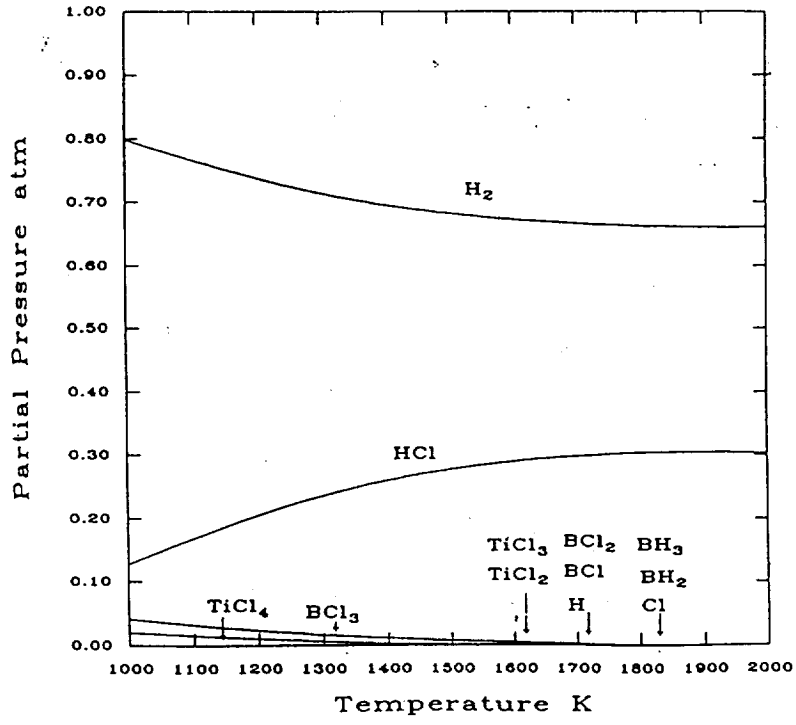

Figure 6: **Equilibrium Gas Phase Composition of the Reaction**

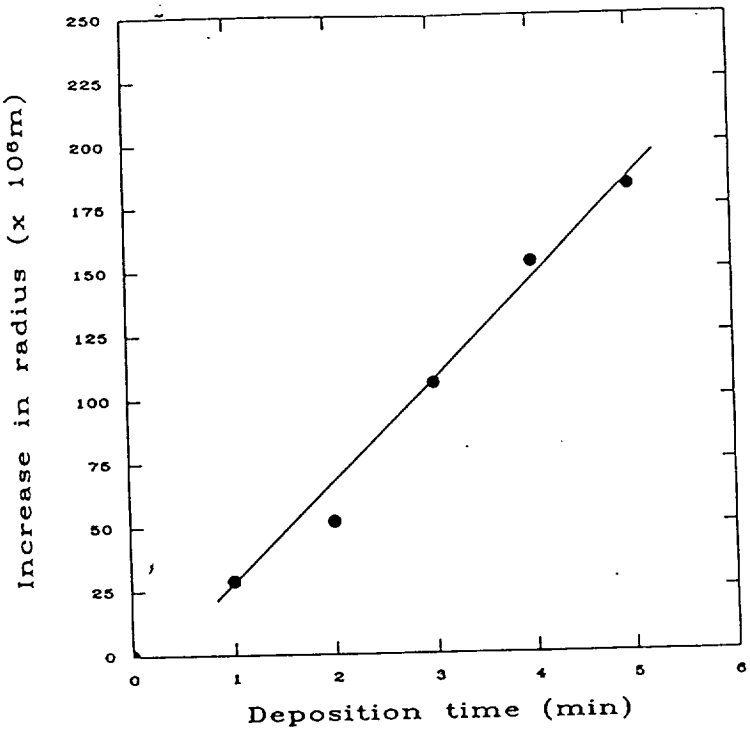

Figure 7: **Dependence of Growth Rate Versus Time**

7.1.2 Kinetic Study

The chemical vapor deposition process is mainly controlled by kinetic, diffusion and thermodynamic factors. Under real conditions, these factors manifest themselves simultaneously and determine the feasibility and direction of the deposition process as a whole. The various parameters studied include total gas flow rate, temperature of the substrate and concentration of the reactants. The operating pressure was maintained at 1 atm.

The rate of growth can be measured by the change of weight, provided the surface area available for deposition is fixed. Therefore, deposition rate must be defined as the weight or volume change per unit surface area. Hence overall deposition rate is expressed as r_2 - r_1/t where r_1 and r_2 are initial and final radius of the fiber and t is the deposition time. The plot of radius versus deposition time at 1250°C showed the linear dependence of growth time (Figure 7).

The effect of total gas flow rate on deposition rate was studied to eliminate the mass transfer limitations. The plot is shown in Figure 8, where the operating temperature was 1250°C with $H_2/TiCl_4$ and $BCl_3/TiCl_4$ ratios are 25 and 2 respectively. It is observed that the deposition rate is independent of total gas flow rate. That means

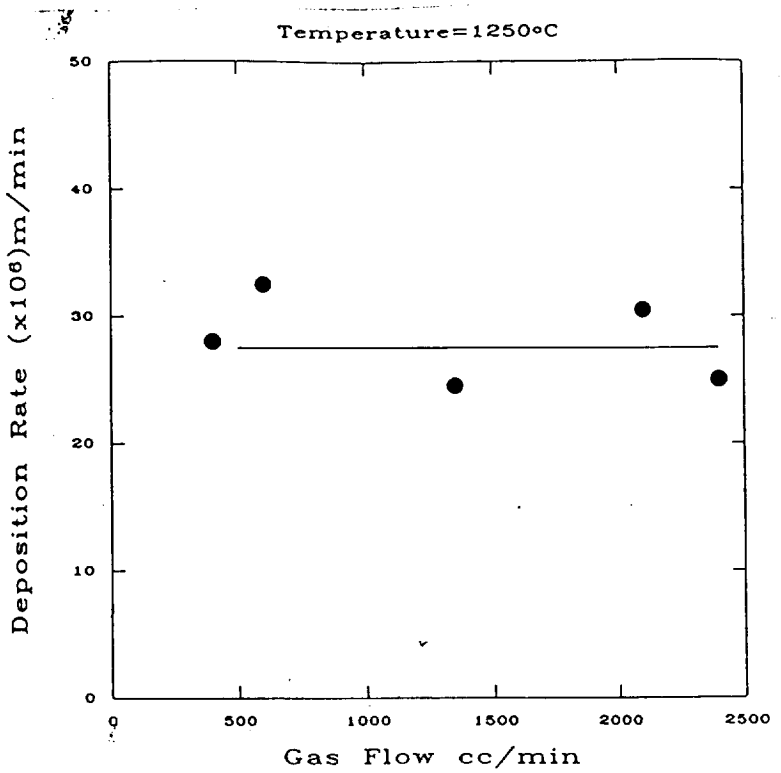

Figure 8: **Effect Total Flow Rate on Deposition**

the rate data is solely influenced by the kinetic and thermodynamic factors and mass transfer limitations are eliminated. This result is similar to that of Mamet'ev et al., (1974). However, at higher temperature and lower total gas flow, the deposition rate drop indicating the change in deposition mechanism.

The rate of deposition of TiB_2 can be expressed as a product of concentration of reactants and temperature, which are independent of each other.

k = k'f(c)

where k is the deposition rate,

k' is a function of temperature, and

$f(c) = C^m_{BCl_3} C^n_{TiCl_4}$, where m and n are the order of the reaction with respect to BCl_3 and $TiCl_4$ respectively.

Since the hydrogen concentration is always in excess, the deposition is assumed to be independent of it. Similarly the concentration of HCl, a reaction product. Since deposition rate is small and hydrogen is used in large excess, the net gas flow rate more or less remains constant. So we varied the input ratios of $H_2/TiCl_4$ and $BCl_3/TiCl_4$ to find out its effect on deposition rate.

The effect of BCl_3 concentration on the deposition rate is shown in figure 9 at

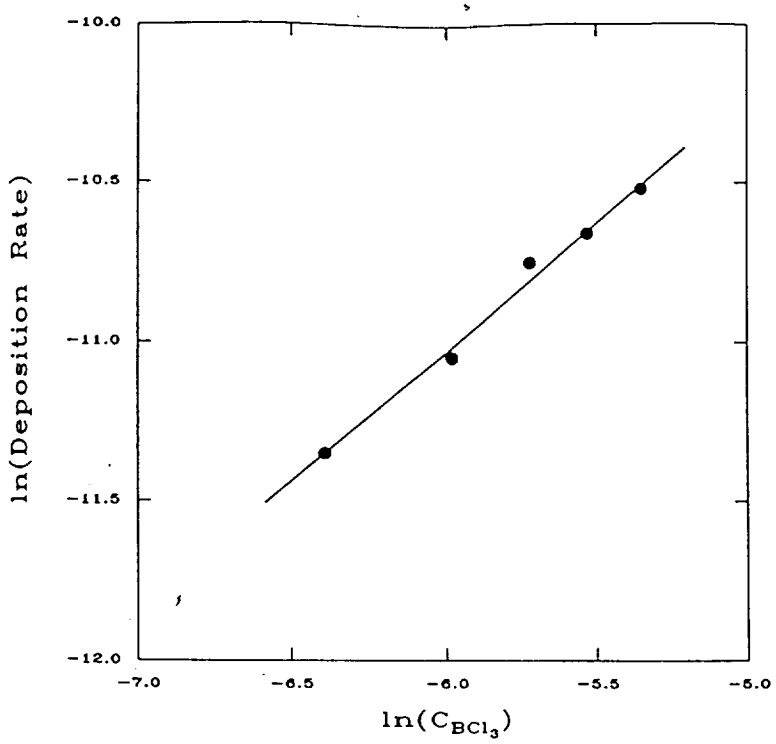

Figure 9: **Effect of BCl_3 Concentration on Deposition Rate at 1250°C and $H_2/TiCl_4$=22**

fixed $H_2/TiCl_4$ ratio (22) and temperature (1250°C).

The graph is linear and slope gives the reaction order with respect to BCl_3 (i.e., m =0.8). Similarly, the concentration of $TiCl_4$ is varied, keeping the $BCl_3/TiCl_4$ ratio constant. This is shown in figure 10. From the plot, it can seen that the concentrations of both BCl_3 and $TiCl_4$ varied simultaneously and the slope gives the overall order (1.0). This gives the order with respect to $TiCl_4$ to be 0.2 (= n). We have also observed the decrease in deposition efficiency with increase in $H_2/(TiCl_4 + BCl_3)$ ratio which is similar to that of Peshev at al., (1965).

Temperature plays an important role on the rate of deposition as well as on the morphology of the deposit. Increasing the temperature, increases the deposition rate rapidly. This is delineated in the Arrhenius plot (figure 11) where η (deposition rate) is plotted against inverse temperature readings between 1200-1450°C for two different concentrations of reactants. It is observed that decreasing the concentration of BCl_3 and $TiCl_4$ decreases the deposition rate but the slope $\frac{E}{R}$ remain unaffected.

Here E is the activation energy (K cal/mol k) and R is the gas constant. This confirms that our data is not governed by mass transfer limitations. The activation

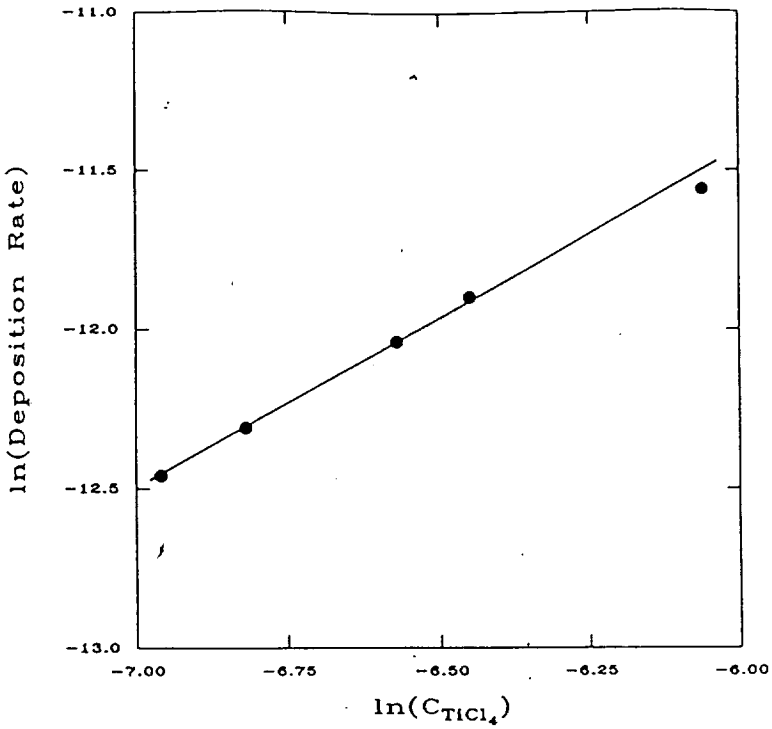

Figure 10: **Effect of $TiCl_4$ Concentration on Deposition for Constant $BCl_3/TiCl_4$ Ratios**

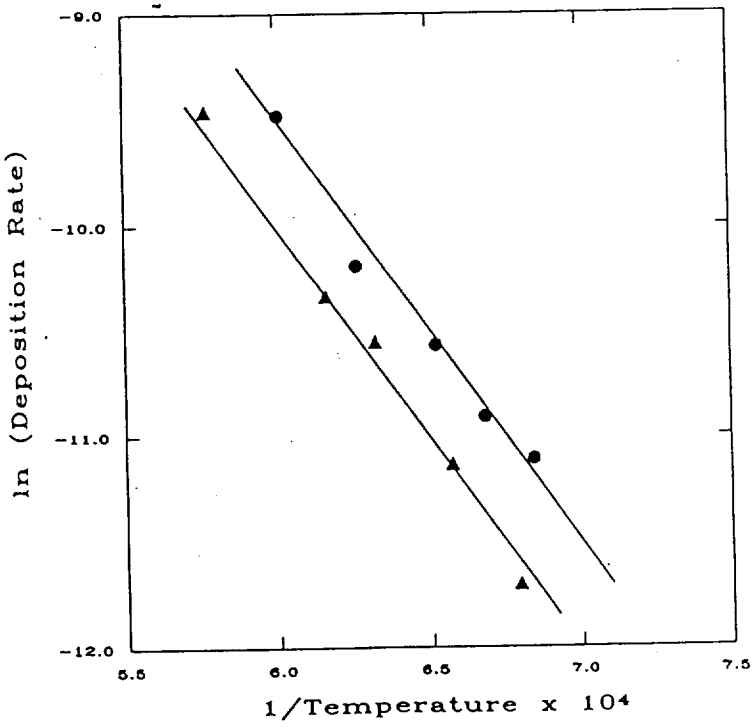

Figure 11: **Arrhenius Plot**

energy obtained from above plot is 40.7 k cal/mol K. This is in an excellent agreement with the values obtained by Bessmann et al. [1977] [40 ±12 K cal/mol K] with the reduction of BCl_3 and $TiCl_4$ by hydrogen. There is no change in slope between 1200-1450°C; shows that only the reaction kinetics controls the deposition rate. However, at higher temperature, the regime shift to a diffusion controlled. But operation at higher temperature resulted in poor fiber quality and morphology which is elaborated in the latter part of this report.

Least square analysis of the deposition rate gave the value of k to be 4900. Hence, the overall deposition rate is expressed as :

$$k = 4900e^{-\frac{40700}{RT}} C_{BCl_3}^{0.8} C_{TiCl_4}^{0.2}$$

where k is the deposition rate in mm/hr,
T is the temperature in Kelvin,
C_{BCl_3} and C_{TiCl_4} are concentrations in mol/lit, and
R is the gas constant =1.987 cal/mol K.

This is the simple expression obtained for our operation. However, actual reaction kinetics is much more complicated due to many side reactions and products.

7.1.3 Morphological Study

Chemical vapor deposited TiB_2 exhibits various morphologies and microstructures depending on the temperature of the substrate and concentration of the reactants. It is advantageous to study and understand this phenomenon with respect to the final property of the fiber since the mechanical properties of the fiber is sensitive to the microstructure of the deposit.

Temperature is one of the important parameter which determines the deposit characteristics. It is well established that at fixed concentration of reactants , increase in temperature, increases the size of the crystallite on the deposit. Vice versa also holds good [Besmann and Spear, 1975; Takahashi and Kamiya, 1974]. That means temperature and supersaturation play opposite to each other in determining the crystallinity. These effects are explained below. In Figure 12, the detailed surface morphology of the deposit at different temperature is shown.

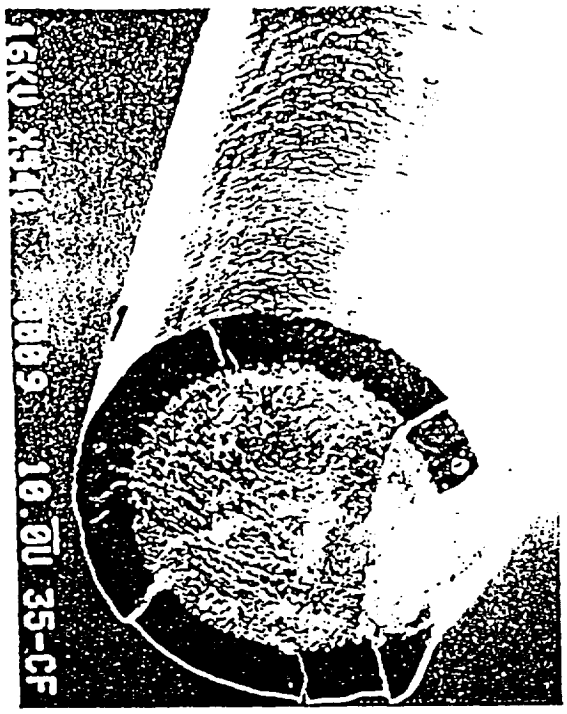

1

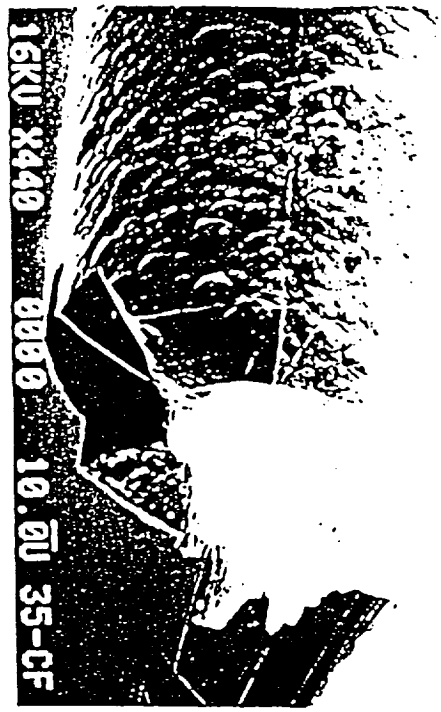

2

Temperature (°C): 1. 1200 2. 1250 3. 1310 4. 1350

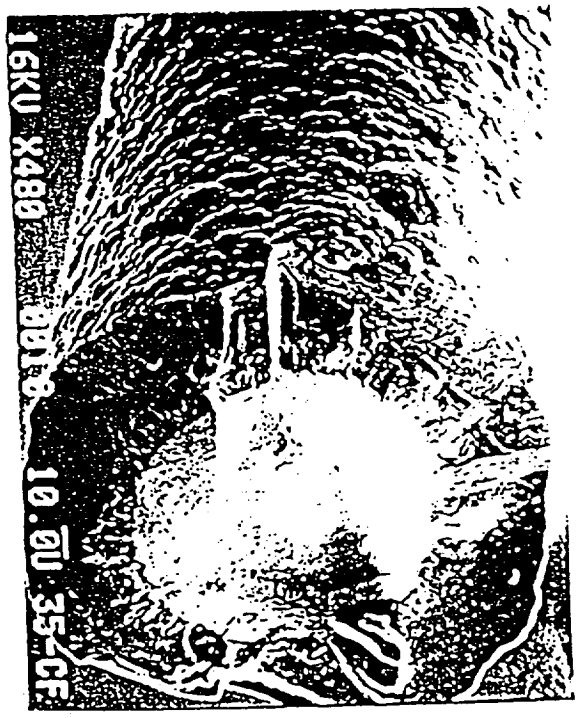

Figure 12: Surface Morphology of the Deposit at Different Temperature

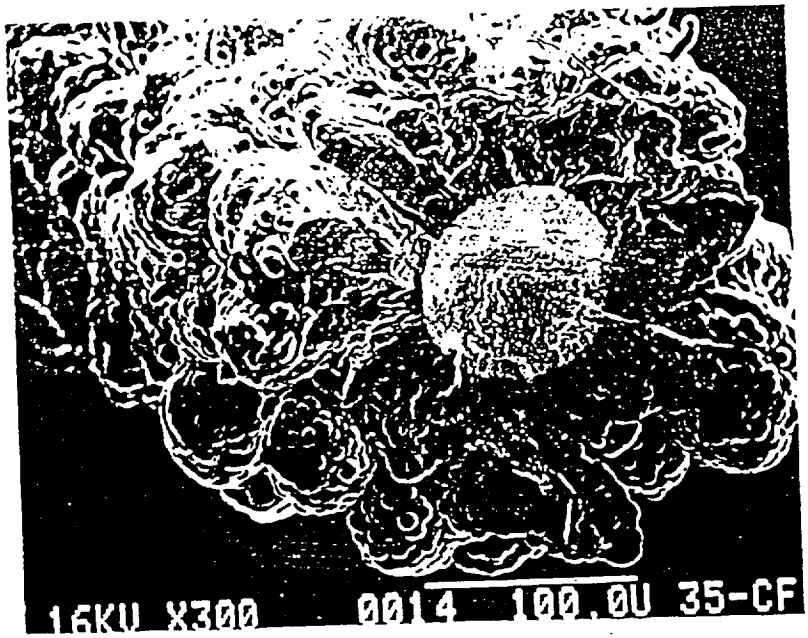

1

Effect of Temperature on Surface Morphology

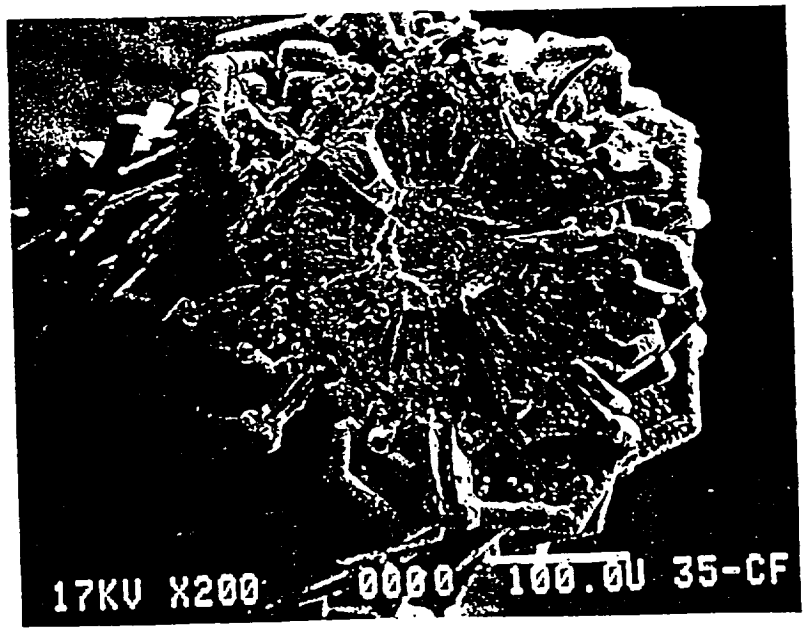

Temperature (°C): 1. 1460 2. 1900

2

The $BCl_3/TiCl_4 = 2$ and $H_2/TiCl_4 = 22$ was maintained throughout the operation. At 1200°C, the coating (deposit) is smooth, microcrystalline without any nodular deposit. As the temperature increases, the surface becomes increasingly nodular. At 1400°C, the surface is seen to be made up of nodules of over 50 μm in size which in turn made up of small grains of 2 to 5 μm size. After careful observation, it is predicted that initial deposit is microcrystalline and nodules appear to grow as a secondary features on it. At very high temperature (>1450°C), the deposit morphology changes from nodular to platelet kind of deposit which can be easily detached from the core [size around 30 x 40 μm]. This may be due to the change in transfer mechanism [changed to mass transfer control]. At low temperatures (<1200°C), the deposit is amorphous in nature and hardly sticks to the substrate.

The effect of concentration of reactants on the surface morphology is also considered in our study. Figure 13 shows the effect of $BCl_3/TiCl_4$ ratio at optimum temperature (1250°C), flow rate (2 l/min) and $H_2/TiCl_4$ ratio (25) on deposit morphology. It is observed that, increase in $BCl_3/TiCl_4$ ratio increases the surface crystallinity leading to more nodular surface. At $BCl_3/TiCl_4$ ratio greater than 2.5, nodules of approximately 10μm size are uniformly distributed on the surface of the fiber. However, at $BCl_3/TiCl_4$ ratio of 2 or below the surface is smooth and perfectly microcrystalline.

The effect of $H_2/TiCl_4$ ratio on fiber morphology is presented in figure 14. The temperature and flow rate were maintained same as above, where as $BCl_3/TiCl_4$ ratio was kept at 2. At $H_2/TiCl_4$ ratio of 7, the surface is very rough with a lot of small nodular growth, which are non-uniformly distributed on the surface. As the ratio increases, this phenomenon starts disappearing. At a ratio of 22, the surface is smoother with preferred crystallinity. Further increase in $H_2/TiCl_4$ ration, no appreciable change in the surface features are observed.

Even though we studied all possible parameters effect on morphological feature of the deposit, it is very difficult to locate the exact mechanism of growth. It may be influenced by impurities (side products), codeposited products, or any of the above parameter. However, optimum conditions for best quality microcrystalline fiber are at 1250°C with $H_2/TiCl_4$ and $BCl_3/TiCl_4$ ratios 25 and 2 respectively.

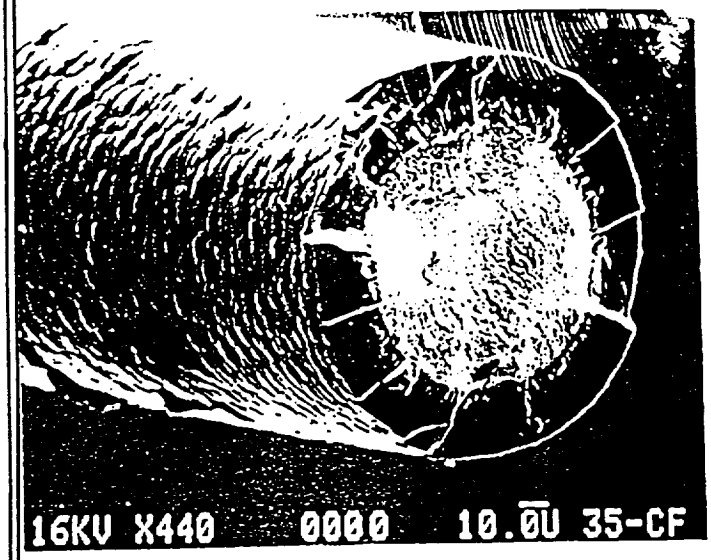

1

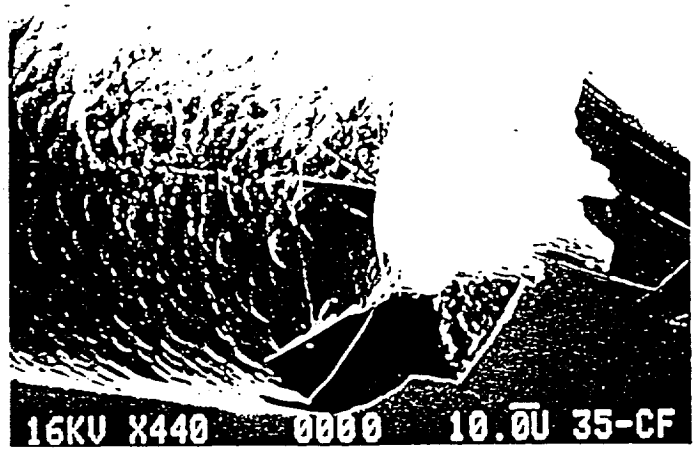

2

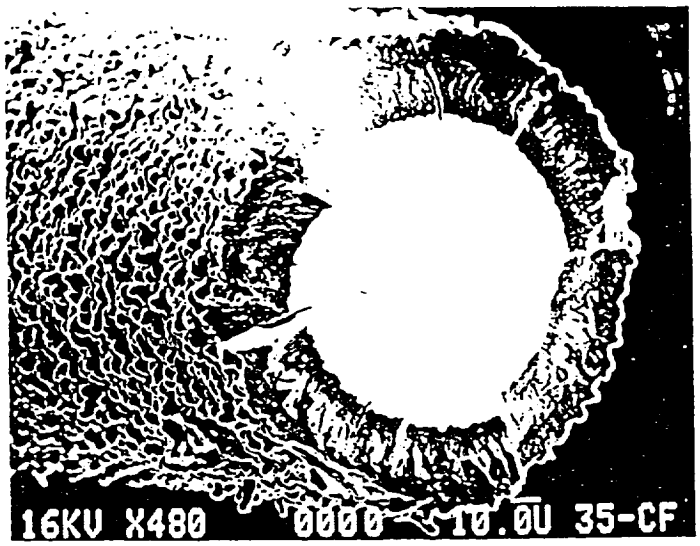

3

$BCl_3/TiCl_4$: 1. 1.2 2. 2.0 3. 2.4

Figure 13: Morphology at 1250°C, for Different $BCl_3/TiCl_4$ Ratio

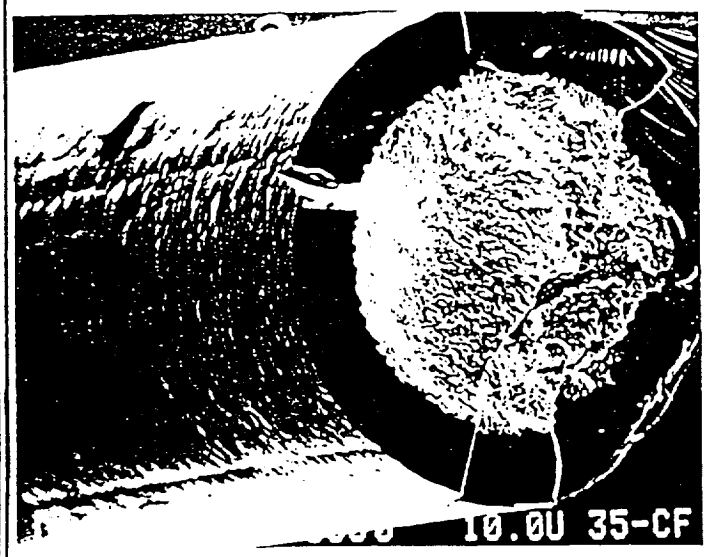

1

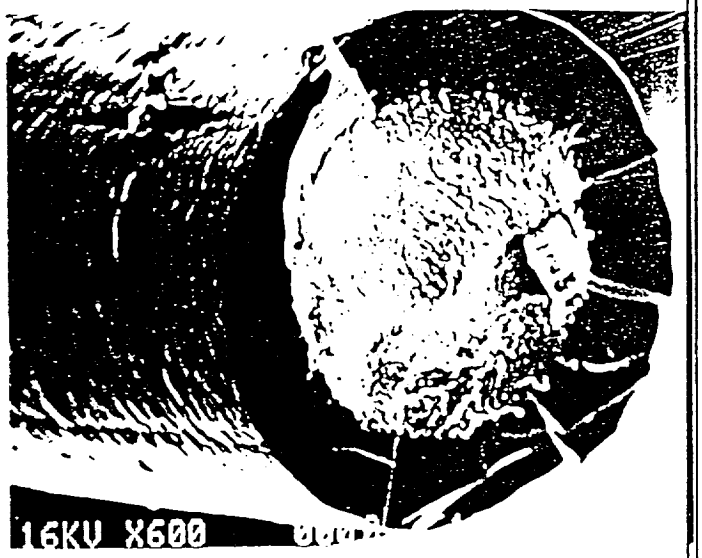

2

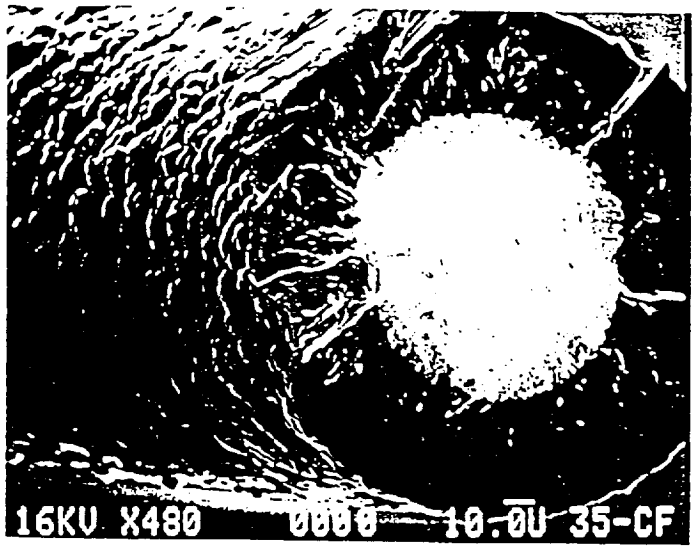

3

$H_2/TiCl_4$: 1. 7 2. 22 3. 40

Figure 14: Morphology for Different $H_2/TiCl_4$ ratio

7.1.4 Thermal Stresses in the Deposition Process

The fibers and their coatings are being exposed to three different stresses: thermal expansion mismatch, thermal stresses and blistering. These three stresses induce micro-cracks in the coating with the subsequent weakening of the final product. The question to answer is which one of these stresses crosses the resistance threshold for the cracks in the coating to appear. For most situations, a slow cooling process suppresses the thermal stress. On the other hand, blistering most likely will appear when coating and core interact to form a tertiary intermediate layer. The solution to thermal expansion mismatch is by incorporating intermediate layer which act as a "cushion" and absorbs stresses on the coating.

The cooling rate of the deposited fiber plays also an important role on the adherence of the TiB_2 film on W core. If the fiber is brought to room temperature very fast, the coating chips off as shown in figure 15. This is due to the thermal stresses created while depositing. The slow cooling process after the reaction will suppress these thermal stresses leading to good adhesion. The parent fiber with the chip is shown in the figure. However, chipped piece showed remarkable good physical and mechanical properties. In our experiments, we limited the interaction between TiB_2 deposit and the W core to avoid blistering. SEM studies were conducted on a radial cross section of the fiber to determine possible interaction.

There is no interaction and a sharp interface is clearly discernable. To further our studies, we mounted the fiber longitudinally. The special technique has to be used here to avoid the damage to the fiber and for accurate results. Fiber is mounted in an epoxy and polished first with alumina and subsequently with diamond wheel. These results are shown in figure 16 where there is absolutely no interaction. The fiber is powdered and x-ray diffraction was carried out. However, there is no trace of tungsten borides as can be seen from x-ray pattern (figure 17).

An intermediate layer of pyrolytic carbon was deposited to improve further the mechanical properties by eliminating blistering effect. Earlier analysis were used to detect the interaction between the core and coatings. Figure 18 does not indicate the presence of any diffusion layer or compound formation between the different layers of coating. This is in agreement with the results of Pierson et al., [1979].

Finally, the solution to mismatching thermal expansion coefficients has been to deposit an intermediate pyrolytic carbon layer; this "spongy" layer acts as a "cushion"

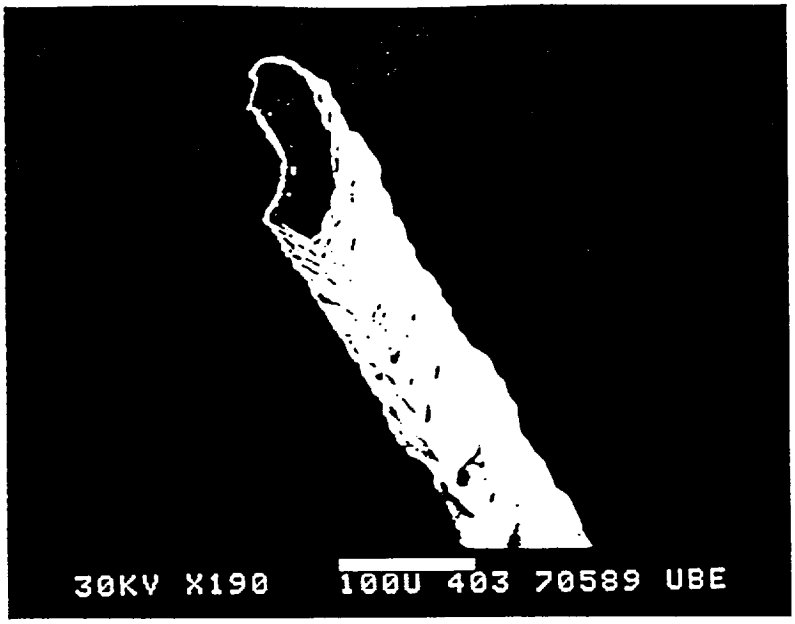

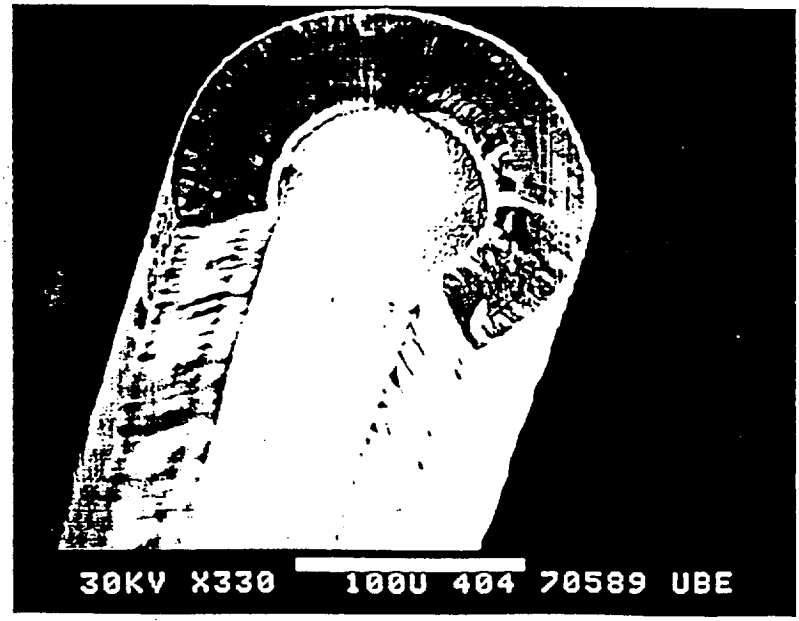

Figure 15: Cooling Effect on Coating Adhesion and Chipped Fiber

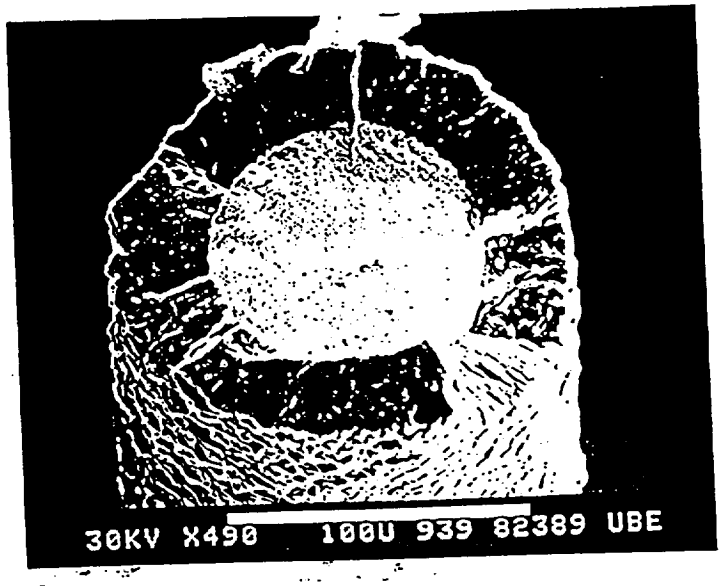

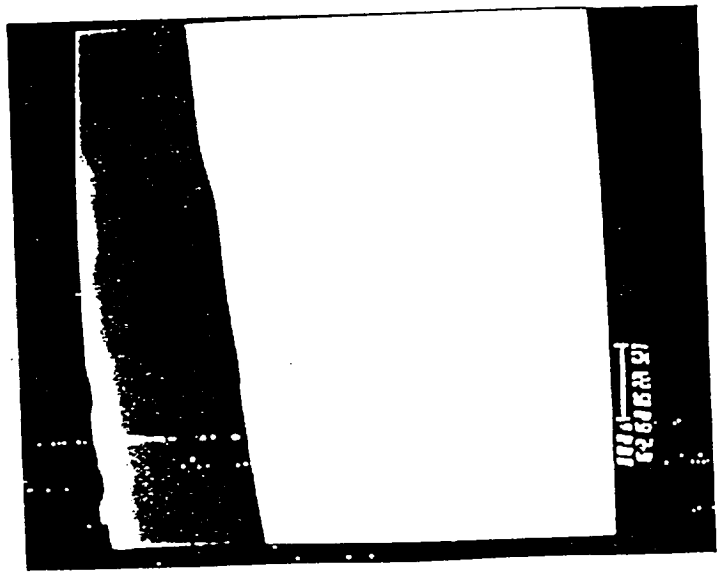

Figure 16: Fiber-Core Interface with Clear Boundary

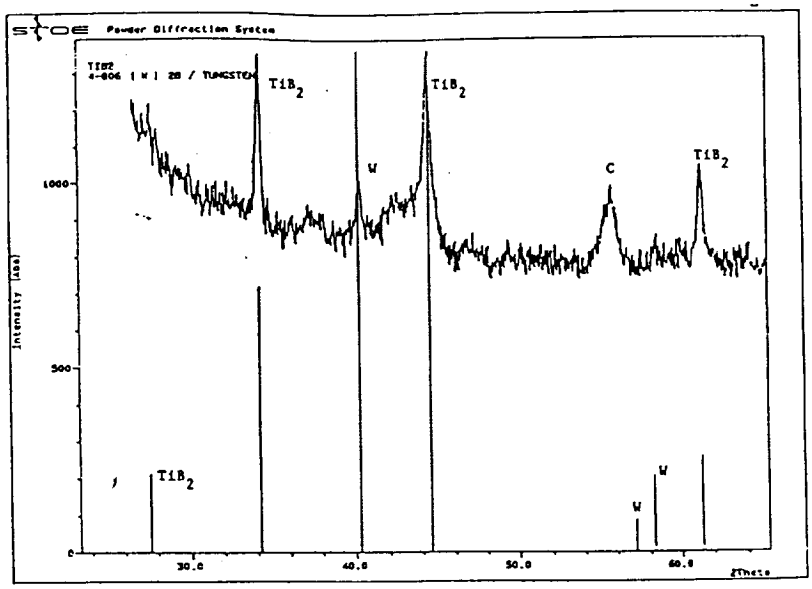

Figure 17: X-ray Diffraction Pattern of TiB_2 on W

and "absorbs" stresses on the coating. However, the pyrolytic carbon layer may have a deleterious effect on the final strength. Figure 19 shows a layer of pyrolytic graphite deposited on W core at 1000°C.

It can be seen that the external surface of graphite was striation corresponding to W core. However, final TiB_2 deposit shows the very smooth surface. That means the pyrolytic carbon (graphitic) layer provides a healing effect to the fiber stresses by smoothening the surface of the core.

7.1.5 Residual Stress Model

A theoretical model is used to estimate the residual stress in CVD of TiB_2 on W core. This provides information on the magnitude of residual stress and the region of maximum stress. The effect of various parameters can be studied and utilized in reducing the stresses. Since the thermal expansion mismatch plays a major role on residual stresses, only this is considered in our study. These stresses arise due to cooling the coating from deposition temperature. However, for high temperature application, for which the fibers are intended, these stresses are expected to diminish.

A composite cylinder model is used [Brugger, 1971; Redston and Stanworth, 1945;

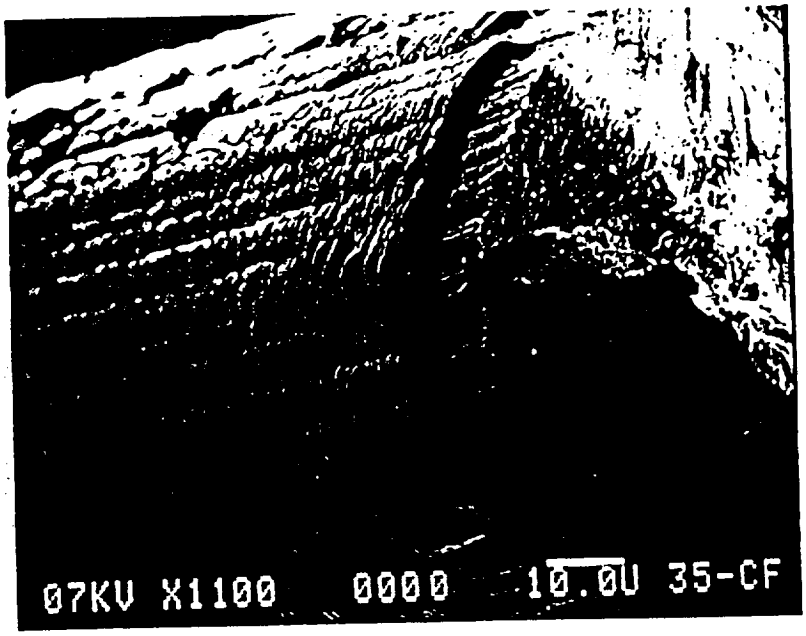

Effect of Pyrolytic Graphite Intermediate Layer on Surface Morphology

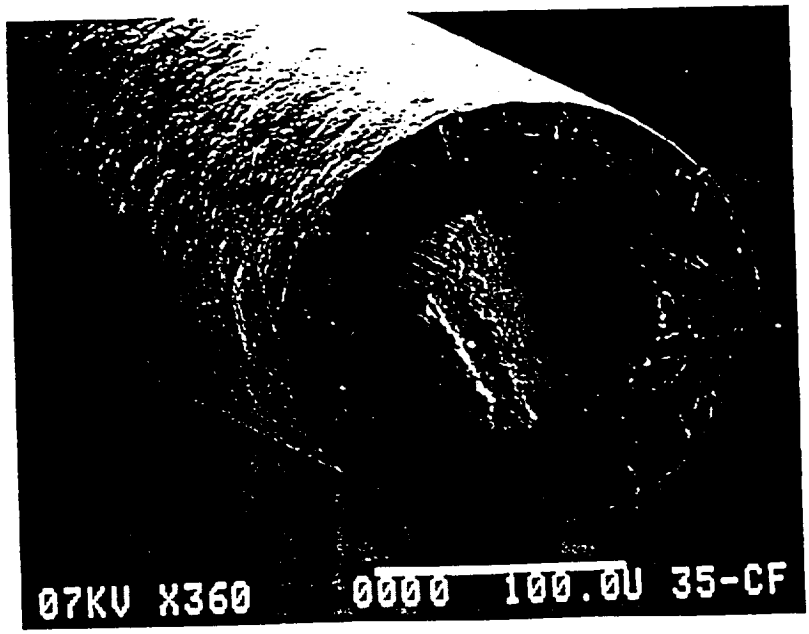

Figure 18: Effect of Intermediate Layer on Fiber-Core Interaction

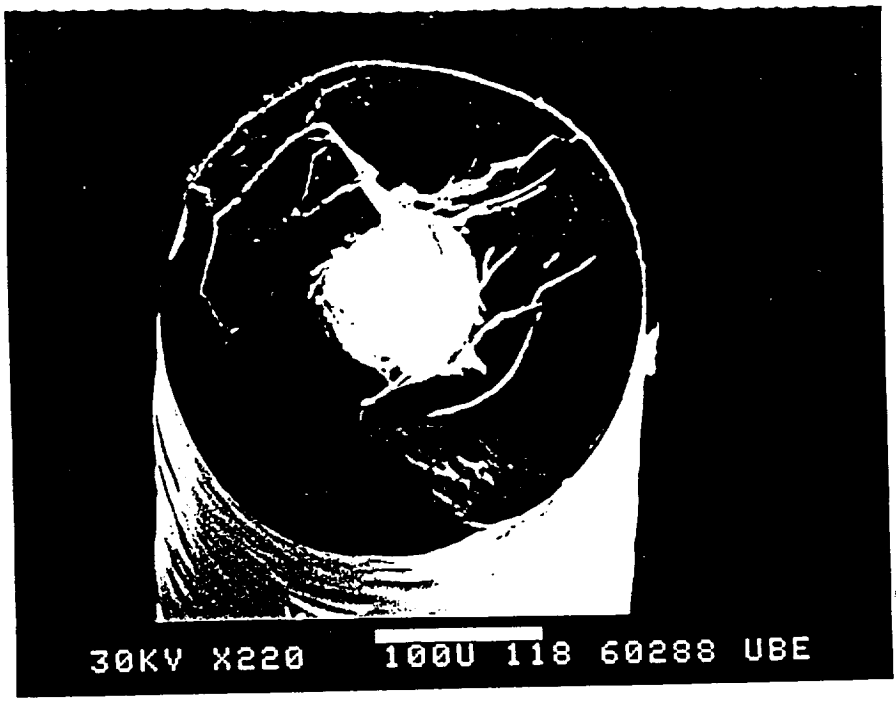

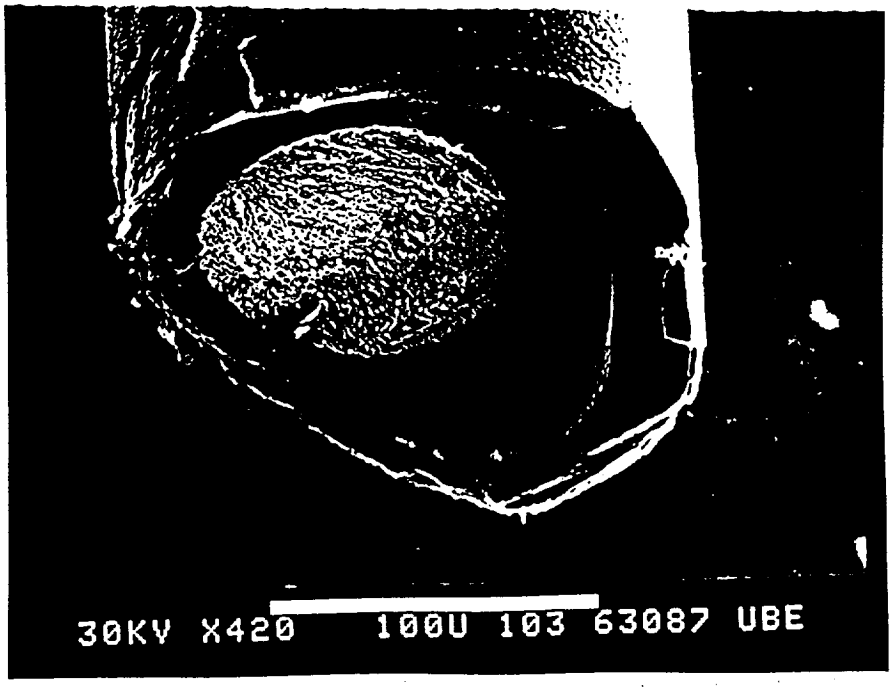

Figure 19: Intermediate "Spongy" Layer

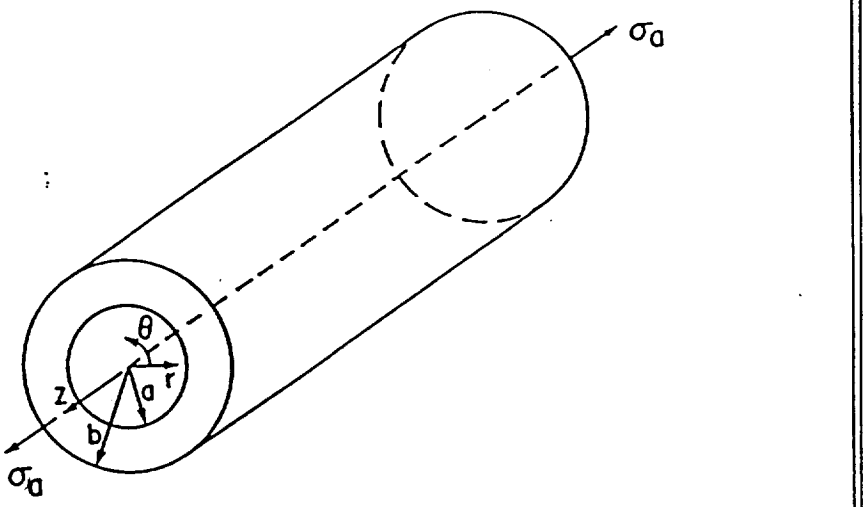

Figure 20: **Co-ordinate System for Stress Analysis**

Jain and Wetherhold, 1989], where coating and the core are assumed to behave elastically in the temperature range considered. Due to anisotropy of the coating, it is modified to take into account the different properties of the coating along the different axes. The coordinate system used is shown in Figure 20. There are three components of stress in the cylindrical composite: axial stress σ_z, radial stress σ_r,and circumferential or hoop stress σ_θ. The constitutive equations and derivations are given in the Ph.D. thesis of Mr. Vikas Lakhotia, SUNY Buffalo (1990).

The stress distribution in composite fiber is shown in Figure 21. The properties of the W were obtained from the literature [Shaffer, 1964]. The stress distribution is calculated for cooling a TiB_2 on W fiber from 1200°C (deposition temperature) to room temperature. Final diameter of the fiber assumed to be 200μm on 75μm W core. It can be seen that the stresses are compressive in the core and tensile in the coating. This is due to higher thermal expansion coefficient of TiB_2 compared to W. The same calculations, assuming the coating to be isotropic are given in Figure 22.

There is not much difference except in the theta stress. In these calculations, it was assumed that the coating exhibited properties of polycrystalline TiB_2. From the above figure, it is seen that the core is subjected to high compressive axial stress. In the coating, the radial stresses are compressive and hence not critical in determining the fracture point of the fiber. The theta and axial stresses are tensile and have a high positive value. The theta value is maximum at the interface and decreases rapidly with

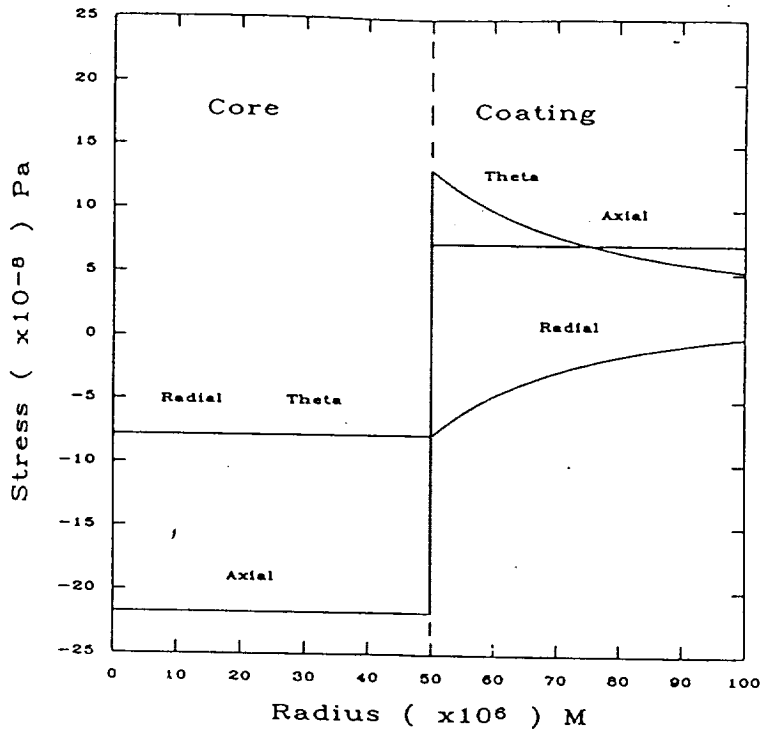

Figure 21: The Stress Distribution in Composite fiber

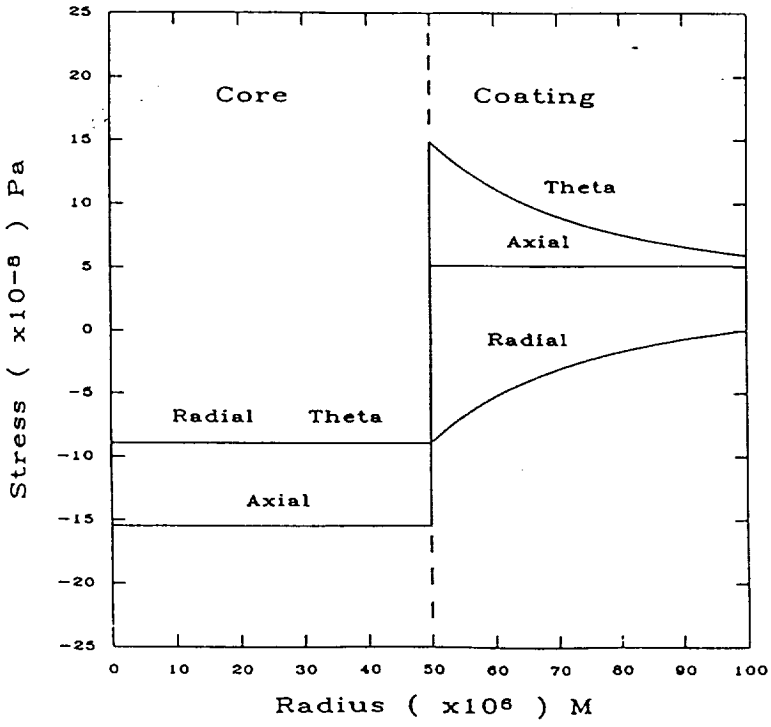

Figure 22: The Stress Distribution Assuming the Coating to be Isotropic

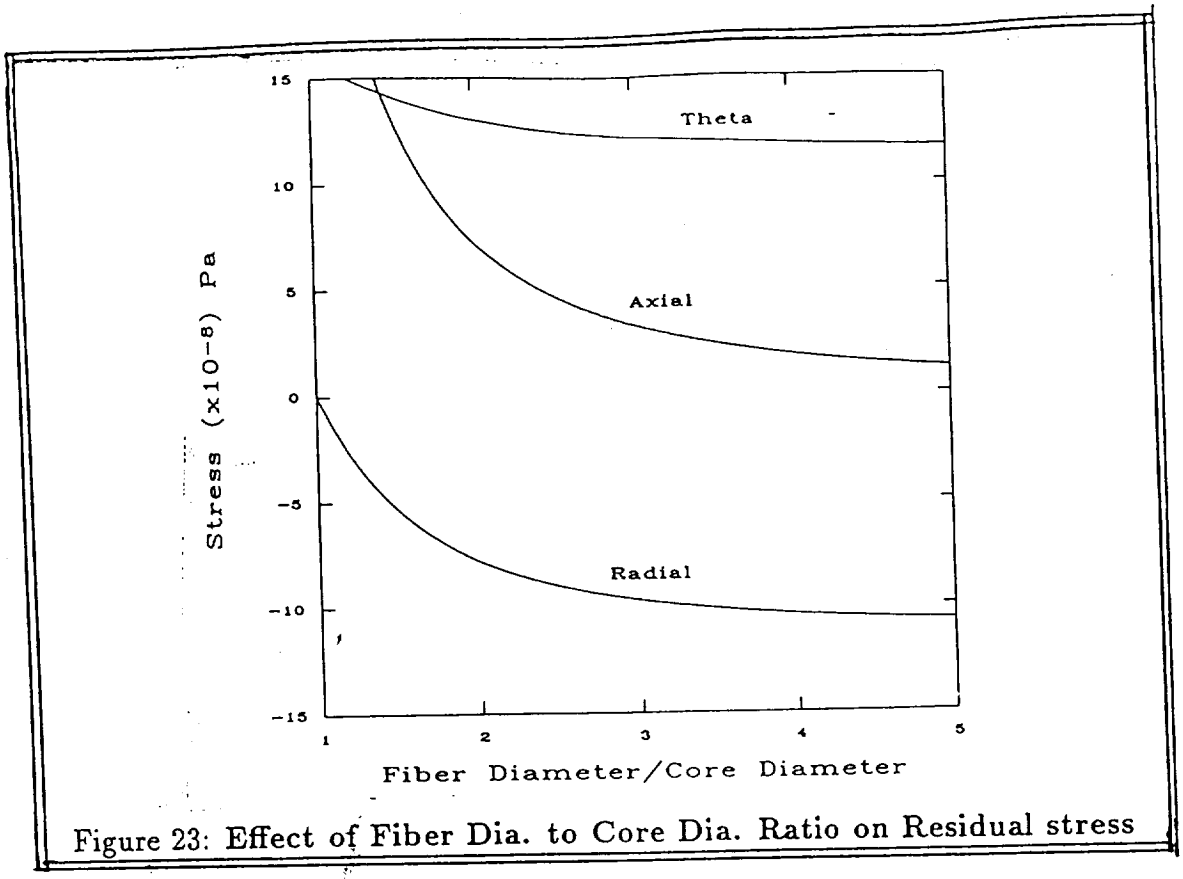

Figure 23: Effect of Fiber Dia. to Core Dia. Ratio on Residual stress

radial distance.

It is interesting to study the relationship between the core diameter to the final fiber diameter with respect to stresses. So we varied the ρ (fiber diameter to core diameter ratio) to calculate the generated stresses from the model. Since the maximum stress occurs at the coating interface, this is plotted in figure 23. It is seen that by increasing the ρ, decreased the stress and their levels off for the ρ value above 3. Above this ratio, stress does not change appreciably.

The effect of deposition temperature on the residual stress is given in figure 24. Here the residual stress increases with temperature, as expected. This is obvious because higher deposition temperature means, greater the thermal expansion mismatch, so the fiber should be deposited in an optimum temperature to get microcrystalline deposit. The effect of internal stress on the stress field is also studied and is discussed in the later part of this report.

7.1.6 Mechanical properties

It is necessary to study the mechanical properties of the fiber to determine the optimum conditions for the deposition to synthesize a fiber. Measurement of the mechanical

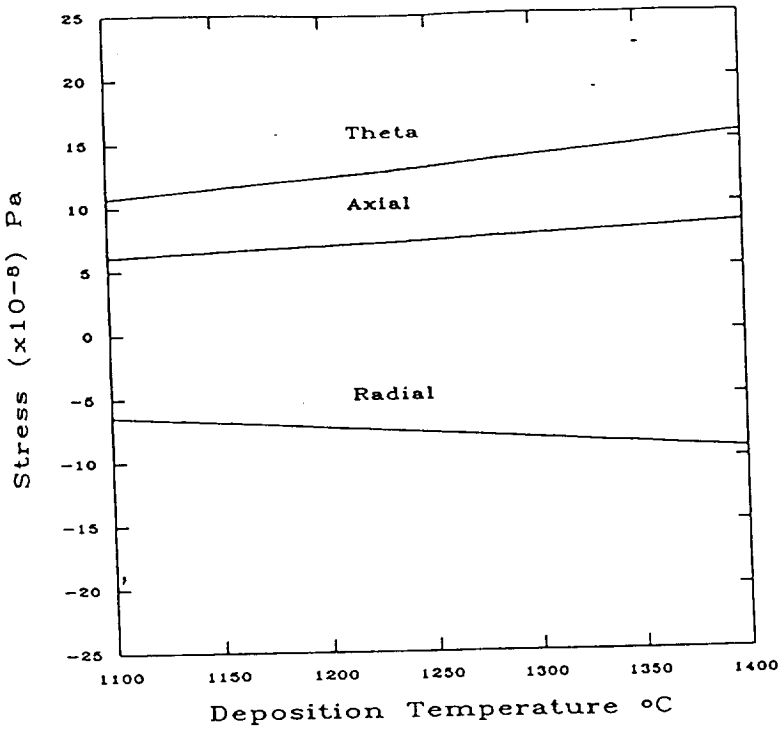

Figure 24: **Effect of Deposition Temperature on Residual Stress**

properties of brittle material like TiB_2 fiber is a difficult task and often the technique used can affect the measured strength. All the tests were conducted on a research grade INSTRON tensile testing equipment. The technique used is the currently accepted standard for testing the brittle fibers.

All the fibers studied fractured in a brittle manner. No separation of the coating from the core is observed. The typical fracture behavior is shown in figure 25. The crack directions on this photograph can be explained in terms of residual stress. This is shown in Figure 26. In the figure, external tensile stress is plotted against stress distribution. As the tensile stress increases, the theta and radial stresses remain unaffected, whereas axial stresses increase rapidly. In general, stress in any direction, causes the fracture in a direction perpendicular to it. Hence in the figure, the fracture is in a plane perpendicular to the fiber axis. Some cases, the cracks are in the radial direction due to reasonably high tensile stresses in theta direction.

The effect of temperature on the strength of the fiber is shown in figure 27. The strengths measured is in the range of 30-50 KSI which is much below the hot pressed TiB_2 (100-150 KSI) and is pass through the maximum at around 1550K. This can be explained by considering both the residual stresses and surface morphology (microcrystallinity). In all the cases the deposition conditions were kept constant (2 min.). From

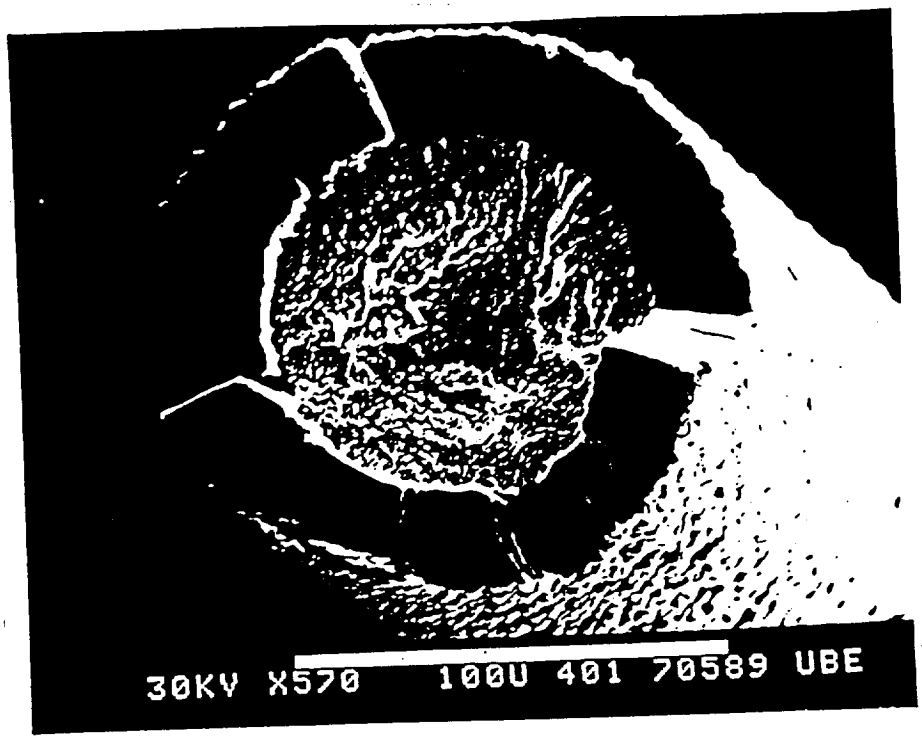

Figure 25: A Typical Brittle Fracture of TiB_2 fiber

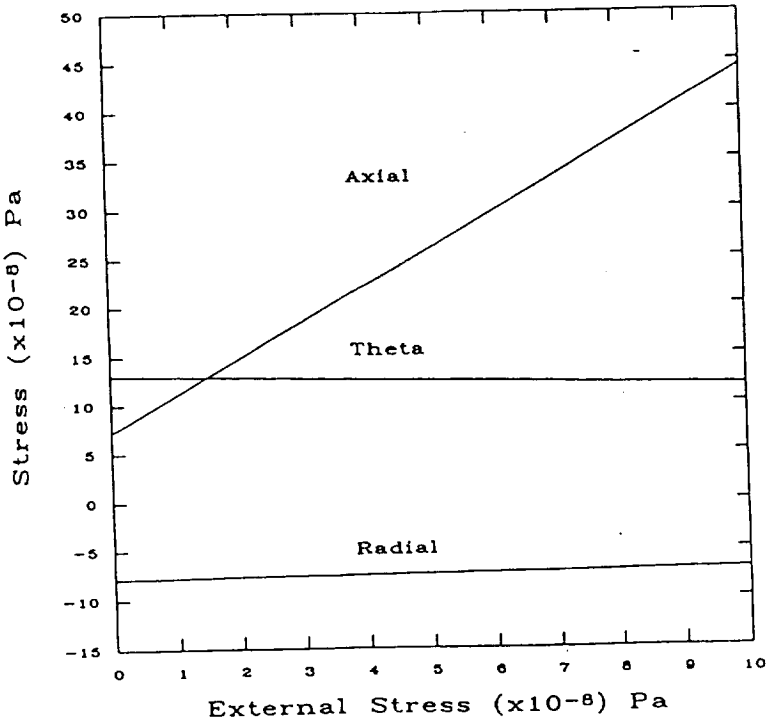

Figure 26: Effect of External Tensile Stress on Stress Distribution

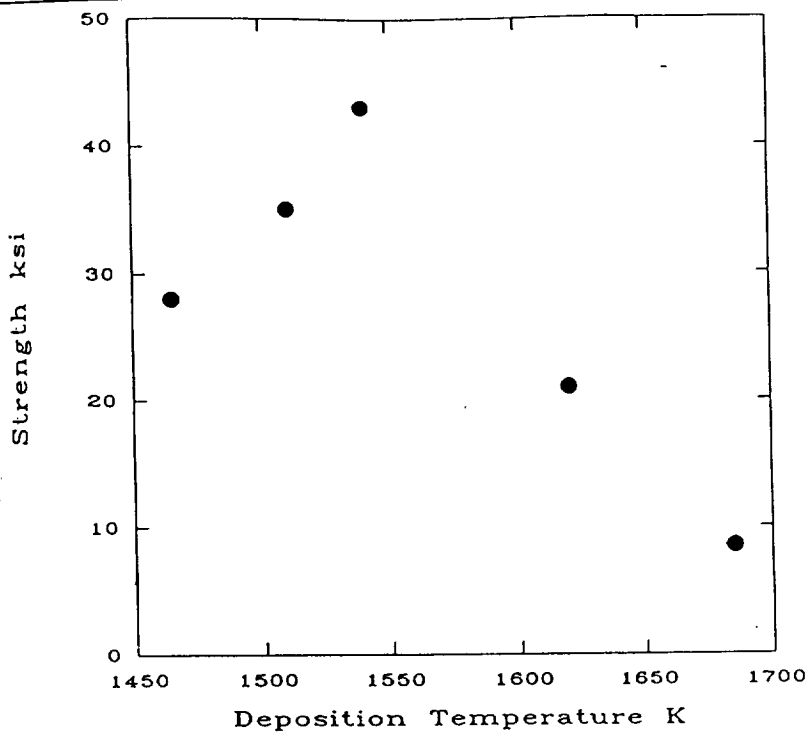

Figure 27: **Strength Dependence on Deposition Temperature**

earlier figure, it is observed that residual stress decreases with coating thickness. This enables the coating to sustain greater external load prior to fracture. Here one should remember the fact that the coating thickness increases with temperature. However, with increase in temperature, the surface micro-crystallinity is lost. The surface becomes more nodular as reported in our morphological studies, resulting in a poor fiber strength. These observations can also be explained by external stress effect plot (figure 28). It shows that an external stress of 2.5 x 10^8 Pa ($\approx$36 KSI), causes axial stress in the coating and the interface, of 16.5 x 10^8 Pa ($\approx$120 KSI). That means the coating is capable of carrying much larger load provided, the residual stresses are reduced.

Various techniques were considered. Among them is the coating of intermediate spongy layer of pyrolytic graphitic carbon. The function of this layer is not clearly understood, but is believed to serve as a spongy layer capable of accommodating the stresses due to thermal expansion difference. The effect of pyrolytic graphitic carbon thickness is shown in figure 29. The tensile strength of the fiber due to the presence of the intermediate layer increases with the thickness. It is passing through maximum at around 3.5 μm for 200 μm TiB_2 fiber. This gives a ratio of intermediate layer to final coating thickness ratio around 60. The modulus of the fiber is around 20-30 MSI, which is not affected by intermediate layer.

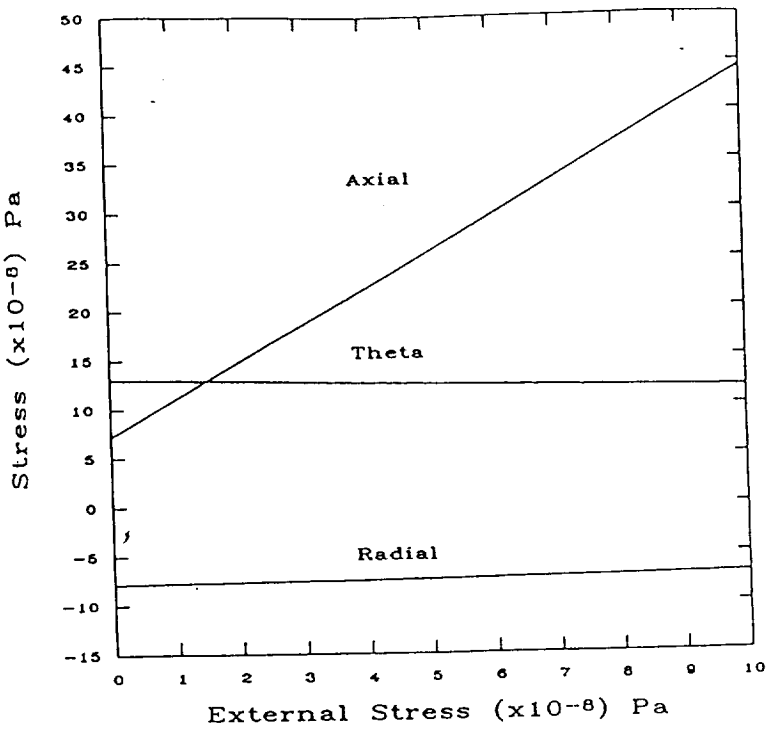

Figure 28: **Effect of External Stress**

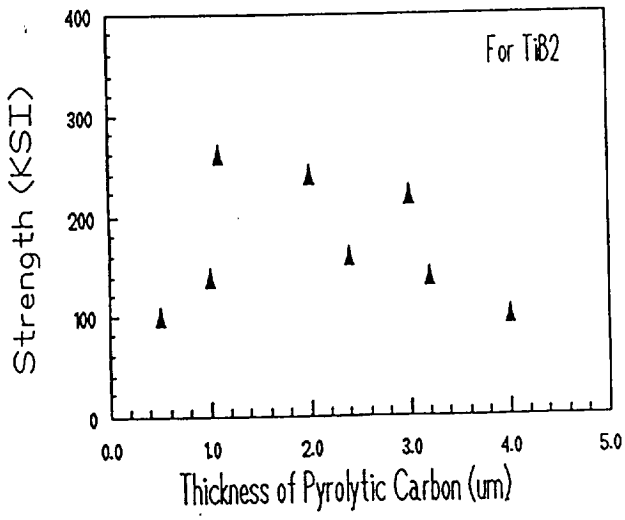

Figure 29: **Graphaite Spongy Layer effect on Strength**

7.1.7 Texture of the Coating

TiB_2 is a hexagonal crystal of AlB_2 type. The lattice parameters are, a = 3.028A, c = 3.228A and $\frac{c}{a}$= 1.064A. It exhibits considerable anisotropy in thermal, mechanical and electrical properties along the two different axes, which is reported in literature [Mersol et al., 1968; Vahldick, 1967; Keihn and Keplin, 1967].

Many researchers observed preferential crystal orientation in TiB_2 deposit [Gannon et al., 1963; Gebhardt and Cree, 1965; Besmann and Spear, 1975]. However, all the studies conducted are on flat substrate where C- axis of the crystal is parallel to the surface. This determination of orientation is fairly simple compared to on a fiber substrate. Following technique is used.

The fibers were cut transversely, mounted in bakelite and polished by alumina and diamond. The coatings were examined metallographically. The samples were then etched with a mixture of nitric acid and hyrofluoric acid. The resultant photomicrographs taken were not able to conclusively prove the existence of orientation of the crystals.

An X-ray diffraction technique described by Cullity was used [Cullity, 1978]. A Debye Scherrer pattern and a pinhole transmission pattern were produced using Ni filtered Cu-Kα radiation. From the diameter of the circle the angle of reflection (2θ) and the d-spacings can be found. Also the d-spacings for the hexagonal TiB_2 crystal are calculated and the results are given in Table 2.

It can be seen that the [001] reflections are absent. This means that the [001] planes are perpendicular to the fiber axis. The Debye Scherrer is shown in figure 30.

The results are confirmed by a pinhole transmission pattern, as shown in Figure 31. The angle θ is calculated from the ring diameter and δ is measured from the normal as indicated in the figure. Using these two, the angle ϕ is calculated by applying the expression, cos ϕ = cos θ cos δ. These are given in 3.

Table 4 gives the interplanar angles between the various planes. It can be seen by comparing the angles that [001] are the indices of the fiber axis. This means that the c-axis of the TiB_2 crystal is parallel to the W-fiber surface. The second ring suggests a second, much less pronounced [011] texture.

TiC and B_4C were also prepared by CVD. These fibers were obtained by decomposition of the corresponding halides with a hydrogen and carbon source.

Table 2: Debye Scherrer Pattern

hk.l	d[A]
00.1	absent
10.0	2.60
10.1	2.029
00.2	absent
11.0	1.509
10.2	1.369
11.1	overlapped
20.0	1.309
20.1	1.213
11.2	1.020
20.2	1.015
10.3	0.992
21.1	0.9472
11.3	0.8774
21.2	0.8444

Table 3: Pinhole Transmission Results

hk.l	θ	δ	ϕ
10.0	17.1	90	90
10.0	17.1	63	64
10.0	17.1	113	112
10.1	22.3	46	50

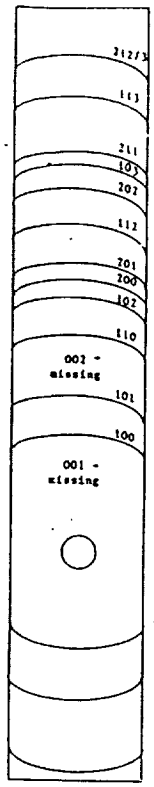

Figure 30: Debye Scherrer Pattern of TiB_2 on W

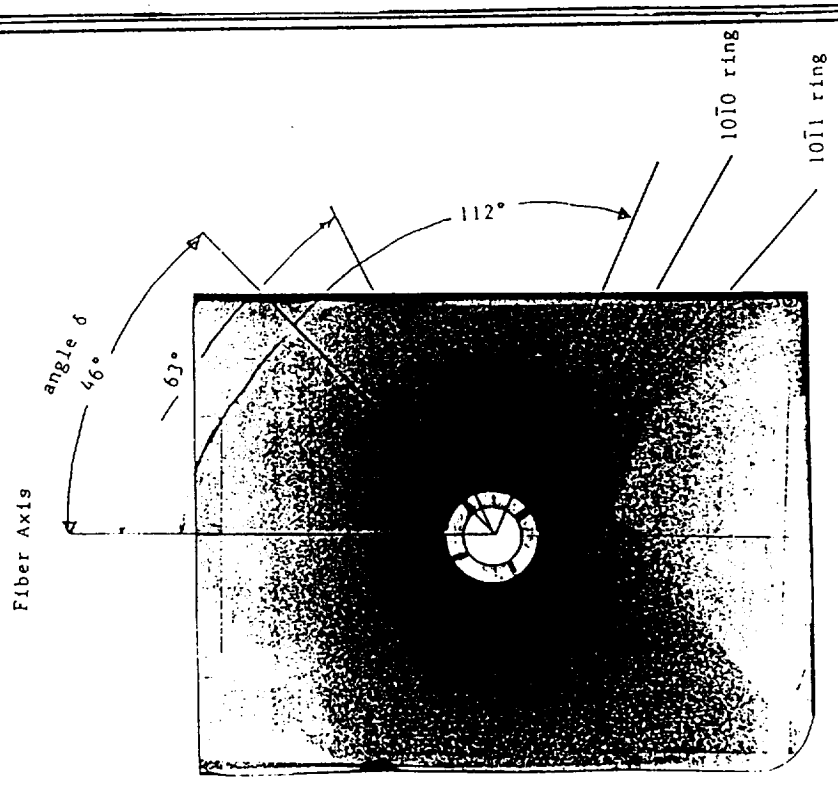

Figure 31: Pinhole Transmission Pattern of TiB_2 on W

Table 4: Interplanar Angles

$\frac{h_1 k_1 . l_1}{h_2 k_2 . l_2}$	$[^o]$
$\frac{00.1}{10.0}$	90.0
$\frac{00.1}{10.1}$	50.0
$\frac{01.1}{10.0}$	67.2
$\frac{01.1}{-10.0}$	112.8
$\frac{01.1}{10.1}$	45.7

8 Boron carbide and titanium carbide fibers

[See Figure 32 and 33].

The CVD process of B_4C is carried out on a carbon core by reducing BCl_3 and CH_4/CCl_4 with hydrogen in the temperature range 1000-1500°C. The concentration of BCl_3, hydrocarbon (CH_4 /CCl_4) and hydrogen gases was varied in our experiments. The nucleation of excess of carbon was observed when CH_4 was used as a precursor. This nucleation of carbon within the deposit is catalyzed by BCl_3 as reported earlier [Brennfleck et al., 1984]. This process leads to local separation of B_4C and carbon deposition. This intergranular carbon deposition exhibits a very low Young's modulus and enables elastic strains of the whole deposit without plastic deformation. The problem of low modulus was partially overcome by using CCl_4 as the carbon source. The optimum reactant concentration expressed in terms of Cl to H ratio was found to be 1:5 at 1300°C. An excess of hydrogen increases the conversion per pass of BCl_3 and reaches the maximum at around 0.002 m^3/sec (total gas flow rate). Our best deposit contained less than 2% of free carbon. Higher temperature gave many side products [$BHCl_2$, BCl_2, and BC1 as reported by Naslain et al., 1979]. The results are given in Table 5. Our fiber has tensile strength of approximately 300-400 KSI with a modus of approximately 35 MSI. The fiber contained less than 2% of free carbon.

Titanium carbide deposition was carried out by reducing $TiCl_4 + CCl_4$ with hydrogen in the temperature range 1300-1500°C. The optimum conditions were: chlorine to hydrogen ratio 1:7 with a flow rate of 0.0015 m^3/sec (at 1400°C) and the residence time in the reactor is 3 min. Here we are faced with a severe problem of heterogeneous

TiC FIBER (CORE - C)

(a) Direct reaction of $TiCl$ with $H : Cl = 5$ at 1400 °C.

(b) Deposition reaction at 1200 ° with $C : Ti = 3$ and $H : Cl = 2.5$

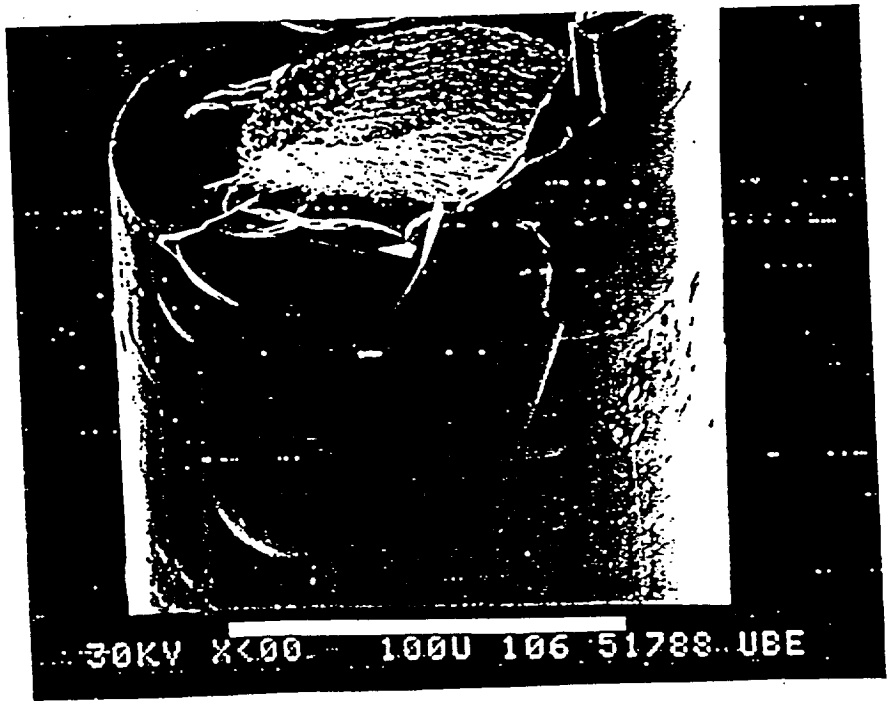

Figure 32: Titanium Carbide CVD Fibers

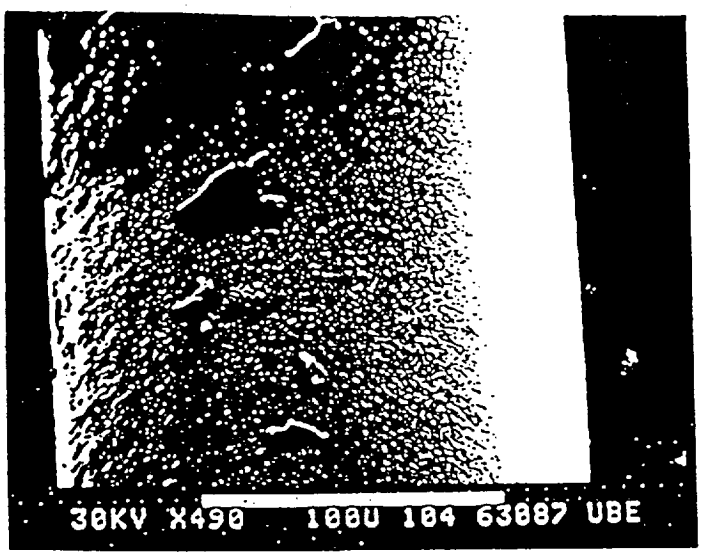

BORON CARBIDE FIBER (CORE -)

BORON CARBIDE FIBER (CORE - C)

(a) Deposition on tungsten core at 1400 °C with $B : C = 2$ and $H : Cl = 2$

(b) At the previous conditions but with CH_4 as carbon source.

Figure 33: Boron Carbide CVD Fibers on Different Cores

Table 5: Properties of fabricated fibers

Fiber	M.P. (°C)	Temp. of deposition (°C)	Thermal expansion $\times 10^6\ °C^{-1}$	Tensile strength KSI	Modulus MSI	Oxidation resistance	Free carbon
TiC	3180	1400	7.6	200-300	25-35	Excellent	<4%
B_4C	2450	1300	5.0	300-400	25-35	Poor	<2%
TiB_2	2980	1000	7.9	200-300	20-30	Moderate	
B	2000	1000		400-500	30-50	Poor	

nucleation and simultaneous deposition of carbon and TiC. In the $CH_4/TiCl_4$ gas mixture, the TiC nucleation is never inhibited if an excess of $TiCl_4$ is used. Carbon core strength (fiber strength) decreases by coating. This decrease is due to the diffusion of carbon from the core substrate to the surface because of the inhibited deposition of carbon from the gaseous phase. Initial analysis showed that the best result for the deposition process can be obtained with a carbon to titanium ratio $\approx$3. Our fibers showed a tensile strength of approximately 200-300 KSI with a modulus of 35 MSI. Free carbon in the mixture is less than 5%. Results are tabulated in Table 5.

9 Chromium Diboride Fibers (CrB_2)

9.1 Introduction

Chromium diboride should be very effective in resolving or reducing severe mechanical and high temperature corrosion problems, especially in severe environments. Furthermore, its ductility, density, good physio- chemical compatibility with metals, high expansion, all make it one of the best candidates among the refractory materials for the metal-matrix composites in the space industry.

The CVD of chromium is well known and the structure-property-process relationship have been extensively studied. [Mazille, 1980; Wakefield, 1969; Hanni and

Hintermann, 1977] However, very few or no investigations have been made using a CrB_2 deposition either on a fiber substrate or any other shaped substrate. The most important aspect in CVD of CrB_2 is obtaining the chromium species in the gaseous phase at a relatively low temperature and with ease. Different precursors have been the subject of many chromium deposition studies in the past, but only few of them have met the above mentioned requirement. These previously investigated precursors are $CrCl_2$ [Hanni and Hintermann, 1977], Cr_2O_3 [Roos, 1959], $Cr(CO)_6$ [Owen and Webber, 1948], Organo-chromium compounds [Wakefield, 1969; Oxley, 1962] and chromium sulphides. Except for $Cr(CO)_6$ and the organo-chromium compounds, the rest of the above mentioned precursors have either a high melting and boiling point or handling difficulty. The carbon content of the lower melting compounds [$Cr(CO)_6$, (organo-chromium compounds)]' lead to the formation of carbides and oxides which are stable compounds at the temperature of deposition. Considering the availability, ease of handling and the high vapor pressure at relatively low temperature [M.pt -96.5°C, B.pt 116.7°C] of chromyl chloride [CrO_2Cl_2], it was decided upon as the chromium containing precursor in this study. Moreover, and as far as we know, no one has been specifically devoted to the in-depth CVD of CrB_2 using this precursor or any other precursor.

In the present work we have used a thermodynamic approach based on the minimization of the total Gibbs free energy of the system, to study the influence of the CVD parameters on the composition of the deposit obtained at equilibrium, from the $CrO_2Cl_2 + H_2 + BCl_3$ reactants system. The emphasis of this study was to obtain pure CrB_2 as a condensed phase. Several experiments were performed to study the morphology of the deposit.

Modelling the kinetics of any chemical process is extremely difficult. This is especially true for deposition processes. In these processes a large number of reactions take place simultaneously, being either gas phase or surface reactions. A classical way around this has been to identify the rate limiting reaction step and then modelling this step accurately. As the rate controlling step is dependent on both the reactant flowrate as well as the reaction temperature, this approach, although sufficient in most cases, cannot be extrapolated for use in scaled-up systems.

The modelling of CVD-kinetics with simultaneous reactions has been done[Coltrin et al., 1986]. Although encouraging results were obtained by this method, a parameter was always used to adjust the calculated deposition rates to the experimentally observed

rates. This is done by adjusting the apparent activation energy of the surface reactions. A detailed description of the flow profiles in the reactor is needed for the theoretical approach. As flow profiles tend to be three dimensional through a horizontal reactor, even with a symmetrical set up, this translates into a very complex problem. [Scholtz 1991]. Experimental work that had been carried out had used a Freundlich isotherm to describe the deposition reaction.

$$\theta = C * P^{\frac{1}{n}} \tag{3}$$

θ Surface coverage
C Rate constant
P Adsorbing gas Pressure
n Real ≥ 1.0

Results obtained from such a study resulted in the curve fitting of the experimental data to a predicted rate equation and did not describe the actual mechanism of deposition. The importance of the different precursors can be identified with such a kinetic expression, but any other detail of the reaction mechanism cannot be deduced from the fitted rate equation. It is important to note that the Freundlich isotherm can be used to approximate most compiled reaction mechanisms. Keeping all these factors in mind a different approach was decided upon to model the reaction kinetics.

9.2 Thermodynamic Analysis for CrB_2 from $CrO_2Cl_2 + H_2 + BCl_3$ CVD system

A thermodynamic approach has been used to study CVD of the CrO_2Cl_2- H_2- BCl_3 system. But, in principle, this may not necessarily give information on the CVD-mechanism or on the deposition characteristics. It can however be used to get a broad overview of the system, assuming that states close to equilibrium are reached in the vicinity of the substrate. In general these conditions may not be reached in each and every case.

The thermodynamic approach which is used here and its application to CVD is based on the minimization of the total Gibbs free energy of the system as described elsewhere. [Colmet et al, 1982; Christin et al, 1979; Zhao et al, 1990]. This method gives the solid, liquid and vapor phase composition at equilibrium for a known initial composition, temperature and pressure. Here one should assume that the deposit is in

equilibrium with different phases and that all the chemical species able to be present are known.

The CVD of CrB_2 from a CrO_2Cl_2 - H_2 - BCl_3 mixture is based on the reduction of CrO_2Cl_2 and BCl_3 by H_2 at the reaction temperature. The actual reaction mechanism may be very complex whose result strongly depends on the deposition parameters.

In the present investigation 53 different possible chemical species were considered: eight in condensed phase (CrB, CrB_2, $CrCl_2$, $CrCl_3$, Cr_2O_3, Cr) six in the liquid phase and the rest of them in vapor phase. The values of their thermodynamic properties (G^o_T- H^o_{298}) were taken from the JANAF table [1970] and Handbook of Thermophysical properties [Barin et al, 1977]. The concentration of all the species formed at equilibrium were investigated as a function of temperature (800 K $\leq$ T $\leq$ 1500 K), total pressure (0.5 atm. $\leq$ P $\leq$ 2.0 atm.) and initial composition of the vapor phase defined by the α= H_2/CrO_2Cl_2 ($1 \leq \alpha \leq 200$) and $\beta = BCl_3/CrO_2Cl_2$ ($1 \leq \beta \leq 10$) ratios.

At a given pressure (1 atm), the nature of the chemical species depends on the temperature a well as the initial reactant concentration of the vapor phase. In order to identify an optimum operating region we varied the α ratio with temperature, keeping β constant at 5. The value for $\beta = 5$ is justified in our later observations. Figure 34 gives the product distribution at three different temperatures with α.

At high α values, the thermodynamic yield of CrB_2 remains constant irrespective of temperature. However, at low α values, CrB_2 increases with temperature before stabilizing. The rate of formation of CrB_2 is highest at low temperature and α values. One of the important condensed species which has an authoritative effect on the material property is free elemental boron. It is observed at high temperature (above 1300 K) for all values of α and increases with temperature.

A study in the variation of the product distribution with a variation in the BCl_3 initial concentration is very important as it will definitely give us some insight in the B to Cr ratio necessary to produce CrB_2. All calculations were carried out at α= 100. From figure 35 it can be seen that only CrB_2, CrB, B and $CrCl_2$ are thermodynamically stable condensed species.

It is interesting to observe the parabolic profile for CrB_2, which is passing through a maximum at a different level, with respect to temperature and the β ratio. Free elemental boron is prominent at a high β ratio and a high temperature. At lower temperature (T = 1100 K), it is present in negligible amount. Chromium dichloride is

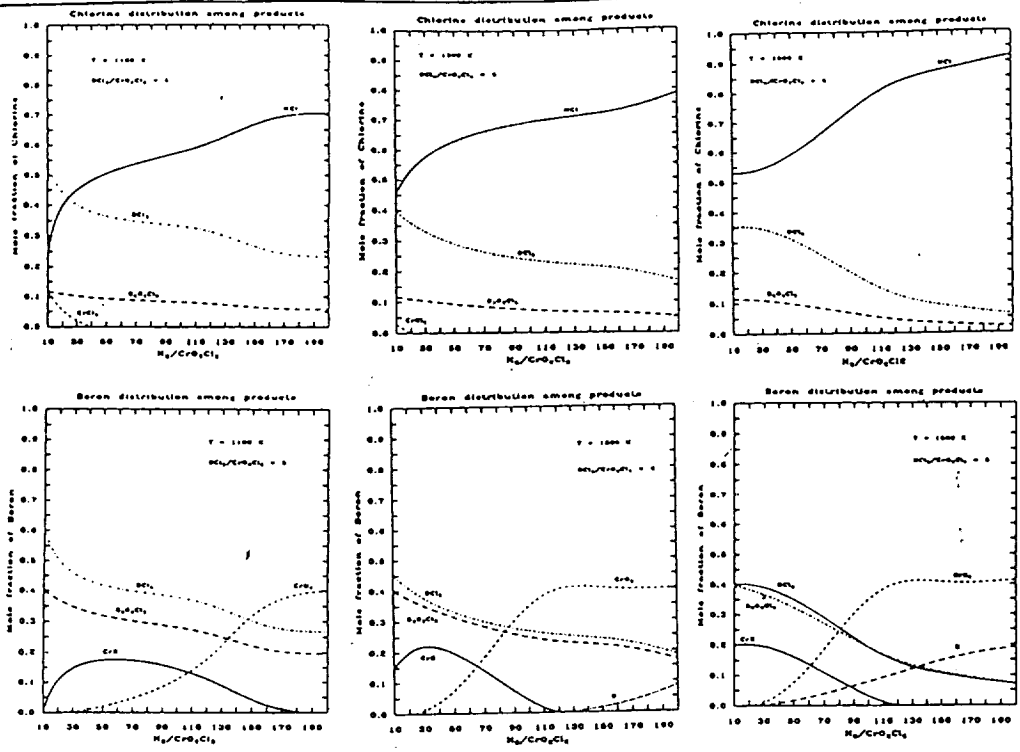

Figure 34: Product Distribution at Different temperature and α

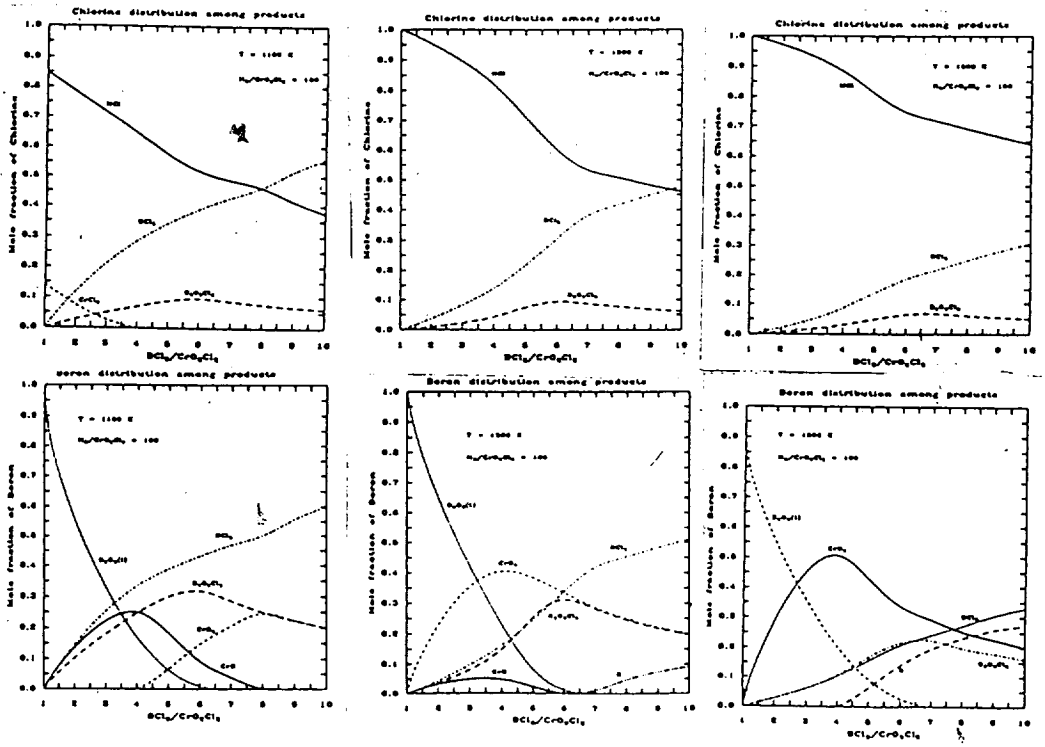

Figure 35: Product Distribution at Different BCl_3 Concentration

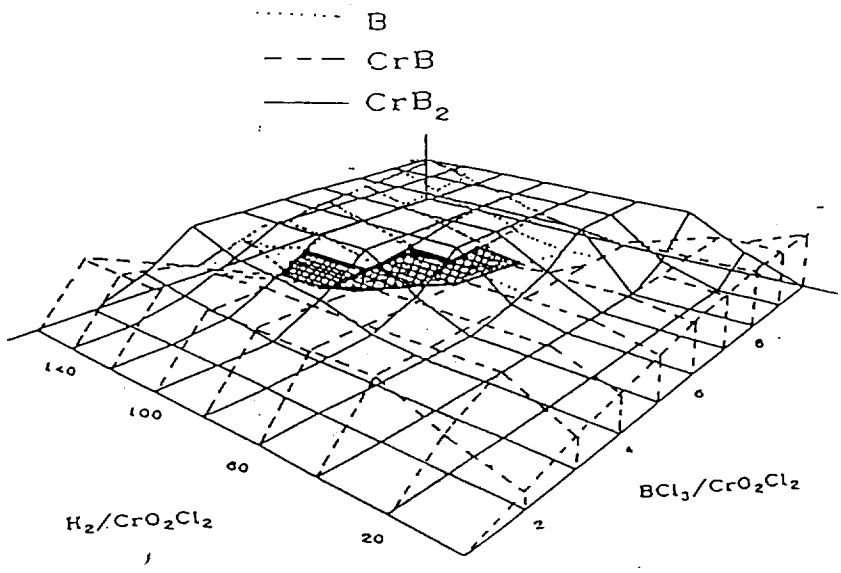

Figure 36: **Overall Product Distribution–A 3D Plot**

observed at low temperature ($\leq$ 1100 K) and low β ratios. This completely disappears at high values of β.

Keeping all this in mind one can conclude that the mechanism of deposition is very complex depending on temperature, α ratios as well as β ratios. At low temperature and low values of α and β, the chromium precursor goes through the $CrCl_2$ phase. This shows that initial mechanism of formation of chromium is possible from $Cr_2O_2Cl_2$ via $CrCl_2$ reduction. As the temperature increases and at high ratios of α this reduction is total. With an increase in operational values, the mechanism seems to change into a replacement reaction mechanism where BCl_3 reacts with chromyl chloride directly and the boron atom displaces the Cr atom from the chromyl chloride molecule. This leads to the formation of mostly of B_2O_3 and $B_3O_3Cl_3$ at high values of β with no CrO_3 formation. From the overall view one can suggest that the majority of the CrB_2 is formed due to a reduction reaction. This leads us to have the following values for our experimental operation: α should be $90 \leq \alpha \leq 110$, β should be $4.5 \leq \beta \leq 6.5$ and the temperature should be between 1100 and 1500 K to get a maximum amount of CrB_2 without any impurities. To get an overall pictorial view, a three dimensional plot was drawn [figure 36].

The effect of pressure on our product distribution was studied by varying the pressure and the α ratio, while keeping both the β ratio and temperature constant at 5 and 1300 K respectively [Figure 37]. Three different pressures (0.5 atm., 1.0 atm. and 2.0 atm) were used and their product distributions were compared with each other. A

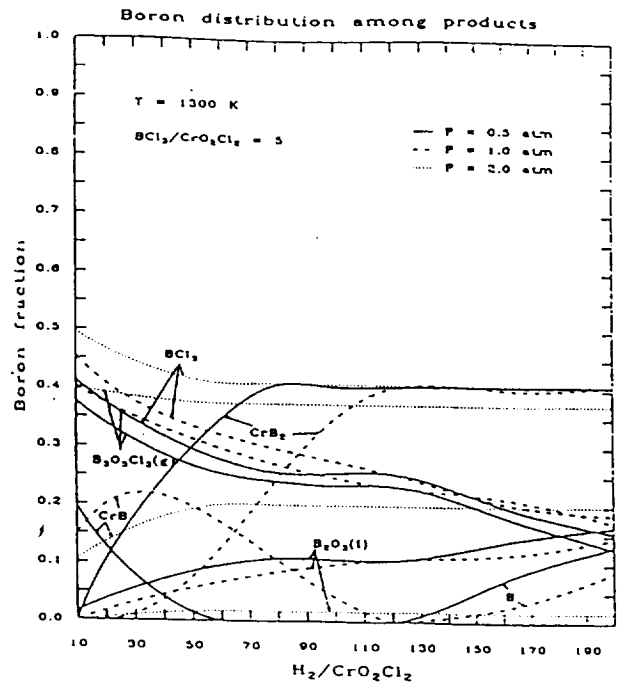

Figure 37: **Effect of Pressure on Product Distribution**

lower pressure increased the formation of all the condensed phases. (CrB, CrB_2, B, B_2O_3(l)) This resulted in the formation of CrB_2 at a lower temperature as well as at α lower a ratio. Unfortunately the formation of B also increased making lower operating pressures not more attractive. Although the CrB_2 formed at lower temperature and α ratio, the ultimate conversion of boron into CrB_2 stayed the same irrespective of pressure.

9.2.1 Results and Discussion

By looking at the phase diagram of chromium and boron, it is apparent that in order to get CrB_2 as the most stable condensed phase we should keep the boron to chromium ratio greater than two. [figure 38].

We divided the borides broadly into two categories, lower borides (CrB) and higher borides (CrB_2). From the experimental results we can however detect many multiple borides such as CrB_4, Cr_2B, Cr_5B_3, etc. by X-ray diffraction spectrograph. How critical these multiple borides are in application to composites is yet to be seen. The typical analysis of the results are discussed below.

The experiments were first carried out at thermodynamical optimum conditions

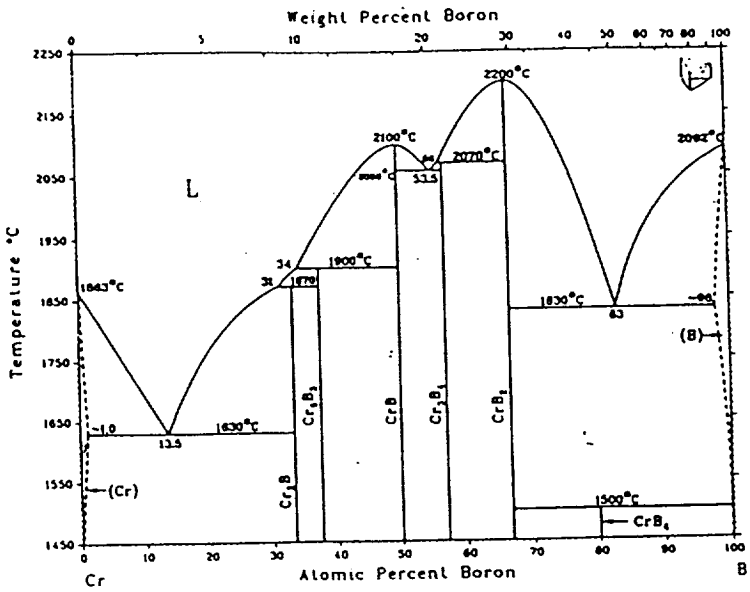

Figure 38: Phase Diagram of Cr-B System

to get exclusively higher borides as the condensed phase. As far as possible we tried to avoid getting free boron in the deposit. The conditions that were used here were α= 110 and β= 5. Since microcrystallinity is also an important parameter for obtaining a better quality fiber, we investigated the deposit structure also with respect to the substrate temperature. Figure 39 gives the SEM photographs at α = 110, β= 5 and various temperatures. At a temperature of 1230 K the deposit is more amorphous and loosely bound to the fiber.

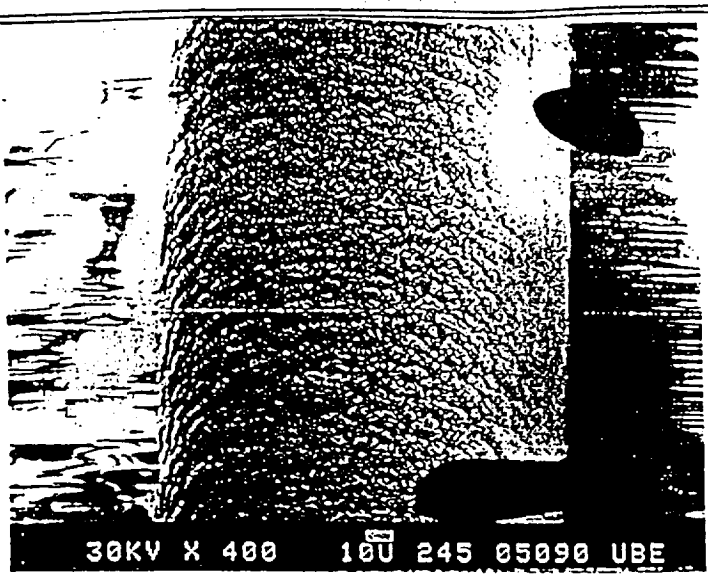

1240°K $\alpha = 110$ $\beta = 5$

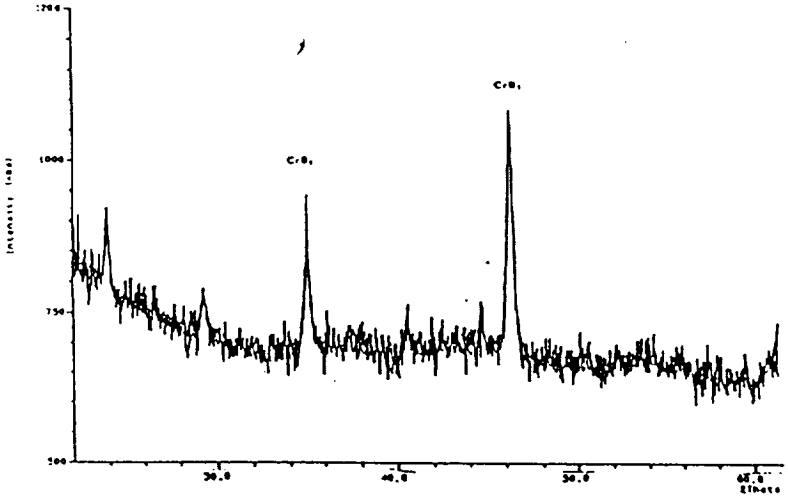

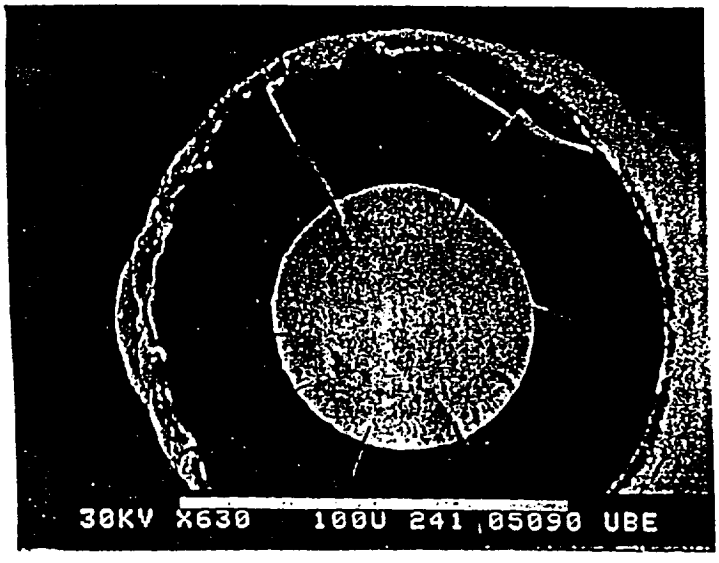

1273°K $\alpha = 110$ $\beta = 5$

Figure 39: SEM Photograph at Different Temperature

$\beta = 5$
$\alpha = 110$
1400K

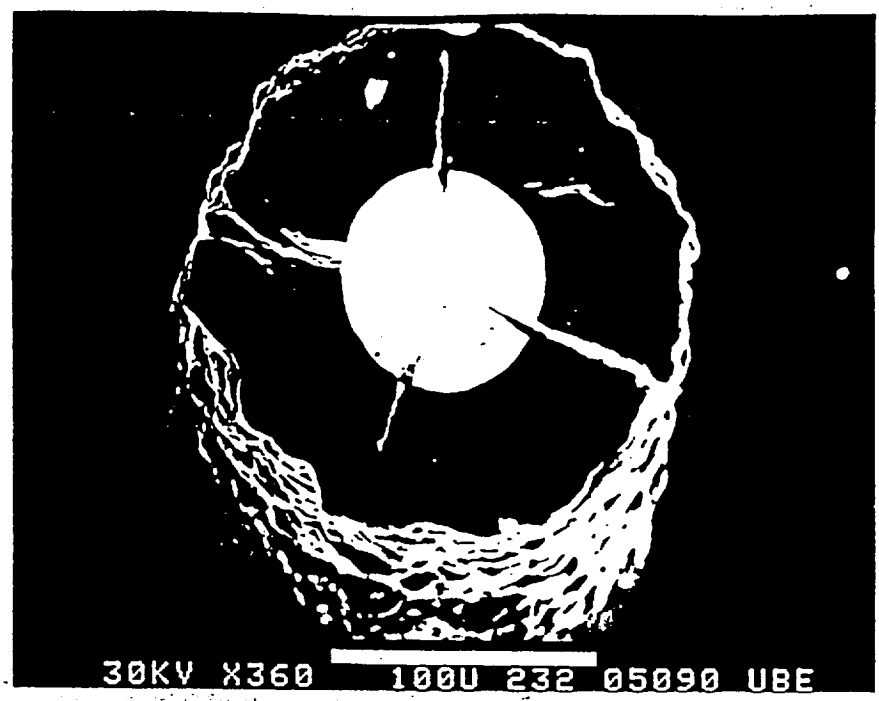

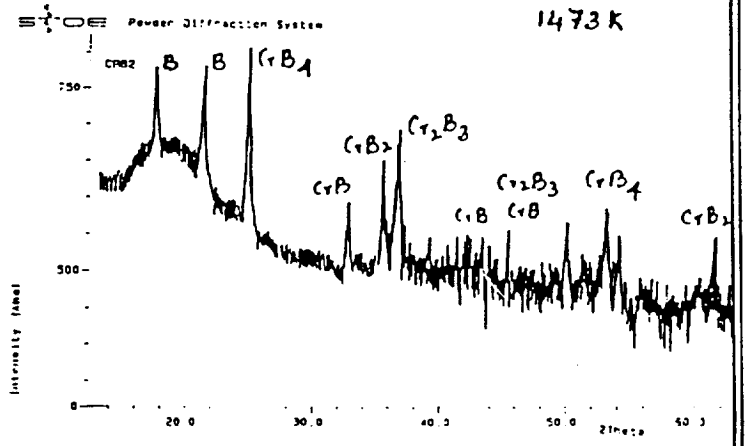

1473°K
$\alpha = 110$
$\beta = 5$

SEM photographs at $\alpha=110, \beta=5$ with X-ray result

With a slight increase in the substrate temperature, the deposit became very smooth and microcrystalline which is the desirable quality for a good quality fiber. This was observed around 1273 K. A further increase in the temperature leads to an increase in crystal size and irregular deposit. One can see the irregularity right from the initial point of deposition. This may be due to the impurity effect which can act as a "catalyst" leading to a non homogeneous growth. Again at high temperature, the mass transfer effect should play an important role as the reaction rate is no longer the controlling deposition parameter. Whatever the reason may be, the fiber quality was very poor. Several runs were taken varying the α and β ratios with temperature and observing their effect on the microstructure a well as the composition of the deposit. It is observed that a higher β ratio results in the incorporation of more free boron in the deposit and a lower α as well as β ratio suppresses the formation of free elemental boron but results in the formation of multiple borides ranging from CrB, CrB_4, CrB_2 to Cr_5B_3. At high temperatures (1553 K) a small amount of Cr_3O_4 was also observed in all the cases which contradicts our thermodynamic predictions.

Experiments were also carried out to see how the precursors $CrCl_3$ and $Cr(CO)_6$ behaved with respect to chromyl chloride. The difficulty of obtaining chromium trichloride in the gas phase, condensation in the feeding lines and uneven deposit limited its analysis. The chromyl hexacarbonyl deposition results at 1350 K are shown in figure 40. This shows an uneven deposit which can be explained because of the large number of impurities in the deposit. From the x-ray diffraction pattern it was observed that mainly B_25C, CrO_2, Cr_23C_6, Cr and a small amount of CrB_2 was found in the deposit.

Finally a strong penetration of deposit into the tungsten substrate was observed. The quality of the fiber is reduced as the core is weakened by the infiltration reaction. To counter this problem some fibers with intermediate carbon layers were deposited. From the results it seems that this gave both an improvement in the quality and appearance of the fiber. This can be seen in figure 41. The fibers from these runs showed the tensile strength up to 167 KSI. The strength analysis was carried out by NASA scientist.

9.3 Kinetic Study of the CrB_2 Deposition Reaction

As a first step in the prediction of a kinetic mechanism for the deposition reaction, a set of elementary reactions were predicted. This system of reactions was derived from

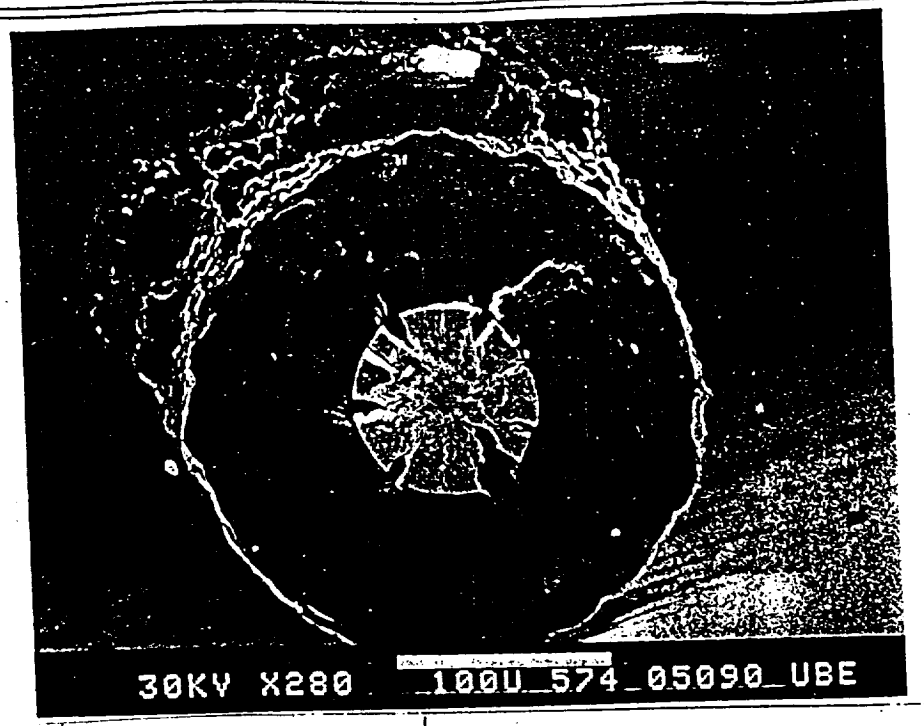

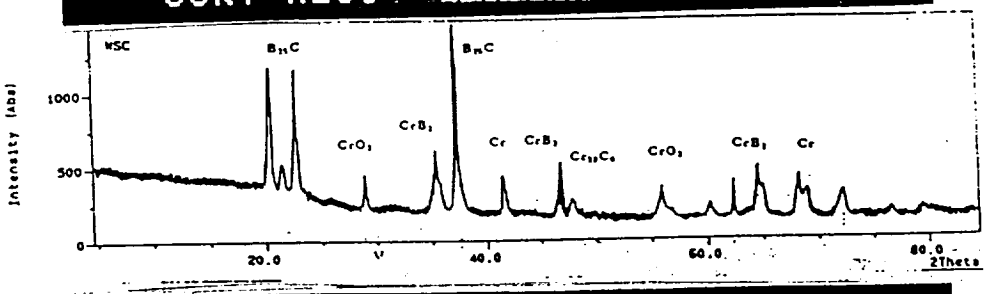

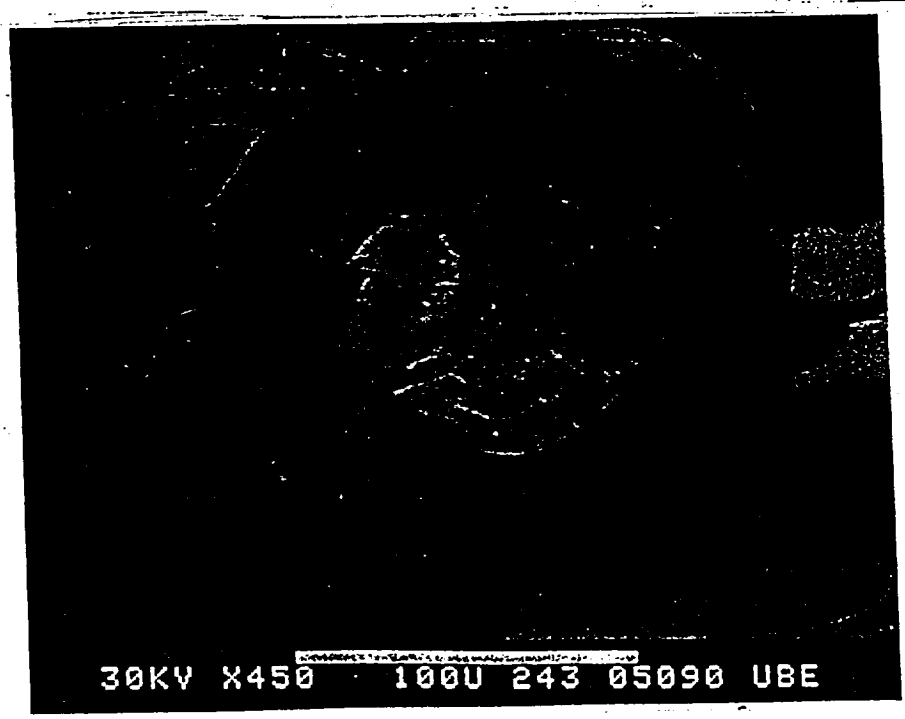

Figure 40: Deposition with Chromium Hexacarbonyl,An Electron Micrograph

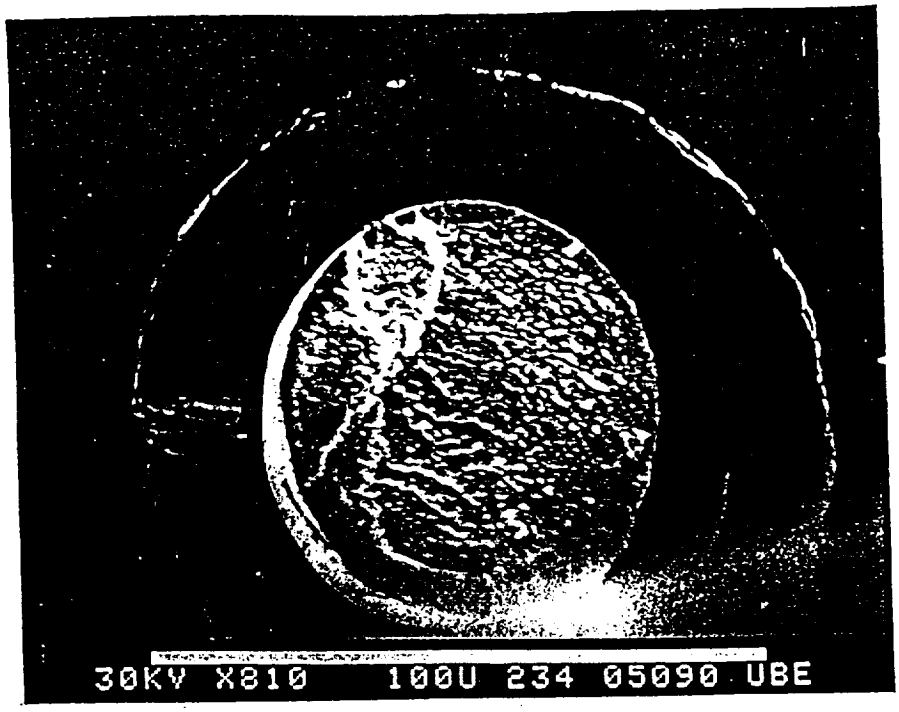

1273°K $\alpha = 110$ $\beta = 5$ Carbon layer 5 μm

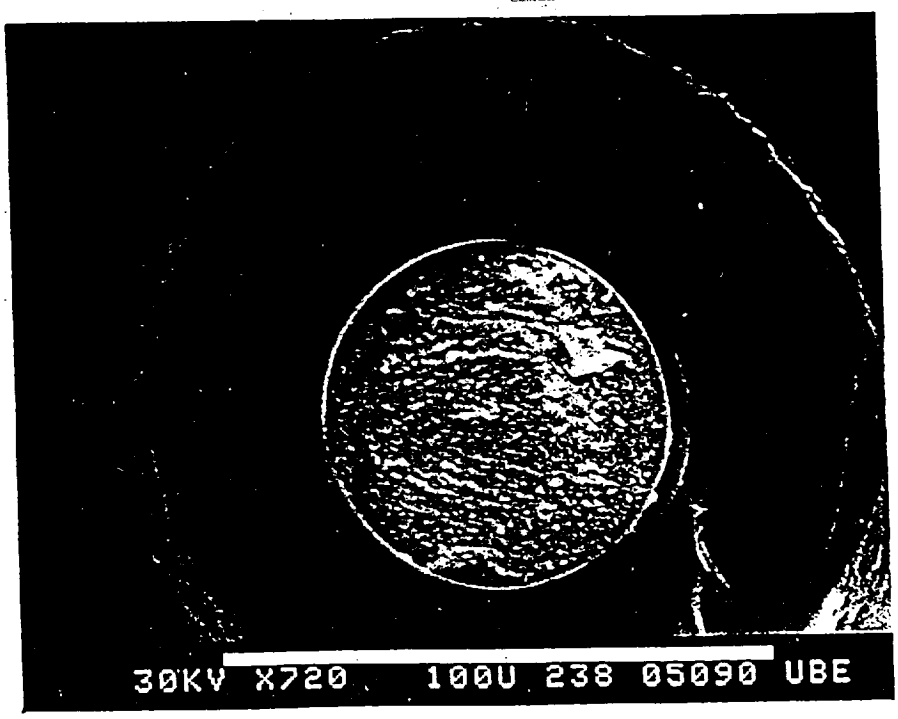

Figure 41: Fiber with Intermediate layer of Carbon

the previously found thermodynamically most stable species and taking into account the bi-molecular bond energies between the different atoms.

$$H_2 \rightleftharpoons 2H \quad (4)$$

$$BCl_3 + H \rightleftharpoons BCl_2 + HCl \quad (5)$$

$$BCl_2 + H \rightleftharpoons BCl + HCl \quad (6)$$

$$BCl + H \rightleftharpoons B + HCl \quad (7)$$

$$CrO_2Cl_2 + BCl \rightleftharpoons BOCl + CrOCl_2 \quad (8)$$

$$CrOCl_2 + BCl \rightleftharpoons CrCl_2 + BOCl \quad (9)$$

$$3BOCl \rightleftharpoons B_2O_3Cl_3 \quad (10)$$

$$CrCl_2 + H \rightleftharpoons CrCl + HCl \quad (11)$$

$$CrCl + H + BCl \rightleftharpoons CrBCl + HCl \quad (12)$$

$$CrBCl + H + BCl \rightleftharpoons CrB_2 + HCl \quad (13)$$

Three different reaction models were proposed and their agreement with experimental results is tested.

It is well known that the deposition reaction is a combination of both gas and surface reactions. The aim of this study was to identify the stage at which adsorption onto the surface, to form the deposit, occurs. It was observed thermodynamically that the chromium containing precursor CrO_2Cl_2, in the presence of both H_2 and BCl_3, is reduced to the previously identified compound $CrCl_2$ at elevated temperatures. It was found that 250°C was achieved in the preheater which was enough to complete the reduction reaction described above. It was thus decided to use the chromium intermediate $CrCl_2$, generated in the preheater, as the starting chromium compound in the modelling of the deposition reaction.

9.3.1 Results and Discussion

All the experiments were done in the kinetically controlled regime. The first approach to test the model was by assuming a pure gas phase reaction and resultant CrB_2 solid deposit (adsorbs) on to the substrate. Taking all the gas reactions at equilibrium, a

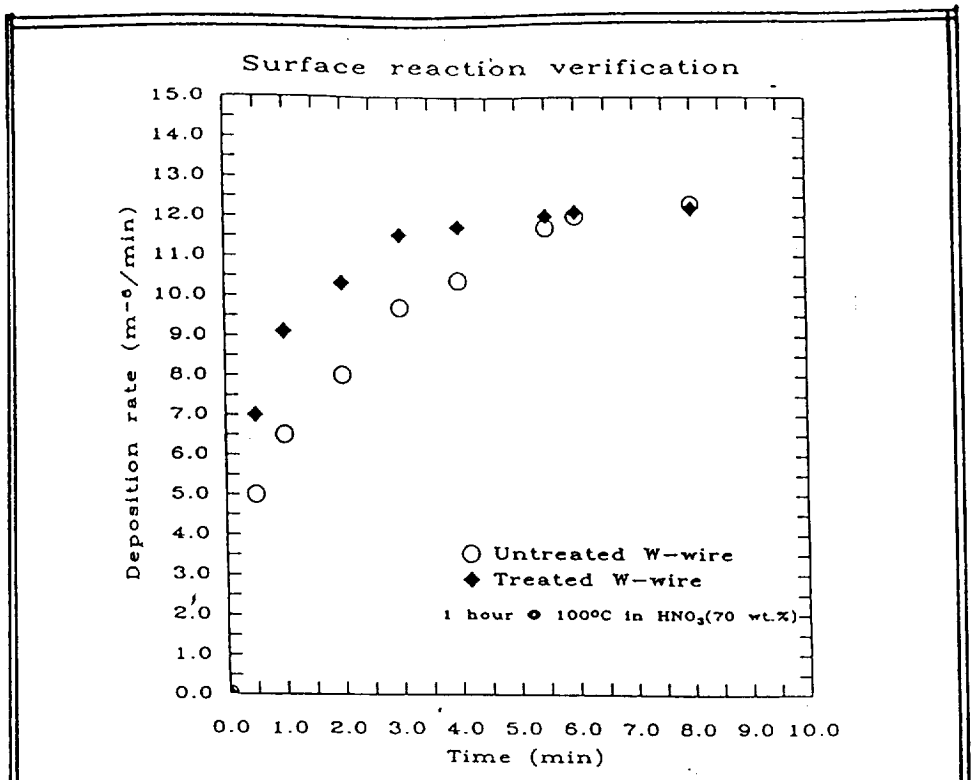

Figure 42: **Effect of Surface Area on Deposition**

simplified model was derived. The rate equation is written as

$$Rate = \frac{K P_{CrCl_2} P_{BCl_3}^4 P_{H_2}^7}{P_{B_2O_3}^2 P_{HCl}^{14}} \tag{14}$$

It is apparent that both the exit and entrance gases should be monitored to investigate this model. However, our measured rate showed a very strong surface reaction dependence. Figure 42 shows the change in surface area of the substrate effect on the deposition rate. From the graph, it is evident that initial deposition is depend on surface area of the substrate. After certain time, both treated and untreated samples (having surface area 0.09 m^2/gm, 0.05 m^2/gm resp) showed the same rate. Hence our first model was not valid.

The two different adsorption model were assumed to test our results: 2nd model, adsorption of the $CrCl_2$ onto the substrate was assumed with subsequent reduction by BCl_3 and H_2. Adopting the Langmuir isotherm, the rate equation is expressed as

$$Rate = \frac{k_1 K_1 P_{CrCl_2} P_{BCl_3}^2 P_{H_2}^4}{1 + K_1 P_{CrCl_2}} \tag{15}$$

Final model (3rd) assumes that both BCl_3 and $CrCl_2$ adsorbs on the surface and reduced in the presence of H_2 to deposit CrB_2. This can be schematically represented

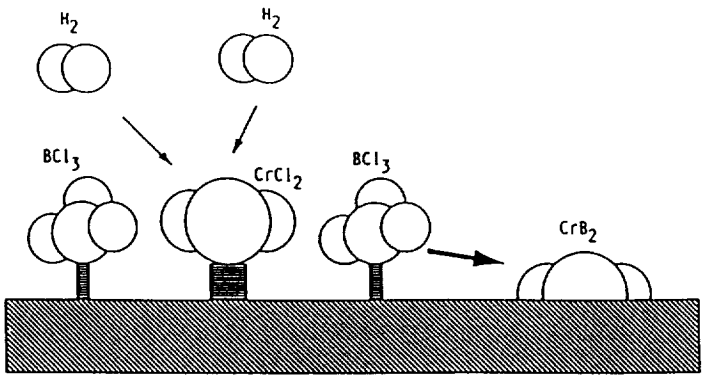

Figure 43: **Schematic Representing the Model**

in the sketch (figure 43). The elementary reactions are:

$$CrCl_2 + S^* \rightleftharpoons CrCl^* \tag{16}$$

$$BCl_3 + S^* \rightleftharpoons BCl_3^* \tag{17}$$

$$2BCl_3^* + 4H_2 + CrCl_2^* \rightleftharpoons CrB_2^* + 8HCl \tag{18}$$

$$CrB_2^* \rightleftharpoons CrB_2 + S^* \tag{19}$$

By assuming Langmuir isotherm, and both BCl_3 and $CrCl_2$ adsorbed species were equally mobile on the substrate, the rate expression is given as

$$Rate = \frac{k_1 K_1 K_2^2 P_{CrCl_2} P_{BCl_3}^2 P_{H_2}^4}{(1 + K_1 P_{CrCl_2} + K_2 P_{BCl_3})^3} \tag{20}$$

Fitting the experimental data to the proposed models created some problems. A non-linear least squares fit is used to find the constants that best approximated the experimental results. The following results were obtained. For the second proposed model (Single adsorption of the $CrCl_2$ onto the substrate), no good fit for the experimental results could be found. Fitting the experimental results to the third proposed model gave much better match. The maximum deviation between the experimental and proposed model was 8%. The agreement between the experiments and the proposed model was plotted on a 3-D graph, to show the variation between the experimentally found deposition rates and the calculated deposition rate. [Figure 44].

A higher resolution plane was generated in the three-Dimensional domain so that the variation of the deposition rate with a variation of the model variables could be

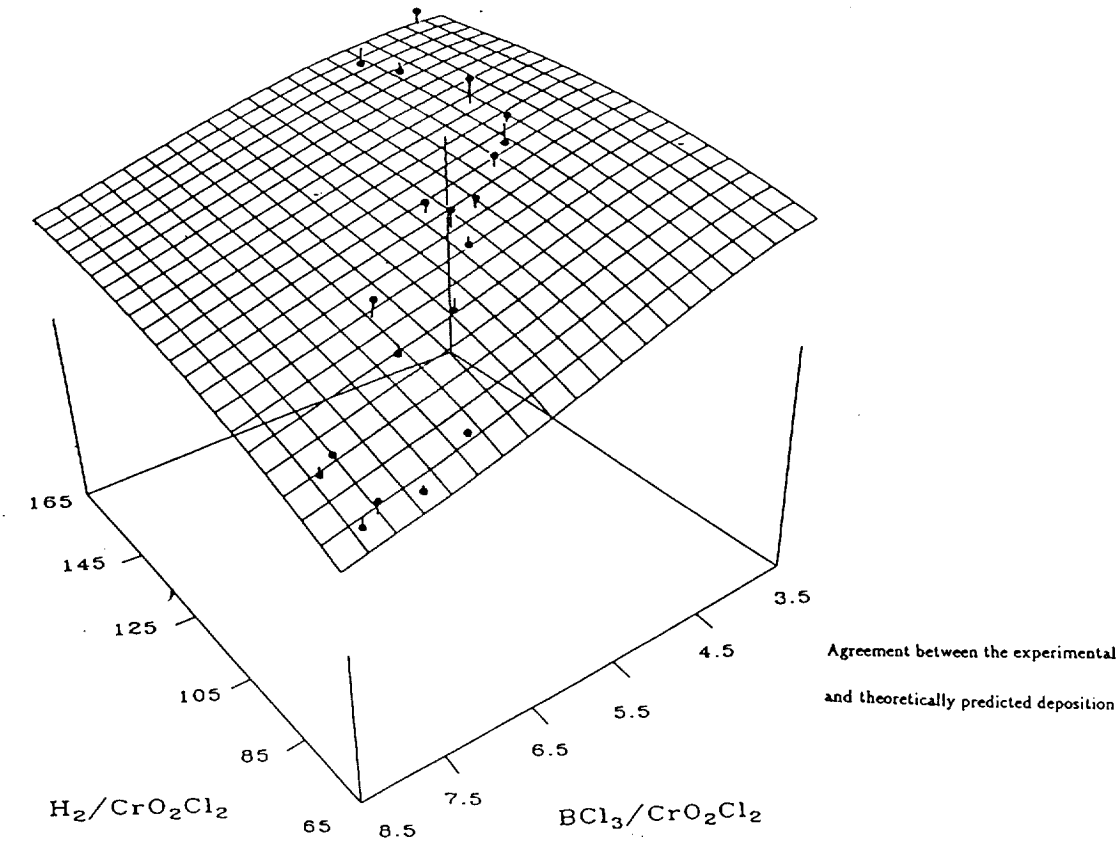

Figure 44: Evaluation of the Model with 3D Plot

observed. At the same time the best fit for the second proposed model was also plotted and the difference in the generated graphs is apparent.

To get a feeling of how good the agreement between the experimental and model results, a comparison between the obtained rates were drawn.

Although the agreement is not excellent, this definitely shows that an adsorption model in which both the BCl_3 and the $CrCl_2$ species adsorb on the surface describes the actual mechanism of the deposition reaction. Using a more refined model, where the surface reaction occurs in a few steps with the slowest step determining the deposition rate, should give better agreement between the experimental and theoretical models. A much improved experimental set-up would be needed to be able to do a more detailed kinetic study.

9.3.2 Implications of the Calculated Rate Constants

Agreement between the experimental and the predicted dubbel adsorption model was quite good and the largest error was of the order 8%. The rate constants were de-

termined by using a least squares fit for the non-linear rate equation. The reaction coefficients were found to be the following values.

k_1 = 113.0 (μm. min^{-1} .atm^{-4})

K_1 = 8.0*10^6

K_2 = 4.0*10^6

These values were found to best represent the experimental results and their relative values were found from the least squares fit used to approximate the non-linear predicted deposition rate. Evaluating the order of magnitude of the constants, might give insight into adsorption efficiency as well as the reaction mechanism characteristics.

10 CONCLUSIONS

The CVD technique was successfully employed to synthesize TiB_2, CrB_2, B, TiC and B_4C fibers on tungsten and carbon substrate. These fibers showed good physical and mechanical properties for the possible use in metal-matrix composite. The main process variables are temperature, compositions of the reactants and total flow rate. The thermodynamic studies on TiB_2 and CrB_2, were used to predict a window for pure product. The rate of deposition of TiB_2 was expressed as:

$$k = 4900e^{\frac{-40700}{RT}} C_{BCl_3}^{0.8} C_{TiCl_4}^{0.2} \tag{21}$$

whereas CrB_2 deposition rate was best expressed by using an adsorption model assuming both the reactant species ($CrCl_2$ and BCl_3) adsorb on to the surface and get reduced with hydrogen to produce CrB_2 .

morphological studies on TiB_2 and CrB_2, showed the optimum deposition condition. The metallographic and X-ray diffraction studies on TiB_2 gave the TiB_2 crystal orientation parallel to the C-axis. The stress distribution due to thermal expression mismatch was studied on TiB_2 deposit and is partially neutralized by using intermediate spongy coating of carbon. The similar experimentation on CrB_2 also produced better results. The tensile strength with TiB_2 reached up to 220 KSI where as with CrB_2 is 167KSI. Exploratory work with TiC, B_4C and B fibers produced the strength result that are comparable to the reported values in the literature. Fibers showed good potential for the use in metal-matrix composite.

11 OVERALL SUCCESS OF THE PROJECT

So far we have successfully developed the CVD process for synthesis of TiB_2, TiC, B_4C, CrB_2 and B fibers and the regimes of deposition, quality of synthesized fibers and qualitative characteristics of the process has been pin pointed. The TiB_2 fibers showed extremely good strength and continuous process fibers (several meters) has been sent to NASA for testing and analysis. With proper encouragement, the process is ready to work continuously. The TiC, B_4C, B fibers matched the properties of the best known reported values. Our exploratory work on CrB_2 gave unexpectedly excellent results. Recent results from NASA showed for non-primary carbon coated fiber, as high as 170 KSI. This process needs more work to go for full scale pilot plant. Overall, this project is fairly successful in developing the fibers with a potential for larger scale production.

12 REFERENCES

Allen, S.D., "Laser chemical vapor deposition: A technical for selective area deposition," J. App. Phys., 52, 6501, 1981.

Anon, Integrated Research on Carbon Composite Mater., Part 1, Tech. Rpt., AFML-TR-66-310-Pt.1, Oct. 1966.

Arya, P.V., "Synthesis of Ceramic Fibers by CVD," M.S. Thesis, SUNY at Buffalo, 1988.

Barin, I., Knacke, O., Kubashewski, O., "Thermochemical Properties of Inorganic Substances," Springer-Verlag, New York, 1977.

Behrendt, D., "Residual Stresses in Boron/Tungsten and Boron/Carbon Fibers," NASA TM X-73616, 1977.

Behrendt, D., "Calculation of Residual Principal Stresses in CVD Boron on Carbon Filaments," NASA TM 81456, 1980.

Behrendt, D., "Longitudinal Residual Stresses in Boron Fibers," Special Tech. Pub., 617, ASTM, 215, 1977.

Besmann, T.M., Spear, K.E., "Analysis of the chemical vapor deposition of Titanium diboride- II. Modelling the kinetics of deposition," J. Electrochem. Soc., 124, No. 5, 790, 1977.

Besmann, T.M., Spear, K.E., "Morphology of CVD TiB ," J. Cryst. Growth, 31, 60, 1975.

Besmann, T.M., Spear, K.E., "Analysis of the chemical vapor deposition of titanium diboride- I. Equilibrium thermodynamic analysis," J. Electrochem. Soc., 124, No. 5, 786, 1977.

Biswas, D.R., "Deposition process for films and coatings," J. Mater. Sci. 21 (7), 2217, 1986.

Biswas, D.R., Ghosh, C., Layman, R., "Vapor phase deposition of aluminum films on quartz substrate," J. Electrochem. Soc., 130, 234, 1983.

Blocher, J. M., Browning, M. F.,and Barret, D. M.,"Chemical Vapor Deposition of Ceramic Materials", Mater. Sci. Res., 17, 299, 1984.

Bouix, J., Vincent, H., Boubehia, M., Viala, J.C., "Titanium diboride- coated Boron fiber for Aluminium matrix composites," J. Less Common Met., 83, 117, 1986.

Brennan, J.J.,and Prewo, K. M.,"Silicon Carbide Fiber Reinforced Glass-Ceramic Matrix Composites Exibiting High Strength and Toughness", J. Mat. Sci.,17, 2371, 1982.

Bryant, W.A., Meier, G.H., "Factors affecting the adherence of chemically vapor deposited coatings," J. Vac. Sci. Technol., 11, No. 4, 719, 1974.

Brugger, K., "Effect of Thermal Stresses on Refractive Index in Clay Fibers," Appl. Opt., 10, 437, 1971.

Bunsell, A.R., "Fiber Reinforcements for Composite Materials," Composite Materials Series, Vol. 2, Elsevier, Amsterdam, 1988.

Bunshah, R.F., Nimmagadda, R., Dunford, W., Movchan, B.A., Demchishin, A.V., Chursanov, N.A., "Structure and properties of refractory compounds deposited by electron beam evaporation," Thin Solid Films, 54, 85, 1978.

Campbell, I.E., High-Temperature Technology, John Wiley and Sons, Inc., N.Y., 105, 1956.

Campbell, I.E., Powell,, D.H., Nowicki, D.H., and Gonser, B.W.,"The Vapor Phase Depósition of Refractory Materials. I.General Conditions and Apparatus, Deposition of Refractory Materials.,96, 318, 1949.

Caputo, A.J., Lackey, W.J., Wright, I.G., Angelini, P., "Chemical vapor deposition of erosion-resistant TiB coatings," J. Electrochem. Soc., 132, No. 9, 2274, 1985.

Chamberlin, R.R., Skarman, J.S., "Chemical spray deposition process for inorganic films," J. Electrochem. Soc., 113, 86, 1966.

Chernyshova, T.A., Tsirlin, A.M., Gerlich, S.O., Rebrov, A.V., Obolenshii, A.V., Poroshk. Met., No. 3 (267), 39, 1985.

Ceramic Source, Vol. 5, pub. Amer. Cer. Soc., NY, 1990.

Christin, F., Naslain, R., Bernard, C., "A Thermodynamic and Experimental Approach of Silicon Carbide CVD. Application to the CVD- Infiltration of Porous Carbon Composites," Proc. 7th Int. Conf. CVD., 499, 1979.

Colmet, R.; Naslain, R. and Hagenmuller, P., "Thermodynamic and experimental analysis of CVD of alumina from $AlCl_3$-H_2-CO_2 gas phase Mixture, J.Electrochem.Soc., 129, 1367,1982.

Coltrin, M.E., Kee, R.J., Miller, J.A., "A Mathematical Model of Silicon Chemical Vapor Deposition," J. Electrochem. Soc., 133(6), p. 1206-1213 ,1986.

Cullity, B.D., Elements of X-ray Diffraction, Addison-Wesley Pub. Co., 303, 1978.

Dan'kin, A.A., Svetlopolyanskaya, T.P., Oreshkin, V.D., Svetlopolyanskii, V.I., "Abrasive wear resistance and character of rupture of the surface layers of Titanium and Zirconium diboride," Poroshk. Met., No. 7 (139), 88, 1974.

DeBolt, H., Krukonis, V., McKee, J., Prescott, R., Wawner, F., "Development and Demonstration of Low Cost Boron Filament Formation Process," AFML-TR-72-271, May 1972.

DiCarlo, J.A., "Fibers for structurally reliable metal and ceramic composites," J. Met., 46, 6, 1985.

Edie, D.D.,"Textile Structure and Their Use in Composite Materials", Int. Fiber. J., 2(2), 6, 1987.

Edie, D. D.,and Dunham, M. G.,"Advanced Engineering Fibers", Chem. Eng. Edu., 21, 186, 1987.

Feldman, C., Satkiewicz, F.G., Jones, G., "Preparation and electrical properties of stoichiometric TiB Thin Films," J. Less Common Met., 22l, 79 (2), 198l.

Frost, A.A., Pearson, R.G., "Kinetics and Mechanism," 2nd ed., Wiley and Sons Inc., New York.

Galasso, F.S., High Modulus, Gordon and Breach Science Publishers, N.Y., 1969.

Gardner, W. B.,"Microbending Loss in Optical Fibers",Bell. Syst. Tech. J., 54, 457, 1975.

Gloge, D.,"Optical Fiber Packing and Its Influence on Fiber Straightness and Loss", Bell. Syst. Tech. J., 54, 245, 1975.

Gannon, R.E., Folweiler, R.C., Vasilos, T., "Pyrolytic synthesis of titanium diboride," J. Am. Ceram. Soc., 46, 496, 1963.

Gebhardt, J.J., Cree, R.F., "Vapor-deposited borides of group IV A metals," J. Am. Ceram. Soc., 48, 262, 1965.

Gordon, S., McBride, B.J., "Computer program for calculation of complex chemical equilibrium compounds, rocket performance, incident and reflected shocks and Chapman-Jouget detonations," NASA SP - 273, 1971.

Ed. Graham, A.K., Electroplating Engineering Handbook, 3rd ed., 56, Van Nostrand Reinhold, N.Y., 1971.

Guinn,K., and Middleman, S.,"continuous Filament Coating by Chemical Vapor deposition", J. Cryst. Growth, 96, 589, 1989.

Hanni, W.; Hintermann, H.E.; "Chemical vapor deposition of chromium," Thin Solid Films, 40, 107, 1977.

Hess, D.W., Jensen, K.F., Anderson, T.J., Reviews in Chemical Engineering, ed., Amundson, N.R., Dan Luss, Vol. 3, No. 2, 97, 1985.

Hoekstra, H.R., Katz, J.J., "The preparation and properties of group IV-B metal borohydrides," J. Am. Chem. Soc., 71, 2488, 1949.

Hough, R.L., "Pyrolytic Titanium diboride filaments for composites," AIAA J., 4(1), 107, 1966.

Irving, R.J., Worsley, I.G., "The Oxidation of Titanium Diboride and Zirconium Diboride at High Temperatures," J. Less Common Met., 16, 103, 1968.

Iwasa, M., Ide, M., Watanabe, S., and Tanji, H.,"Properties and Cycle-Life of Pyrolytic BN-Crucibles", Proc. 10^th Int. Conf. CVD, Eds. Cullen, G. W. and Blocher, J. M. Jr., 1106, 1987.

Jain, L.K., Wetherhold, R.C., "Viscoelastic Analysis of Concentric Cylinders for Composite Materials and Seals," J. Am. Ceram. Soc., 72(10), 1844, 1989.

Janaf Thermochemical Tables, J. Phys. Chem. Ref. Data., 14, 1983.

Janaf, "Thermochemical Tables," 2nd edn., D.R. Stull; H. Prophet et al., NSRS-NBS, 1970.

Johnson, S. M., Brittain, R. D., and Lamoreaux, R. H.,"Degradation of SiC Fibers", J. Electrochem. Soc., 134, 470, 1987.

Kaufman, L., Clougherty, E.V., "Boride compounds for high temperature application," Plansee Proc. 5th Sem., 772, 1964.

Keihn, F.G., Keplin, E.J., "High-Temperature Thermal Expansion of Certain Group IV and Group V Diborides," J. Am. Ceram. Soc., 50, No. 2, 81, 1967.

Keller, R., Jarrett, N., "New materials new approaches in Aluminium electrolysis," New Mater. New Processes, 2, 452, 1983.

Kirk, J.A., Flinn, D.R., Lynch, M.J., "Wear of TiB Coatings," Wear, 72, 315, 1981.

Lennon, J.W., "Status of polycrystalline ceramic fibers," Symp. on Fibrous Composite Eng. Mater., Madison, Wisconsin, Oct. 7-8, 1965.

Mamet'ev, R. Yu., Pavlov, S.M., Sharpin, D.N., Yurkinskaya, L.V., "Static regularities of titanium diboride deposition from gaseous phase," Poroshk. Met., No. 3, (135), 1974.

Matsera, V.E., "Heat resistant fibers and their use in the manufacture of composite materials," Poroshk. Met., No. 11 (83), 45, 1969.

Mazille, H.; "Chemical vapor deposition of chromium onto Nickel," Thin Solid Films, 65, 67, 1980.

Mersol, S.A., Lynch., C.T., Vahldiek, F.W., "Defect Structure of Single-Crystal Titanium Diboride," Anisotropy in Single Crystal Refractory Compounds, Plenum Press, 41, N.Y. 1968.

Miller, G.H., "Method of making continuous length super conducting wires using chemical vapor deposition," IEEE Transactions on Magnetics, Mag. 17, No. 1, Jan. 1981.

Misra, A.K., "Thermodynamic analysis of compatibility of several reinforcement materials with beta phase NiAl alloys," NASA CR - 4171, 1988.

Misra, A.K., "Thermodynamic analysis of compatibility of several reinforcement materials with beta phase FeAl alloys," NASA CR - 4172, 1988.

Moers, K., "Die Reindarstellung hochschmelzender Carbide, Nitride and Boride nach den," Z. anorg. u. allegm. Chem., 198, 243, 1931.

Monney, J.B., Radding, S.B., "Spray pyrolysis processing," Ann. Rev. Mater. Sci., 12, 81, 1982.

Motojima, S., Kosaki, H., "Resistivities against sea-water corrosion and sea-sands abrasion of TiB -coated copper plate," J. Mater. Sci. Let., 4, 1350, 1985.

Mullendore, A.W., Whitley, J.B., Pierson, H.O., Mattox, D.M., "Mechanical properties of chemical vapor deposited coatings for fusion reactor application," J. Vac. Sci. Technol. 18(3), 1049, 1981.

Mueller, W.M., Blackledge, J.P. Libowitz, C.G., Metal Hydrides, Academic Press, N.Y., 1968.

Mutaftschiev, B.; "Adsorption and Crystal Growth," Chem. and Phys. of Solid Surfaces, Vol. 1, CRC-Press Inc., Boca Raton, Florida.

Nakano, K., Matsubara, H., Imura, T., "High Temperature Hardness of Titanium Diboride Single Crystal," Japan, J. Appl. Phys., 13, No. 6, 1974.

Neronov, V.A., Korchagin, M.A., Aleksandrov, V.V., Gusenko, S.N., "Investigation of interaction between Boron and Titanium," J. Less Common Met., 125, 82, 1981.

Owen, B.B.; Webber, R.T.; Metals Technology, Jan. 1948, 693, 1948.

Oxley, J.H.; Browning, M.F.; Vergel, N.D. and Blocher, J.M.Jr.; Ind. Eng. Chem. Prod. Res. and Dev., 1, 102, 1962.

Perry, R.H., Green, D., Perrys Chemical Engineers Handbook 6th ed., McGraw-Hill Book Co., N.Y., 1984.

Peshev, P., Niemyski, T., "Preparation de diboure de cristallin au moyen dune reaction en phase gazeuse," J. Less-Common Met., 10, 133, 1965.

Pierson, H.O., Randich, E., "Titanium diboride coatings and their interaction with the substrates," Thin Solid Films, 54, 119, 1978.

Pierson, H.O., Randich, E., Mattox, D.M., "The Chemical Vapor Deposition of TiB on Graphite," J. Less-Common Met., 67, 381, 1979.

Pierson, H.O., Mullendore, A.W., "Thick boride coatings by chemical vapor deposition," Thin Solid Films, 95, 99, 1982.

Pierson, H.O., Mullendore, A.W., "The chemical vapor deposition of TiB from diborane," Thin Solid Films, 72, 511, 1980.

Ed. Powell, C.F., Oxley, J.H., Blocher, J.M. Jr., Vapor Deposition, John Wiley and Sons, Inc., N.Y., 1966.

Powell, C.F., Campbell, I.E., Gonser, B.W., Vapor-Plating, John Wiley and Sons, Inc., N.Y., 1955.

Randich, E., "CVD boride coatings for erosion applications," Sandia Laboratories, New Mexico, SAND 78-2249C, 1978.

Randich, E., Gerlach, T.M., "The calculation and use of chemical vapor deposition phase diagrams with applications to the Ti-B-Cl-H system between 1200 and 800 K," Thin Solid Films, 75, 271, 1981.

Rauch, H.W., Sutton, W.H., McCreight, L.R., "Ceramic fibers and fibrous composite materials," Vol. 3, Academic Press, N.Y., 1968.

Redston, G.D., Stanworth, J.E., "Glass to Metal Seals," J. Soc. Glass Technol., 29, 72, 1945.

Revankar, V.V.S.; Hlavacek V.; "Synthesis of TiB fibers by CVD," High Temp. Mat. and Proc., 1990 (in press).

Revankar, V.V.S.; Schultz, J.; Hlavacek, V.; "Synthesis of ceramic fibers by CVD, A model study;" Ceram. Eng. and Sci. Proc., 1988.

Richerson, S. M.,"Modern Ceramic Engineering", p 136, Marcel Dekker Publ.,N.Y, 1984.

Roos, A.; Chimie and Industrie, 82, 339, 1959.

Samsonov, G.V., Portnay, K.I., Report FTD-TT-62-430, Wright-Patterson Air Force Base, Ohio, 1962.

Samsonov, G.V., Grebekina, V.G., "Temperature Coefficient of Electroresistance of Some High-Melting Compounds," Poroskh. Met. 8(2), 35, 1968.

Sato, T., Kudo, M., Tachikawa, T., "Synthesis of titanium boride by a reactive ion plating method," Denki Kagaku, 55, 542, 1987.

Scholtz, J.H., "The Coating of Fibrous Substrates by CVD: Modelling and Simulation," Ph.D. Thesis, SUNY at Buffalo, 1991.

Shaffer, P.T.B., No. 1 Materials Index, Plenum Press, NY, 1964.

Sherman, A., Chemical Vapor Deposition of Microelectronics Principles, Technology and Applications, Noyes Publication, 1987.

Shinko, J. S. and Lennartz, J. W.,"CVD Silicon Nitride Crucibles Produced Using SPC Techniques to Correlate and Optimize Processing Variables", Proc. 10^th Int. Conf. CVD, Eds. Cullen, G. W. and Blocher, J. M. Jr., 1106, 1987.

Smith, J.M., "Chemical Engineering Kinetics," McGraw-Hill, New York, 3rd Ed. (1981).

Spear, K. E.,"Principles and Applications of Chemical Vapor Deposition(CVD)", Pure Appl. Chem, 54, 1297, 1982.

Takahashi, T., Kamiya, H., "Chemical vapor deposition of Titanium diboride," J. Cryst. Growth, 26, 203, 1974.

Talley, C., "High Modulus, High Strength Reinforcements for Structural Composites," Tech. Doc. Rept. No. ML-TDR-64-88, Part I - Nov. 1963, Part II - Dec. 1964, Part III - Aug. 1965.

Thebault, J., Pailler, R., Bontemps-Moley, G., Bourdeau, M., Naslain, R., "Chemical compatibility in boron fiber-titanium composite materials," J. Less. Common. Met., 47, 221, 1976.

Touloukian, Y.S., Kirby, R.K., Taylor, R.E., Lee, T.Y.R., Thermophysical Properties of Matter, 12, NY, 1983.

Touloukian, Y.S., Kirby, R.K., Taylor, R.E., Lee, T.Y.R., Thermophysical Properties of Matter, 13, NY, 1983.

Tungsten Wire, General Catalog 7215, General Electric, Sept. 1983.

Vahldiek, F.W., "Electrical Resistivity, Elastic Modulus, and Debye Temperature of Titanium Diboride," J. Less Common Met., 12, 202, 1967.

Van-der Valk, H.J.L., Grondl, J.H.F., "Chemical vapor deposition of Titanium diboride on metallic substrates," Solid State Ion, 16, 99, 1985.

Viguie, J.C., Spitz, J., "Chemical vapor deposition at low temperature," J. Electrochem. Soc., 122, No. 4, 585, 1975.

Vincent, H., Boubehira, M., Bouix, M., "Caractistiques mecaniques des fibers de bore revetues de TiB par CVD reactive. Morphologie de depot," J. Cryst. Growth, 75, 504, 1986.

Wahl, G., and Schmadere, F.," ReviewS in Chemical Vapor Deposition of Superconductor", J. Mater. Sci, 24, 1141, 1989.

Warth, A.H., Bull. Maryland Acad., 3, 3, 1923.

Wakefield, G.F.; "Chromium coatings prepared by chemical vapor deposition," J. Electrochem. Soc., 116, 5, 1969.

Wawner, F., Teng, A., Nutt, S., "Microstructural Characterization of SiC (SCS) Filaments," Metal Matrix Carbon and SiC Composites, NASA Conf. Pub. 2291, 29, 1983.

Witucki, R., "High Modulus, High Strength Filaments and Composites," Tech. Rept. AFML-TR-66-187, May 1967.

Yee, K. K, "Protective Coating for Metals by Chemical Vapor Deposition", Int. Met. Rev., 23, 19, 1978.

Zeman, F., Mayerhofer, J., Kulmberg, A., "Abscheidung von TiB - Schichten uber die gasphase," High Temp. High Pr., 14, 341, 1982.

Zhao, G.Y., Revankar, V.V.S., Hlavacek, V., "Hydrogen-Chlorine Flame For Synthesis of Ultra Fine Powders," J. Less Common Metals, 163 , 269, 1990.

13 APPENDIX

13.1 Titanium Diboride Fibers

13.2 chromium Diboride Fibers

SYNTHESIS OF HIGH PERFORMANCE CERAMIC FIBERS BY CHEMICAL VAPOR

DEPOSITION FOR ADVANCED METALLICS REINFORCING

Final Technical Report for the Project Grant No. NAG3-897 to be Submitted to NASA Lewis Research Center, Cleveland, OH 44135-3191 for the period 1988-1991

13 APPENDIX

13.1 Titanium Diboride Fibers

Titanium diboride	TiB_2	Reference
Formula weight :	69.54 g/mol	82
Melting point :	2980 °C	
Density :	4.52 g/cc	

Chemical

Theoretical analysis : 31.12 % boron

68.88 % titanium

Reactivity :

1. Does not react with HCl, HF.
2. Reacts with hot H_2SO_4.
3. Soluble in HNO_3-H_2O_2.

4. Decomposed by fused alkali, carbonates and bisulfates.

5. Reacts violently with Na_2O_2 and brown lead oxide.

6. Air oxidation becomes noticeable at 700 °C. 83

Electrical 84

Resistivity : 9.1 $\mu\Omega$-cm. at 300 °C.

The temperature coefficient of electroresistance is 0.84 x 10^{-3} deg^{-1}

Mechanical 85

Knoop Hardness	15-36 GPa
Transverse Rupture Strength	700-1000 MPa
Fracture Toughness, K_{1c}	6-8 MPa $m^{1/2}$
Youngs Modulus	514-574 GPa
Poissons Ratio	0.09-0.28

Thermal

Conductivity	65-120 W/m K at 300 K
	54-122 W/m K at 2300 K
Specific Heat	632 J $(kg\ K)^{-1}$ at 300 K
	1155 J $(kg\ K)^{-1}$ at 1400 K

APPENDIX I

Expansion

// a-axis : $\Delta L/L_o = - 0.114 + 3.092 \times 10^{-4} T + 2.806 \times 10^{-7} T^2 - 3.996 \times 10^{-11} T^3\%$

// c-axis : $\Delta L/L_o = - 0.197 + 5.959 \times 10^{-4} T - 2.770 \times 10^{-7} T^2 - 4.369 \times 10^{-11} T^3\%$

polycrystalline : $\Delta L/L_o = - 0.142 + 4.054 \times 10^{-4} T + 2.786 \times 10^{-7} T^2$

$- 4.097 \times 10^{-11} T^3\%$

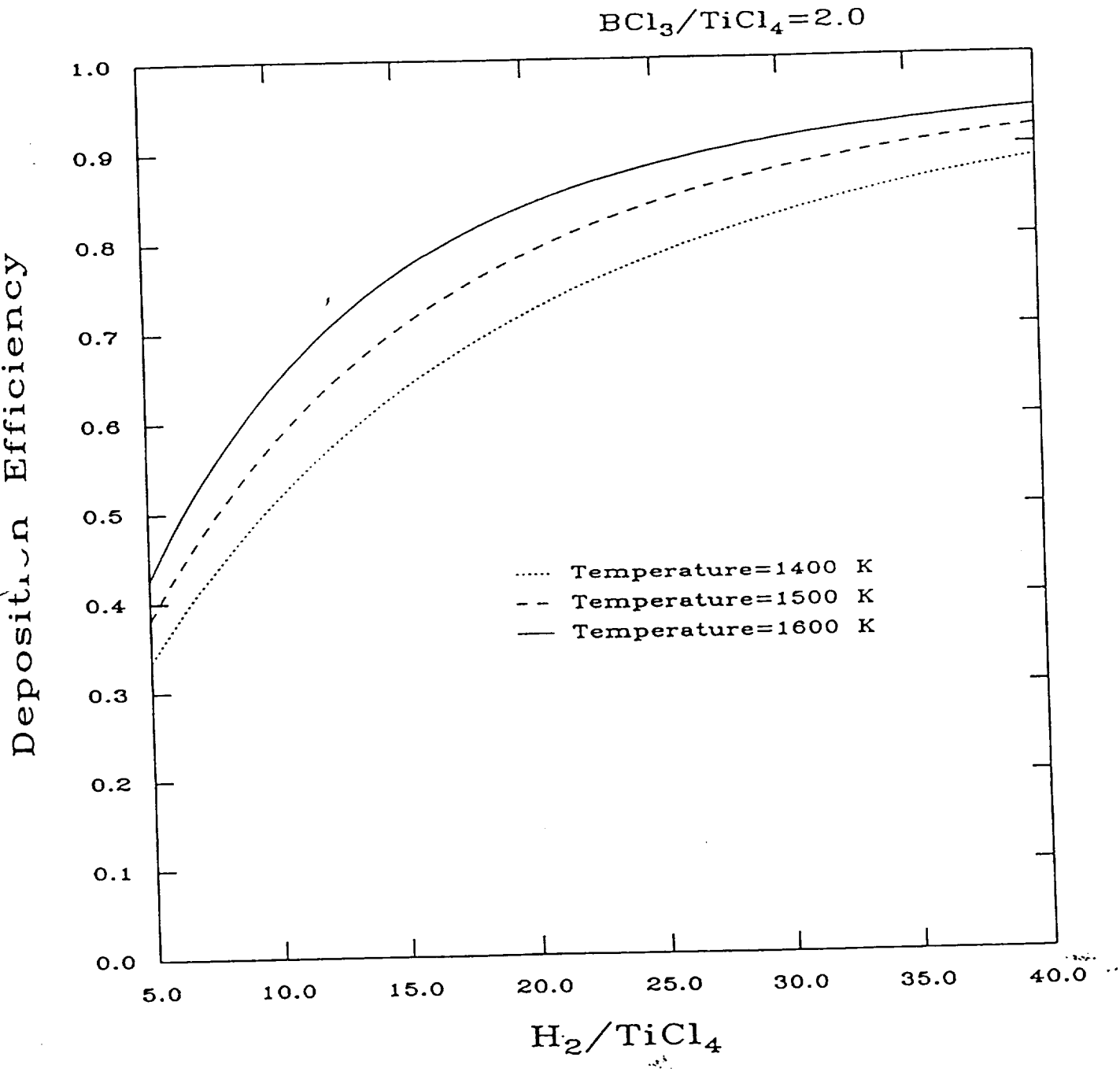

Effect of $H_2/TiCl_4$ ratio on Deposition Efficiency

TABLE 3.1

Physical Properties of Tungsten (W)[61]

Melting Point	3417 °C
Boiling Point	5930 °C
Vapor Pressure (mm Hg)	
1527 °C	1.93×10^{-15}
Specific Heat at 20 °C (cal/gm-atom)	6.25
Thermal Conductivity (cal/sq cm/cm/sec/°C)	
20 °C	0.310
927 °C	0.275
1127 °C	0.268
1527 °C	0.253
Density (g/cc)	19.17
Coefficient of Linear Expansion	
mean value 0 - 500 °C	4.98×10^{-6} $(°C)^{-1}$
Elastic Properties (at 25 °C)	
Young's Modulus	41×10^3 kg/mm^2
Shear Modulus	16×10^3 kg/mm^2
Poissons Ratio	0.27
Electrical Resistivity ($\mu\Omega$-cm)	
24 °C	5.89
700 °C	22.43
1100 °C	34.65
1500 °C	49.66

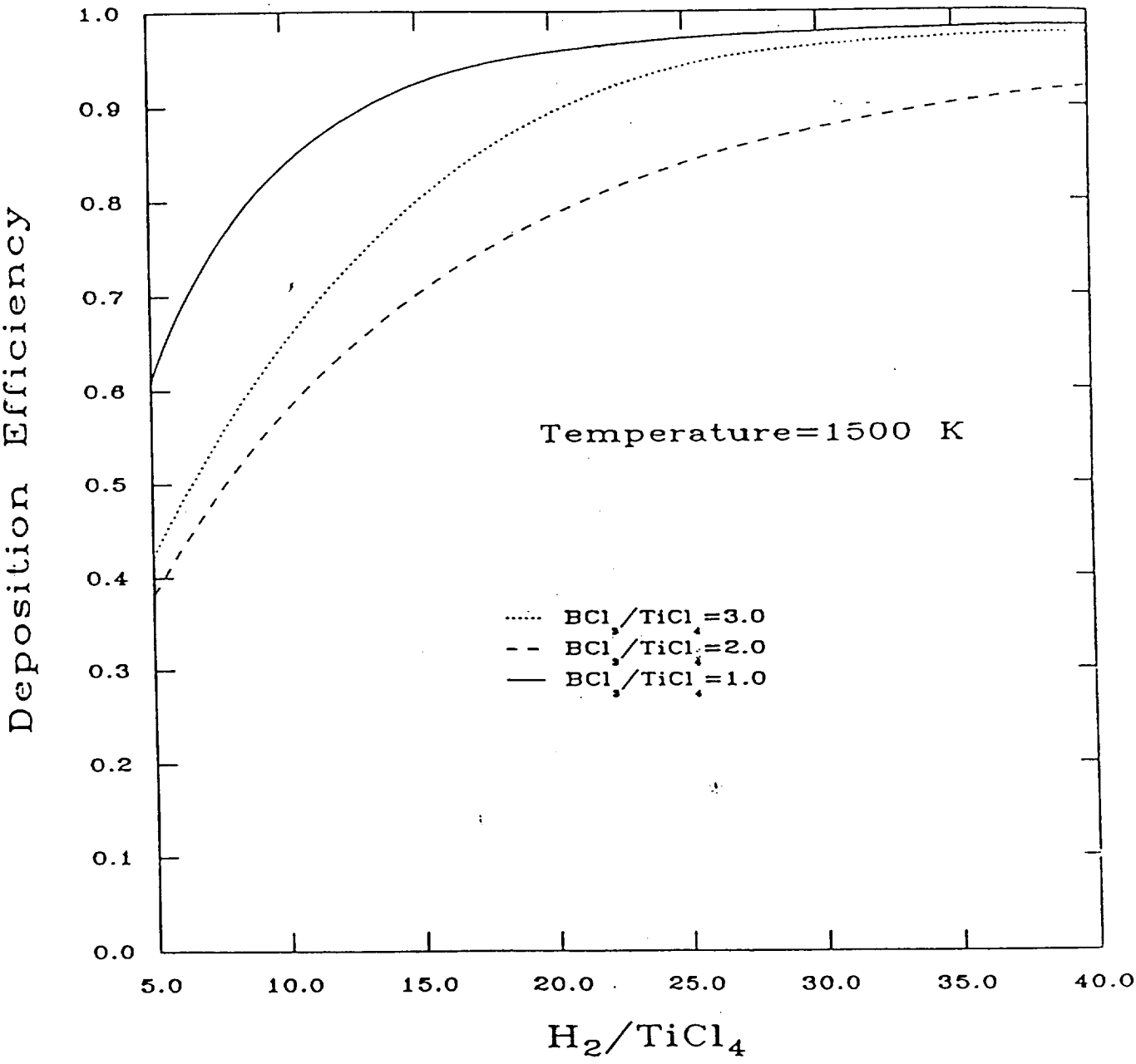

Effect of $H_2/TiCl_4$ Ratio on Deposition Efficiency

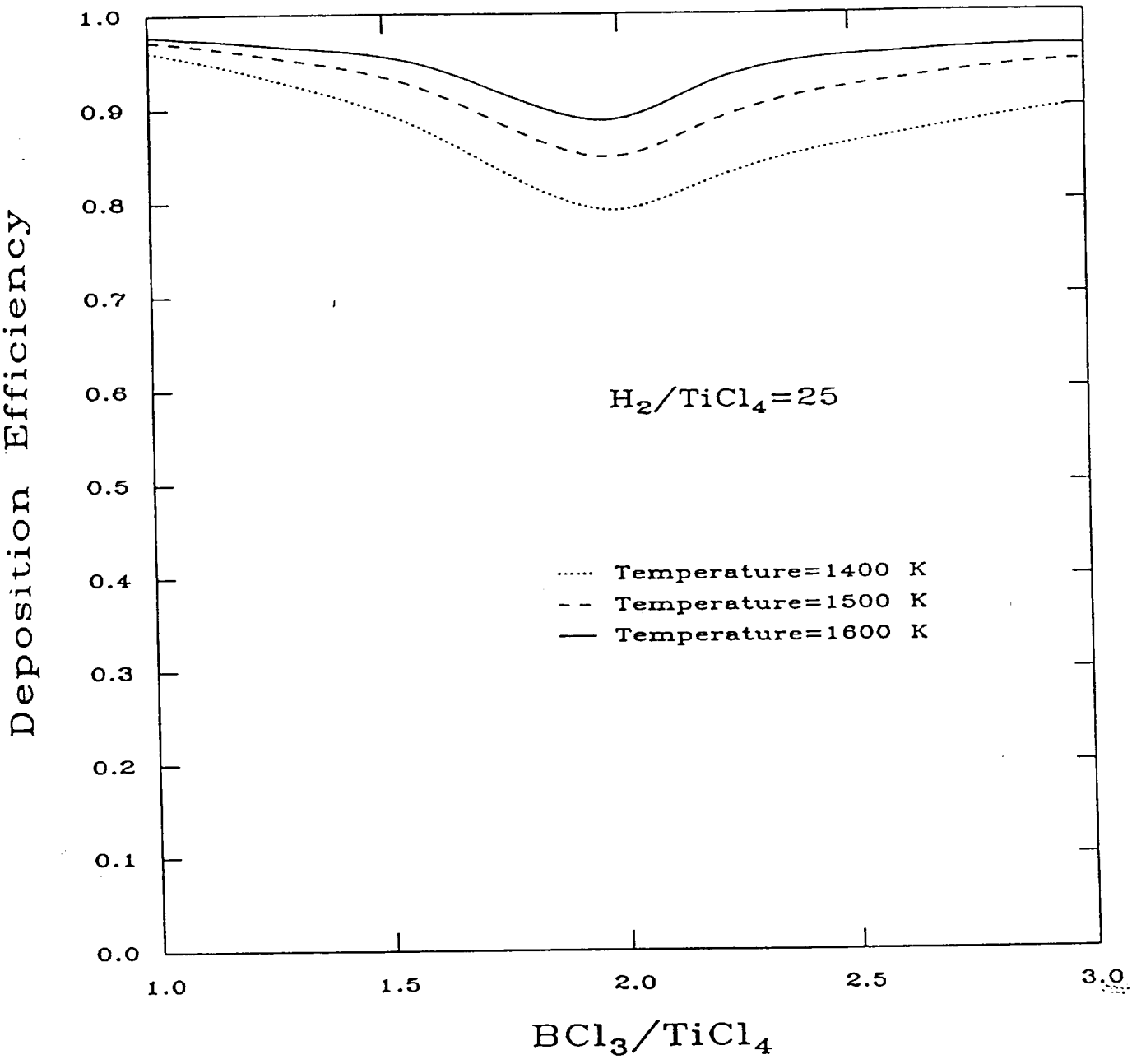

Effect of $BCl_3/TiCl_4$ ratio on Deposition Efficiency

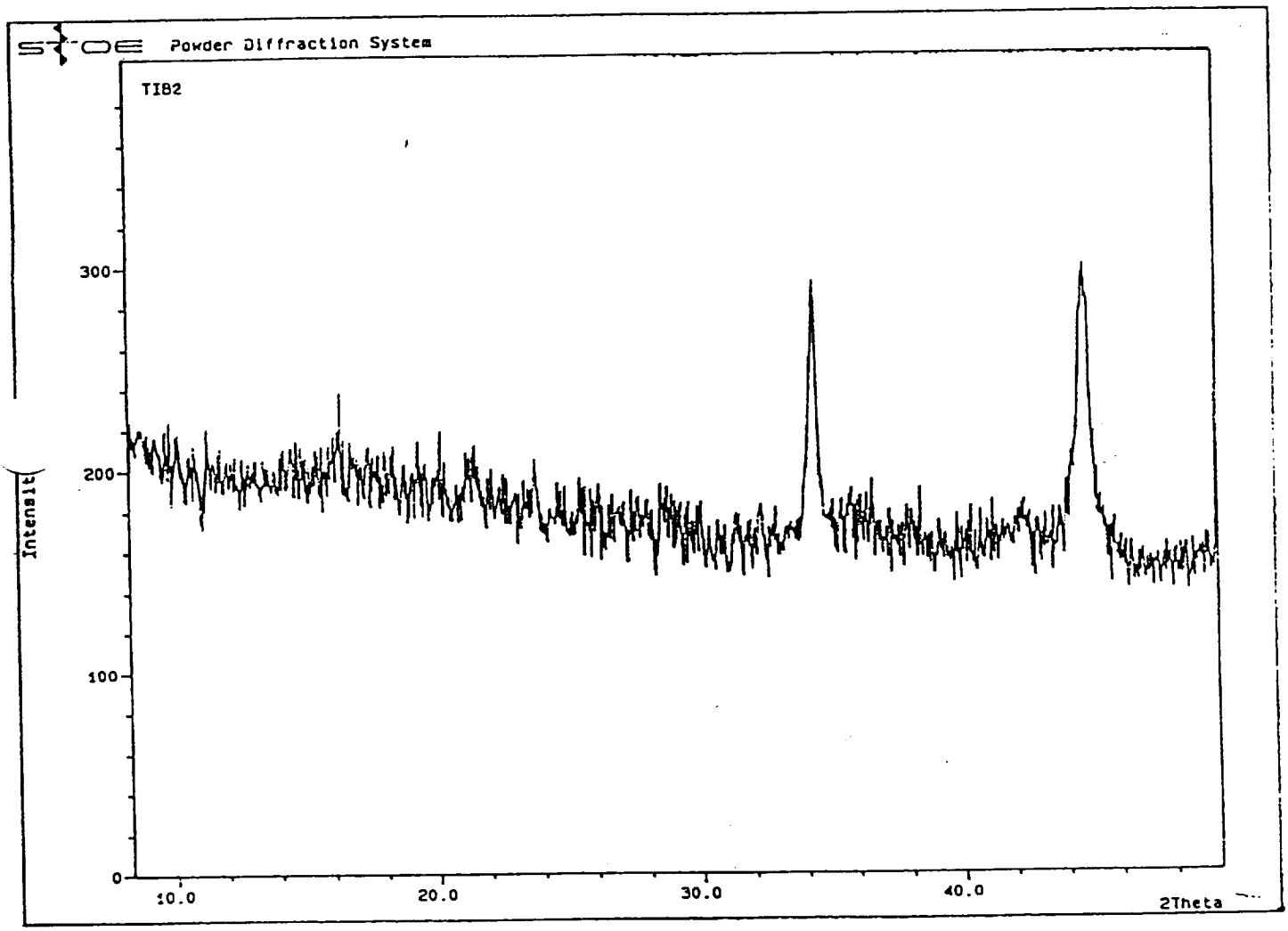

X-ray diffraction of the TiB_2 fiber to determine codeposited B

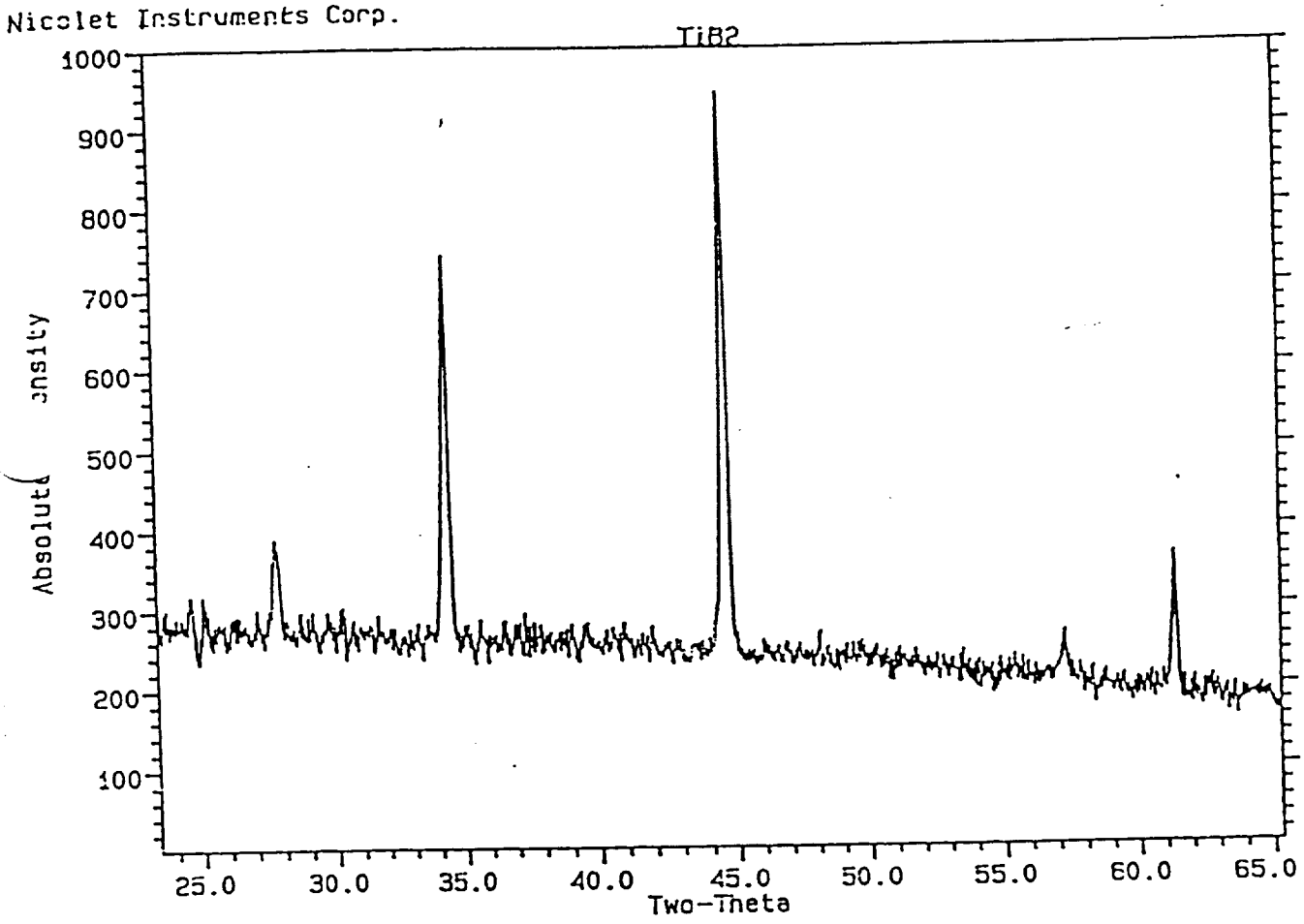

X-ray Diffraction of TiB_2 Powder

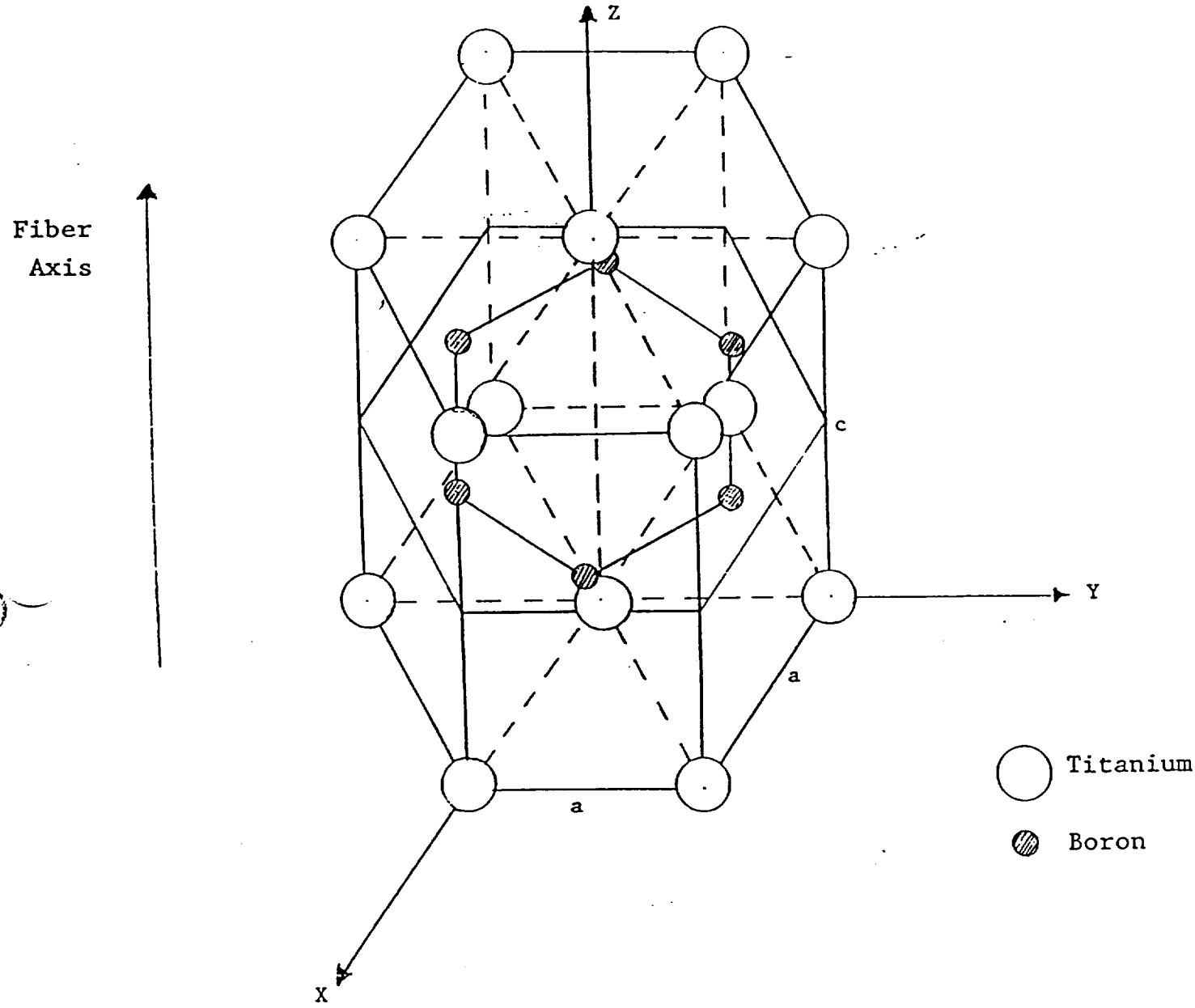

The coordinates of the atoms in a unit cell are:

1 Ti	0, 0, 0		
2 B	1/3, 2/3, 1/2	and	2/3, 1/3, 1/2

Crystal Structure of TiB_2

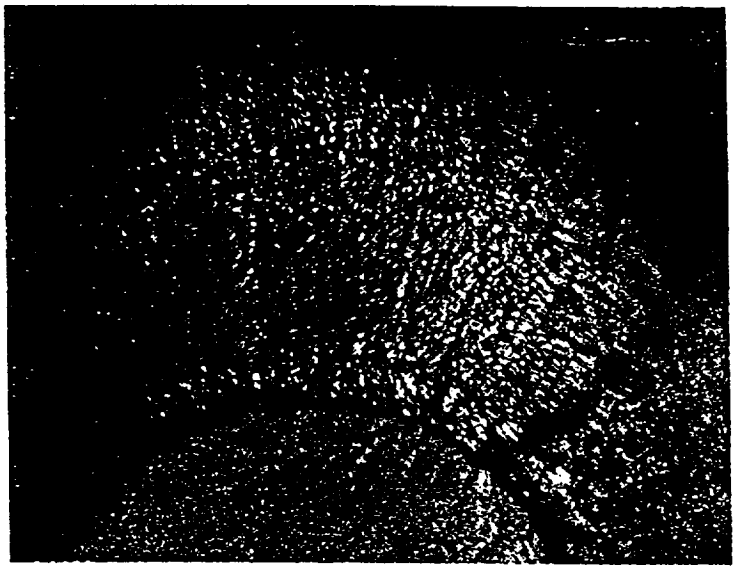

Metallograph of CVD TiB_2

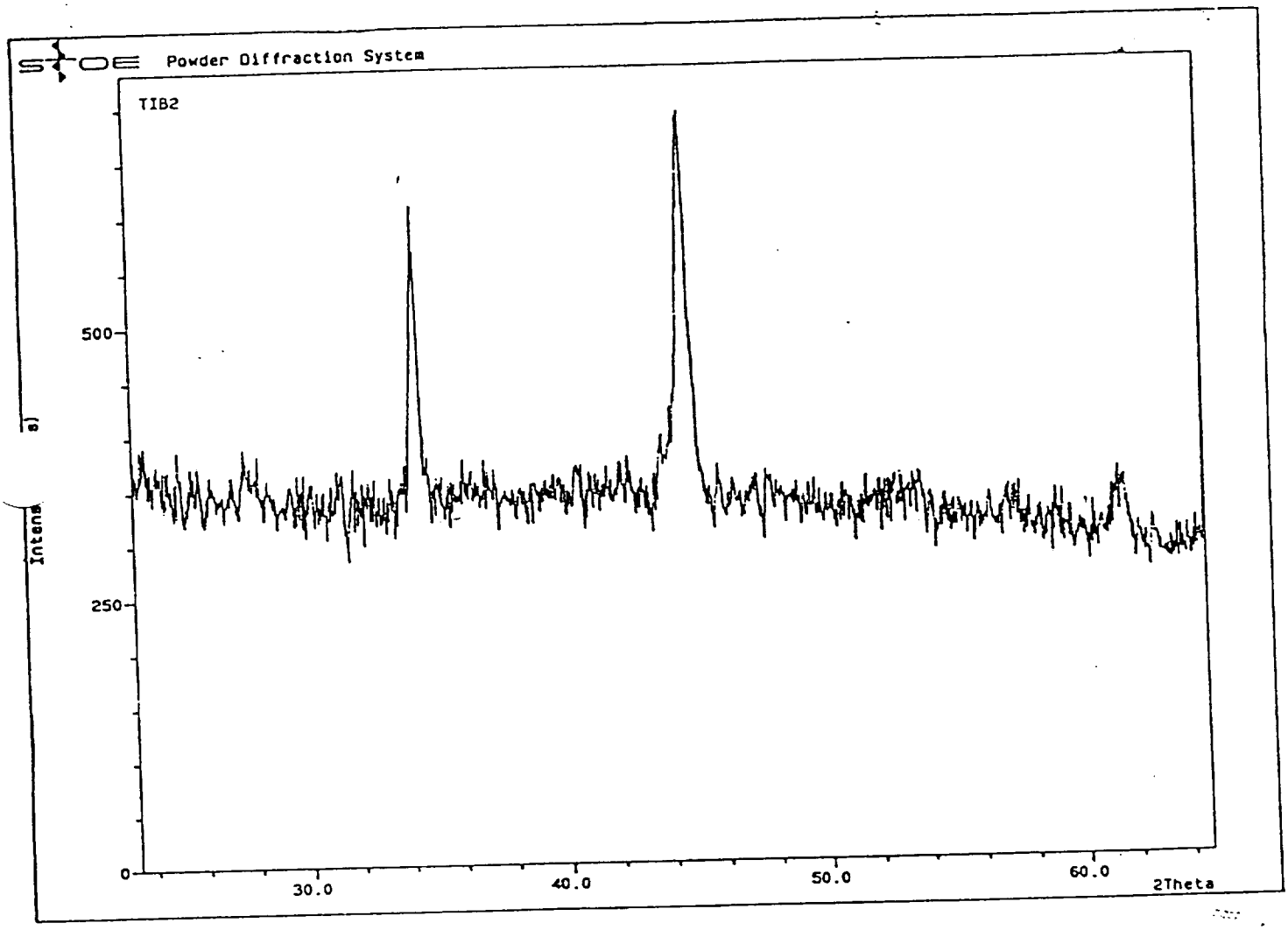

X-ray diffraction of the TiB_2 fiber

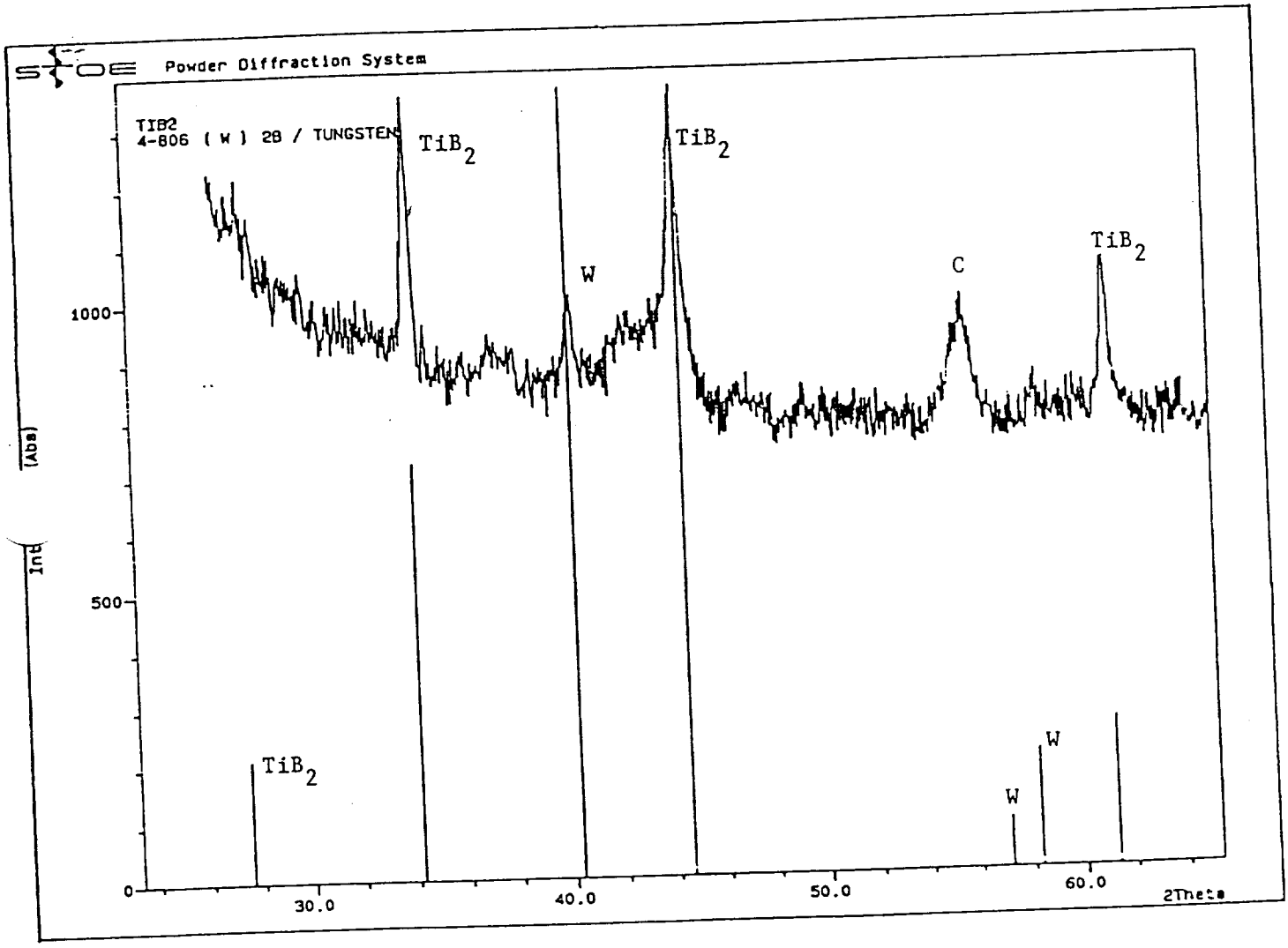

X-ray Diffraction Pattern of TiB_2 Coating on W with Graphite Intermediate Layer

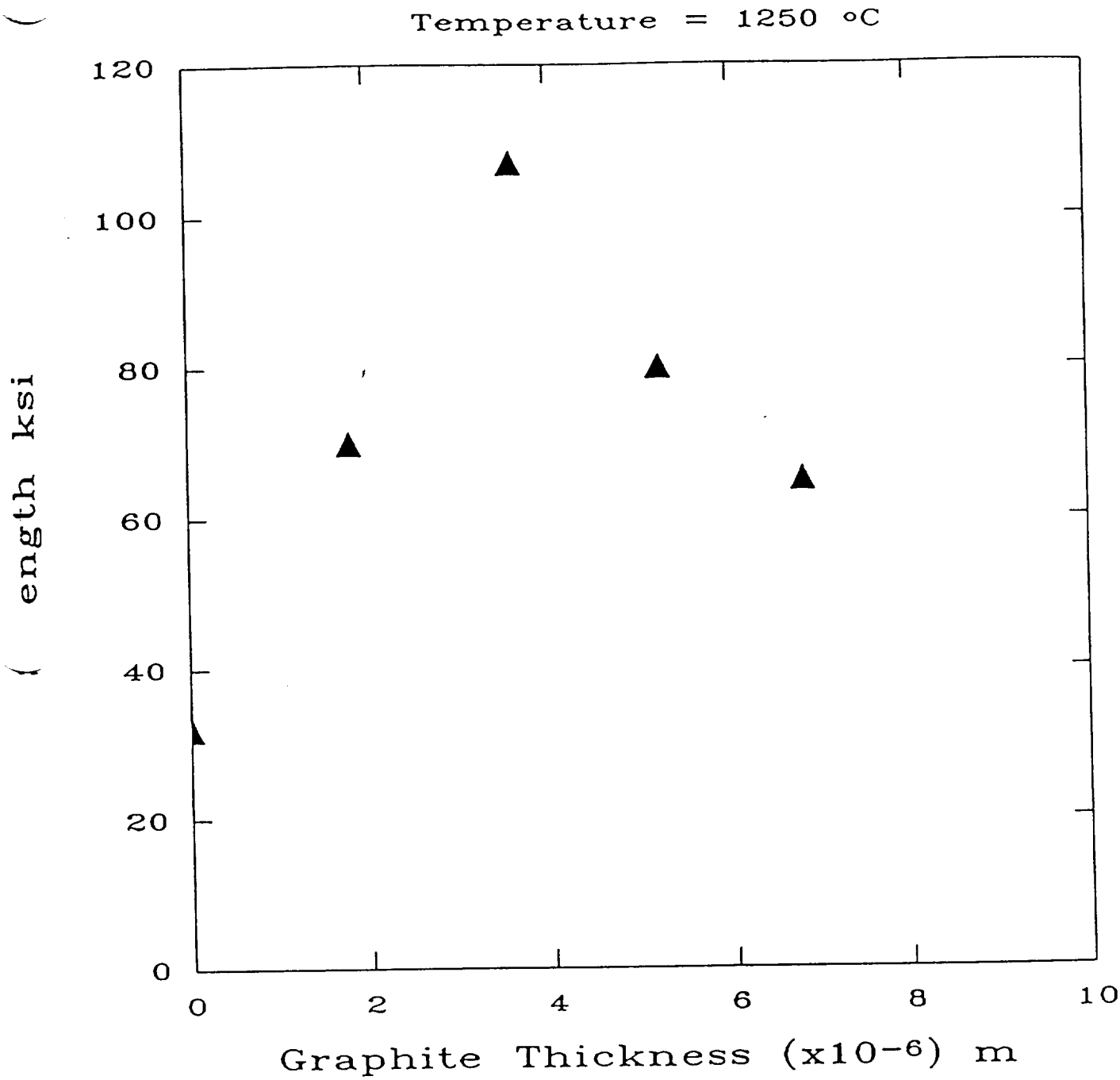

Effect of Intermediate Pyrolytic Graphite Layer on Strength

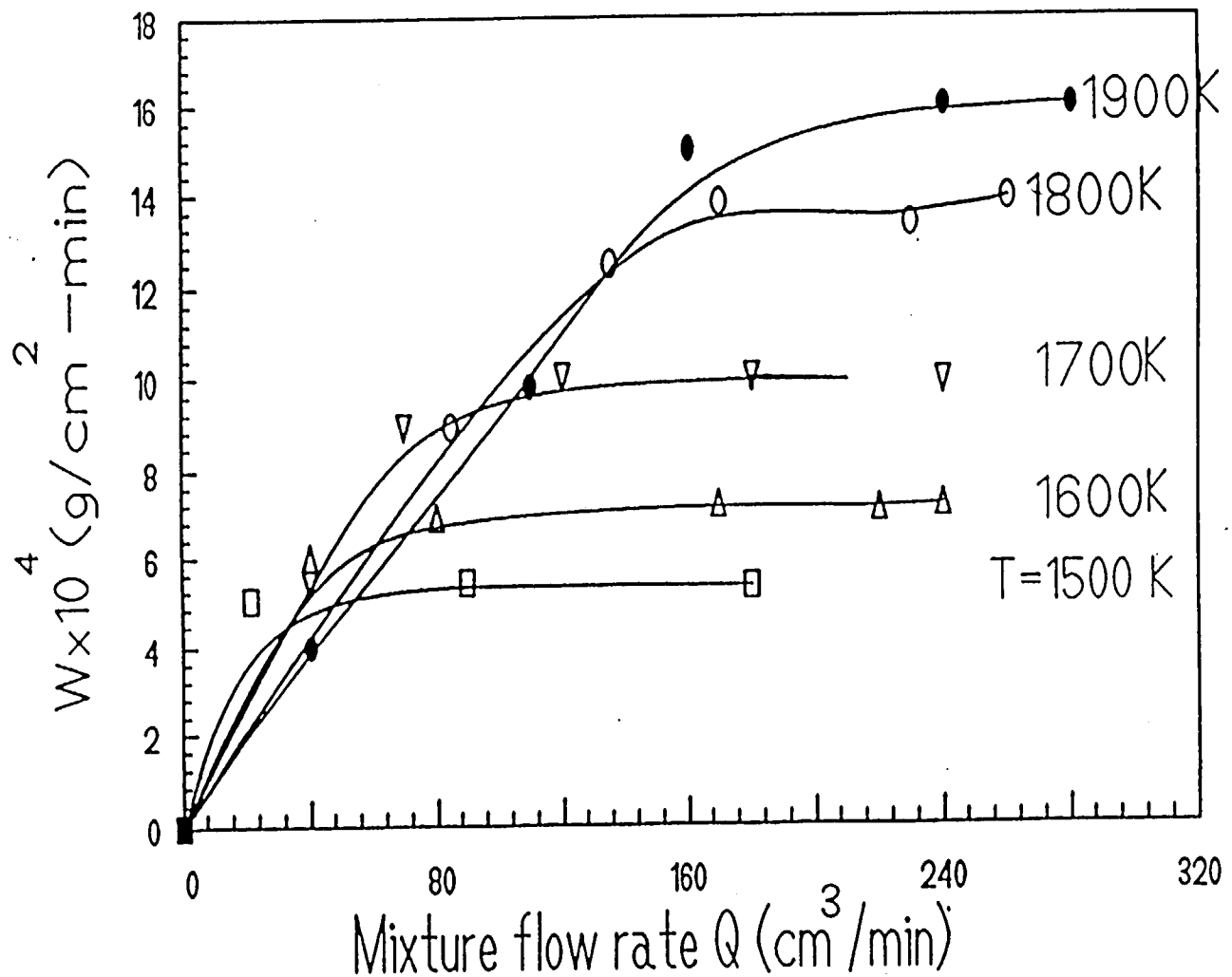

Variation of Deposition Rate of Titanium Diboride with Volume Rate of Flow of Reagents

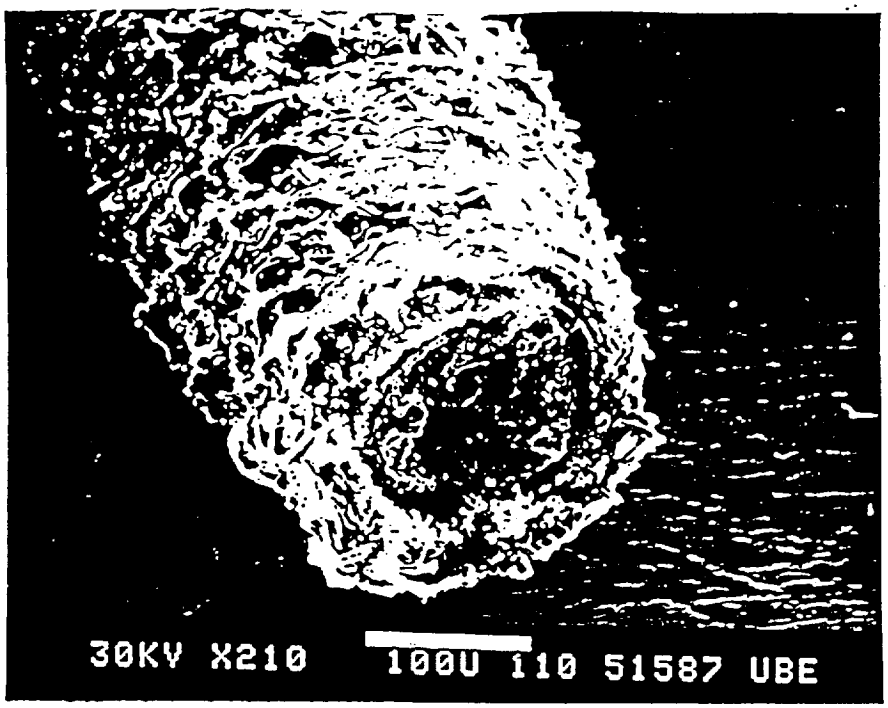

Fiber produced from direct boriding

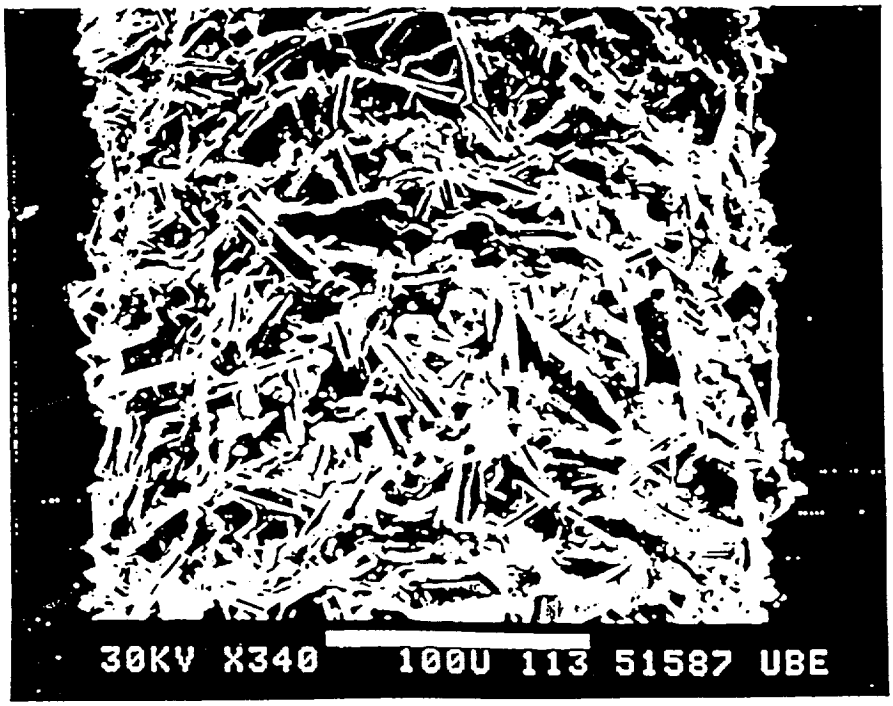

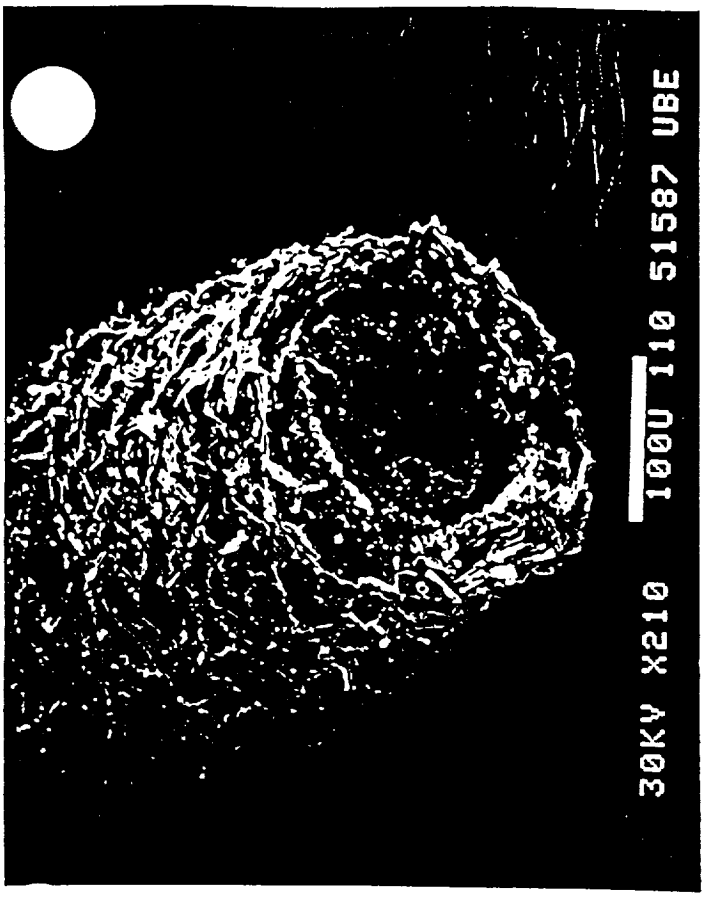

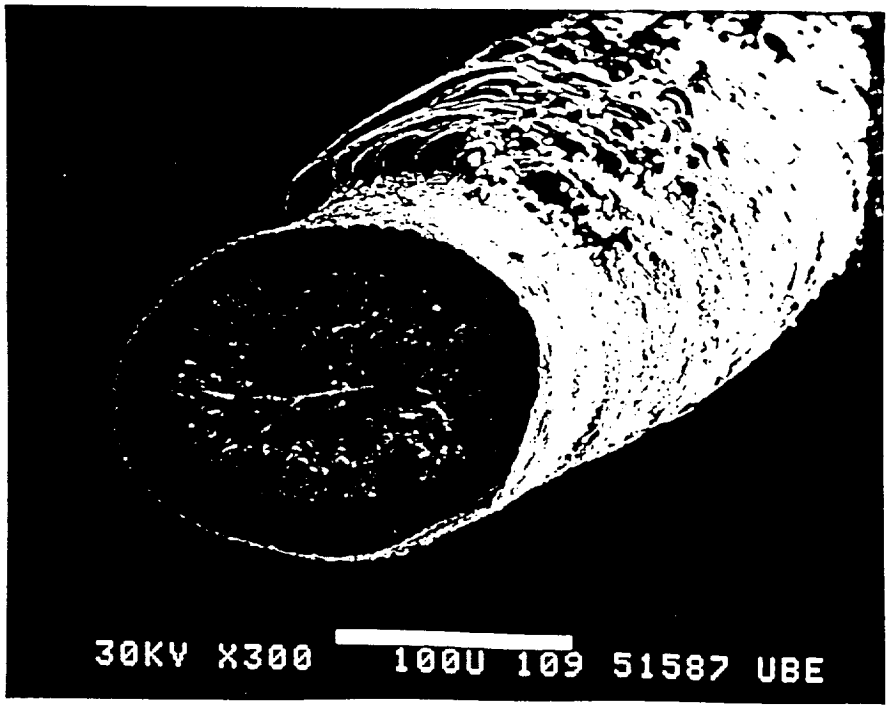

A. Ti + BCl_3 + H_2 at 1400°C

B. Ti fiber + boron powder + hydrogen carrier gas at 1350°C

C. Ti fiber + BCl_3 + H_2 + Ar at 1200°C

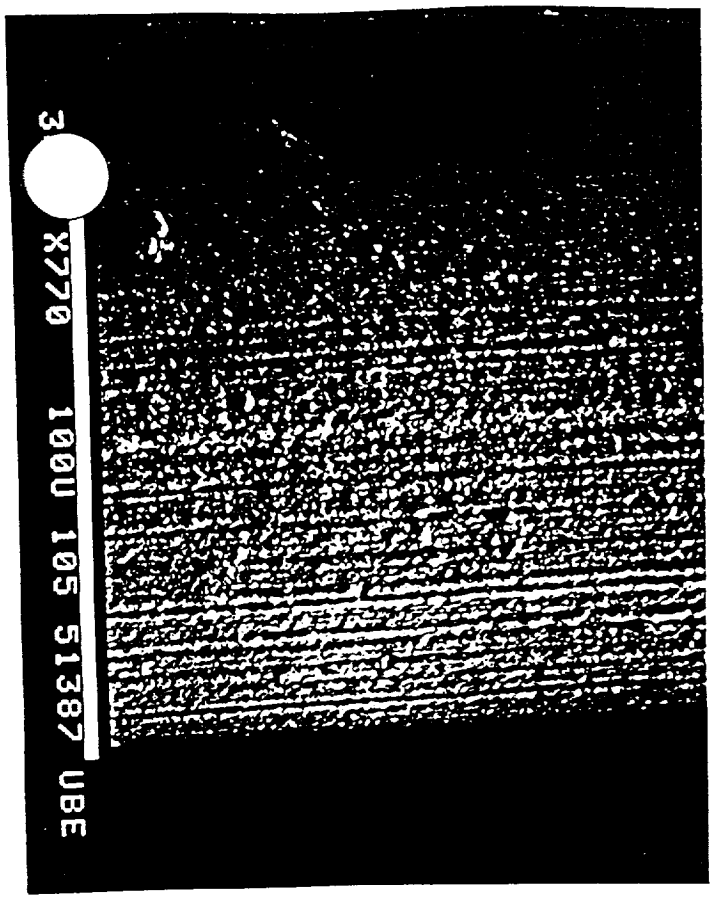

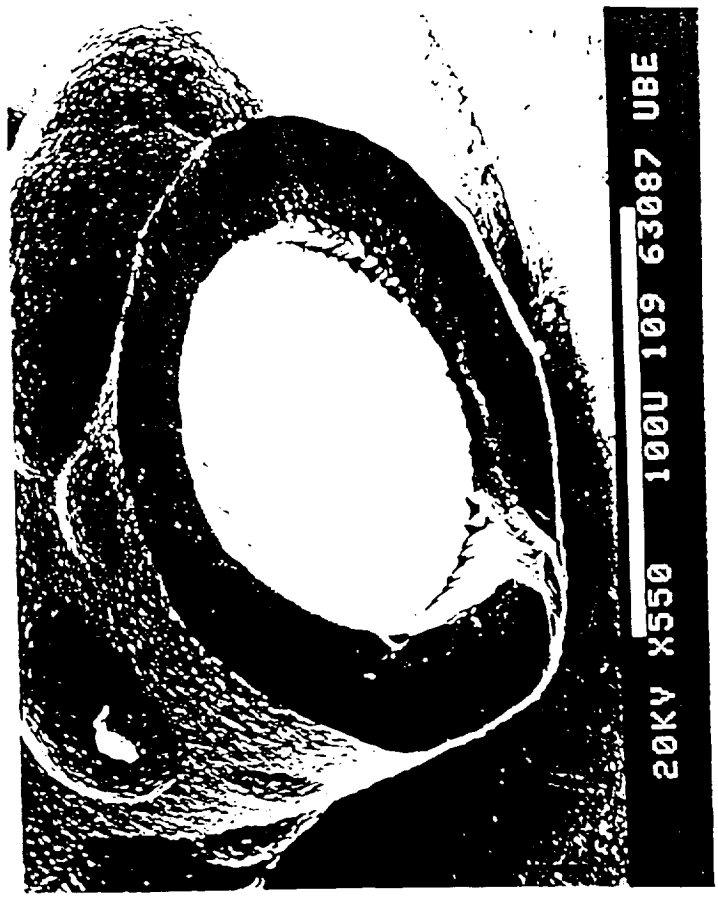

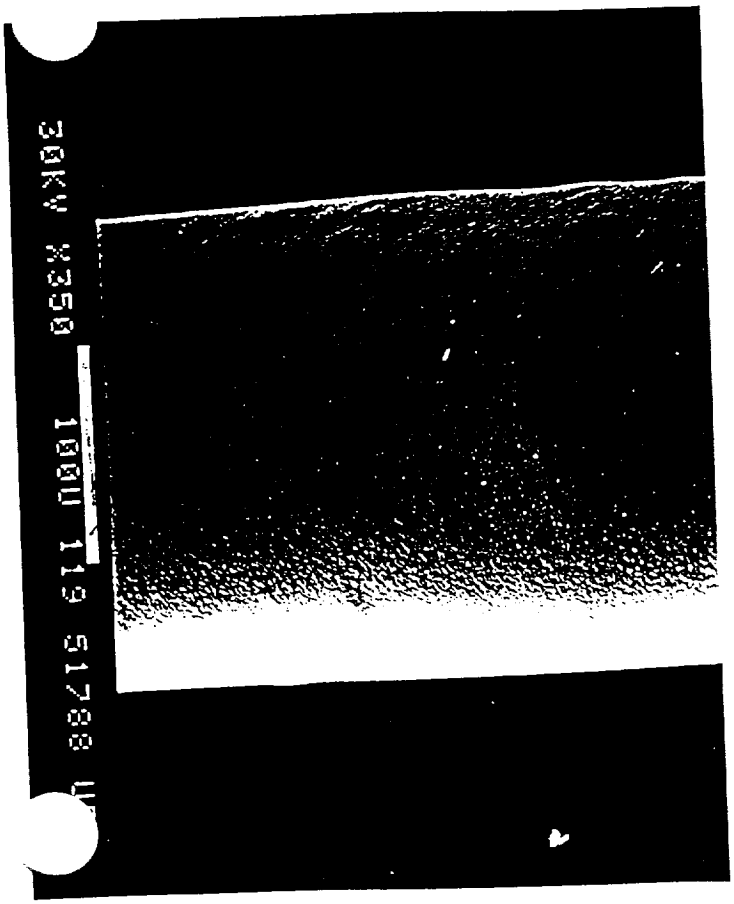

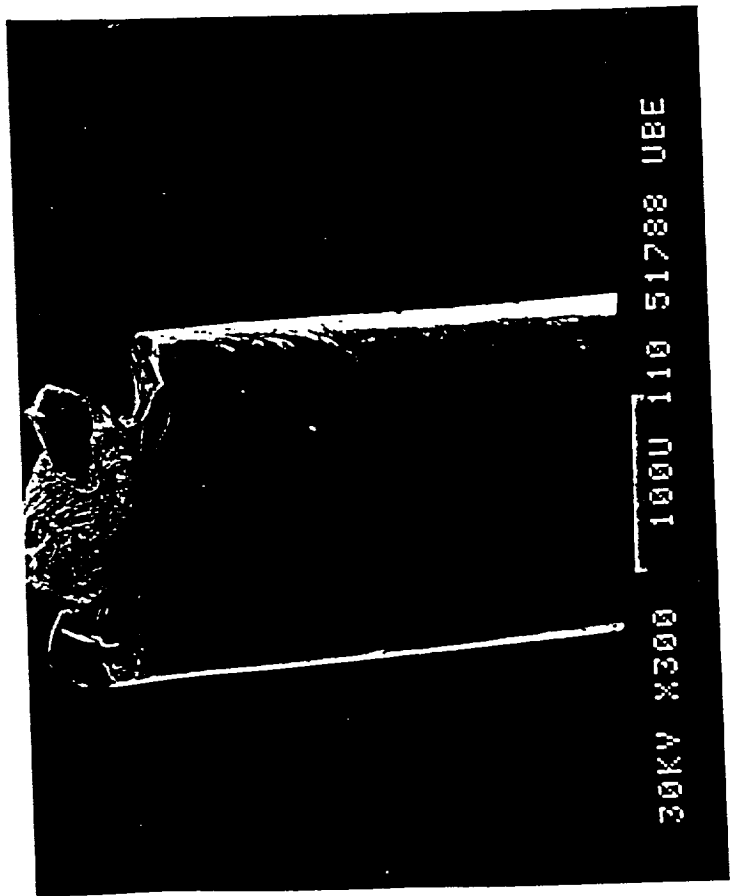

1. 1000°C
2. 1100°C H:Cl ratio - 7
3. 1150°C
4. 1220°C B:Ti ratio - 2.5

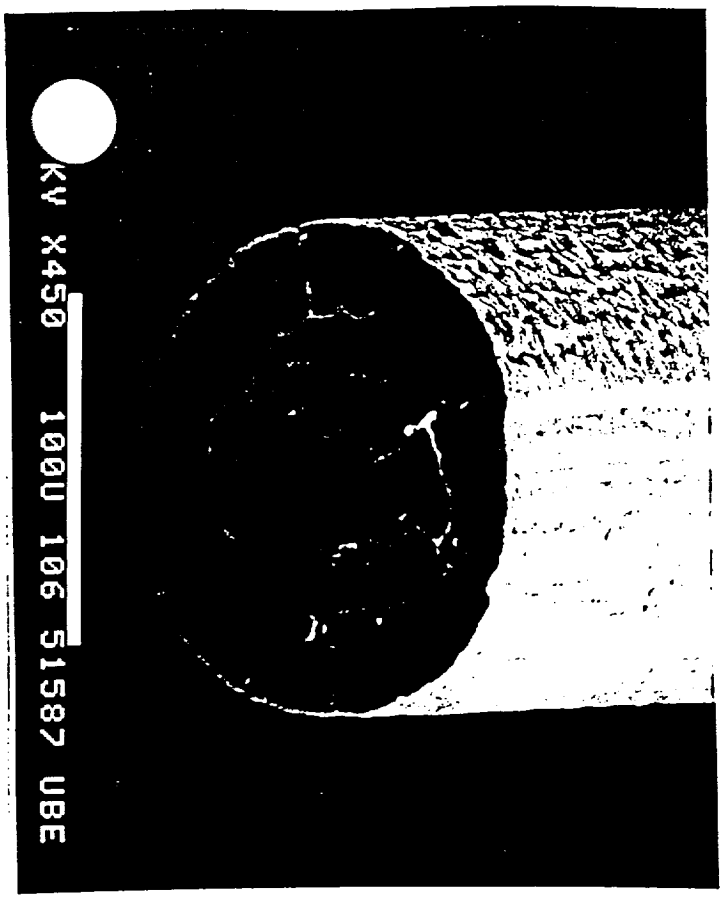

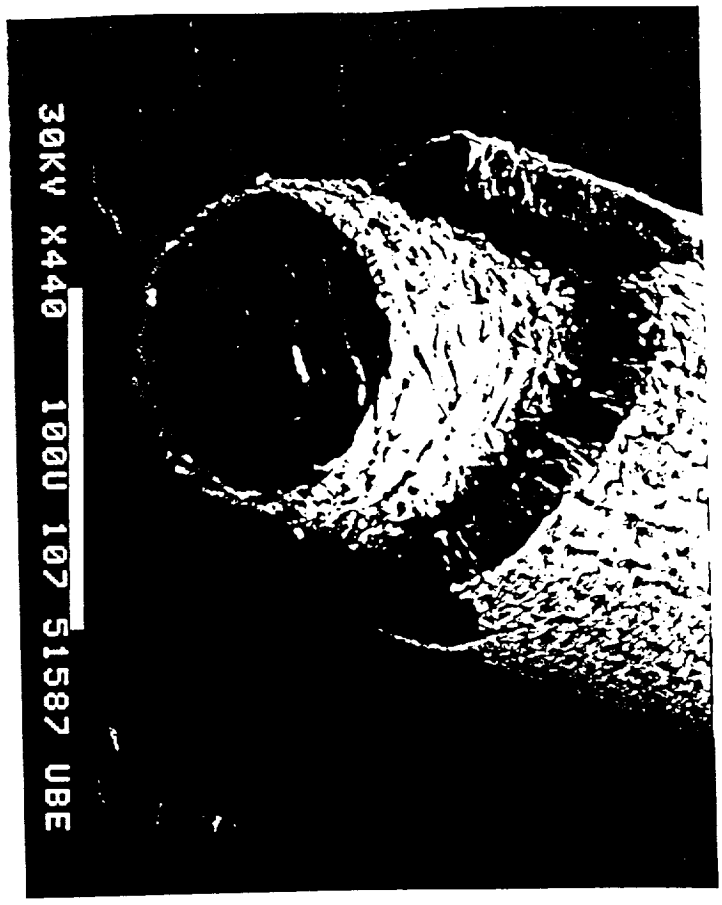

a

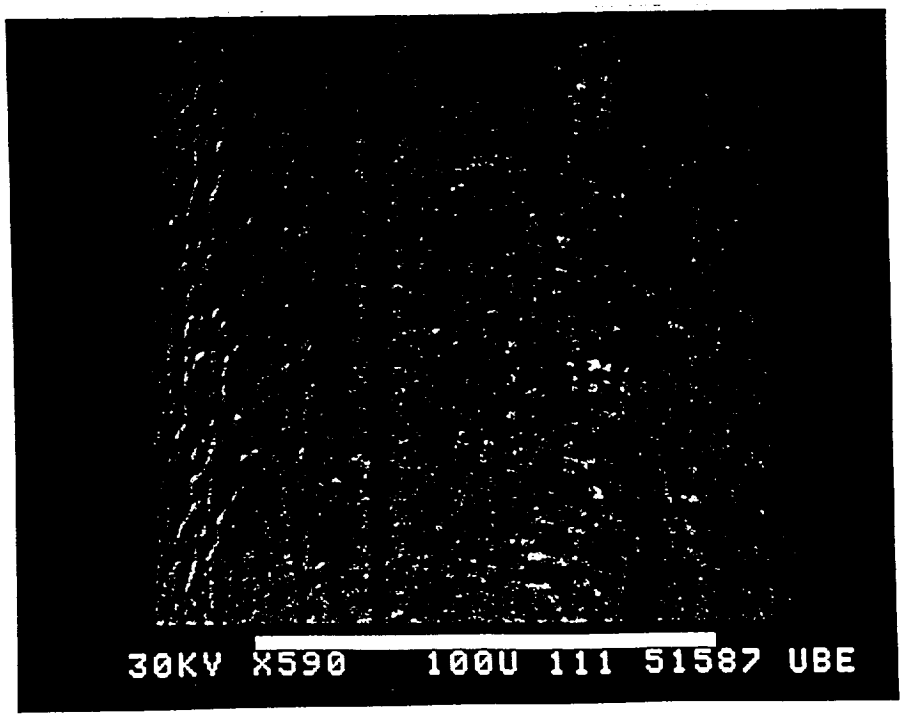

TiB_2 fibers

(a) Ti core
(b) Mo core
(c) Ti Core

} at Optimum Conditions Obtain with Tungsten Core

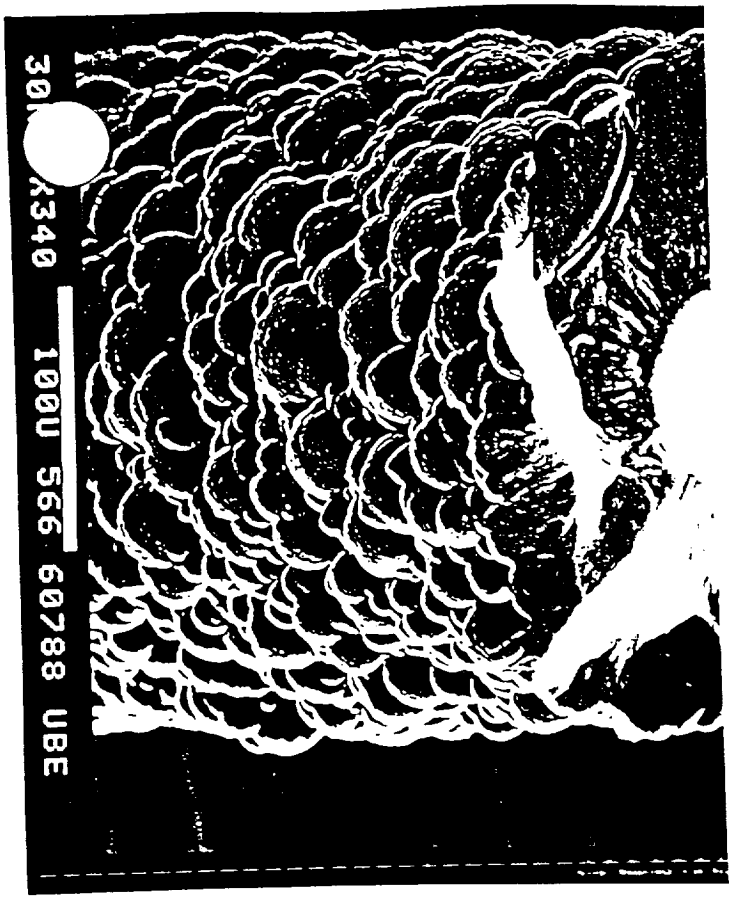

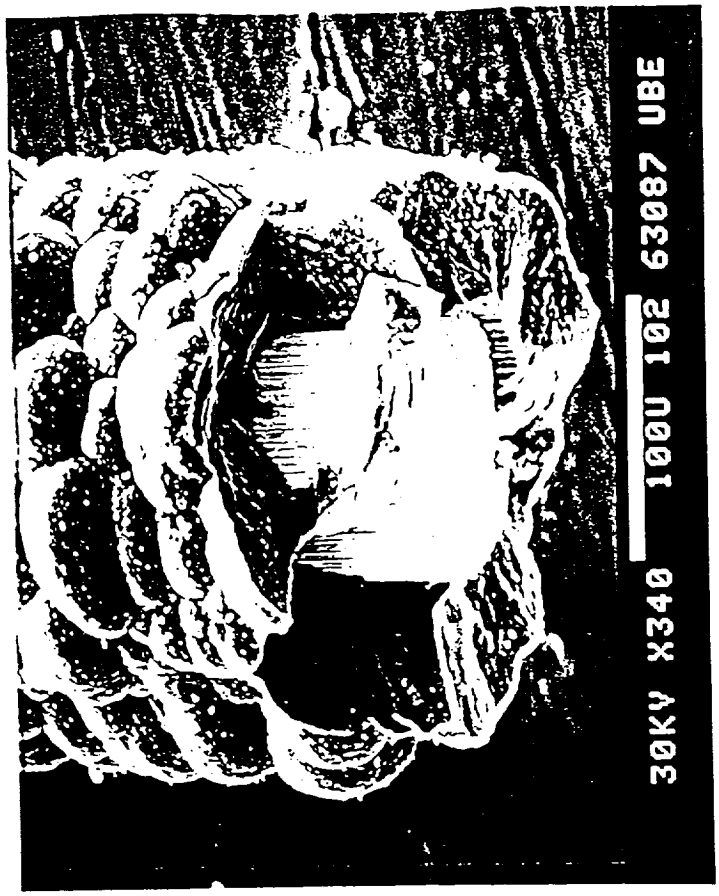

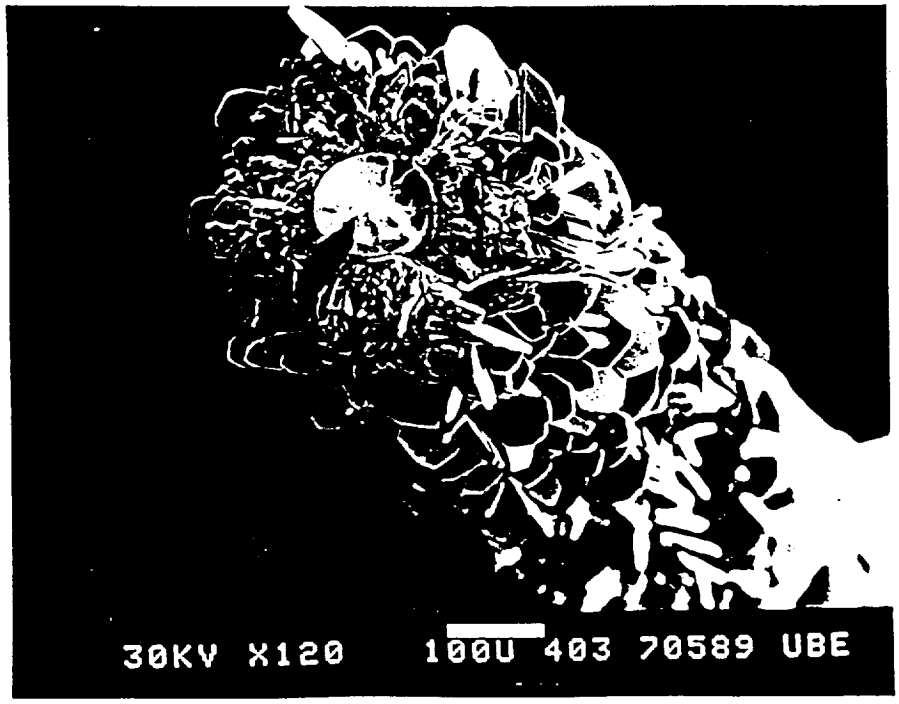

9. 1400°C

10. 1450°C

11. >1450°C

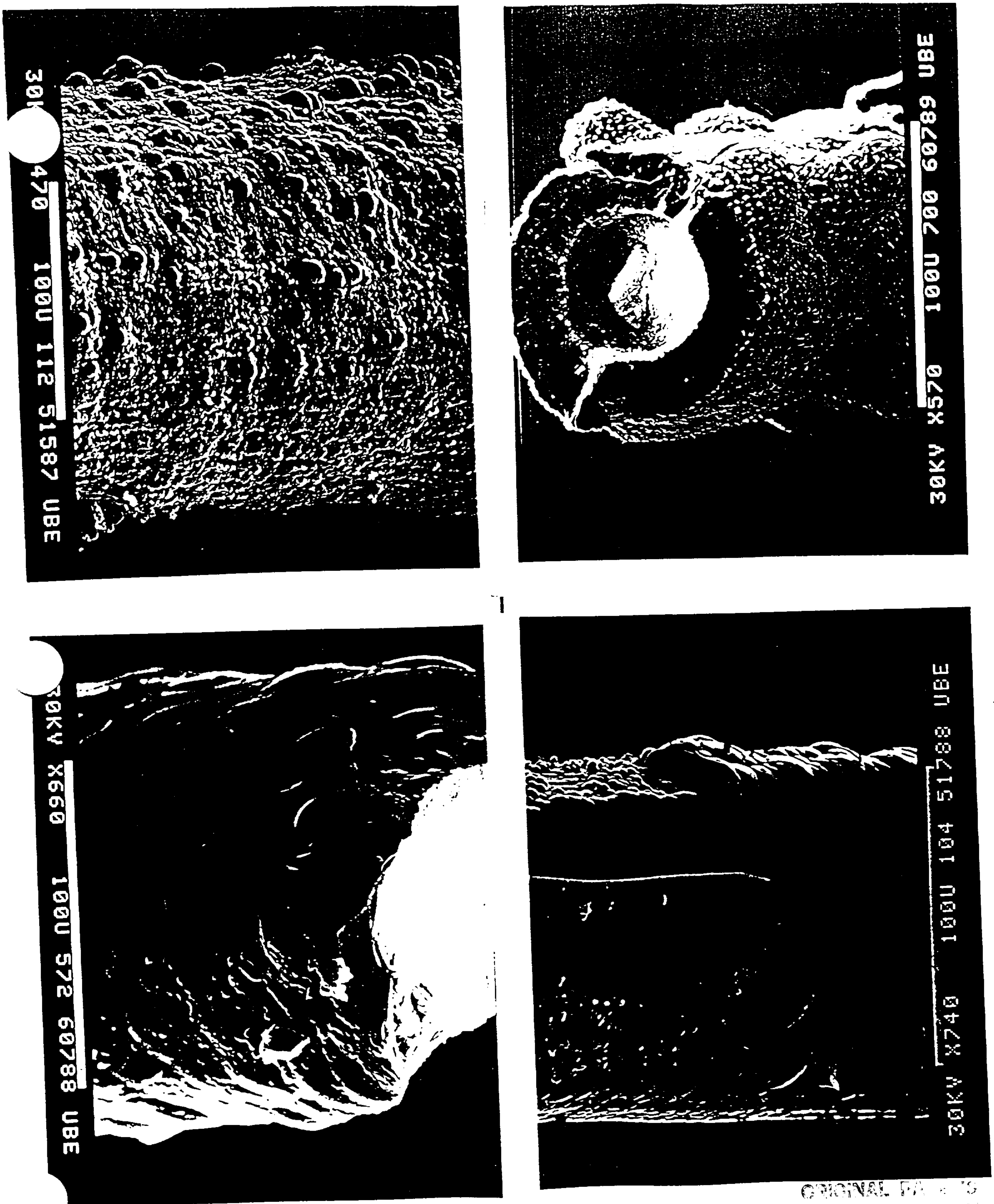

A. 1060°C

B. 1100°C

C. 1140°C

D. 1200°C

H:Cl ratio 7

B:Ti ratio

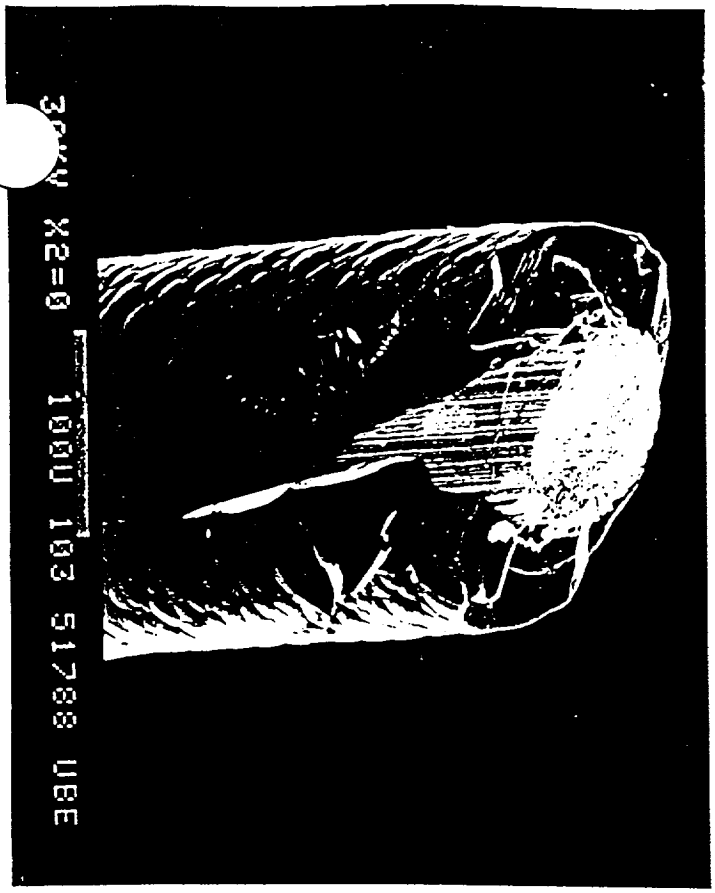

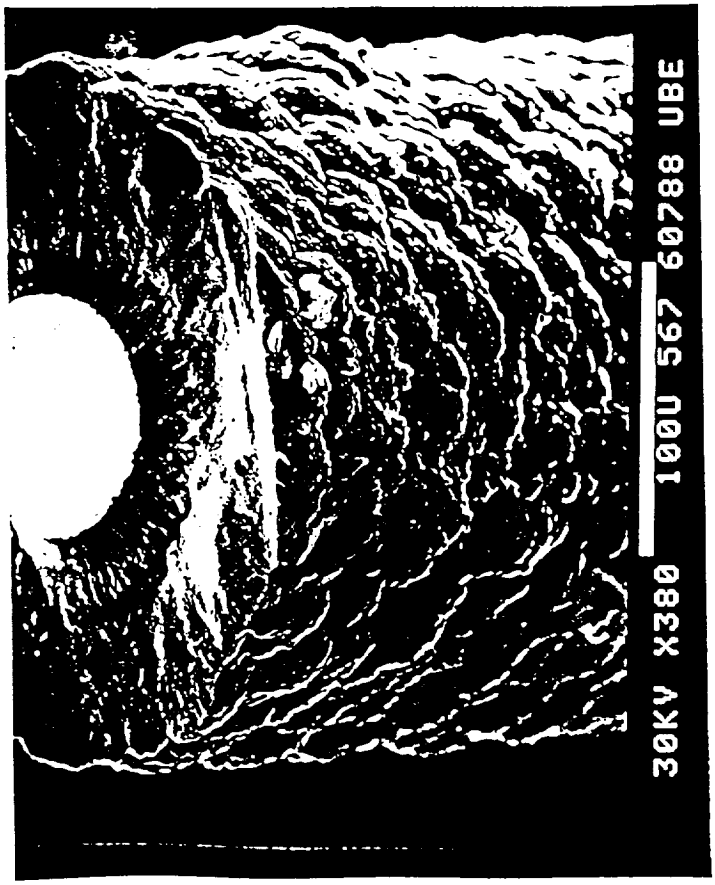

5. 1250°C

6. 1250°C

7. 1330°C

8. 1350°C

ORIGINAL PAGE IS
OF POOR QUALITY

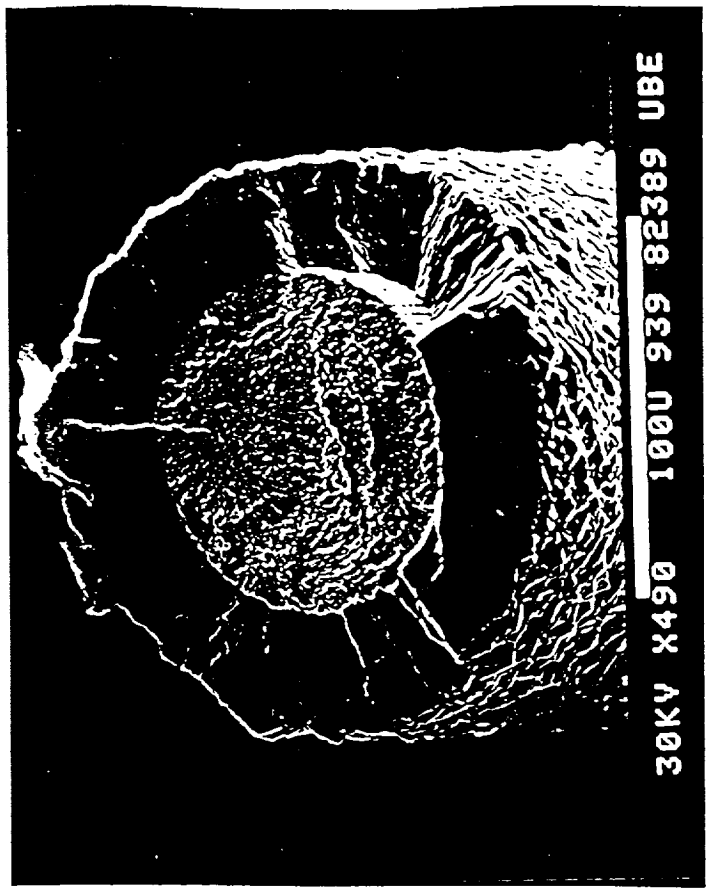

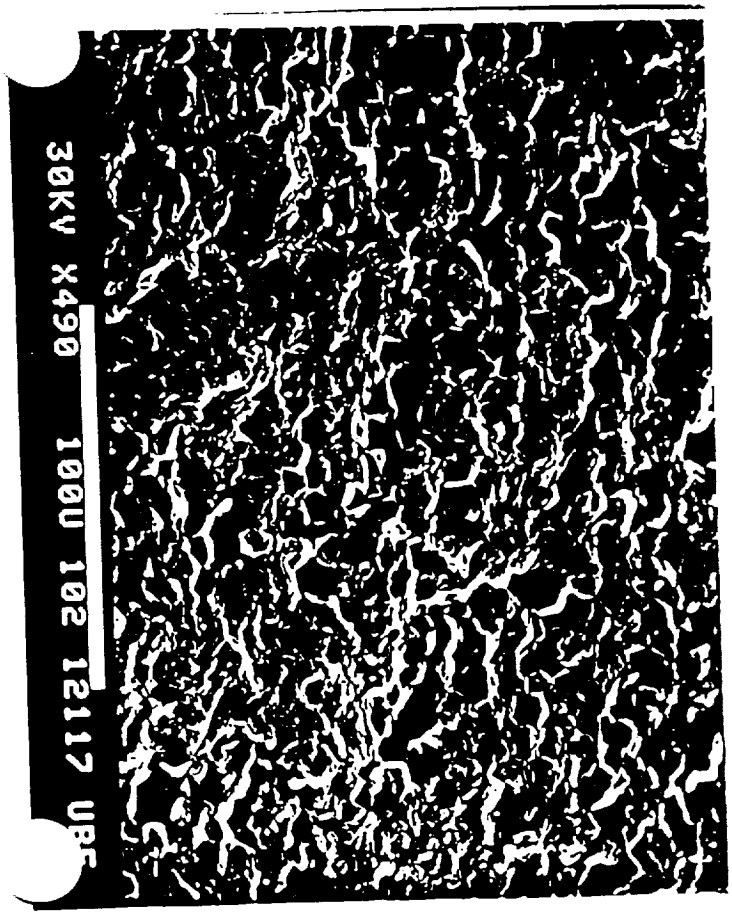

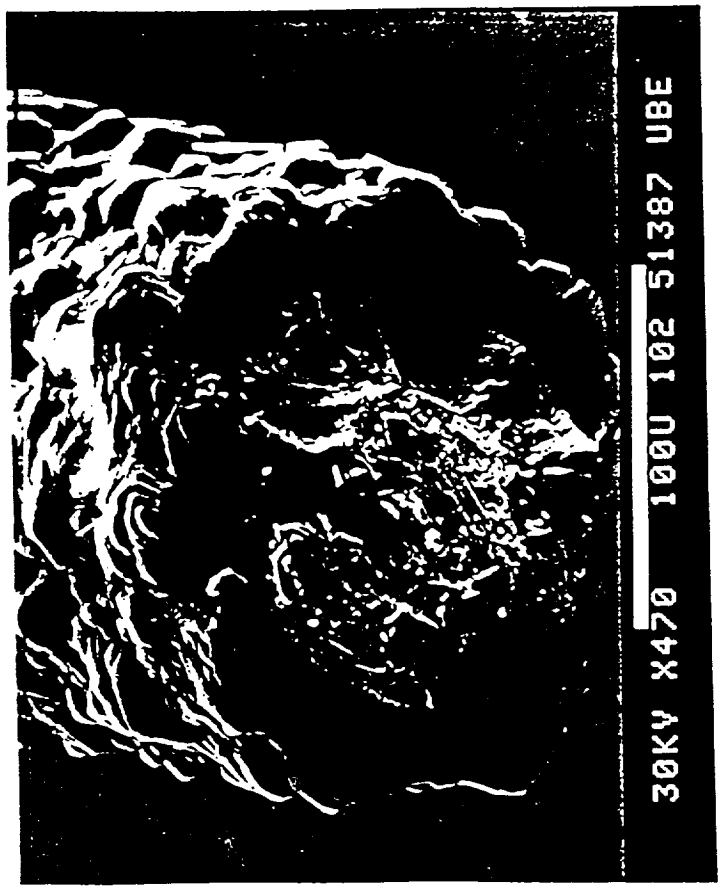

E. 1250°C

F. 1250°C

G. 1300°C

H. 1300°C

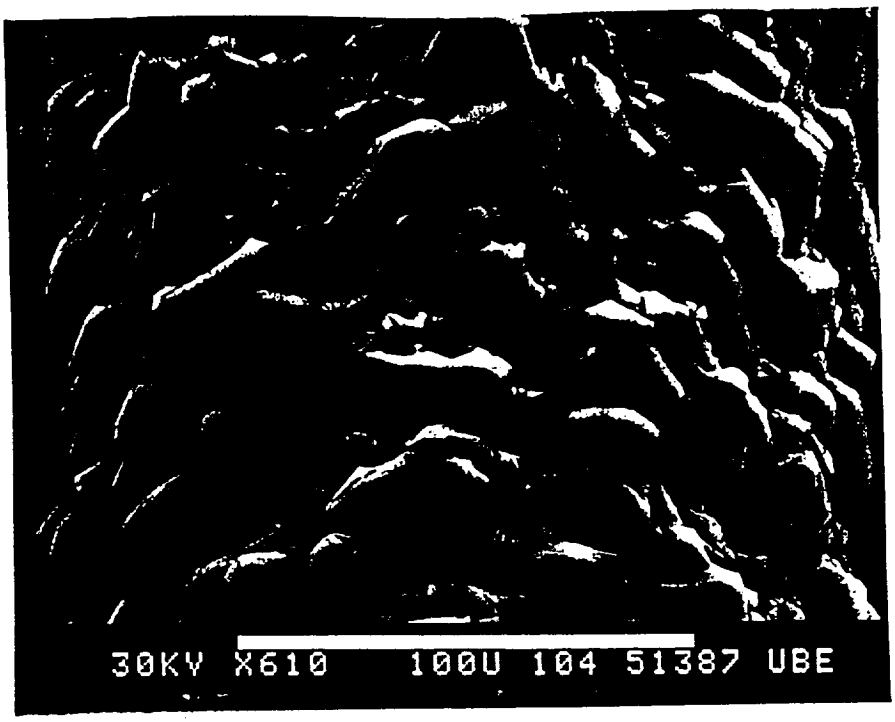

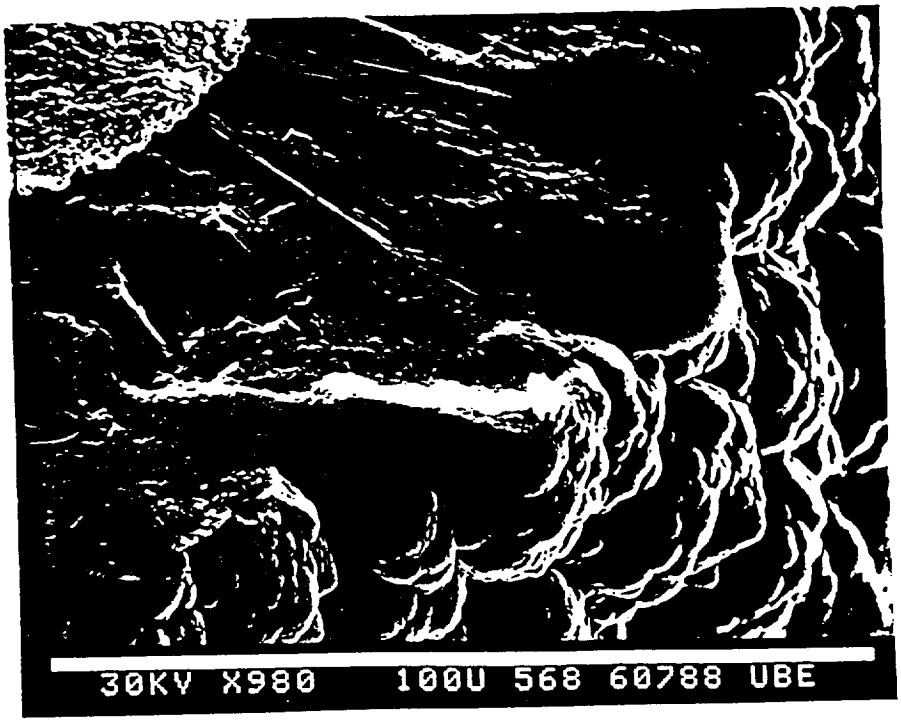

I. 1400°C

J. greater than 1400°C

ORIGINAL PAGE IS
OF POOR QUALITY

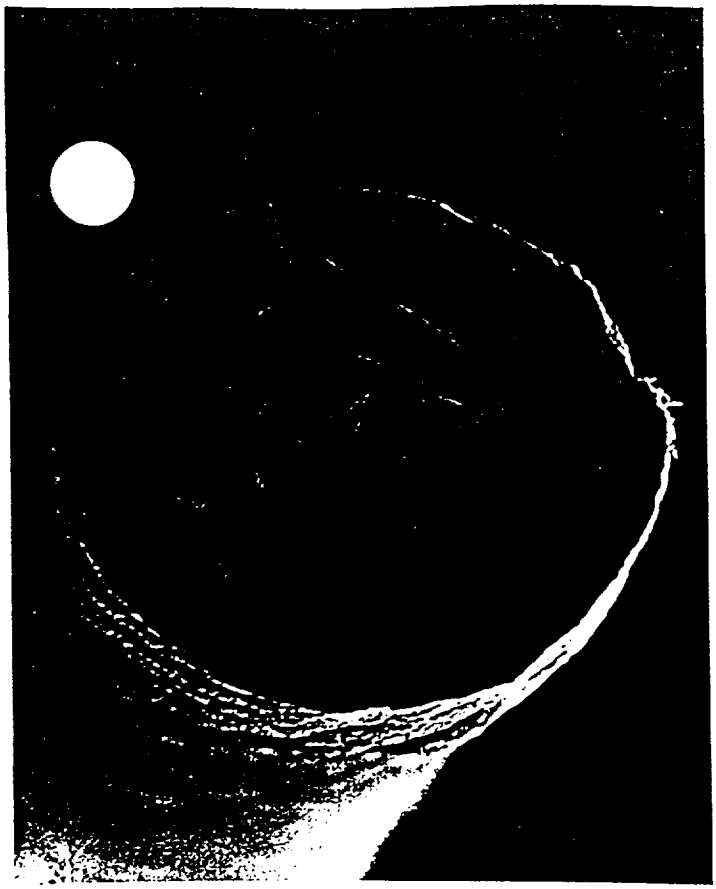

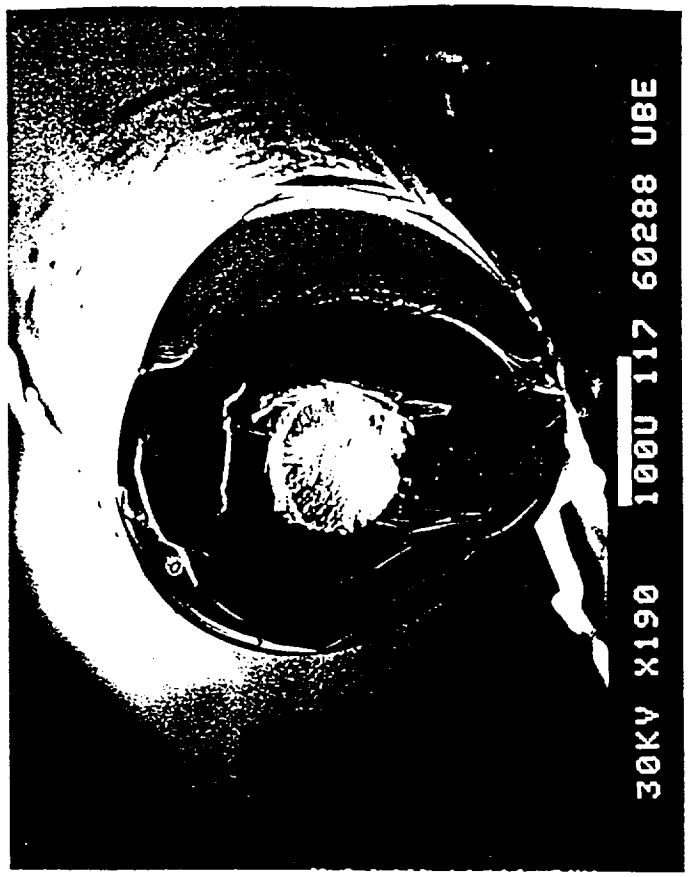

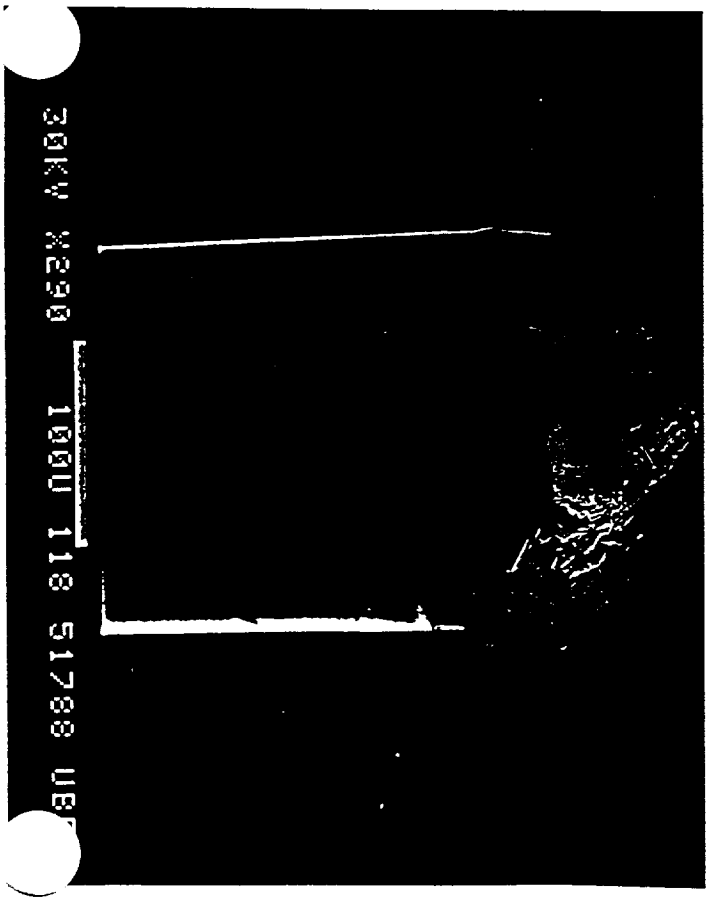

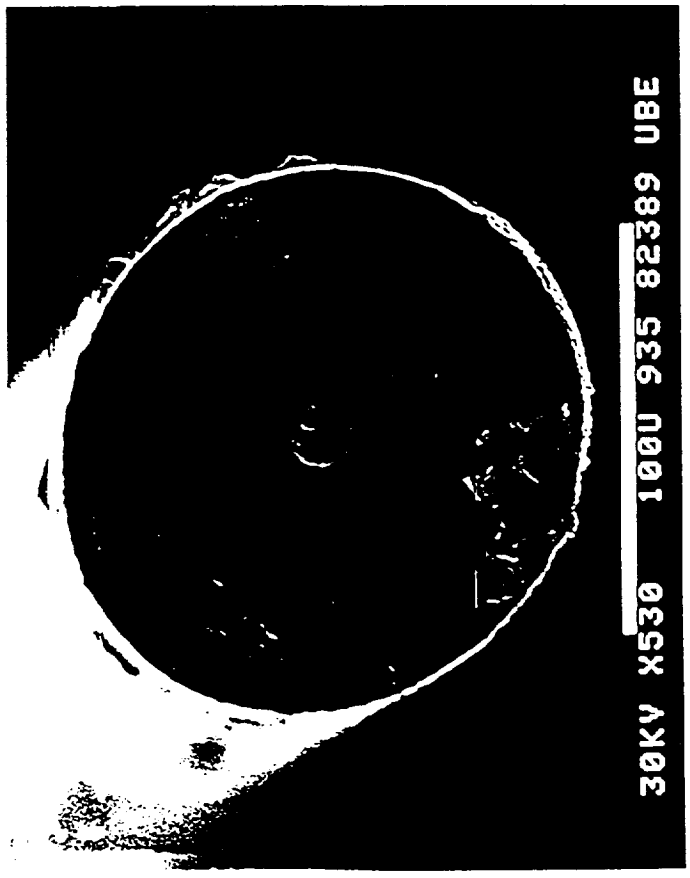

ORIGINAL PAGE IS
OF POOR QUALITY

TITANIUM DIBORIDE FIBERS

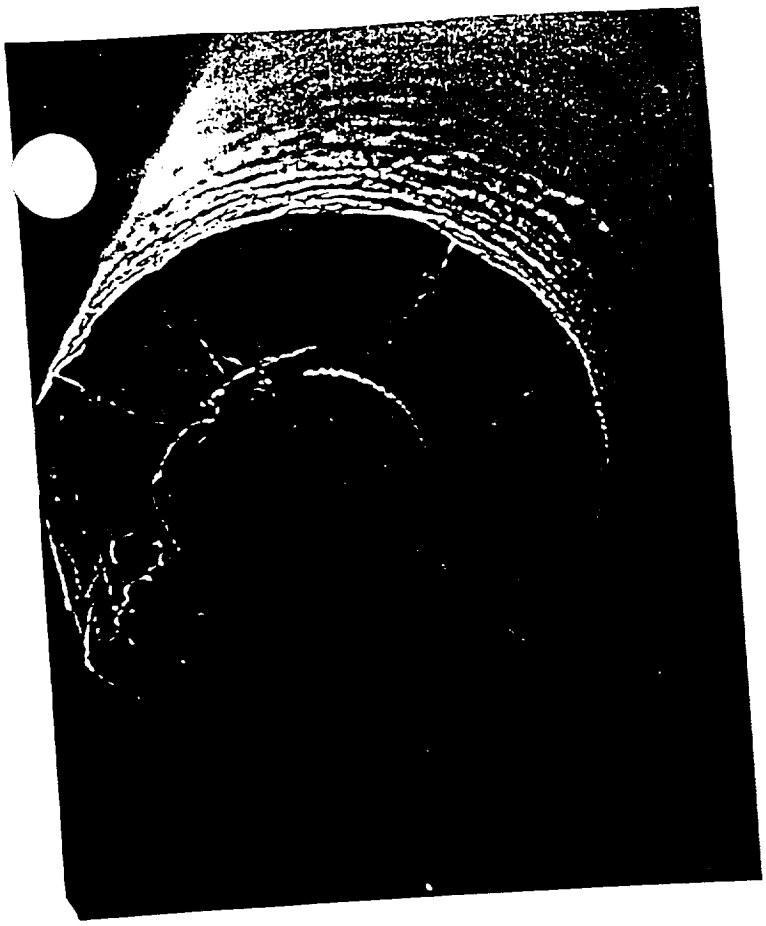

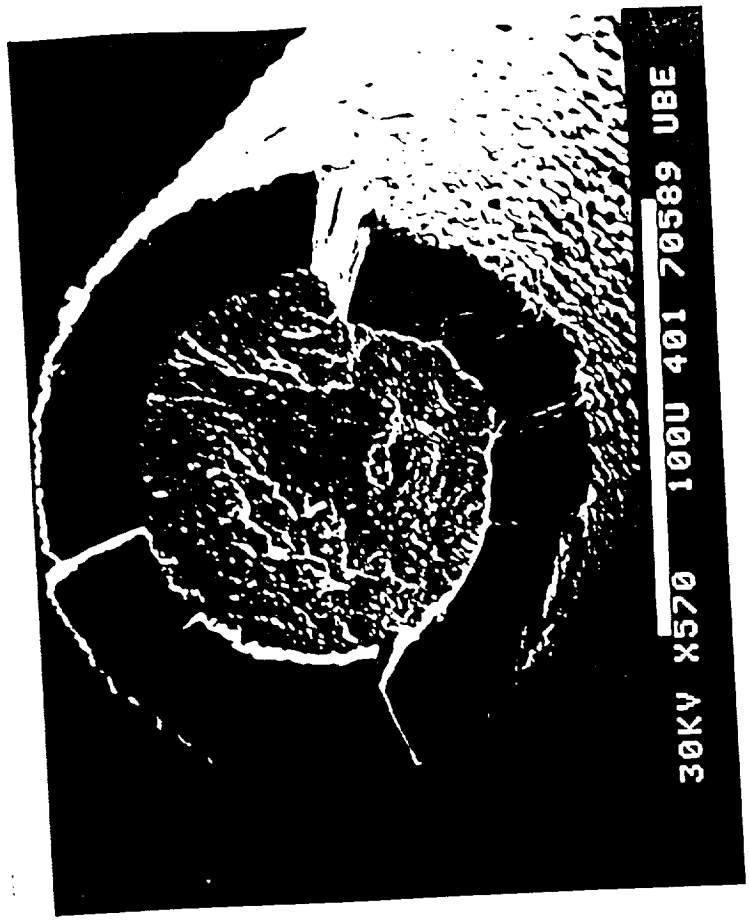

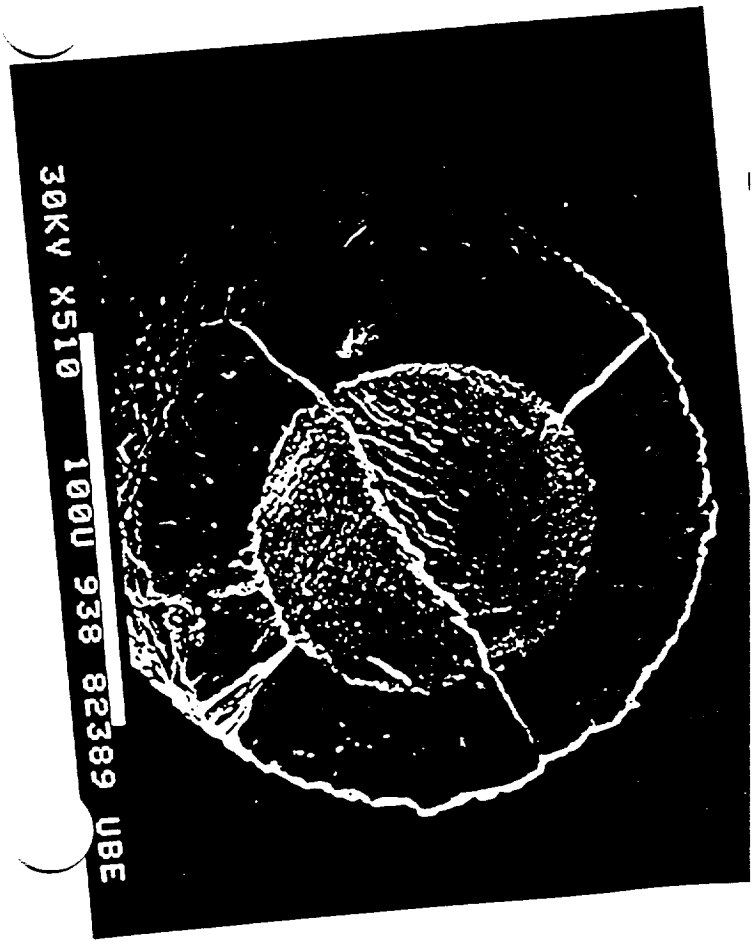

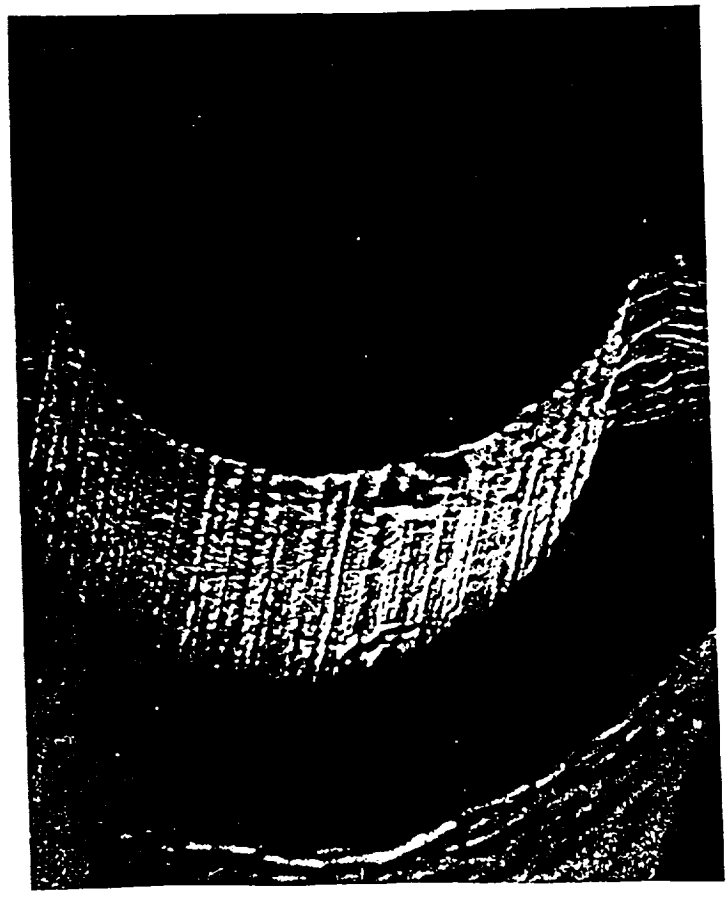

WITHOUT INTERMEDIATE LAYER

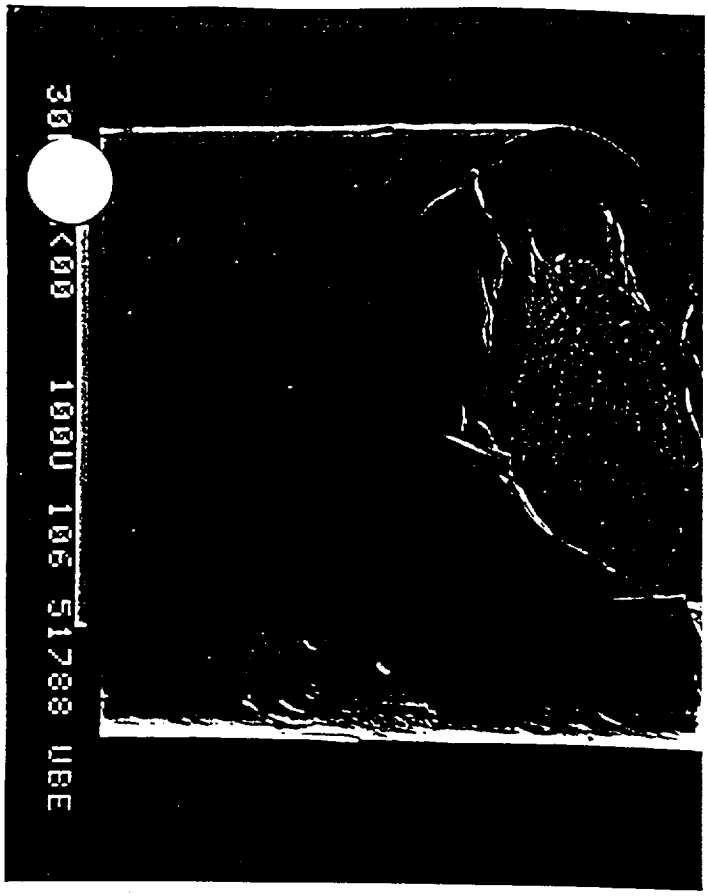

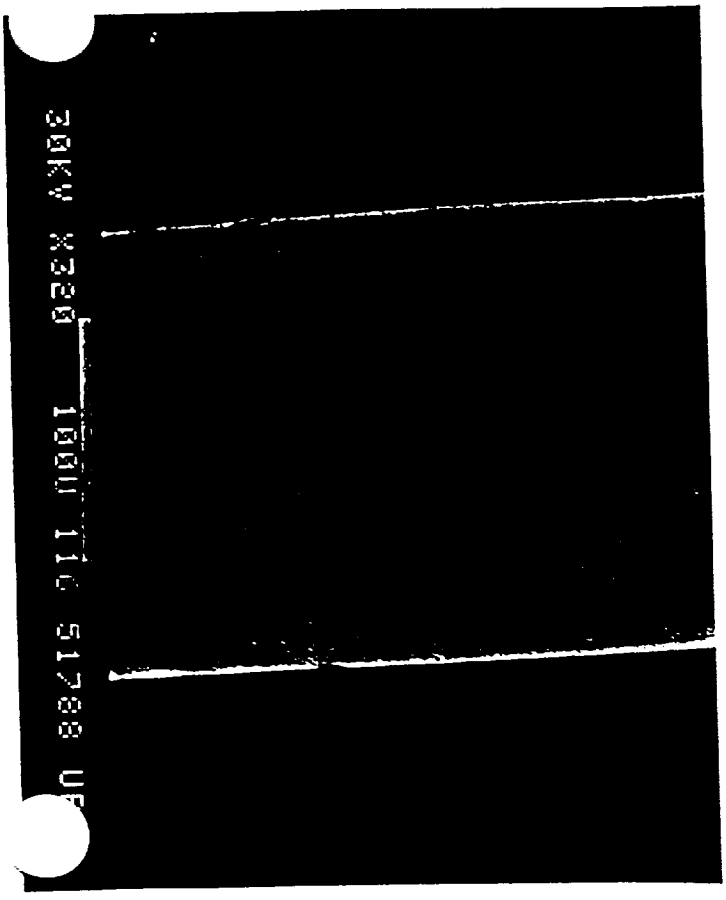

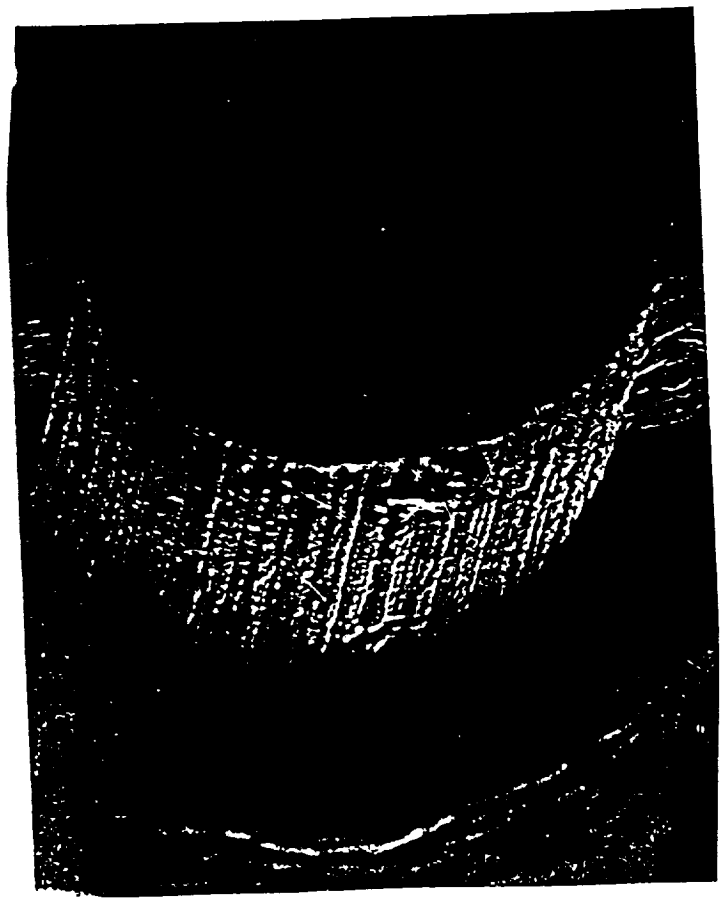

ORIGINAL PAGE IS
OF POOR QUALITY

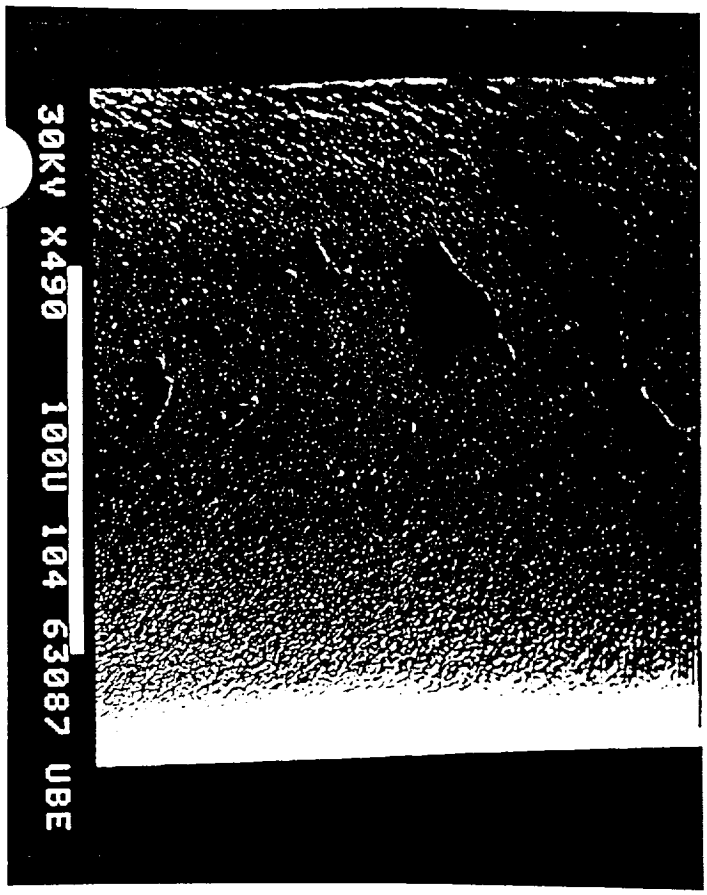

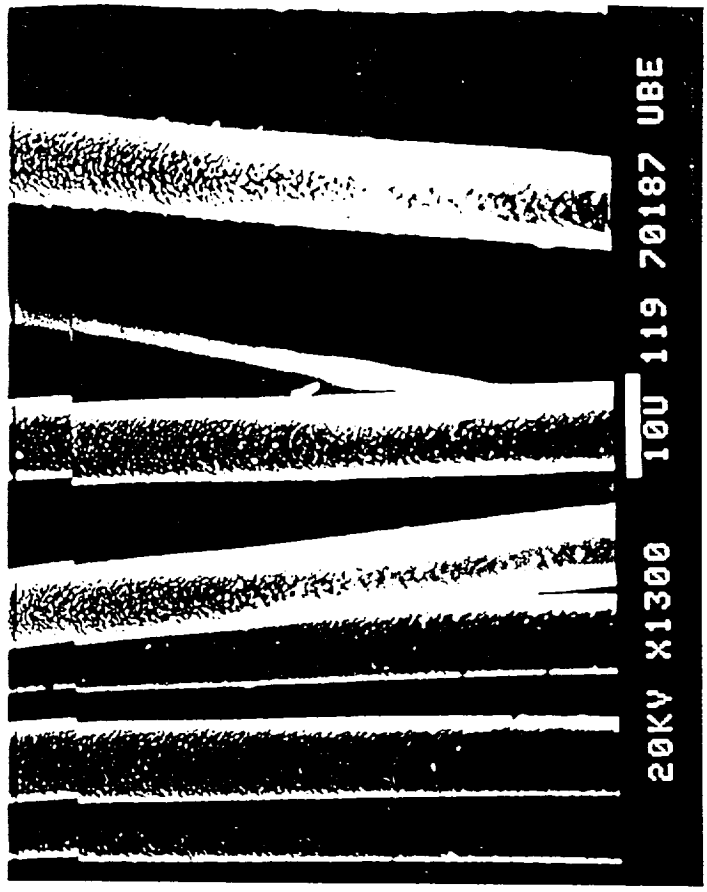

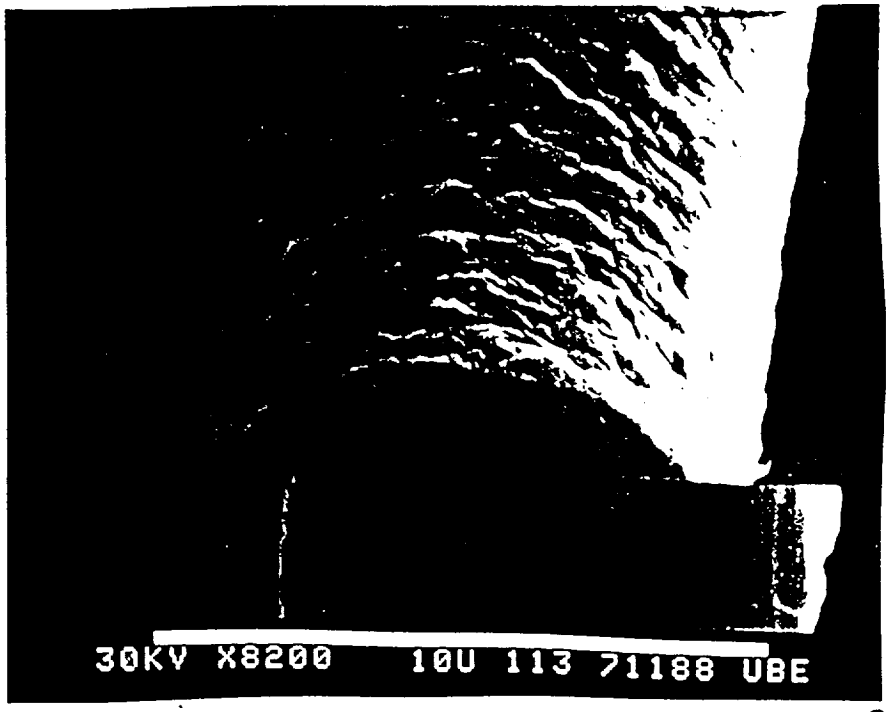

TiC FIBERS ON CARBON CORE

(a) $TiCl_4$ deposition with CCl_4 at 1200°C with C:Ti = 3; H:Cl = 7.5

(b) insitu conversion at 1300°C

(c) $TiCl_4$ + CCl_4 deposition at 1300°C with C:Ti = 3; H:Cl = 7.5

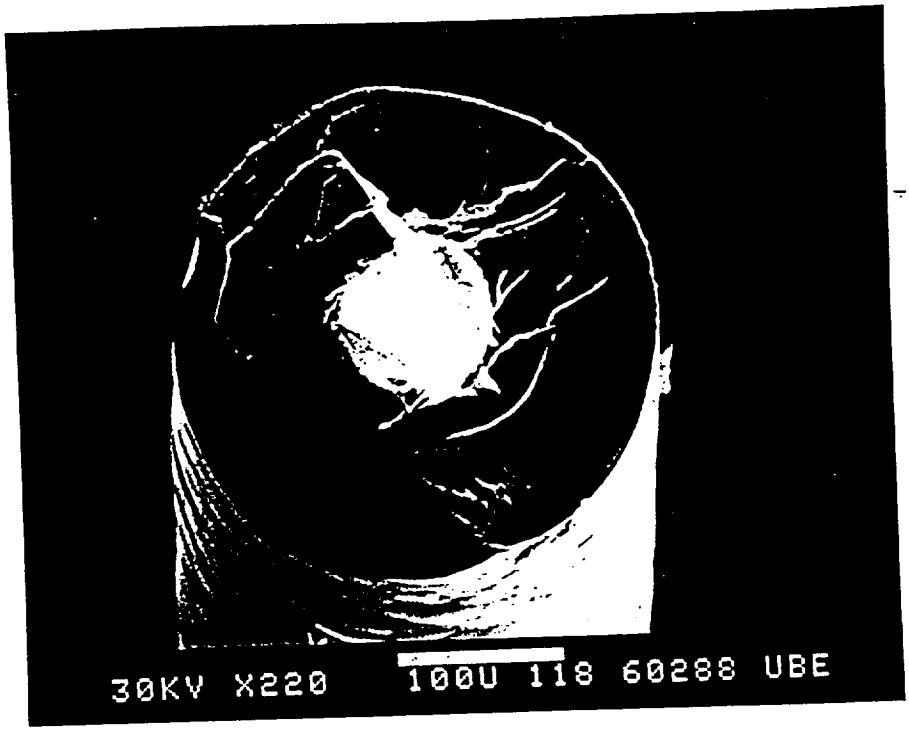

TiB_2 with graded deposition of carbon

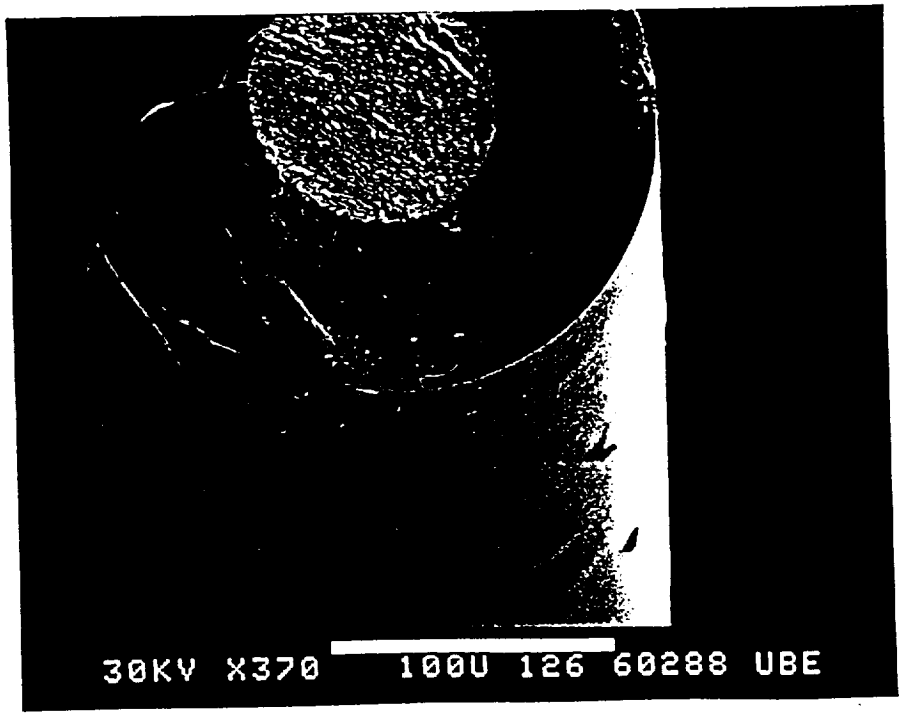

APPENDIX II

```
C-----------------------------------------------------------------C
C-----------------------------------------------------------------C
C       AUTHOR : VIKAS LAKHOTIA                                   C
C       DATE   : OCT., 1989                                       C
C-----------------------------------------------------------------C
C      THIS IS A PROGRAM USED TO CALCULATE THE THERMODYNAMIC      C
C      CONSTANTS a1..a7 FOR THERMODYNAMIC EQUILIBRIUM CALCULATION.C
C      THESE CONSTANTS ARE USED IN THE PROGRAM NASAF TO OBTAIN    C
C      EQUILIBRIUM COMPOSITION OF REACTING MIXTURES. THIS PROGRAM C
C      USES SEVERAL SUBROUTINES AVAILABLE IN IMSL LIBRARY         C
C-----------------------------------------------------------------C
```

APPENDIX II

```
      PROGRAM LSQ

      IMPLICIT DOUBLE PRECISION(A-H,O-Z)
      INTEGER    LDA, NOBS, NPARM, NEQNS, LDB, NB, NCA, NRA,LDC,
     *  NCZ,NCC,NRZ,NRC
      PARAMETER  (NOBS=8, NPARM=5, NEQN=3,LDA=NOBS*NEQN,
     *  LDB=NPARM,NB=NPARM,NCA=NPARM,NRA=NOBS*NEQN,
     *  LDZ=NOBS*NEQN,LDC=NPARM,NRZ=NOBS*NEQN,NCC=1,
     *  NCZ=1,NRC=NPARM,IPATH=1)
      REAL*8   A(LDA,NCA),B(LDB,NB),Y(LDA),Z(LDA,NCZ),
     * C(NPARM,NCC),D(NPARM),F(NPARM),X(NOBS),DHF,R,
     * Q(NOBS),S298,SQ(NOBS),SUM,SUM1
      CHARACTER*32 FILNAM
      EXTERNAL   DMXTXF,DMXTYF,DLSARG,DWRRRN

        write(*,*)'please enter the filename from which data is
     *  to be read'
        read(*,100) filnam
100     format(a32)
        open(13,file=filnam,status='old')
        open(14,file='lsq1.dat',status='unknown')
        ne=0
        R=8.314
```

APPENDIX II

```
C       R is the gas constant
        read(13,*) dhf
        read(13,*) S298
C       dhf is the heat of formation of a substance at 298 K.
C       S298 is the entropy at 298 K.
C       This loop reads the value of specific heat, entropy and
C       enthalpy at any temperature, t, and arranges them in a
C       column. It is used to calculate the five constants a1..a5.
C       It calculates the elements of the matrix on
C       the right hand side which when multiplied with the
C       constants give the specific heat, entropy or enthalpy.

        do 56 i=1,nobs
        read(13,*) x(i)
        t=x(i)
        read(13,*) y(ne+i)
C       Here y(ne +i) is the specific heat.
        y(ne+i)=y(ne+i)/R
        A(ne+i,1)=1.
        A(ne+i,2)=t
        A(ne+i,3)=t**2
        A(ne+i,4)=t**3
        A(ne+i,5)=t**4
```

```
      ne=ne+1
      read(13,*) y(ne+i)
C     Here y(ne+i) is the entropy.
      aa=y(ne+i)
      sq(i)=aa
      y(ne+i)=(y(ne+i)-S298)/R
      A(ne+i,1)=log(t/298.)
      A(ne+i,2)=t-298.
      A(ne+i,3)=(t**2-298.**2)/2.
      A(ne+i,4)=(t**3-298.**3)/3.
      A(ne+i,5)=(t**4-298.**4)/4.
      ne=ne+1
      read(13,*) y(ne+i)
C     Here y(ne+i) is the enthalpy
      aa=y(ne+i)
      q(i)=aa
      y(ne+i)=y(ne+i)*1000./R
      A(ne+i,1)=t-298.
      A(ne+i,2)=(t**2-298.**2)/2.
      A(ne+i,3)=(t**3-298.**3)/3.
      A(ne+i,4)=(t**4-298.**4)/4.
   56 A(ne+i,5)=(t**5-298.**5)/5.
      do 57 i=1,nobs*neqn
```

```
      aa=y(i)
57    z(i,1)=aa
C     The following loop makes all the elements of the matrix of the
C     same order.
      do 61 i=1,lda
      A(i,1)=A(i,1)
      A(i,2)=A(i,2)*1.0E-03
      A(i,3)=A(i,3)*1.0E-06
      A(i,4)=A(i,4)*1.0E-09
61    A(i,5)=A(i,5)*1.0E-12
C     The subroutine DMXTXF multiplies the transpose of the matrix
C     A with itself. The end result is a square matrix.
      CALL DMXTXF(NRA,NCA,A,LDA,NB,B,LDB)
C     All the dwrrrn subroutines are used to display the results
C     of the calculations on screen and can be omitted without
C     any difference to the results.
C     CALL DWRRRN('B=trans(A)*A',NB,NB,B,LDB,0)
C     The subroutine DMXTYF multiplies the transpose of A with Z.
C     This is done to maintain equality of the two sides.
      CALL DMXTYF(NRA,NCA,A,LDA,NRZ,NCZ,Z,LDZ,NRC,NCC,C,LDC)
C     CALL DWRRRN('C=trans(A)*B',NRC,NCC,C,LDC,0)
      do 58 i=1,nparm
      aa=c(i,1)
```

```
 58     d(i)=aa
C       This subroutine solves a system of linear equations.
C       It brings back the value of the constants a1..a5.
        CALL DLSARG(NPARM,B,LDB,D,1,F)
C       CALL DWRRRN('F',1,NPARM,F,1,0)
C       The following loop makes the elements of the correct magnitude
C       and corrects for the changing of order of magnitude earlier.
        a1=f(1)
        a2=f(2)*1.0E-03
        a3=f(3)*1.0E-06
        a4=f(4)*1.0E-09
        a5=f(5)*1.0E-12
C       The folowing lines calculates the value of a6 using the
C       enthalpy values.
        sum=0.
        do 92 i=1,nobs
        t=x(i)
        q(i)=(q(i)+dhf)*1000./R-a1*t-a2/2.*t**2-a3/3.*t**3-a4/4.
     *  *t**4-a5/5.*t**5
 92     sum=sum+q(i)
        a6=sum/nobs
C       The following lines calculate the value of a7 using the
C       entropy values.
```

APPENDIX II

```
      sum1=0.
      do 93 i=1,nobs
      t=x(i)
      sq(i)=sq(i)/R-a1*log(t)-a2*t-a3/2.*t**2-a4/3.*t**3-
     *  a5/4.*t**4
93    sum1=sum1+sq(i)
      a7=sum1/nobs
      write(14,41) a1,a2,a3,a4,a5
      write(14,42) a6,a7
41    format(5e15.8)
42    format(2e15.8)
      end
```

APPENDIX III

```
C-----------------------------------------------------------------C
C-----------------------------------------------------------------C
C       AUTHOR : VIKAS LAKHOTIA                                   C
C       DATE   : FEB.,1990                                        C
C-----------------------------------------------------------------C
C       THIS PROGRAM IS USED TO CALCULATE THE RESIDUAL STRESSES   C
C       ARISING IN A CVD FIBER DUE TO THERMAL EXPANSION MISMATCH  C
C       BETWEEN THE COATING AND THE CORE. THE TEMPERATURE USED IN C
C       THESE CALCULATIONS IS THE DIFFERENCE IN DEPOSITION        C
C       TEMPERATURE AND ROOM TEMPERATURE. IT ACCOUNTS FOR THE     C
C       ANISOTROPIC NATURE OF THE TiB2 COATING                    C
C-----------------------------------------------------------------C
```

APPENDIX III

```
      PROGRAM STRESS

      IMPLICIT DOUBLE PRECISION(A-H,O-Z)
      Open(11,File='input.dat',status='unknown')

C     E11, v11 and et11 are the Elastic modulus, Poissons ratio
C     and Thermal expansion of tungsten.
C     E12, v12 and et12 are the Elastic modulus, Poissons ratio
C     and Thermal expansion of titanium diboride parallel to c-axis.
C     E22, v22 and et22 are the Elastic modulus, Poissons ratio
C     and Thermal expansion of titanium diboride parallel to a-axis.
C     T is the deposition temperature.
C     p is the ratio of fiber diameter to core diameter.
C     Sa is the external stress applied.
C     b is the final fiber diameter.
C     r is the radial distance.
      Read(11,*) E11, v11
      Read(11,*) E12, v12
      Read(11,*) E22, v22
      Read(11,*) T, p, Sa
      et21=-0.205+5.959E-04*T+2.77E-07*T**2-4.369E-11*T**3
      et22=-0.118+3.092E-04*T+2.806E-07*T**2-3.996E-11*T**3
      et11=-4.3E-03+4.266E-04*(T-293)+8.479E-08*(T-293)**2
```

APPENDIX III

```
      $ -1.974E-11*(T-293)**3
C       A negative sign is used in the folowing equations since
C       the fiber is being cooled. A factor of 0.01 is used as
C       the reported values of thermal expansion are in percantage.
        et121=-0.010*(et11-et21)
        et122=-0.010*(et11-et22)
       AA1=E11**2*E22*et122 - E11*E21*E22*et122- E11**2*E22*et122*p**2+
      -  2*E11*E21*E22*et122*p**2 - E11*E21*E22*et122*p**4 -
      -  E11*E21*E22*et121*v1 + 2*E11*E21*E22*et121*p**2*v1 -
      -  E11*E21*E22*et121*p**4*v1 + E11**2*E22*et121*v21 -
      -  E11**2*E22*et121*p**2*v21 +  Sa*(-(E11*E22*p**2*v1) +
      -   E11*E22*p**4*v1 + E11*E22*p**2*v21 - E11*E22*p**4*v21)
       CC1=E11**2*E21*et121 - E11*E21*E22*et121 + 2*E11*E21*E22*et121*
      -  p**2 - E11**2*E21*et121*p**4 - E11*E21*E22*et121*p**4 +
      -  E11*E21*E22*et121*v1 - 2*E11*E21*E22*et122*v1 -
      -  2*E11*E21*E22*et121*p**2*v1 + 4*E11*E21*E22*et122*p**2*v1 +
      -  E11*E21*E22*et121*p**4*v1 - 2*E11*E21*E22*et122*p**4*v1 +
      -  2*E11**2*E21*et122*v21 - 2*E11**2*E21*et122*p**2*v21 -
      -  E11**2*E21*et121*v22 + 2*E11**2*E21*et121*p**2*v22 -
      -  E11**2*E21*et121*p**4*v22 +
      -  Sa*(E11**2*p**2 - E11*E22*p**2 + E11**2*p**4 + E11*E22*p**4 +
      -  E11*E22*p**2*v1 - E11*E22*p**4*v1 + 2*E11*E22*p**2*v1*v21 -
      -  2*E11*E22*p**4*v1*v21 - 2*E11**2*p**2*v21**2 -
```

APPENDIX III

```
-  E11**2*p**2*v22 +   E11**2*p**4*v22)
 DET=E11**2 - E11*E21 - E11*E22 + E21*E22 + E11**2*p**2 +
-  E11*E22*p**2 - 2*E21*E22*p**2 + E11*E21*p**4 + E21*E22*p**4 +
-  E11*E22*v1 -  E21*E22*v1 - E11*E22*p**2*v1 +
-  2*E21*E22*p**2*v1 -  E21*E22*p**4*v1 -
-  2*E21*E22*v1**2 + 4*E21*E22*p**2*v1**2 - 2*E21*E22*p**4*v1**2+
-  2*E11*E21*v1*v21 + 2*E11*E22*v1*v21 - 2*E11*E21*p**2*v1*v21 -
-  2*E11*E22*p**2*v1*v21 - 2*E11**2*v21**2 - E11**2*v22 +
-  E11*E21*v22 + E11**2*p**2*v22 - 2*E11*E21*p**2*v22 +
-  E11*E21*p**4*v22
    A1=AA1/DET
    C1=CC1/DET
    C2=C1/(1-p**2)+Sa*p**2
    A2=A1/(1-p**2)
    Sr1=A1
    St1=A1
    Sz1=C1
    Sz2=C2

    write(*,*) 'CORE STRESSES'
    write(*,*) 'Radial Stress=Theta Stress'
    write(*,10) Sr1
    write(*,*) 'Axial Stress='
```

APPENDIX III

```
      write(*,*) Sz1
      write(*,*) 'COATING STRESSES'
      write(*,*) 'Radial Stress= (1-(b/r)**2)*'
      write(*,10) A2
      write(*,*) 'Theta Stress= (1+(b/r)**2)*'
      write(*,10) A2
      write(*,*) 'Axial Stress='
      write(*,10) Sz2
10    format(2x,e16.8)
      end
```

Appendix-III

Graphical representations

13.2 chromium Diboride Fibers

In the deposition of chromium in the form of a thin film on an inert substrate many different precursors have been used.The main aim beeing to get the chromium in the gas phase at a relatively low temperature.The most important were the following.

1. $CrCl_2$ [1]
2. Cr_2O_3 [2]
3. $Cr(CO)_6$ [3]
4. Cr_2S_3

Considering these and others the most appealing,considering availability and toxicity,were the following.

Precursor	Melting point(C)	Boiling point(C)
CrO_2Cl_2	-96.5	117
$Cr(CO)_6$	83	210
$CrCl_3$	1150	1300

Chromyl Chloride as precursor

In comparing the different compounds the use of chromyl chloride seemed very attractive because of its low melting point.As this compound had not been used in any previous research it was of major interest to us to see how it would behave combined with the carrier gas H_2 and the secondary reaction component BCl_3.Hopefully it would be possible to deposit a pure film of CrB_2 on our inert surface according to the overall equation :

$$CrO_2Cl_2 + H_2 + BCl_3 = CrB_2 + HCl + ... \quad (1)$$

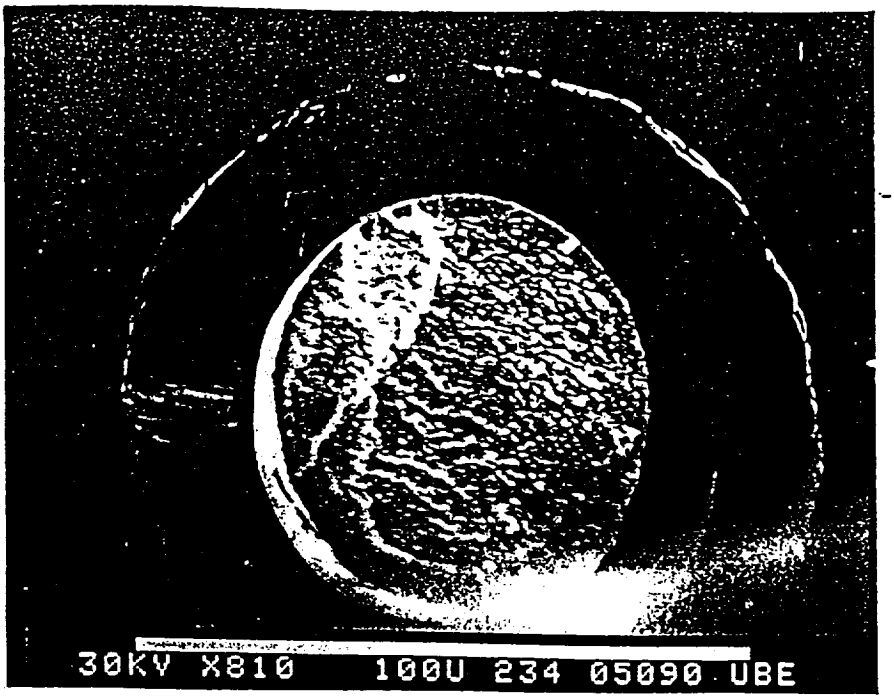

Carbon layer 5 μm

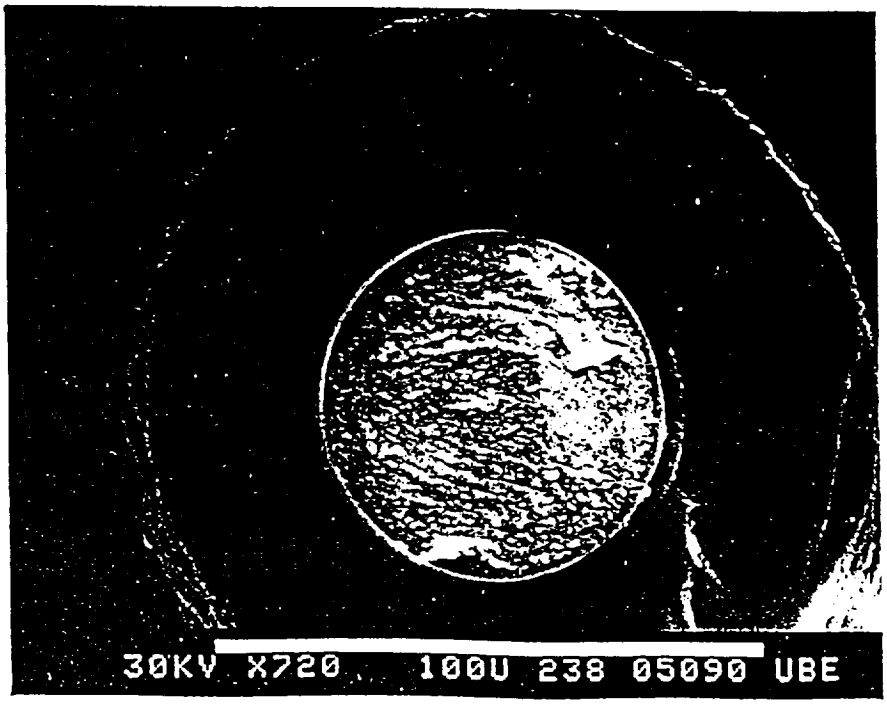

1273°K $\alpha = 110$ $\beta = 5$

Samples with intermediate layer of carbon.

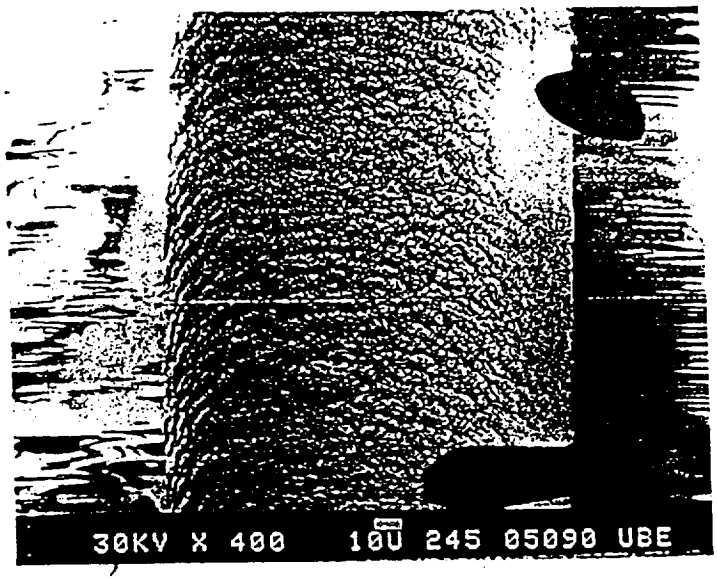

1240°K $\alpha = 110\ \beta = 5$

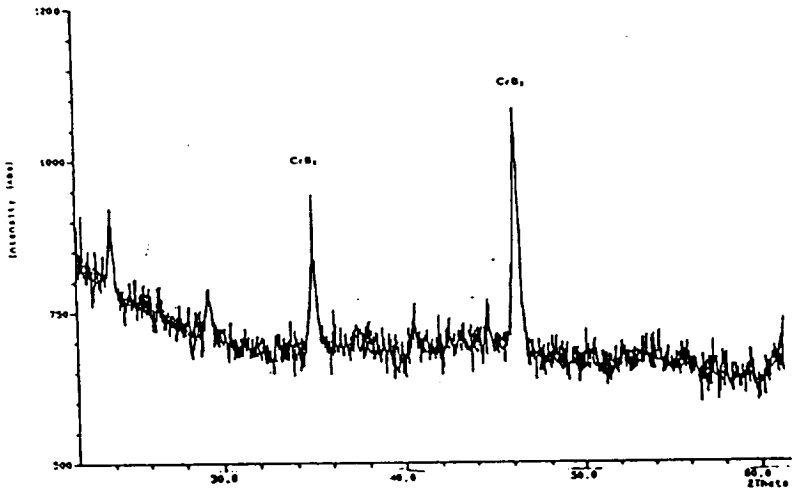

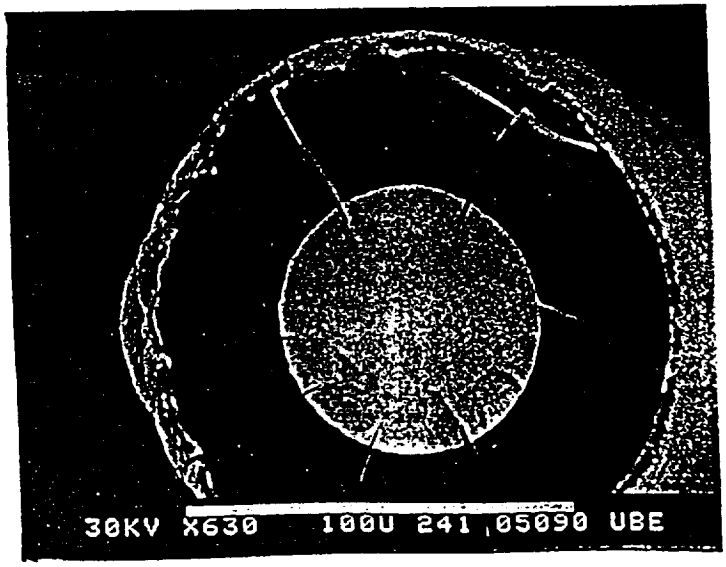

1273°K $\alpha = 110\ \beta = 5$

SEM photographs at α=110,β=5 with X-ray result.

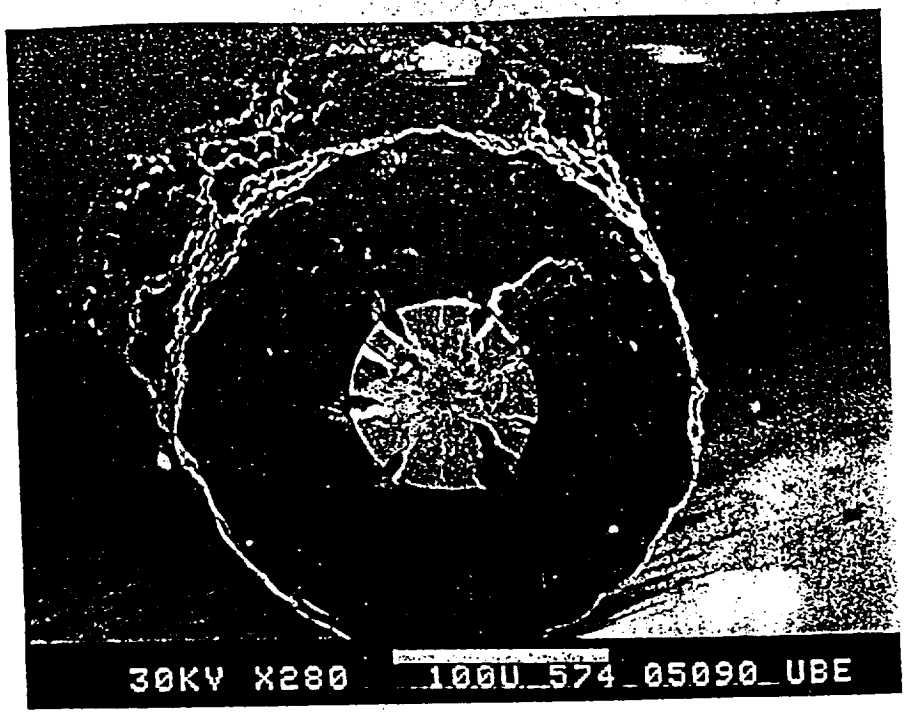

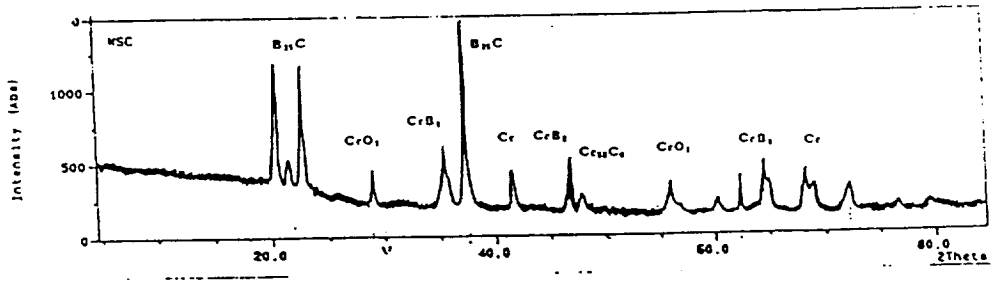

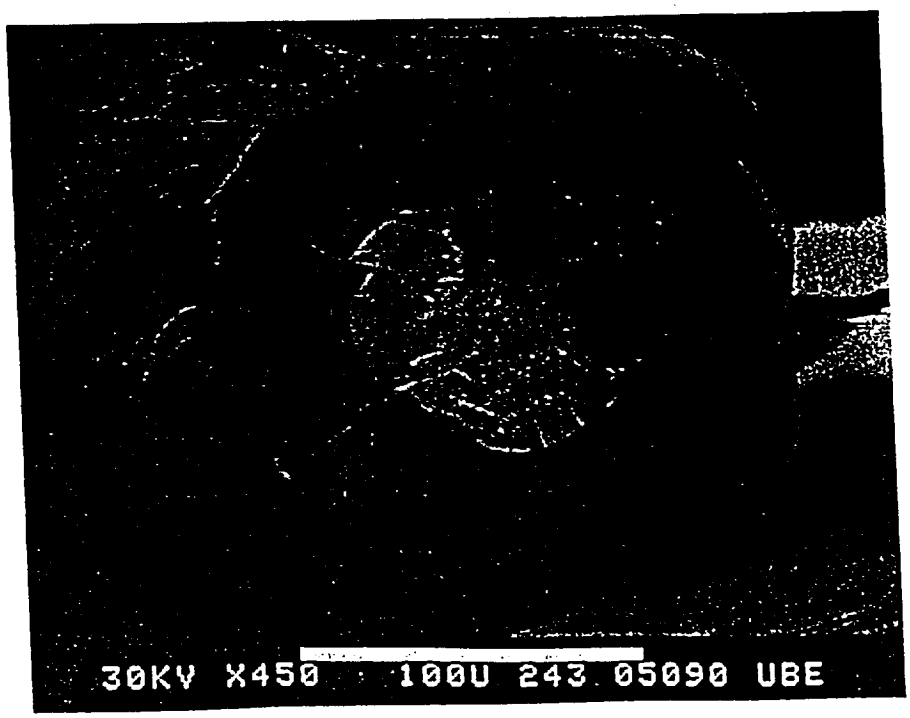

SEM and X-ray for $Cr(CO)_6$ deposition sample.

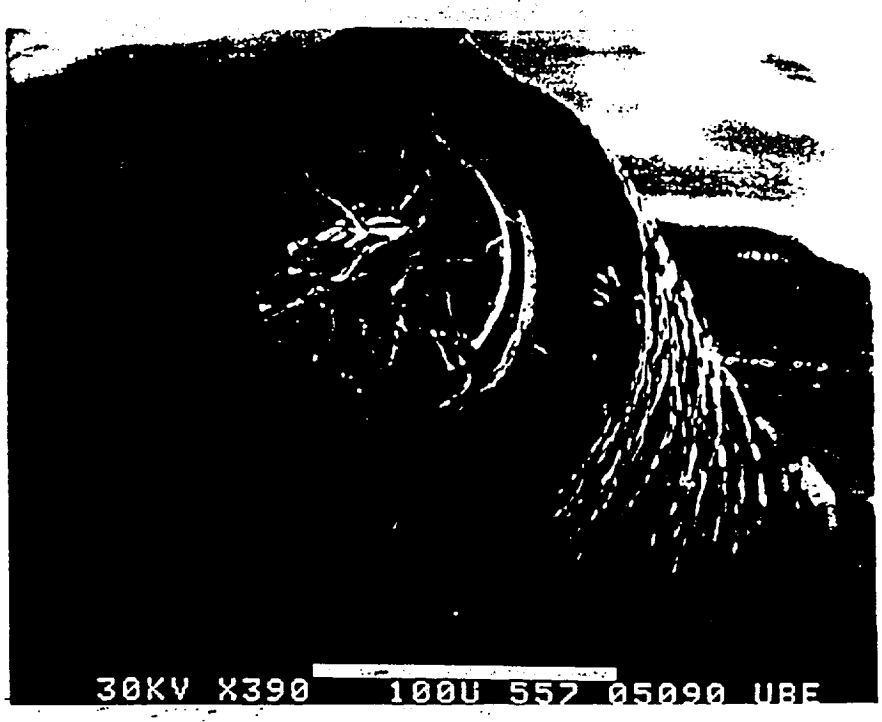

T = 1323°K

α = 110

β = 5

D = 164 μm

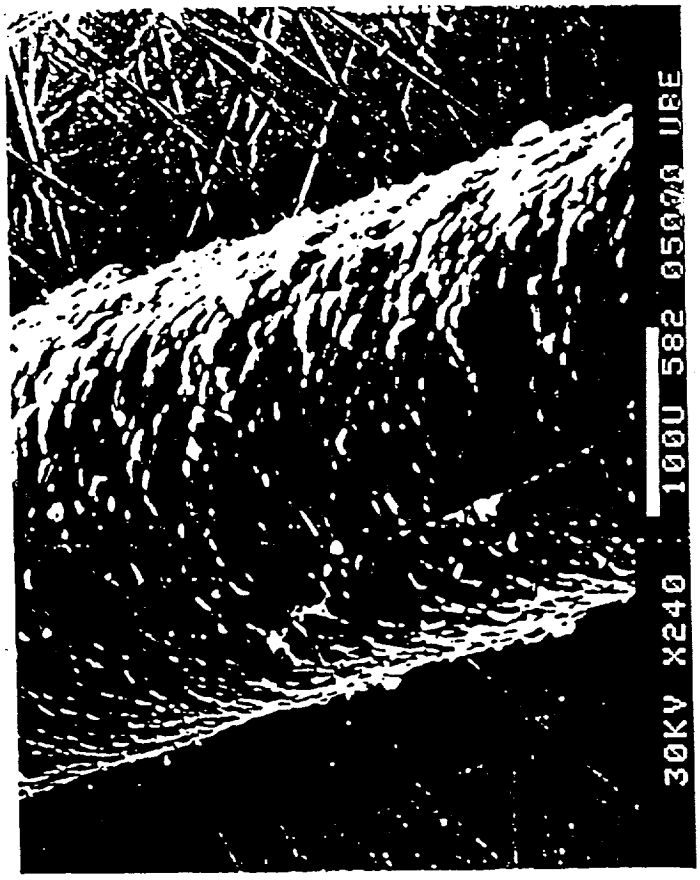

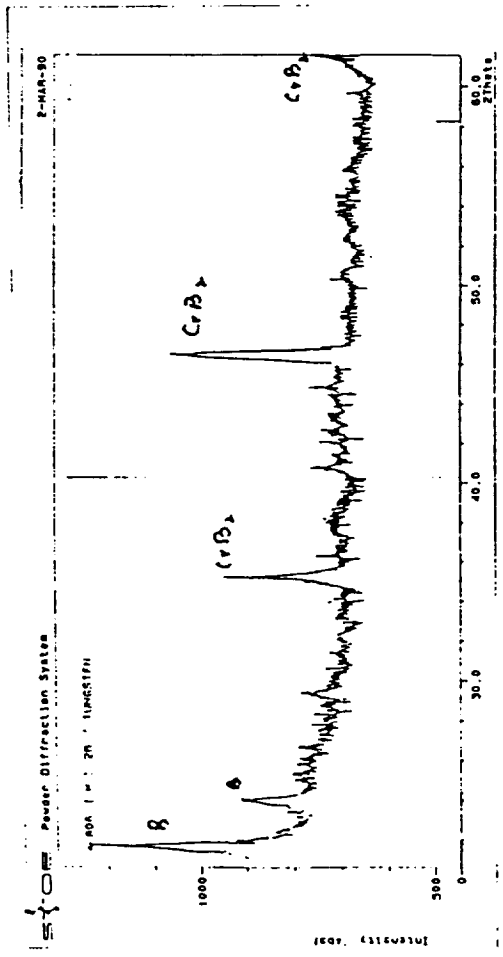

T = [illegible]

α = 110

β = 5

D = 209 μm .

Surface is quite smooth except [illegible]

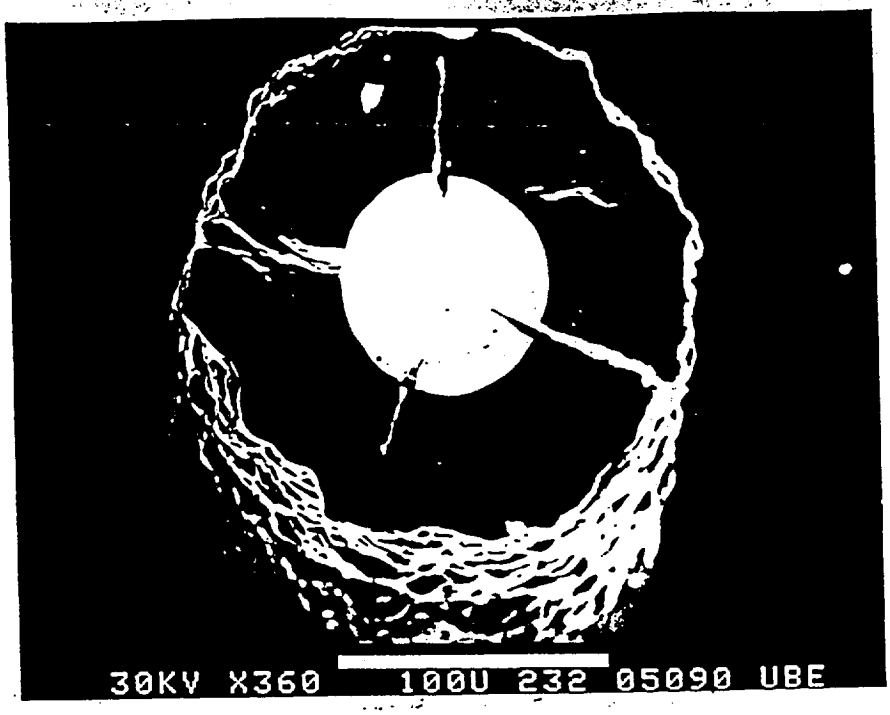

1480 K
α = 110
β = 5

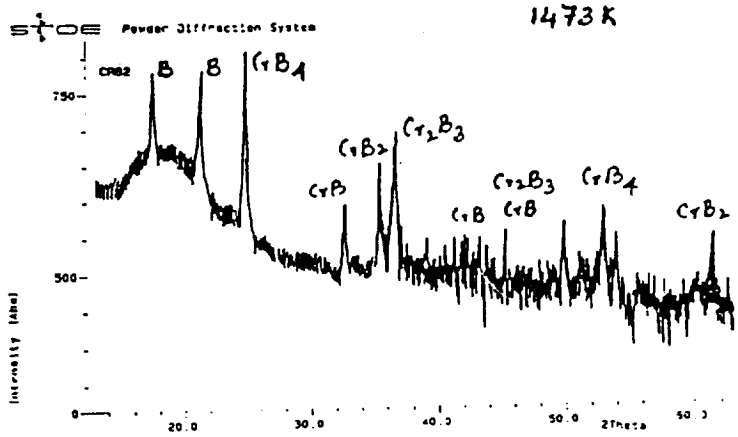

1473° K
α = 110
β = 5

Fig 8. Cont:

T = 1273°K

$\alpha = 150$

$\beta = 8$

D = 190 μm

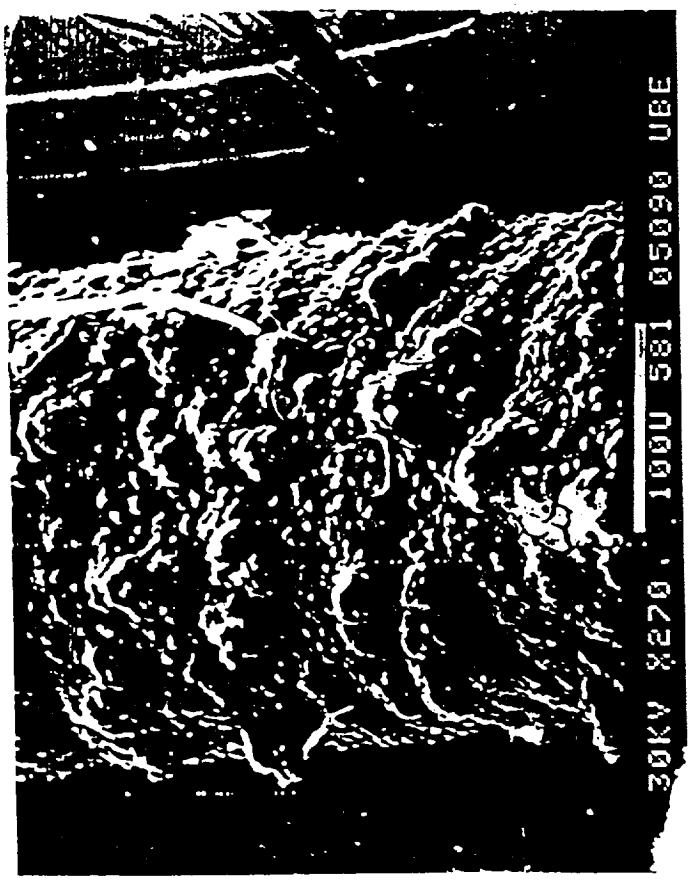

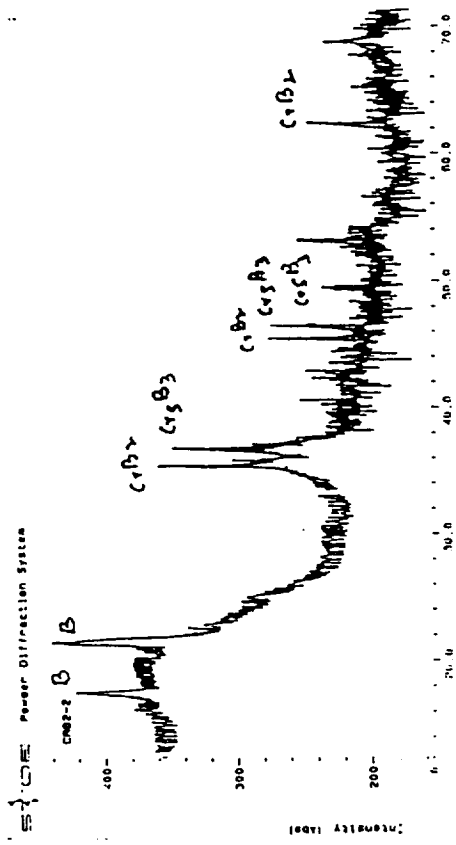

D = 239 μm

$\alpha = 150$

$\beta = 8$

T = 1433°K

When there is more boron, dendritic growth is more accelerated.

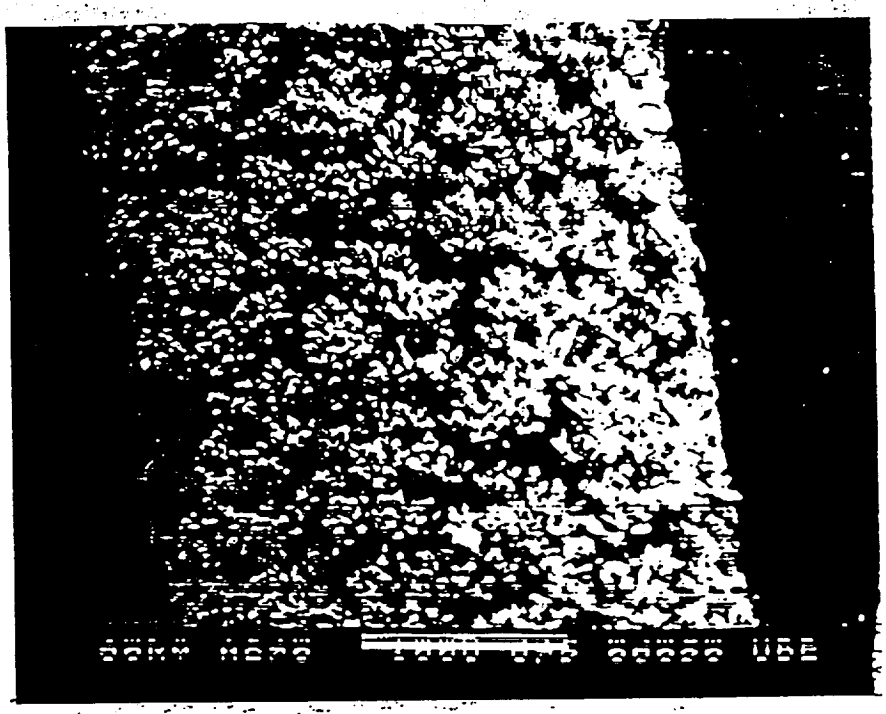

T = 1523 K
α = 110
β = 5
D = 290 μm

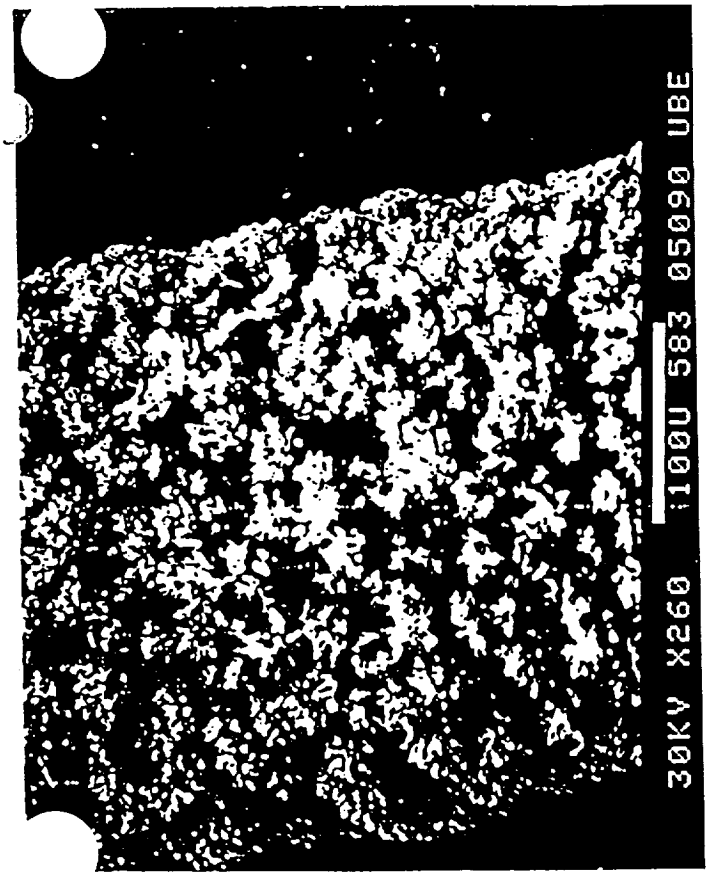

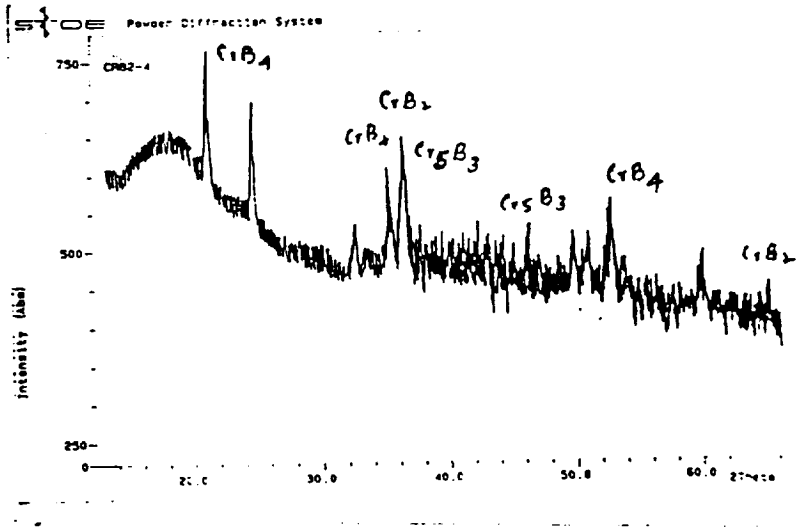

T = 1553 K
α = 110
β = 5
D = 309 μm.

As the temperature increases, the secondary grain is more dendritic. This increases with temperature at same α & β. This may be the [illegible] effect of impurities even though we didn't detect any in X-ray.

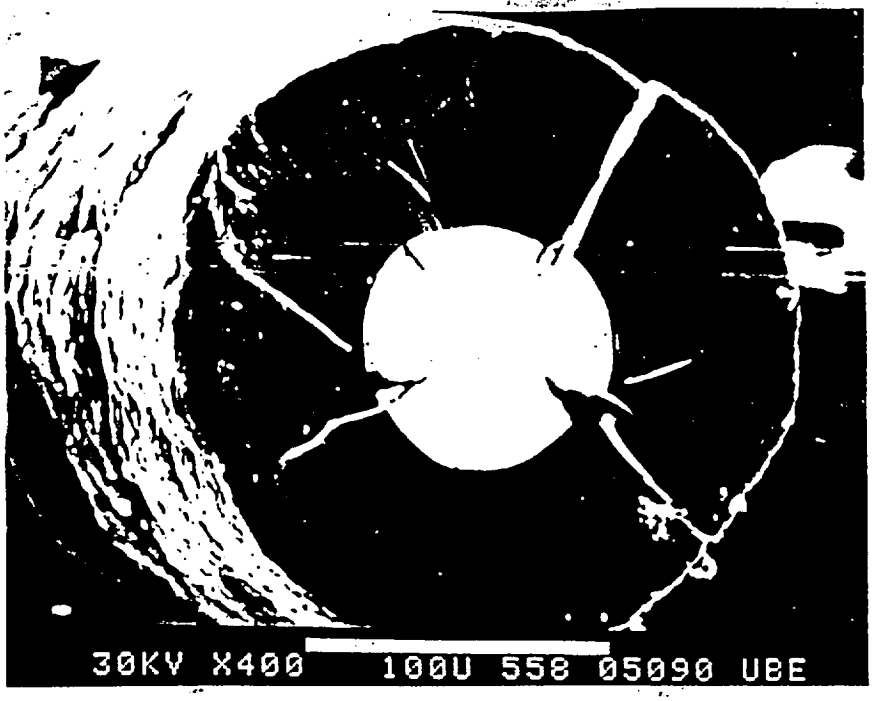

T = 1373 K

α = 110

β = 5

D = 205 μm

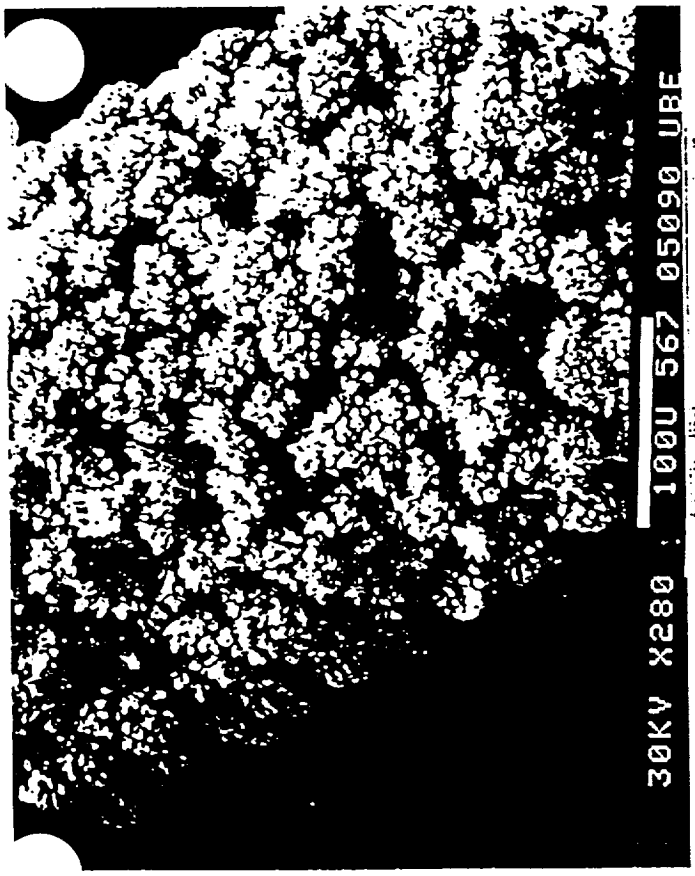

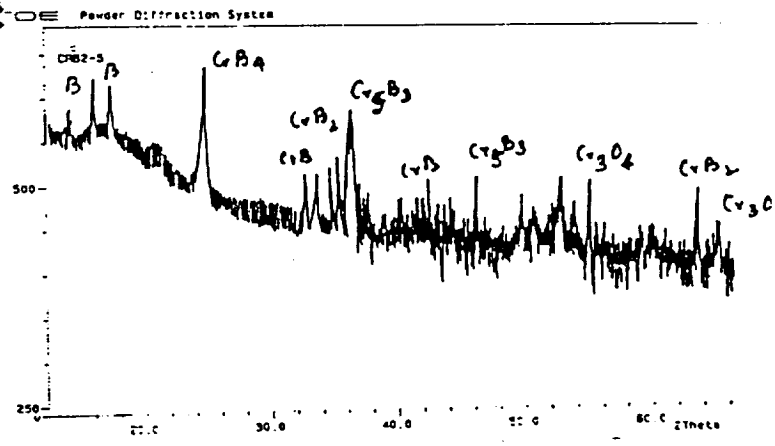

T = 1553 K

α = 110

β = 5

D = 309 μm

High temperature shows some oxides in the deposit.

Structure is showing dendritic growth right from the begining

T = 1273°K

$\alpha = 50$

$\beta = 3$

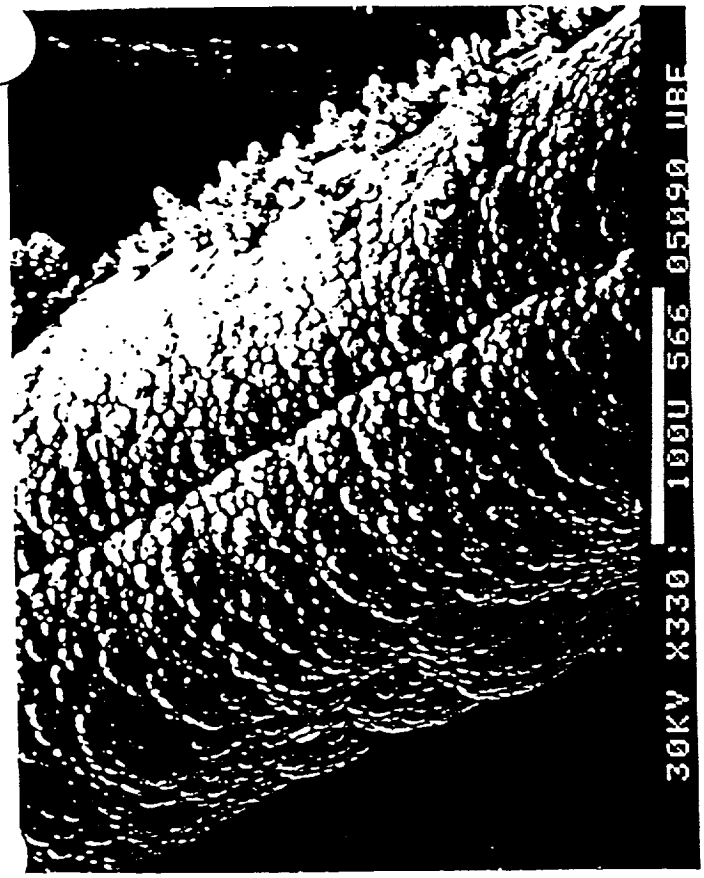

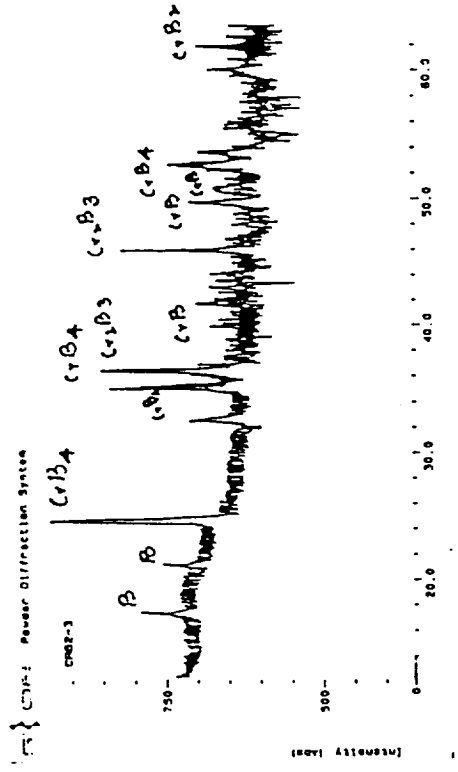

$\alpha = 50$

$\beta = 3$

T = 1373 K

Fiber shows some uneven growth

[illegible] to lot of free boron in the deposit.

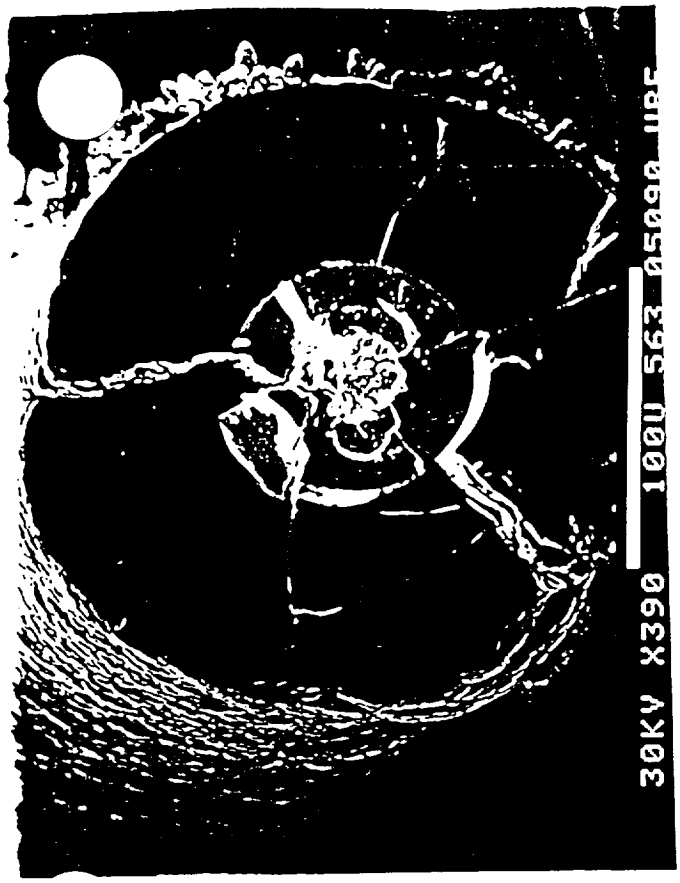

α=150 T=1373°K D=207 μm
β=5

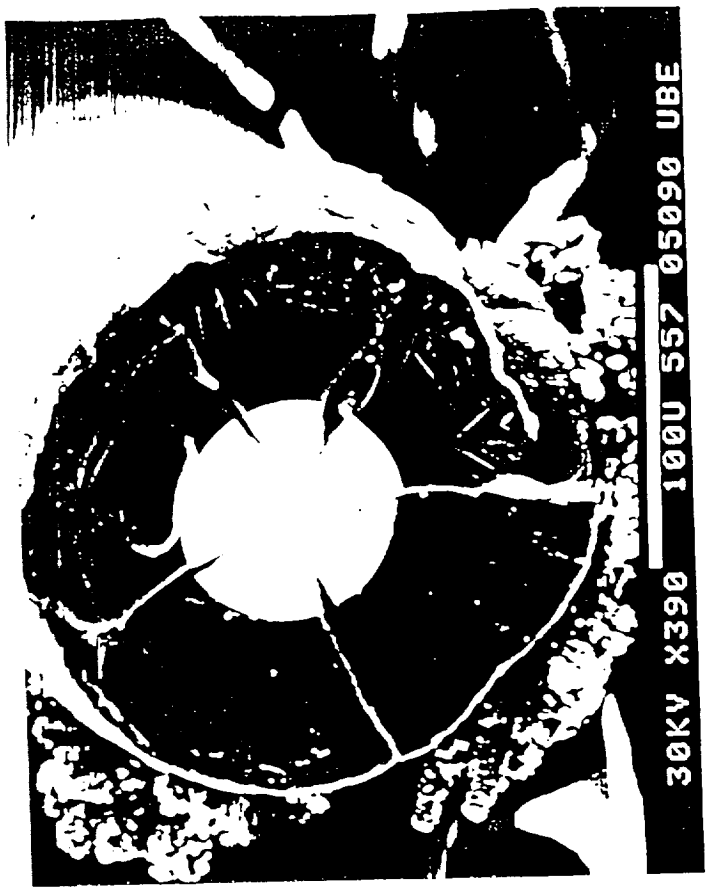

α=110 T=124[illegible]°K D=[illegible] μm
β=5

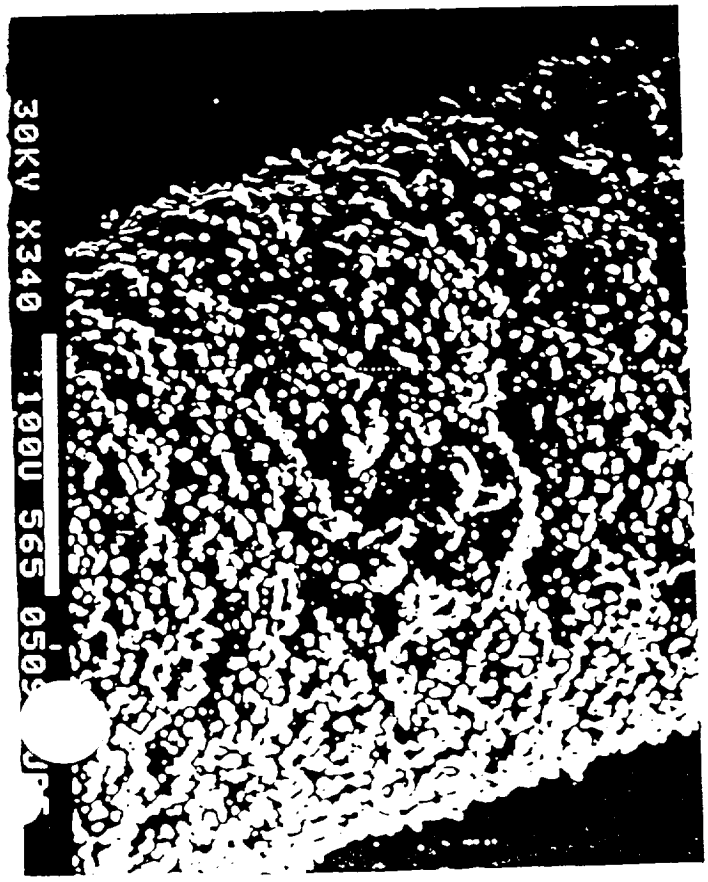

ORIGINAL PAGE IS
OF POOR QUALITY

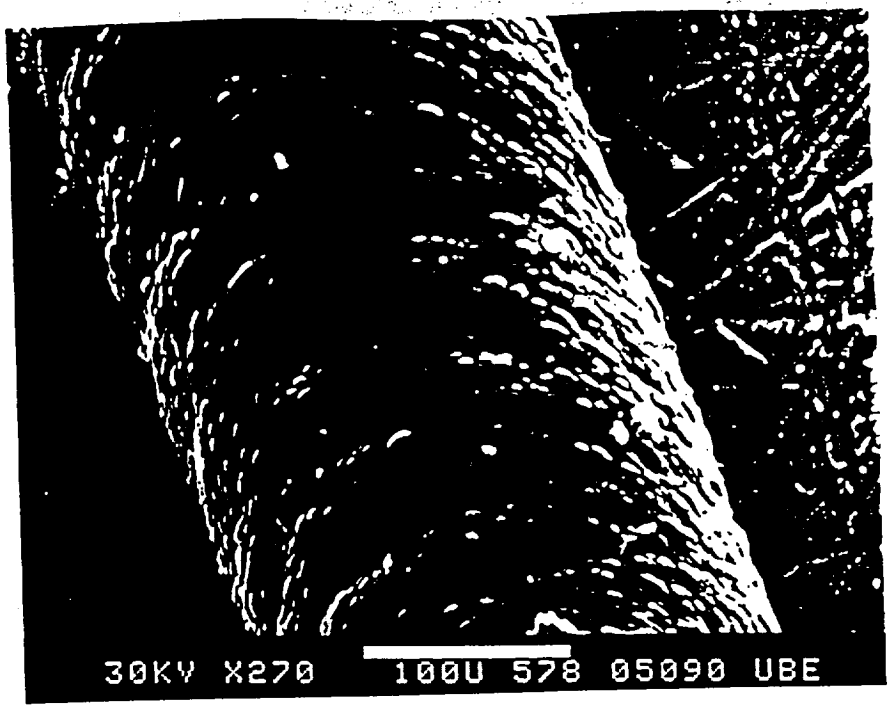

239 μm

1323°K

D = 239 μm

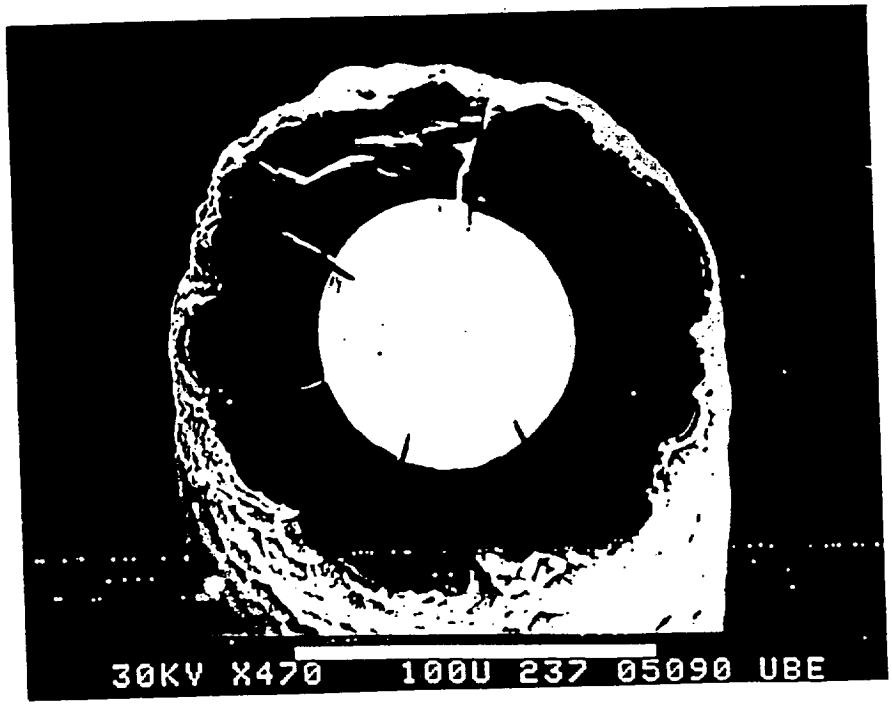

T = 1353°K

D = 144 μm.

α = 50

β = 3

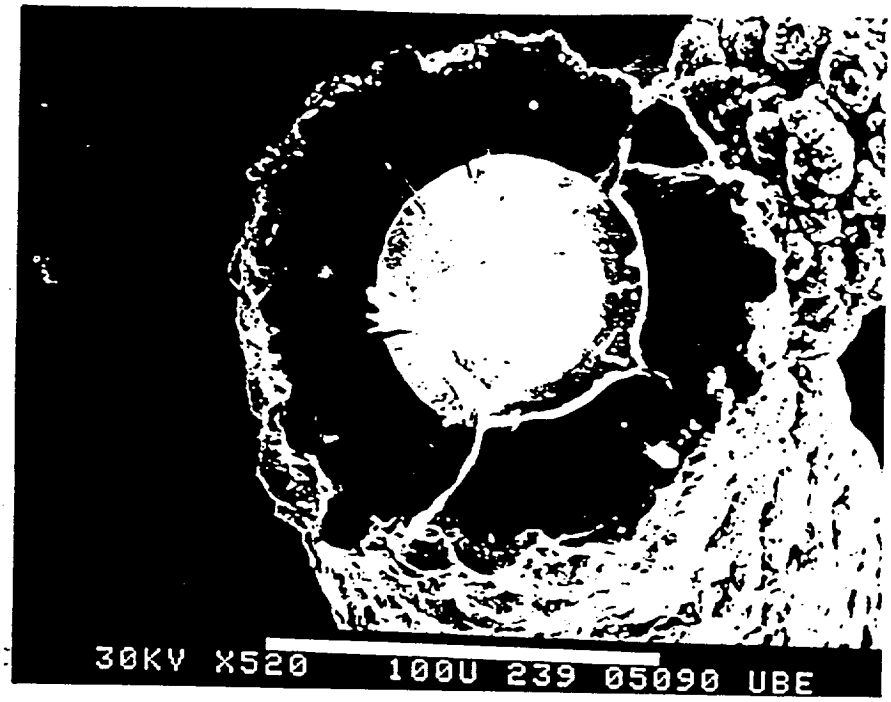

$T = 1423^{\circ}K$ $D = 127\,\mu m$

$H_2 / Cr(CO)_6 = 100$

$BCl_3 / Cr(CO)_6 = 5$

Due to presence of carbides and oxides, as impurities, secondary growth takes place as a globules. Even though there is change in flow phenomenon (slight increase in Re no) the impurity effect is the main cause for this growth.

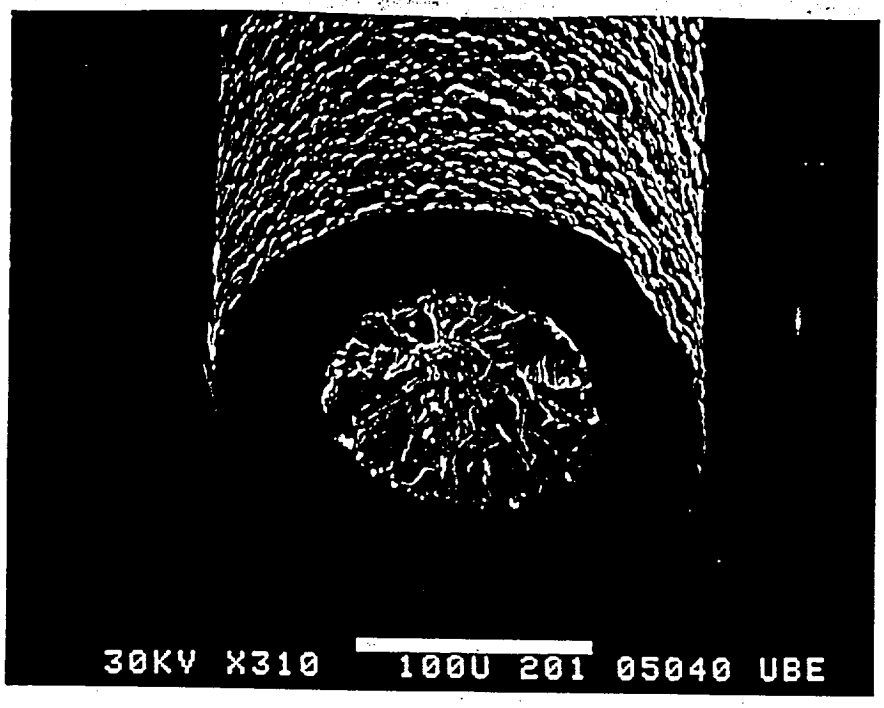

CrO_2U_2
1200°C

Crystal orienta
Just like Ti

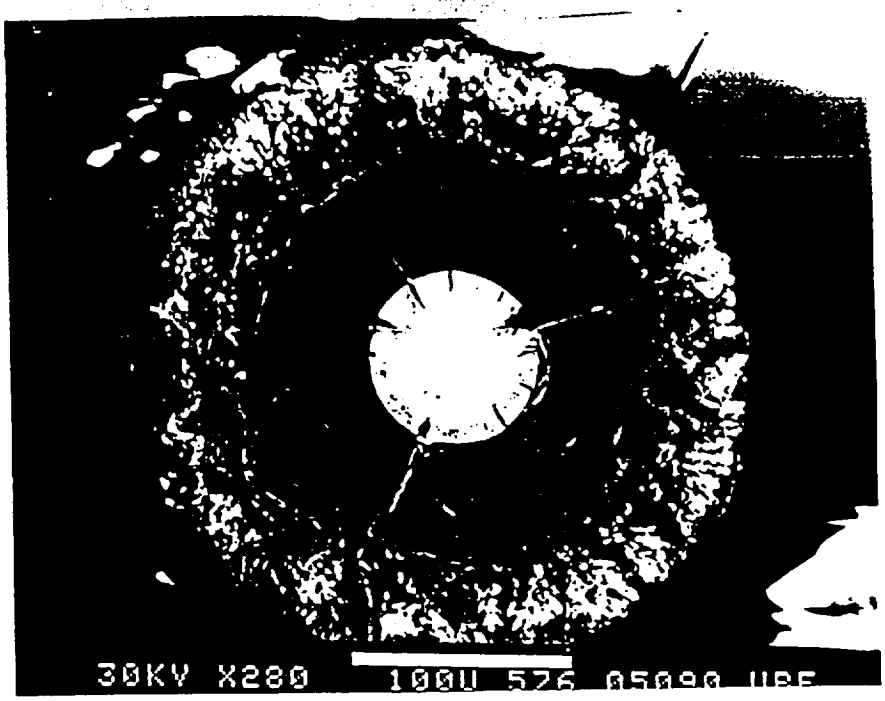

T = 1523 K
α = 50
β = 3

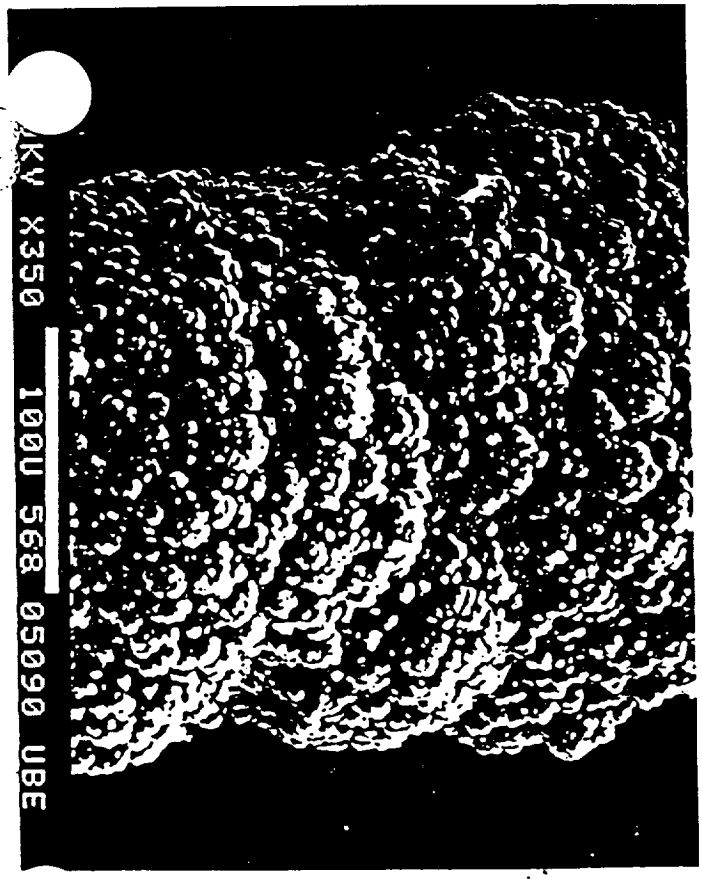

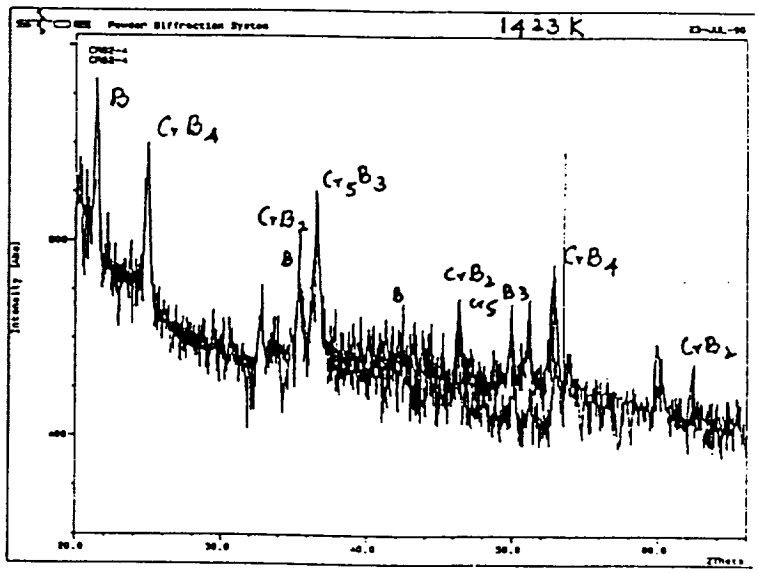

T = 1423 K
α = 150
β = 8

Figure 9. SEM photographs at different α and β ratios.

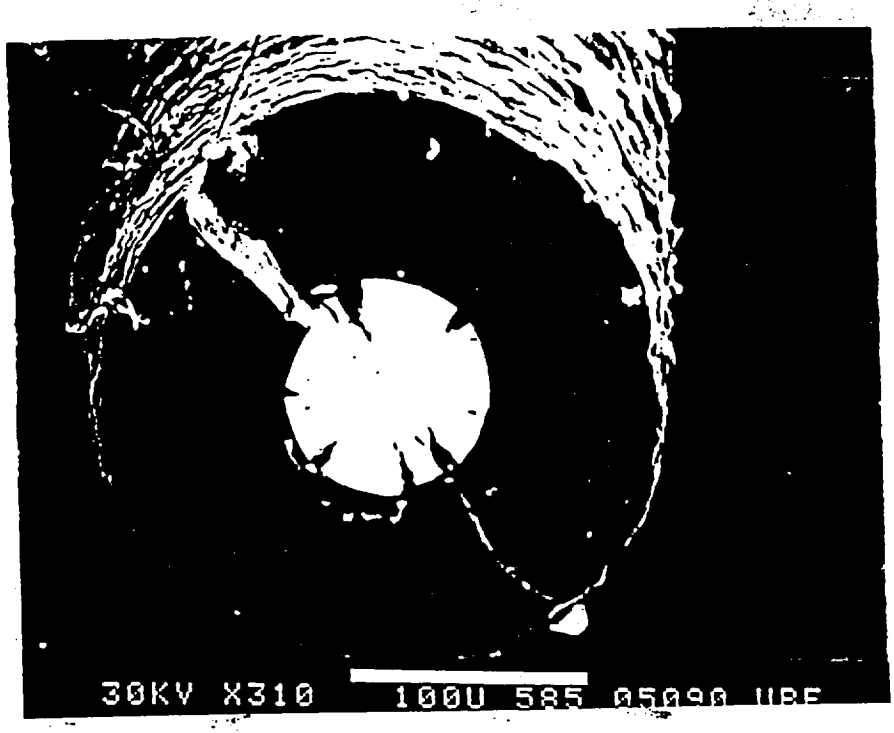

T: 1373 K

$\alpha = 110$

$\beta = 5$

D = 235 μm

10μm intermediate layer

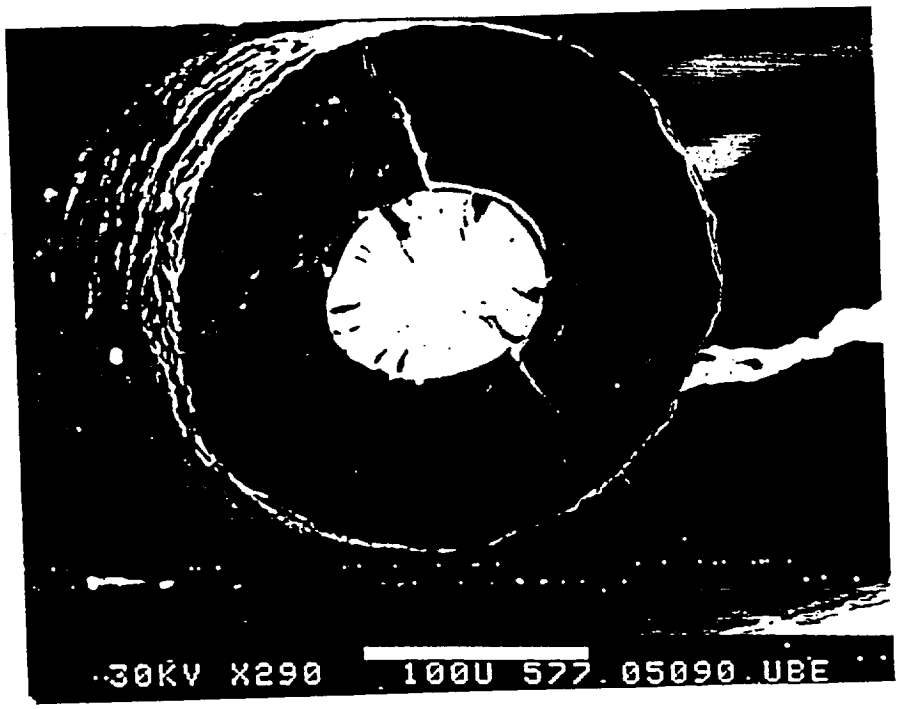

T = 485 K

$\alpha = 110$

$\beta = 5$

D = 241 μm

10 μm of intermediate la

These two samples are with intermediate layer of carbon.

It can be seen that as the temperature increases (> 1273 K)

the intermediate layer is having minor effect.

```
RE      TS
CR     0000  CL  2.0000  O    2.0000       0.0000  00  0.0000     1.000000  M        0.00  G
 300.000           0.00000
    1.0000  CL  3.0000       0.0000       0.0000  00  0.0000     5.000000  M        0.00  G
 300.000           0.00000
H   2.0000       0.0000       0.0000       0.0000  00  0.0000   120.000000  M        0.00  G
 300.000           0.00000
 NAMELISTS
SINPT2
KASE    =            1,
T       =   1000.000     ,   1100.000     ,   1200.000     ,   1300.000     ,
  500.0000     , 21*0.0000000E+00,
P       =   1.000000     , 25*0.0000000E+00,
PSIA    = F,
MMHG    = F,
NSQM    = F,
V       = 13*0.0000000E+00,
RHO     =   1.000000     , 25*0.0000000E+00,
ERATIO  = F,
OF      = F,
FPCT    = F,
FA      = F,
MIX     = 20*0.0000000E+00,
IP      = T,
HP      = F,
S       = F,
T       = F,
UV      = F,
PV      = F,
KT      = F,
SHOCK   = F,
DETN    = F,
OTTO    =  0.0000000E+00,
CR      =  0.0000000E+00,
SO      =  0.0000000E+00,
SO      =  0.0000000E+00,
IONS    = F,
IDEBUG  =            0,
TRACE   =  1.0000000E-06,
SIUNIT  = F,
PHI     = F,
INHG    = F
SEND

NO INPT2 VALUE GIVEN FOR OF, EQRAT, FA, OR FPCT

SPECIES BEING CONSIDERED IN THIS SYSTEM
    HTP 90  CRB(S)          HTP 90  CRB2(S)         HTP 90  CRCL2(S)        HTP 90  CRC
L2(L)         HTP 90  CRCL3(S)
    HTP 90  CRO2CL2         J12/64  B(S)            J12/64  B(L)             J12/64  B
              J12/64  BCL
    ' 6/72  BCL2            J12/64  BCL3            J12/64  BH              J12/64  BH2
              J12/64  BH3
    J 6/68  BO              J 3/65  BOCL            J 6/68  BO2             J12/64  B2
              J 6/66  B2O
    J12/64  B2O2            J 6/71  B2O3(L)         J 6/71  B2O3            J 3/65  B3O
3CL3          J 6/72  CL
    J 6/61  CLO             J 3/61  CLO2            J 9/65  CL2             J12/65  CL2
O             J 6/73  CR(S)
```

```
 6/73  CR(L)              J 6/73  CR              J12/73  CRO             J12/73  CRO
2          J12/73  CRO3
  /73  CR2O3(S)           J12/73  CR2O3(L)        J 3/77  H               J12/75  HBO
           J12/64  HBO2
  J 9/64  HCL             J 3/64  HO2             J 3/77  H2              L 3/81  H2O
(S)        J 3/79  H2O(L)
  J 3/79  H2O             L 2/69  H2O2            J12/64  H3B3O6          J 3/77  O
           J 6/77  OH
  J 3/77  O2              J 6/61  O3              J 3/61  H2(L)

OF =   0.000000

                          EFFECTIVE FUEL          EFFECTIVE OXIDANT       MIXTURE
ENTHALPY                    HPP(2)                  HPP(1)                HSUBO
(KG-MOL)(DEG K)/KG      -0.31158582E+03         0.00000000E+00        -0.31158582E+03

KG-ATOMS/KG                 BOP(I,2)                BOP(I,1)              BO(I)
      CR                0.10176423E-02          0.00000000E+00        0.10176423E-02
      CL                0.17299918E-01          0.00000000E+00        0.17299918E-01
      O                 0.20352845E-02          0.00000000E+00        0.20352845E-02
      B                 0.50882113E-02          0.00000000E+00        0.50882113E-02
      H                 0.24423414E+00          0.00000000E+00        0.24423414E+00
 1     20.735  -29.635  -53.604   -2.503   -8.789   17.000 1000.000
ADD CRB2(S)
 1     -6.829  -28.929  -51.093   -5.720   -8.802    8.000 1000.000
ADD CRB(S)
 1    -11.116  -29.355  -52.810   -3.577   -8.790    5.000 1000.000
P   'E CRB2(S)
      -10.546  -29.222  -52.374   -4.146   -8.793    3.000 1000.000
AD  B203(L)
 1    -10.644  -29.222  -52.594   -4.048   -8.793    3.000 1000.000
 2    -11.341  -28.338  -49.078   -2.937   -8.915    4.000 1100.000
ADD CRB2(S)
 2    -10.740  -28.199  -48.677   -3.539   -8.918    4.000 1100.000
 3    -10.452  -27.298  -45.171   -3.535   -9.039    5.000 1200.000
REMOVE CRB(S)
 3    -10.741  -27.325  -45.267   -3.391   -9.038    3.000 1200.000
 4    -12.013  -26.726  -42.815   -2.666   -9.147    5.000 1300.000
 5     11.604  -39.326  -91.239  -19.091   -8.107    6.000  500.000
ADD CRCL3(S)
 5    -18.166  -43.962 -101.162   -4.206   -8.068    6.000  500.000
REMOVE CRB2(S)
 5    -27.888  -40.721  -94.569  -14.095   -8.077    7.000  500.000
ADD CRCL2(S)
 5    -30.060  -39.997  -93.113  -16.281   -8.090    4.000  500.000
REMOVE CRCL3(S)
 5    -29.188  -40.434  -93.991  -14.963   -8.081    4.000  500.000
```

THERMODYNAMIC EQUILIBRIUM PROPERTIES AT ASSIGNED

TEMPERATURE AND PRESSURE

ASE NO. 1

ENERGY	STATE	TEMP	DENSITY		MOLES
	CHEMICAL FORMULA				
CAL/MOL		DEG K	G/CC		
FUEL	CR 1.00000	CL 2.00000	O 2.00000		1.000000 -1
28656.680	G	300.00	0.0000		
FUEL	B 1.00000	CL 3.00000			5.000000 -
96276.109	G	300.00	0.0000		
FUEL	H 2.00000				120.000
13.324	G	300.00	0.0000		

O/F= 0.0000 PERCENT FUEL= 100.0000 EQUIVALENCE RATIO=12.2857 PHI= 0.0000
REACTANT DENSITY= 0.0000

THERMODYNAMIC PROPERTIES

P, ATM	1.0000	1.0000	1.0000	1.0000	1.0000
T, DEG K	1000.0	1100.0	1200.0	1300.0	500.0
RHO, G/CC	9.4172-5	8.5462-5	7.8167-5	7.2142-5	1.9059-4
H L/G	-1.0036	110.84	227.11	333.08	-555.29
U /G	-258.16	-172.53	-82.706	-2.6028	-682.35
G, AL/G	-5547.52	-6107.36	-6677.89	-7257.57	-2951.33
S, CAL/(G)(K)	5.5465	5.6529	5.7542	5.8390	4.7921
M, MOL WT	7.727	7.714	7.697	7.696	7.820
(DLV/DLP)T	-1.00000	-1.00147	-1.00002	-1.00013	-1.00000
(DLV/DLT)P	1.0000	1.0315	1.0007	1.0043	1.0000
CP, CAL/(G)(K)	1.0056	1.1941	1.0408	1.0861	0.9721
GAMMA (S)	1.3436	1.2955	1.3305	1.3152	1.3540
SON VEL,M/SEC	1202.4	1239.3	1313.3	1359.1	848.4

MOLE FRACTIONS

CRB(S)	7.7898-3	4.3348-3	0.0000 0	0.0000 0	0.0000 0
CRB2(S)	0.0000 0	3.4403-3	7.7535-3	7.7544-3	0.0000 0
CRCL2(S)	0.0000 0	0.0000 0	0.0000 0	0.0000 0	7.8568-3
BCL2	4.219 -8	3.553 -7	1.749 -6	9.684 -6	1.627-19
BCL3	1.7182-2	1.3880-2	1.0102-2	9.8263-3	2.8373-2
BH3	1.337 -8	7.277 -8	2.284 -7	1.123 -6	7.140-19
BOCL	9.030 -8	1.026 -6	7.338 -6	4.168 -5	6.836-20
B203(L)	1.6020-3	1.7699-3	2.3484-3	2.0771-3	4.8026-3
B303CL3	3.5910-3	3.4114-3	2.8053-3	2.9959-3	4.3532-4
H	2.129 -9	2.416 -8	1.834 -7	1.028 -6	6.606-21
	3.993 -7	4.888 -6	3.568 -5	2.344 -4	4.840-20
	7.654 -9	9.899 -8	8.866 -7	4.546 -6	5.021-21
CL	7.0109-2	8.0301-2	9.3078-2	9.3296-2	3.1427-2
	8.9973-1	8.9286-1	8.8387-1	8.8375-1	9.2710-1
H2O	8.727 -8	3.301 -7	1.164 -6	2.234 -6	2.997-13

ADDITIONAL PRODUCTS WHICH WERE CONSIDERED BUT WHOSE MOLE FRACTIONS WERE LESS THAN 0.10000 E-05 FOR ALL ASSIGNED CONDITIONS

Cl L)	CRCL3(S)	CRO2CL2	B(S)	B(L)	B	BCL
BH	BH2	BO				
)2	B2	B2O	B2O2	B2O3	CL	CLO
CLO2	CL2	CL2O				
CR(S)	CR(L)	CR	CRO	CRO2	CRO3	CR2O3(S)
CR2O3(L)	HO2	H2O(S)				
:O(L)	H2O2	H3B3O6	O	OH	O2	O3
H2(L)						

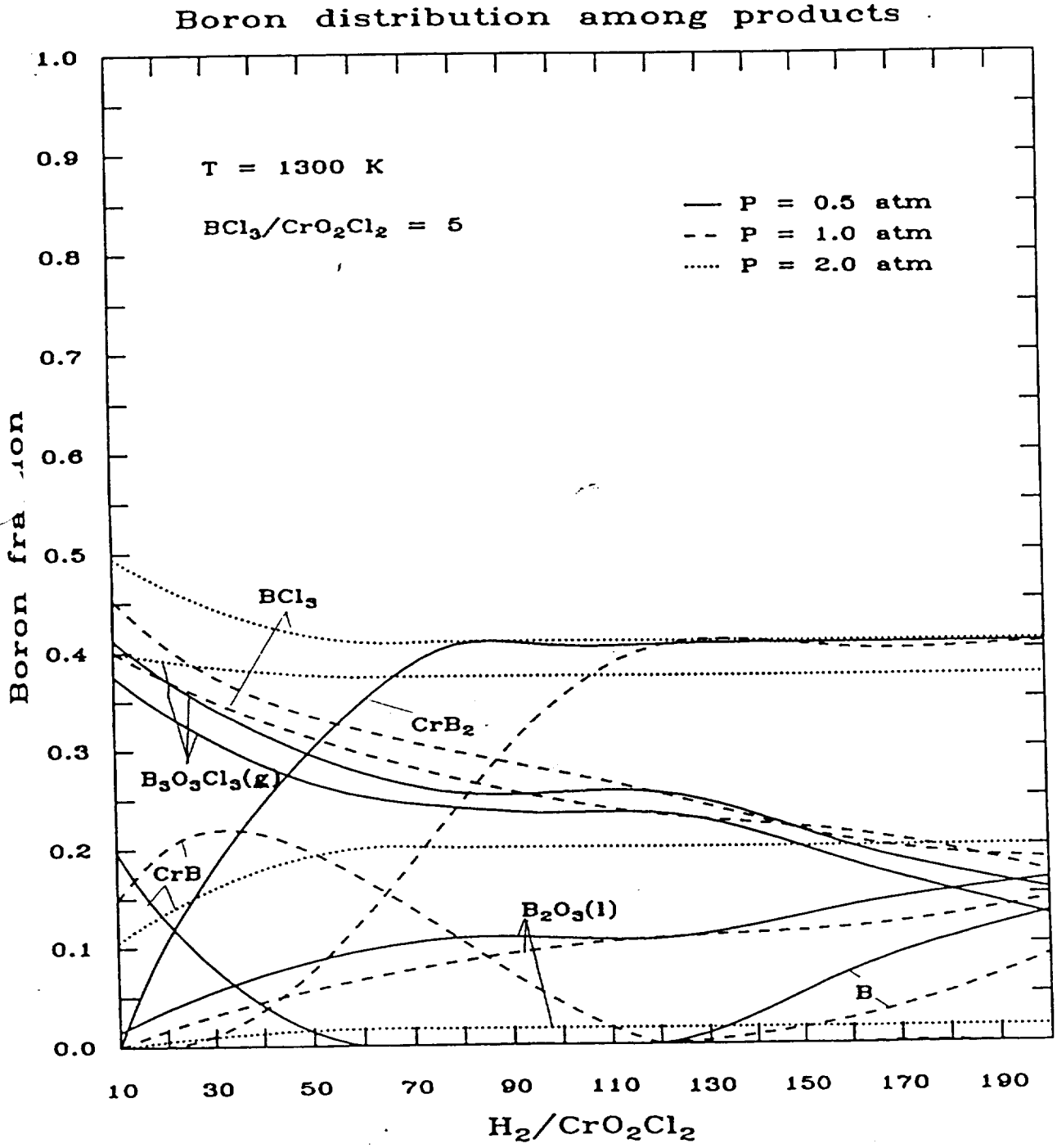
Boron distribution among products
T = 1300 K
BCl_3/CrO_2Cl_2 = 5
P = 0.5 atm
P = 1.0 atm
P = 2.0 atm
Boron fraction
BCl_3
CrB_2
$B_3O_3Cl_3(g)$
CrB
$B_2O_3(l)$
B
1.0
0.9
0.8
0.7
0.6
0.5
0.4
0.3
0.2
0.1
0.0
10
30
50
70
90
110
130
150
170
190
H_2/CrO_2Cl_2

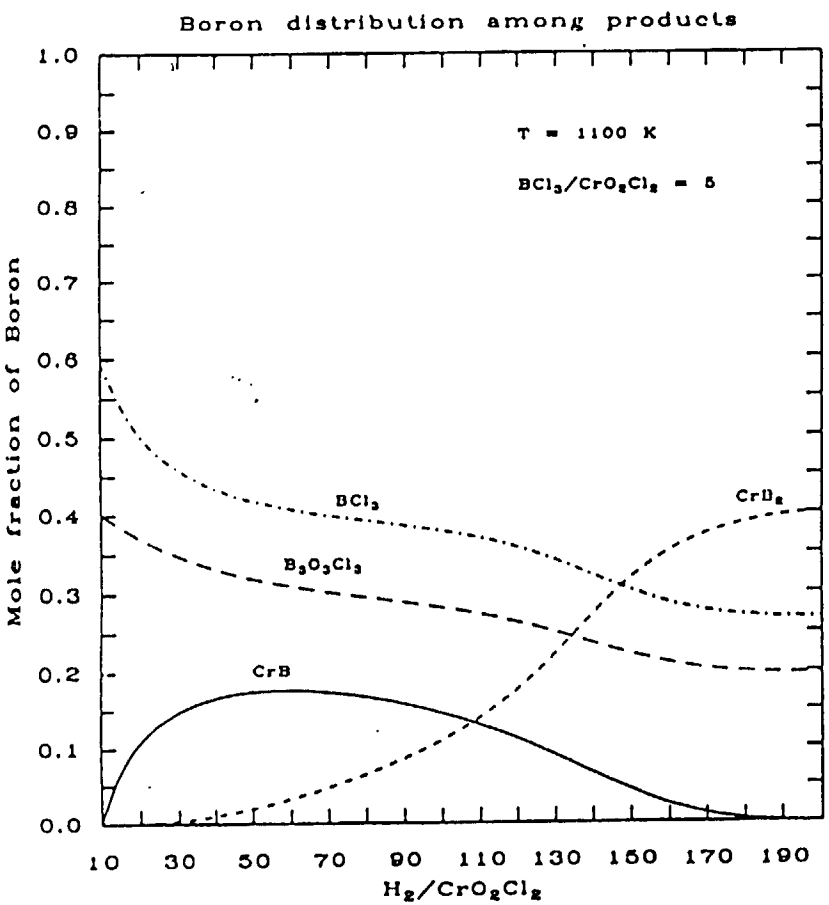
Boron distribution among products
T = 1100 K
BCl_3/CrO_2Cl_2 = 5
Mole fraction of Boron
BCl_3
$B_3O_3Cl_3$
CrB
CrB_2
1.0
0.9
0.8
0.7
0.6
0.5
0.4
0.3
0.2
0.1
0.0
10 30 50 70 90 110 130 150 170 190
H_2/CrO_2Cl_2

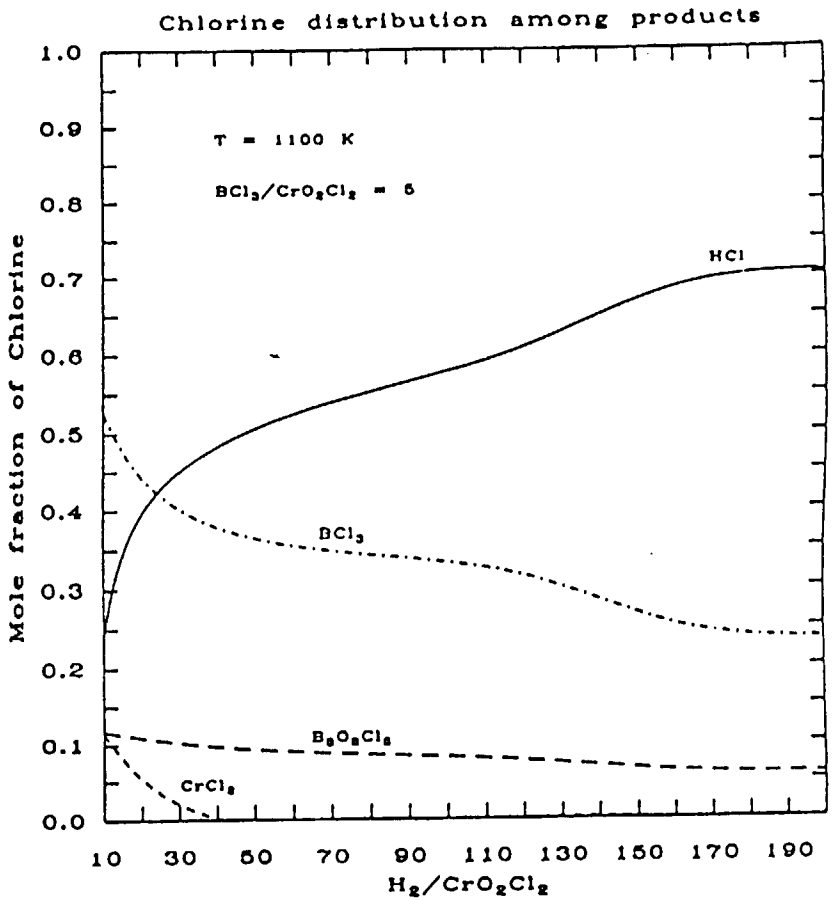
Chlorine distribution among products
T = 1100 K
BCl_3/CrO_2Cl_2 = 5
Mole fraction of Chlorine
HCl
BCl_3
$B_3O_3Cl_3$
$CrCl_2$
1.0
0.9
0.8
0.7
0.6
0.5
0.4
0.3
0.2
0.1
0.0
10 30 50 70 90 110 130 150 170 190
H_2/CrO_2Cl_2

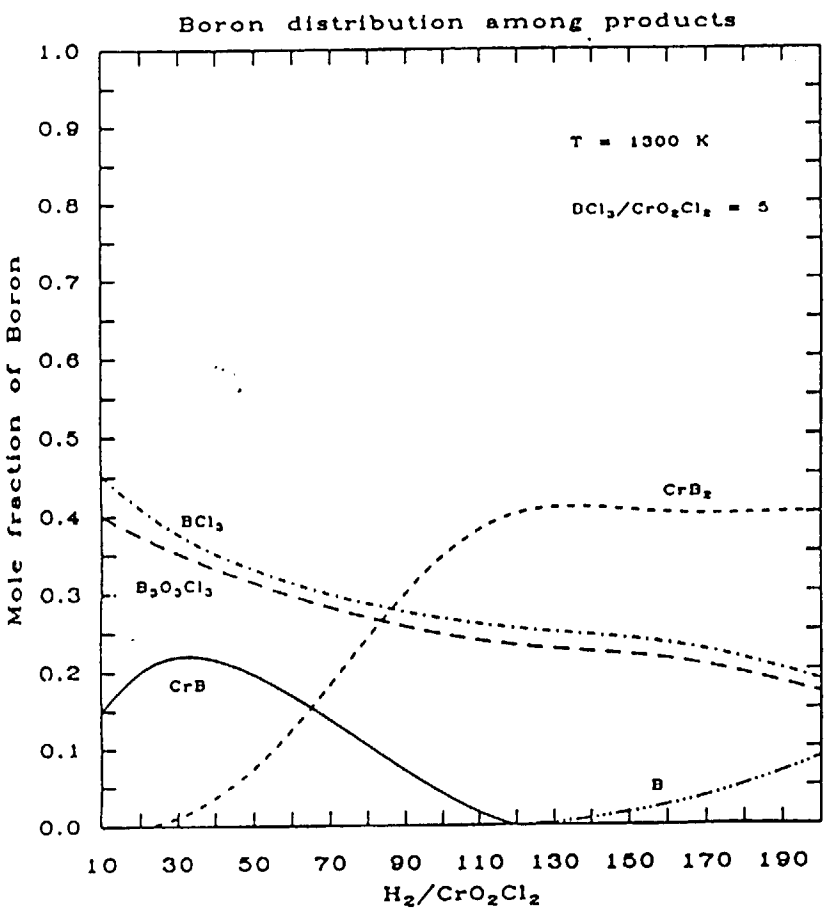
Boron distribution among products
T = 1300 K
BCl_3/CrO_2Cl_2 = 5
Mole fraction of Boron
H_2/CrO_2Cl_2
BCl_3
$B_3O_3Cl_3$
CrB
CrB_2
B
1.0
0.9
0.8
0.7
0.6
0.5
0.4
0.3
0.2
0.1
0.0
10 30 50 70 90 110 130 150 170 190

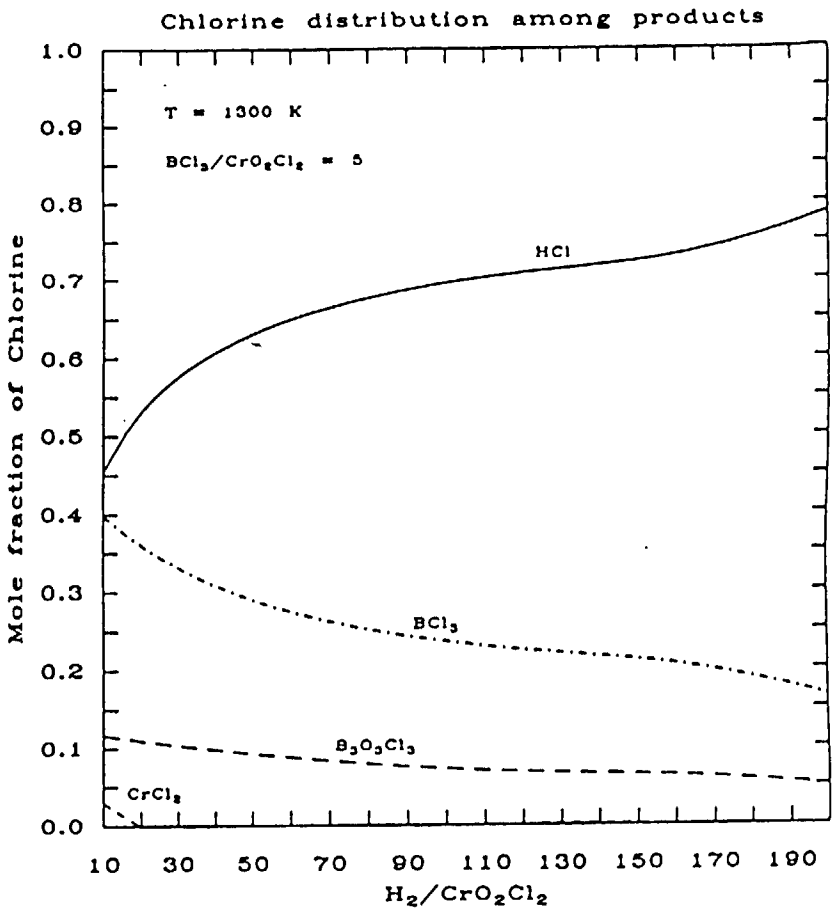
Chlorine distribution among products
T = 1300 K
BCl_3/CrO_2Cl_2 = 5
Mole fraction of Chlorine
H_2/CrO_2Cl_2
HCl
BCl_3
$B_3O_3Cl_3$
$CrCl_2$
1.0
0.9
0.8
0.7
0.6
0.5
0.4
0.3
0.2
0.1
0.0
10 30 50 70 90 110 130 150 170 190

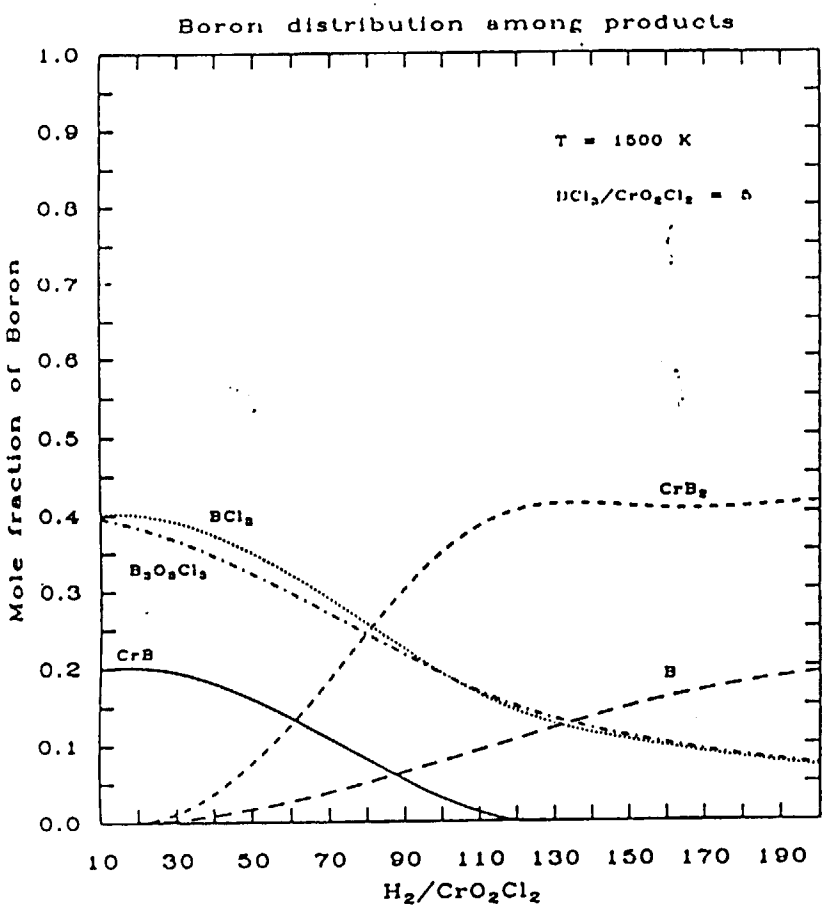
Boron distribution among products
T = 1500 K
BCl_3/CrO_2Cl_2 = 5
Mole fraction of Boron
H_2/CrO_2Cl_2
BCl_3
$B_3O_3Cl_3$
CrB
CrB_2
B
1.0
0.9
0.8
0.7
0.6
0.5
0.4
0.3
0.2
0.1
0.0
10 30 50 70 90 110 130 150 170 190

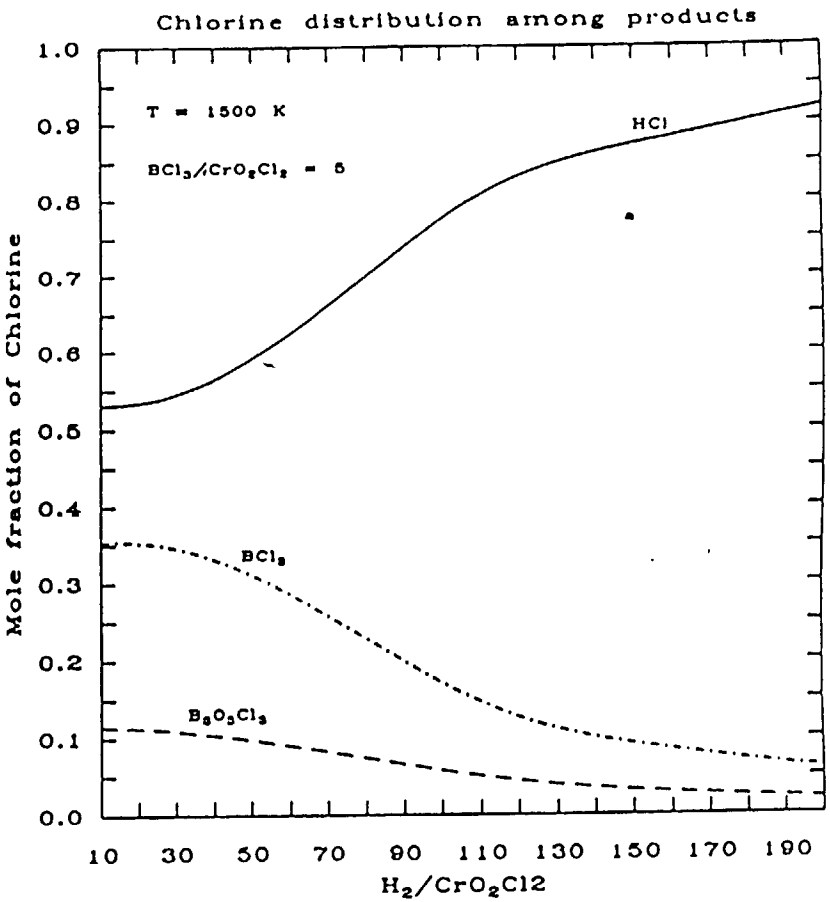
Chlorine distribution among products
T = 1500 K
BCl_3/CrO_2Cl_2 = 5
Mole fraction of Chlorine
H_2/CrO_2Cl2
HCl
BCl_3
$B_3O_3Cl_3$
1.0
0.9
0.8
0.7
0.6
0.5
0.4
0.3
0.2
0.1
0.0
10 30 50 70 90 110 130 150 170 190

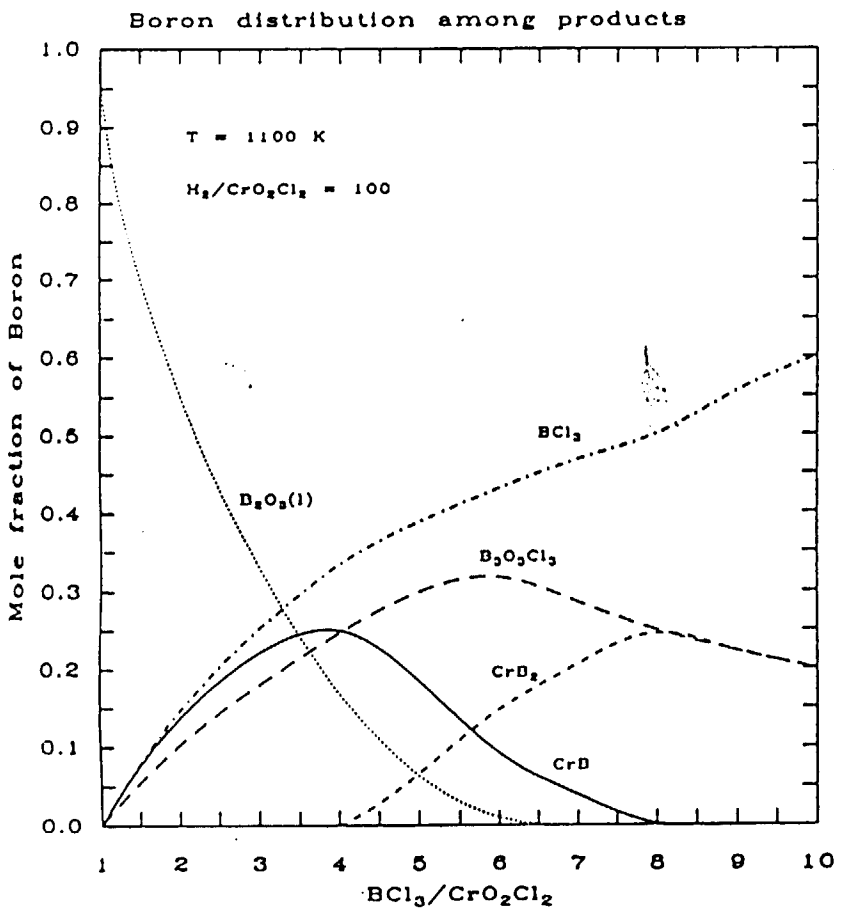
Boron distribution among products
T = 1100 K
H_2/CrO_2Cl_2 = 100
Mole fraction of Boron
BCl_3
$B_2O_3(l)$
$B_3O_3Cl_3$
CrB_2
CrB
BCl_3/CrO_2Cl_2

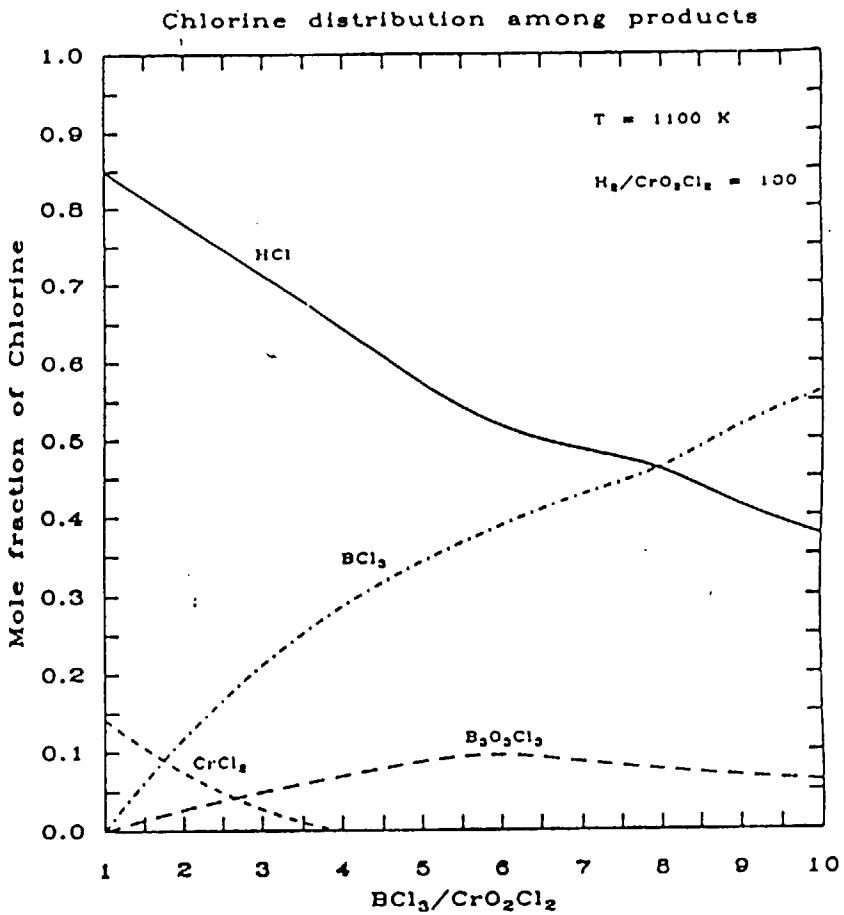
Chlorine distribution among products
T = 1100 K
H_2/CrO_2Cl_2 = 100
Mole fraction of Chlorine
HCl
BCl_3
$CrCl_2$
$B_3O_3Cl_3$
BCl_3/CrO_2Cl_2

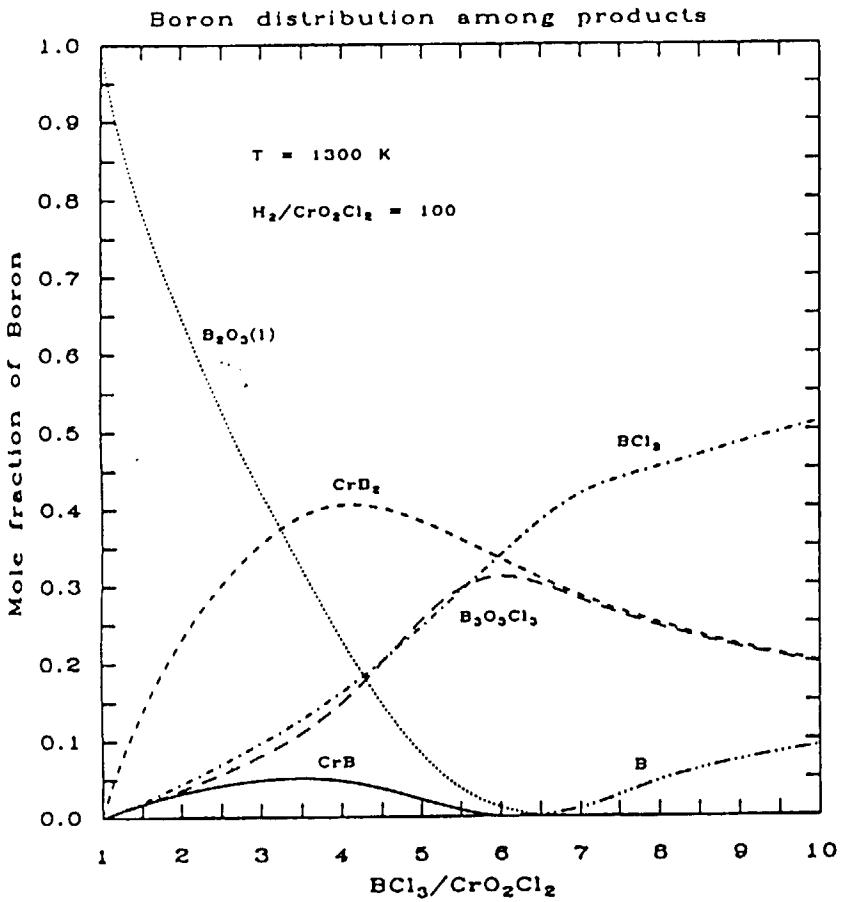
Boron distribution among products
T = 1300 K
H_2/CrO_2Cl_2 = 100
$B_2O_3(l)$
BCl_3
CrB_2
$B_3O_3Cl_3$
CrB
B
Mole fraction of Boron
BCl_3/CrO_2Cl_2

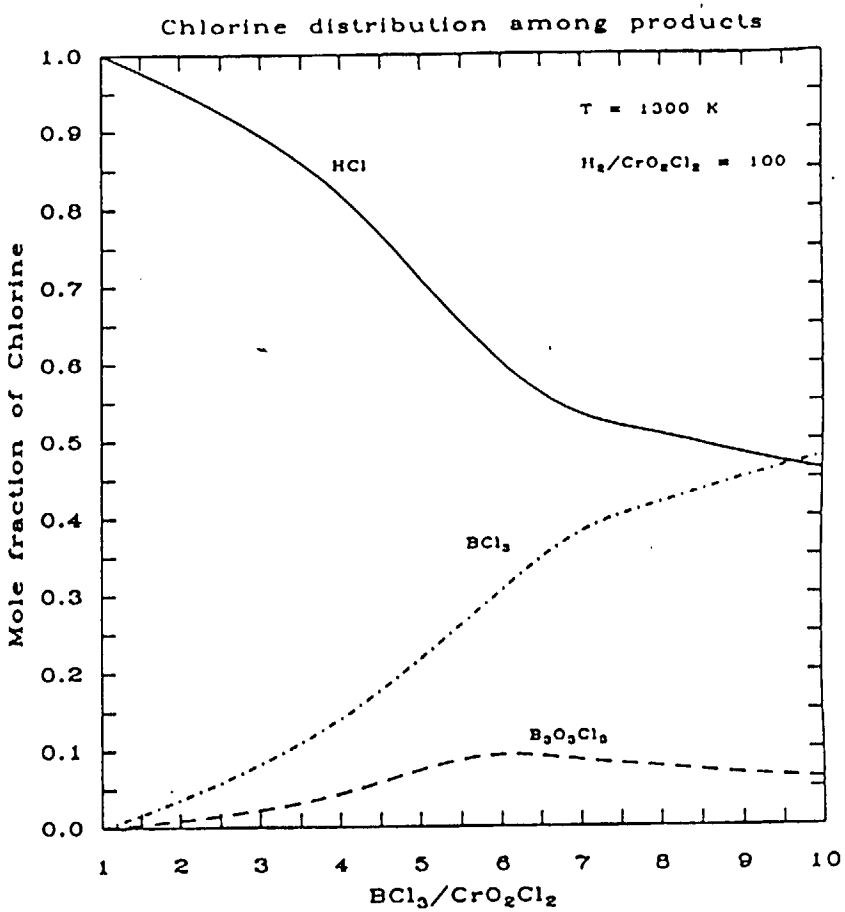
Chlorine distribution among products
T = 1300 K
H_2/CrO_2Cl_2 = 100
HCl
BCl_3
$B_3O_3Cl_3$
Mole fraction of Chlorine
BCl_3/CrO_2Cl_2

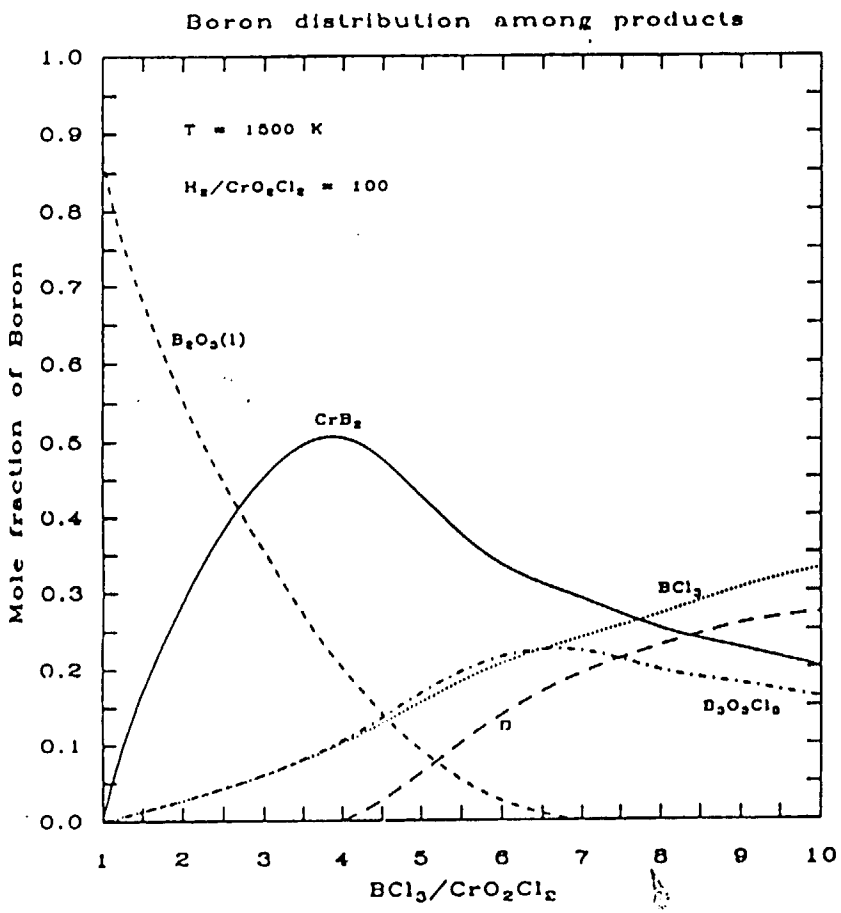
Boron distribution among products
T = 1500 K
H_2/CrO_2Cl_2 = 100
$B_2O_3(l)$
CrB_2
BCl_3
D
$B_3O_3Cl_3$
Mole fraction of Boron
BCl_3/CrO_2Cl_2

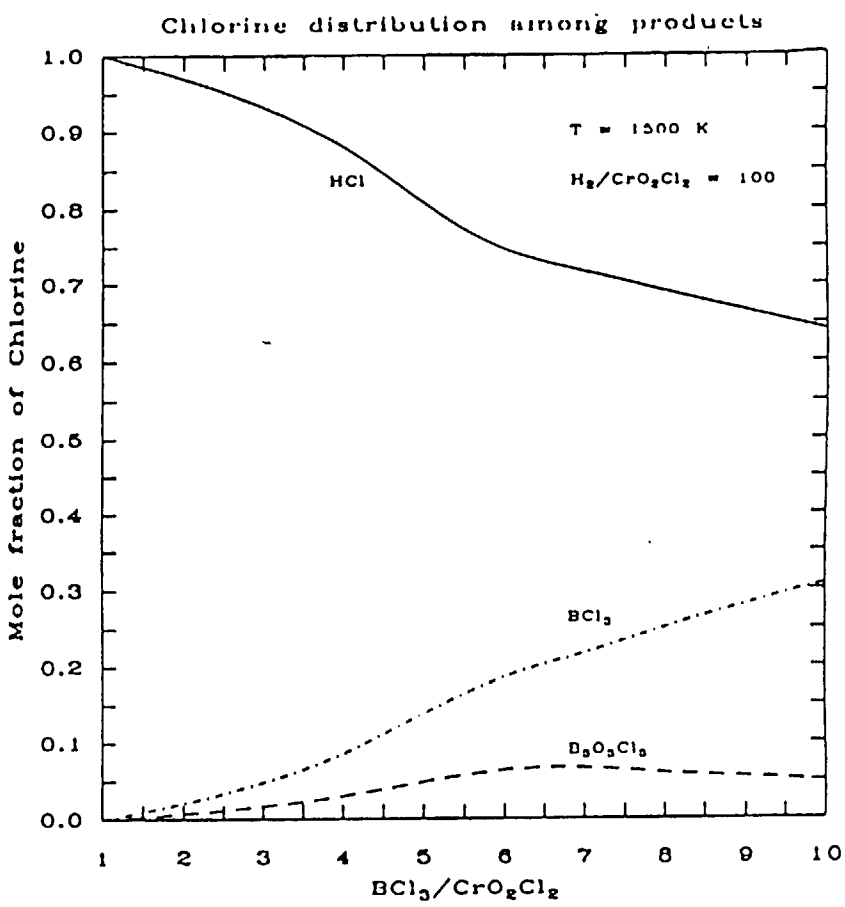
Chlorine distribution among products
T = 1500 K
H_2/CrO_2Cl_2 = 100
HCl
BCl_3
$B_3O_3Cl_3$
Mole fraction of Chlorine
BCl_3/CrO_2Cl_2

CrB_2 1100 K

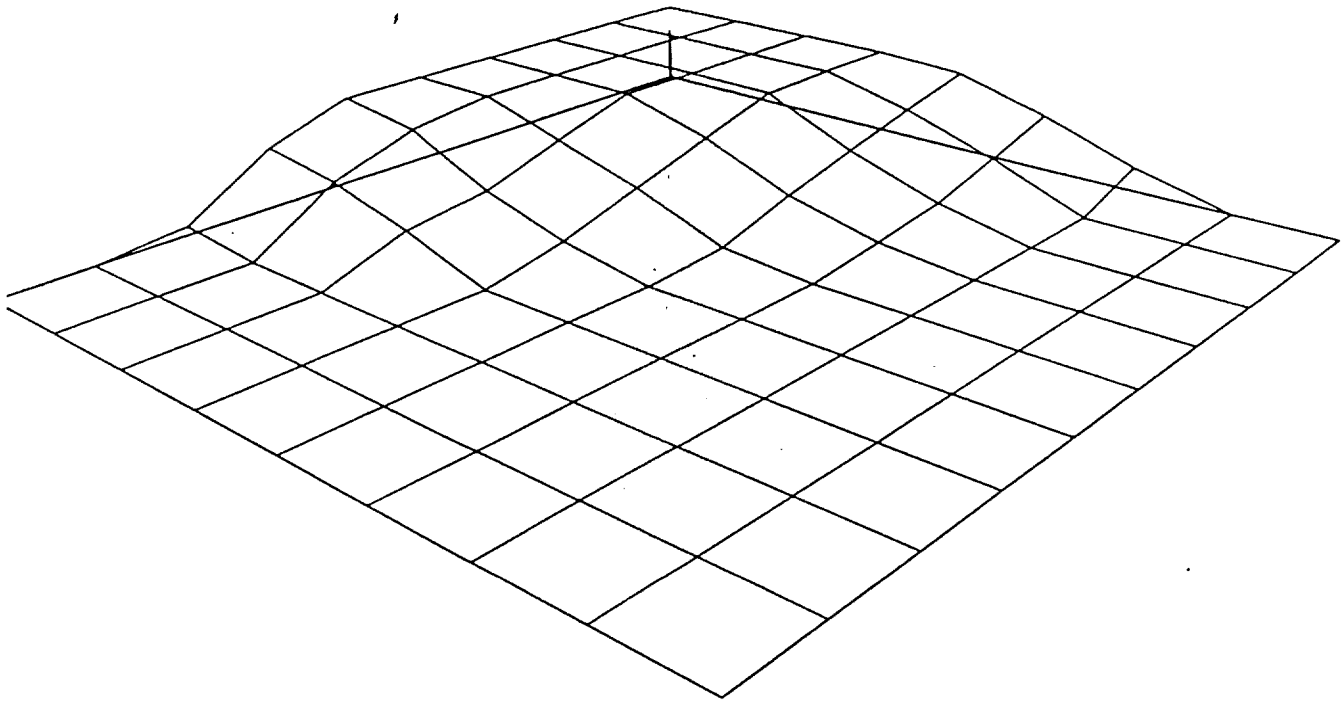

C_1B_2, 1500 K

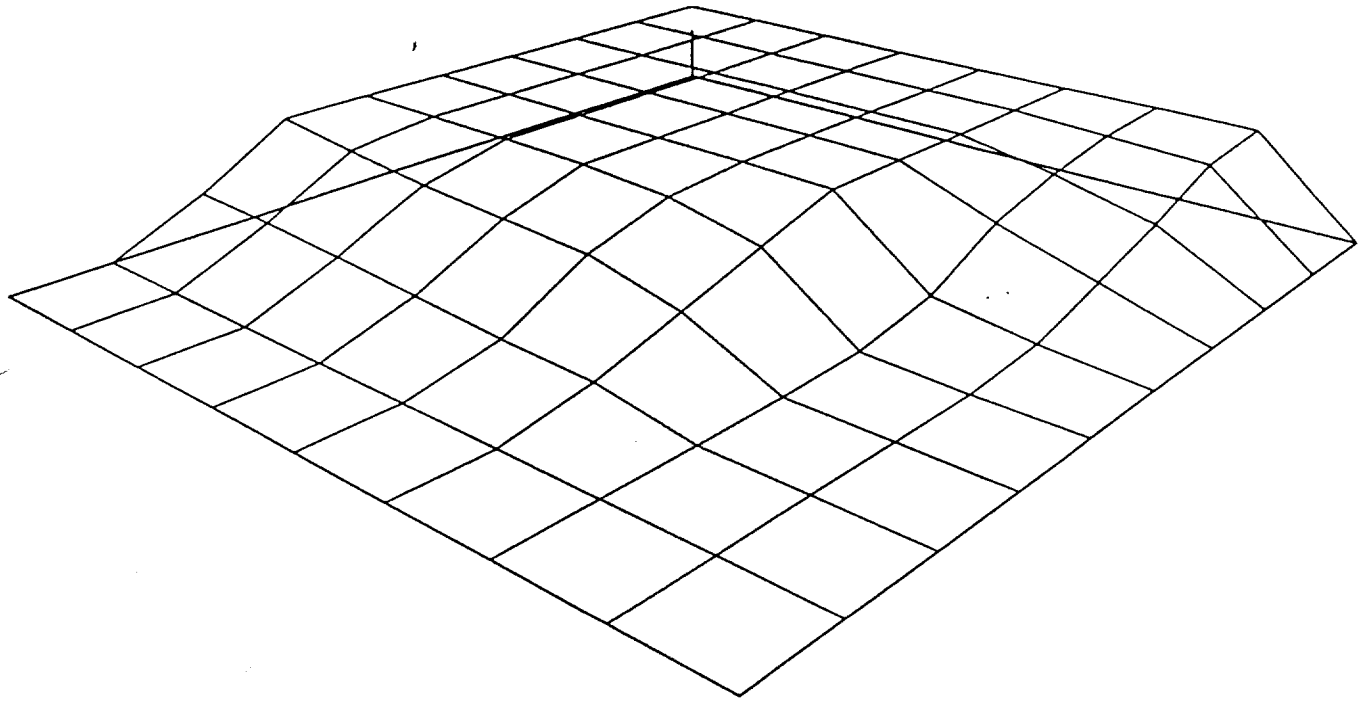

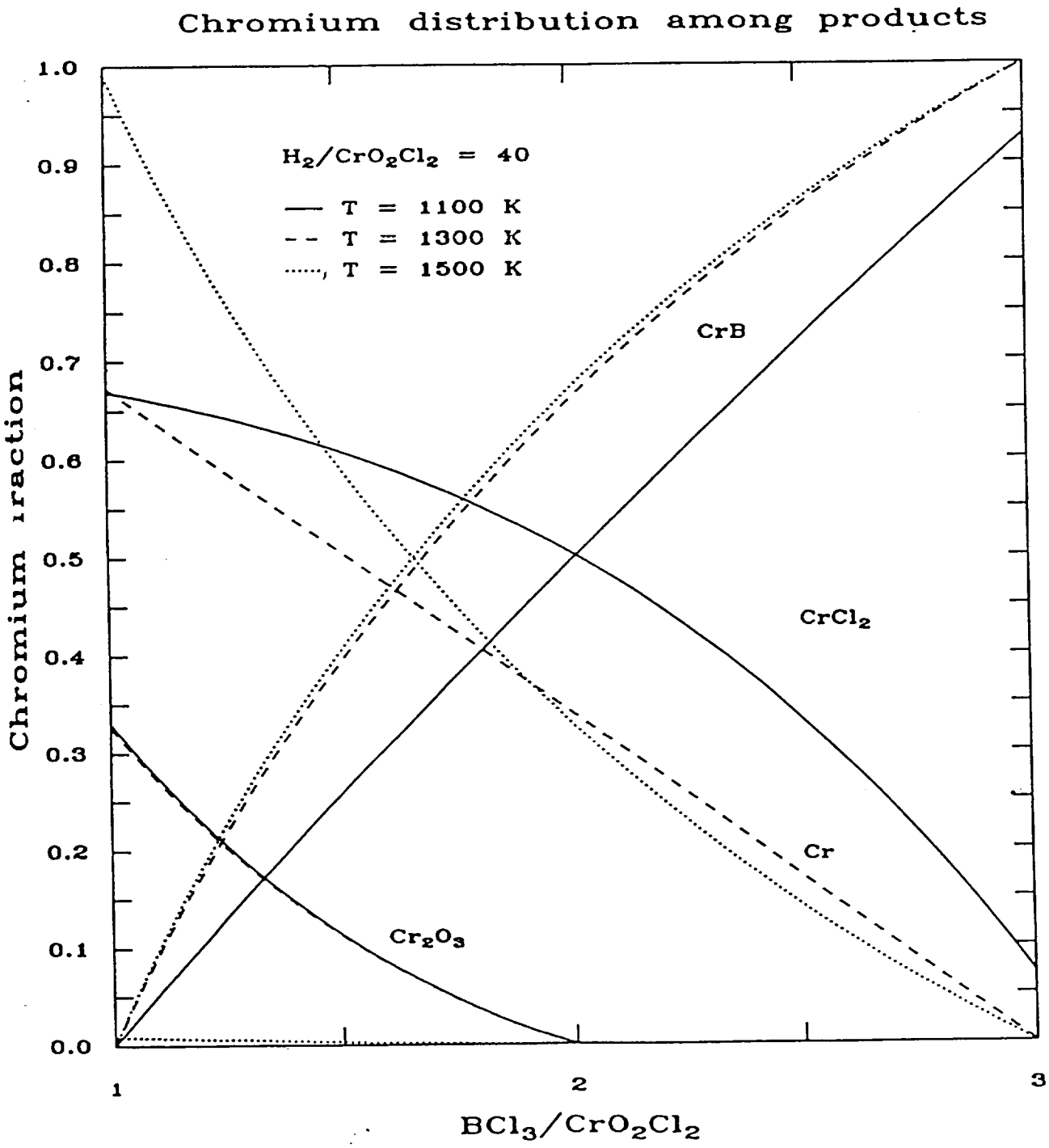
Chromium distribution among products
H_2/CrO_2Cl_2 = 40
T = 1100 K
T = 1300 K
T = 1500 K
CrB
$CrCl_2$
Cr
Cr_2O_3
Chromium fraction
1.0
0.9
0.8
0.7
0.6
0.5
0.4
0.3
0.2
0.1
0.0
1
2
3
BCl_3/CrO_2Cl_2

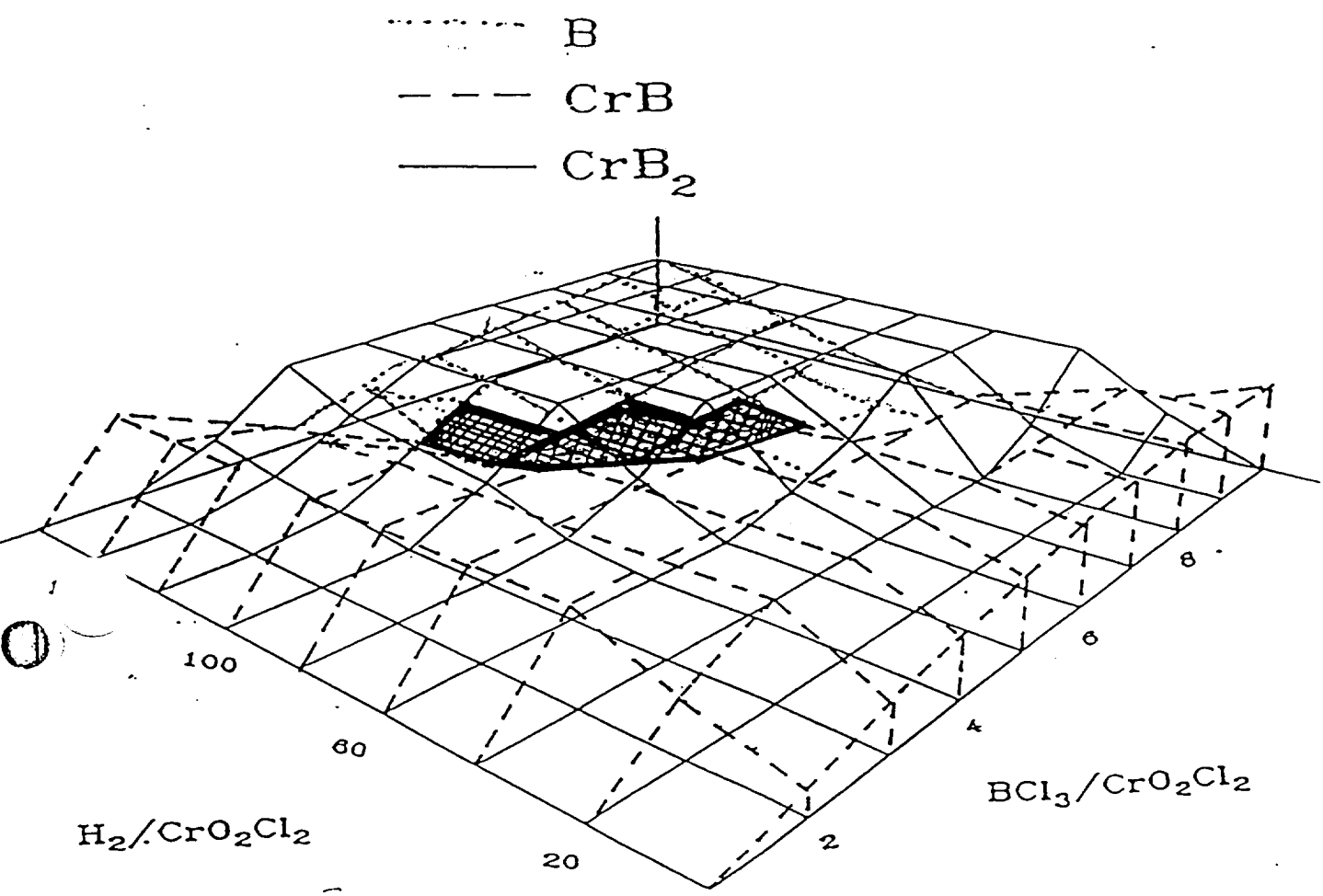
B
CrB
CrB_2
100
60
20
H_2/CrO_2Cl_2
2
4
6
8
BCl_3/CrO_2Cl_2

CrB

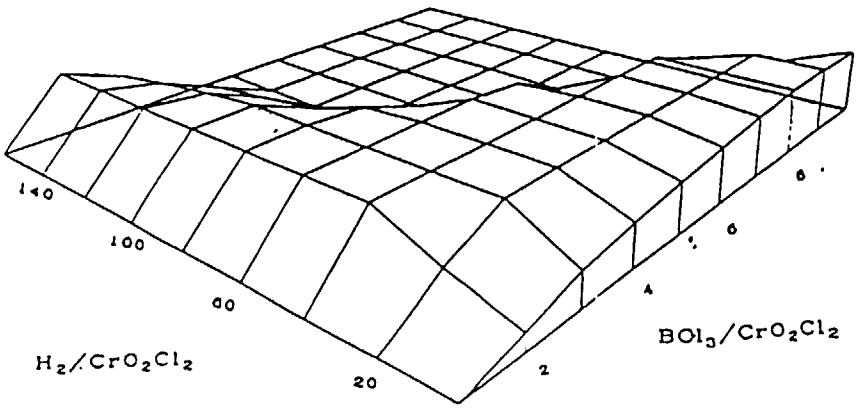
140
100
60
20
H_2/CrO_2Cl_2
2
4
6
8
BCl_3/CrO_2Cl_2

CrB_2

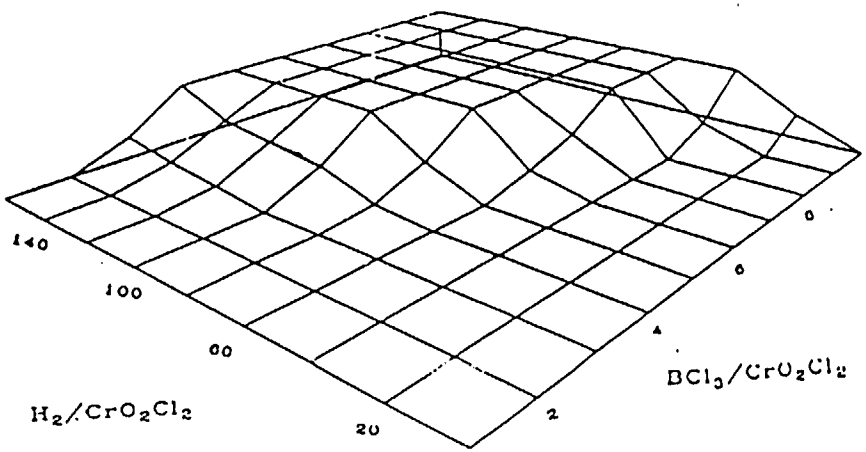
140
100
60
20
H_2/CrO_2Cl_2
2
4
6
8
BCl_3/CrO_2Cl_2

B

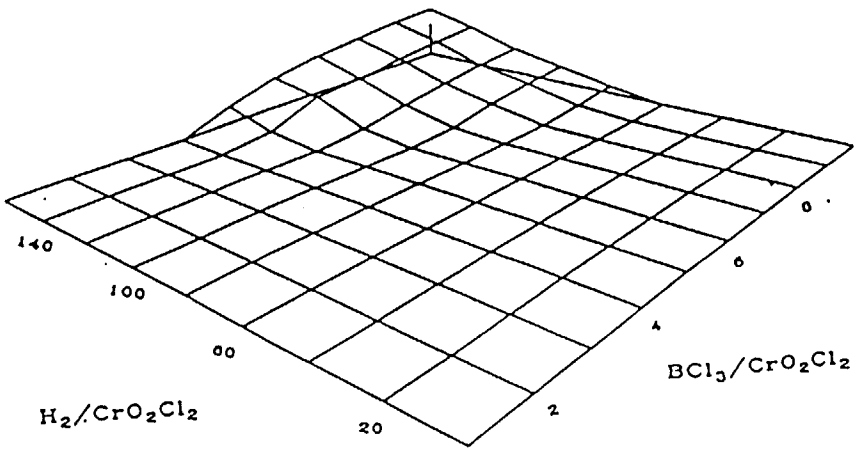
140
100
60
20
H_2/CrO_2Cl_2
2
4
6
8
BCl_3/CrO_2Cl_2

Appendix

Appendix

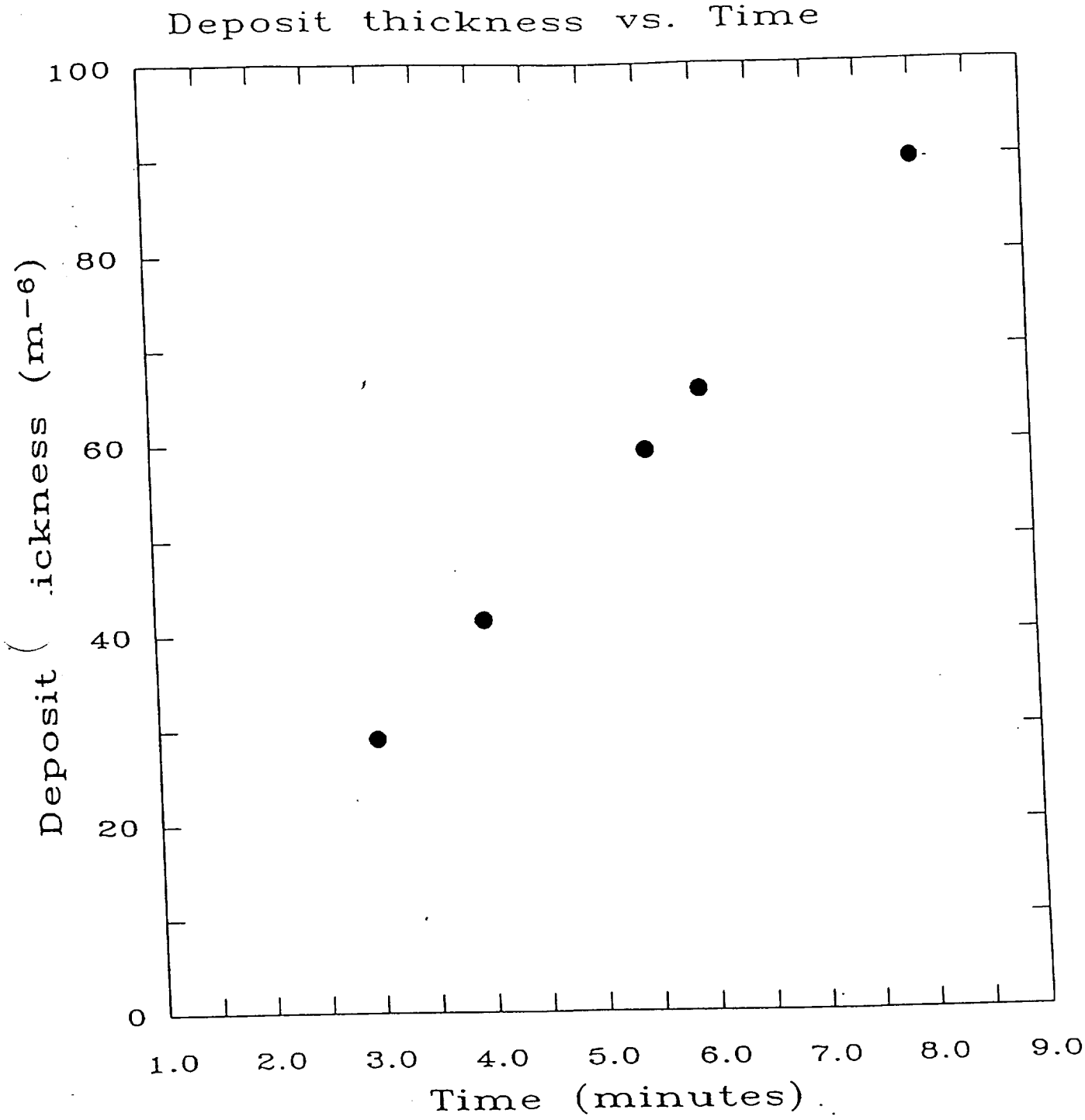

Linear dependence between deposition rate and Increase of the diameter of the deposited fiber

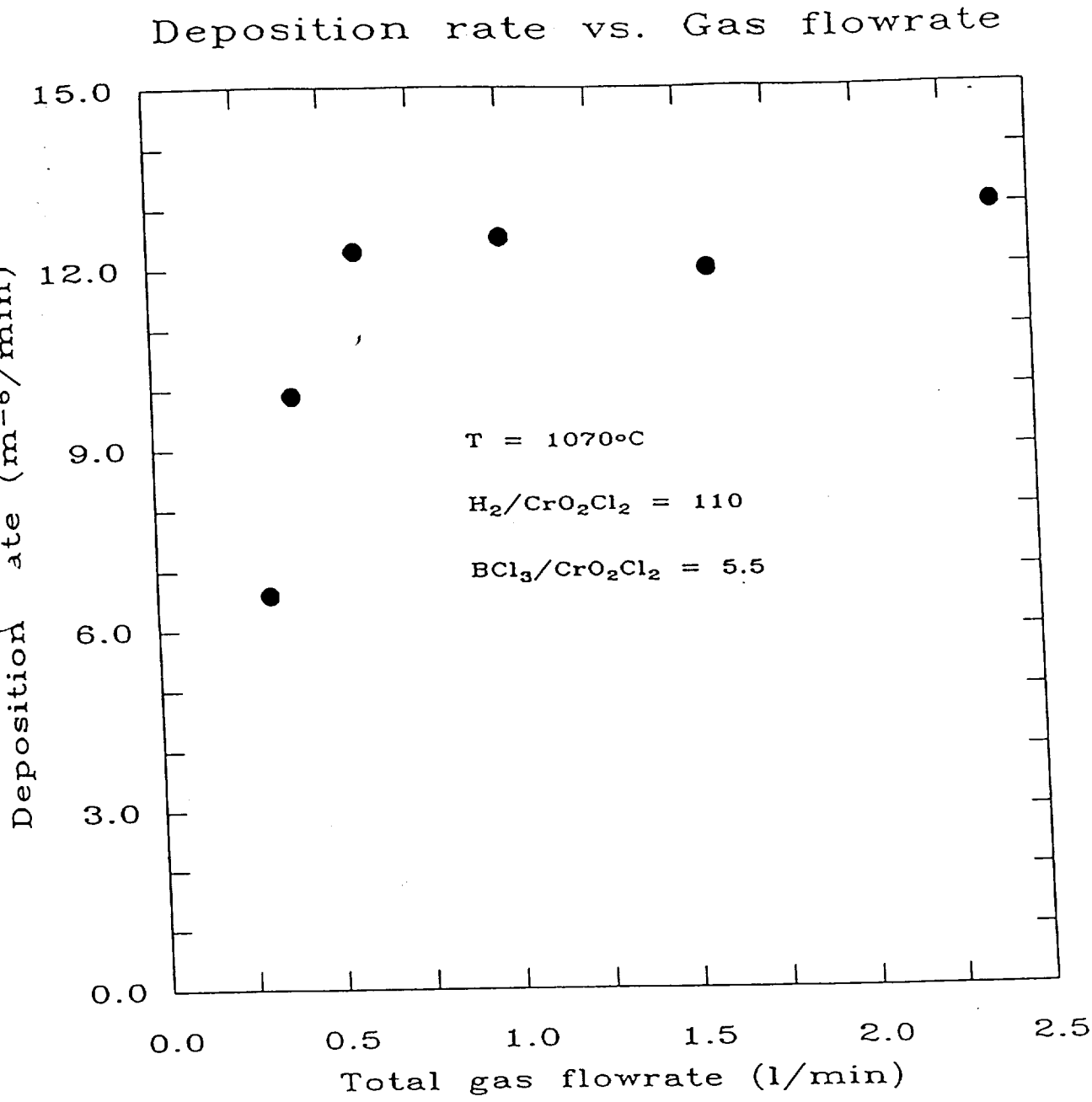

Deposition rate versus total gas flowrate

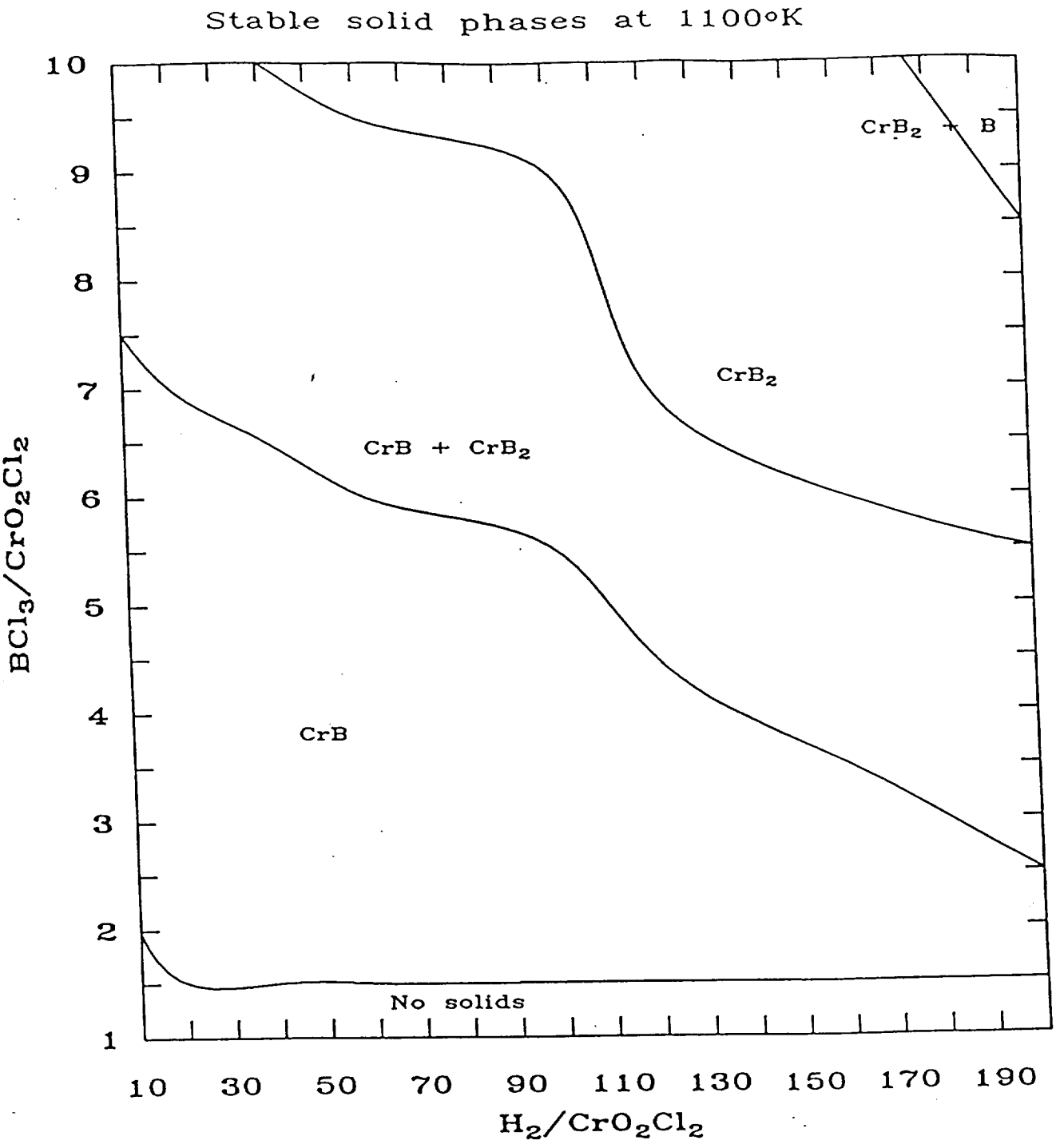

Stable solid phases at 1100 K for the CVD system

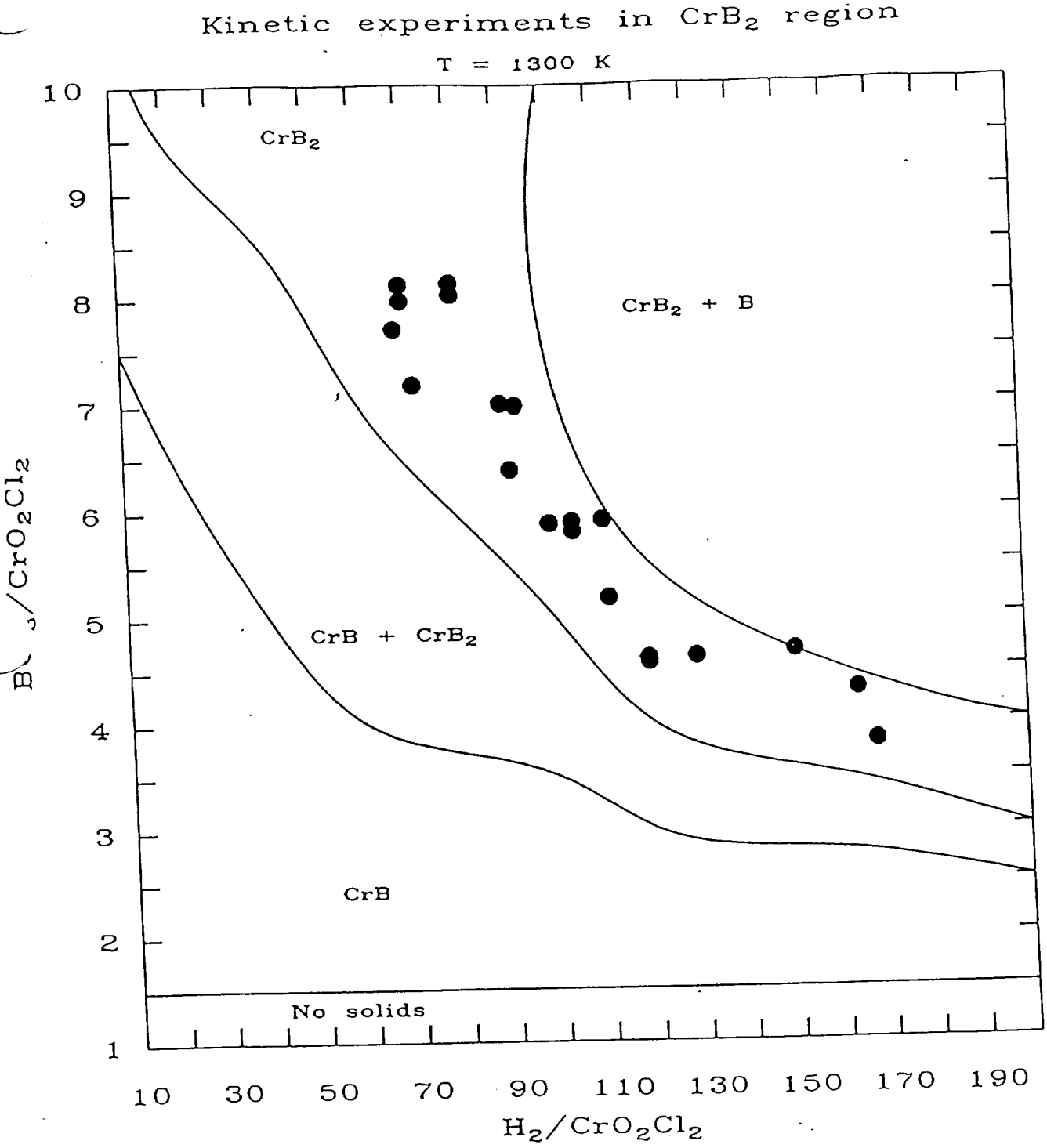

Stable solid phases at 1300 K with the points indicating at which conditions experiments were done.

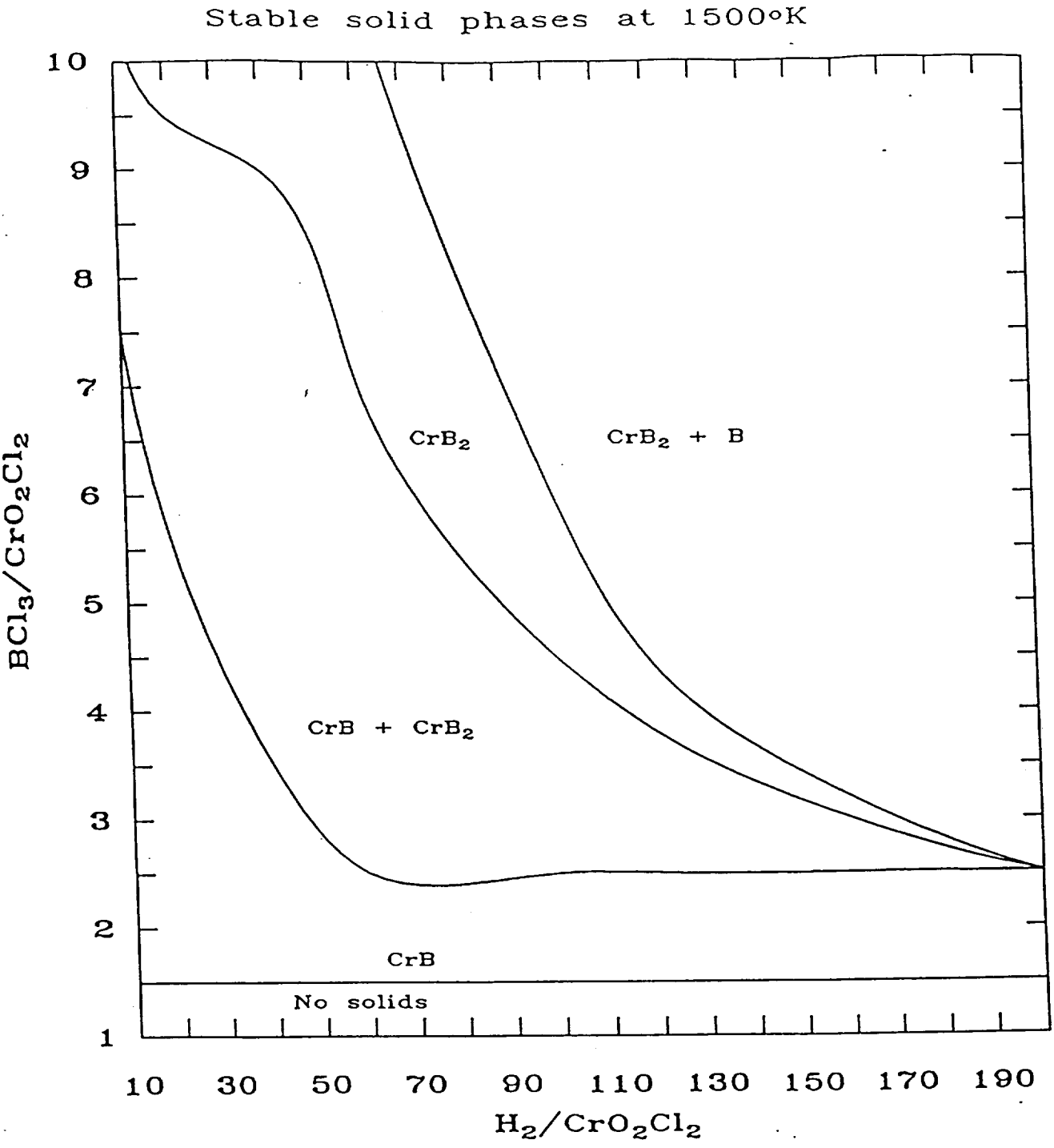

Stable solid phases at 1500 K for the CVD system

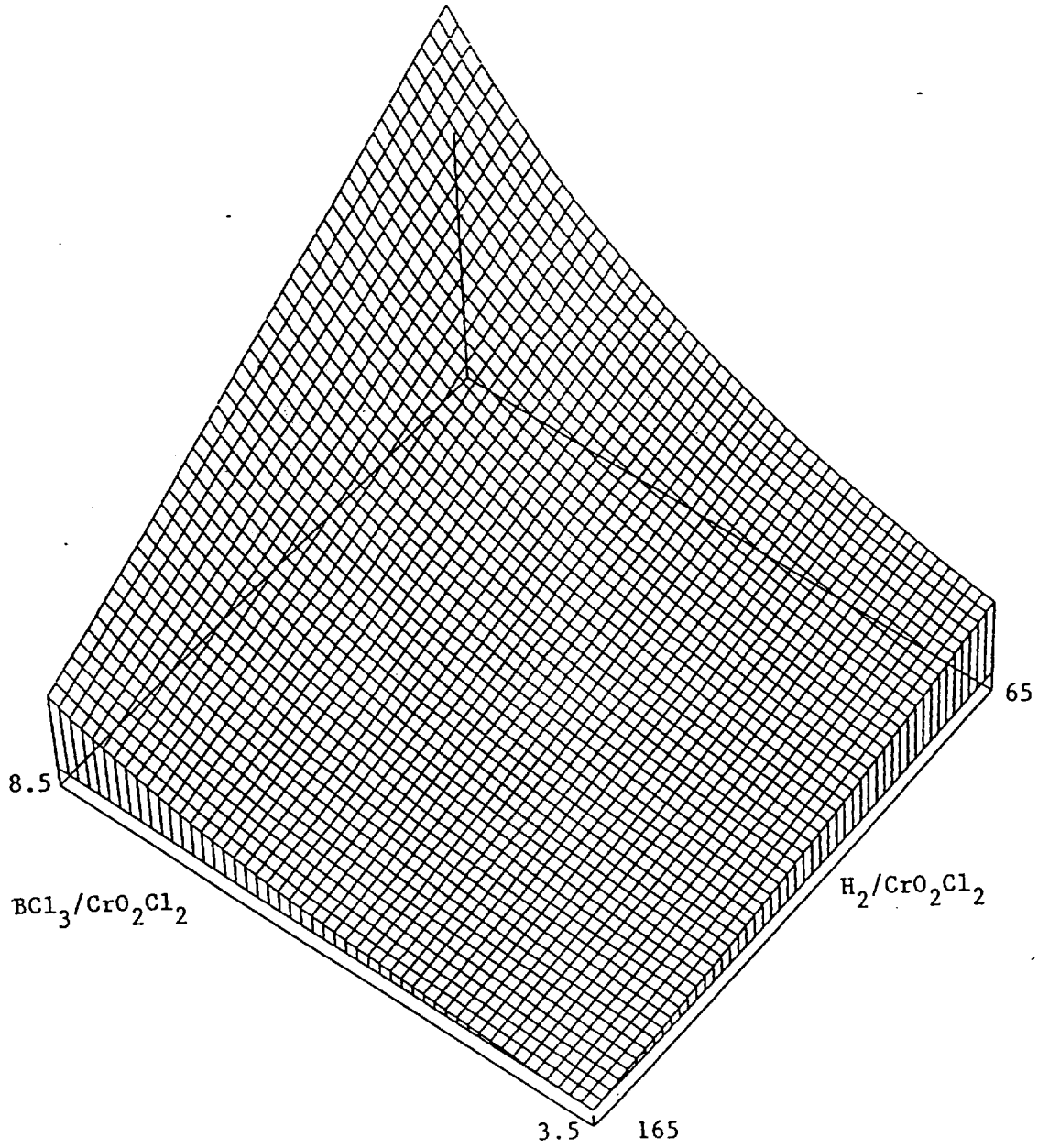

Proposed deposition rate from the second Model.

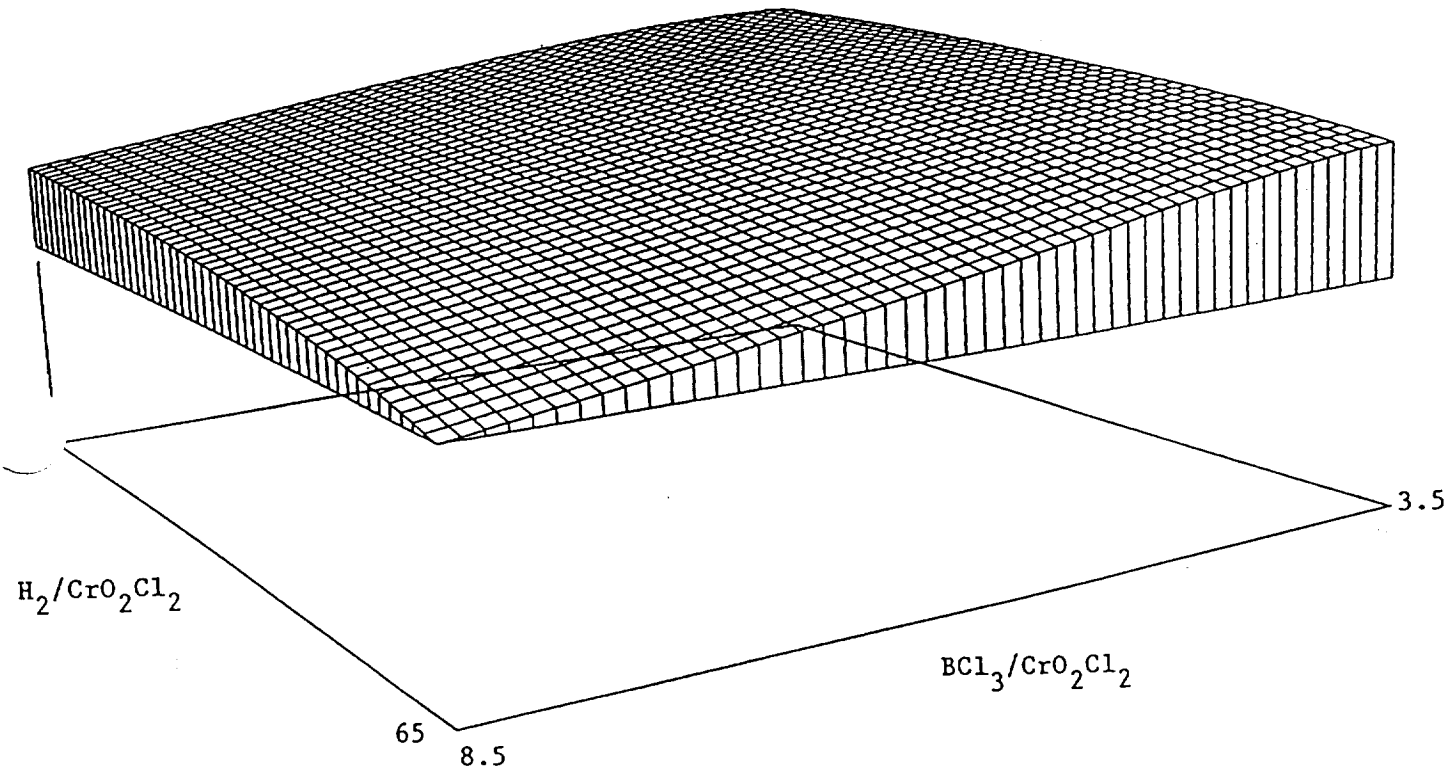

Proposed deposition rate from the third Model.

Experiment #	H_2/CrO_2Cl_2 (α)	BCl_3/CrO_2Cl_2 (β)	Rate (Exp) $\mu m.min^{-1}$	Rate (Model) $\mu m.min^{-1}$	Deviation %
1	129.5	4.62	15.2	14.1	8.2
2	119.4	4.61	13.0	13.9	-6.3
3	110.7	5.91	12.8	12.5	2.1
4	99.5	5.87	12.4	12.2	1.3
5	90.0	7.0	10.5	10.8	-2.1
6	80.3	8.03	9.3	9.4	-0.4
7	69.8	7.98	8.4	8.9	-5.1
8	104.2	5.89	13.4	12.3	7.2
9	80.2	8.13	9.11	9.3	-1.8
10	69.6	8.13	8.4	8.8	-3.2
11	150.6	4.67	14.7	14.3	2.4
12	163.8	4.68	13.8	14.5	-5.0
13	104.3	5.8	12.6	12.4	1.1
14	93.0	6.98	11.7	10.9	7.3
15	71.8	7.18	9.7	9.7	-0.8
16	91.6	6.38	10.9	11.4	-4.8
17	167.6	3.81	15.4	15.0	2.6
18	111.5	5.18	13.6	13.2	3.1
19	68.2	7.71	9.1	9.0	0.9
20	119.4	4.68	13.7	13.9	-1.2

Experimental vs. Theoretical deposition rates

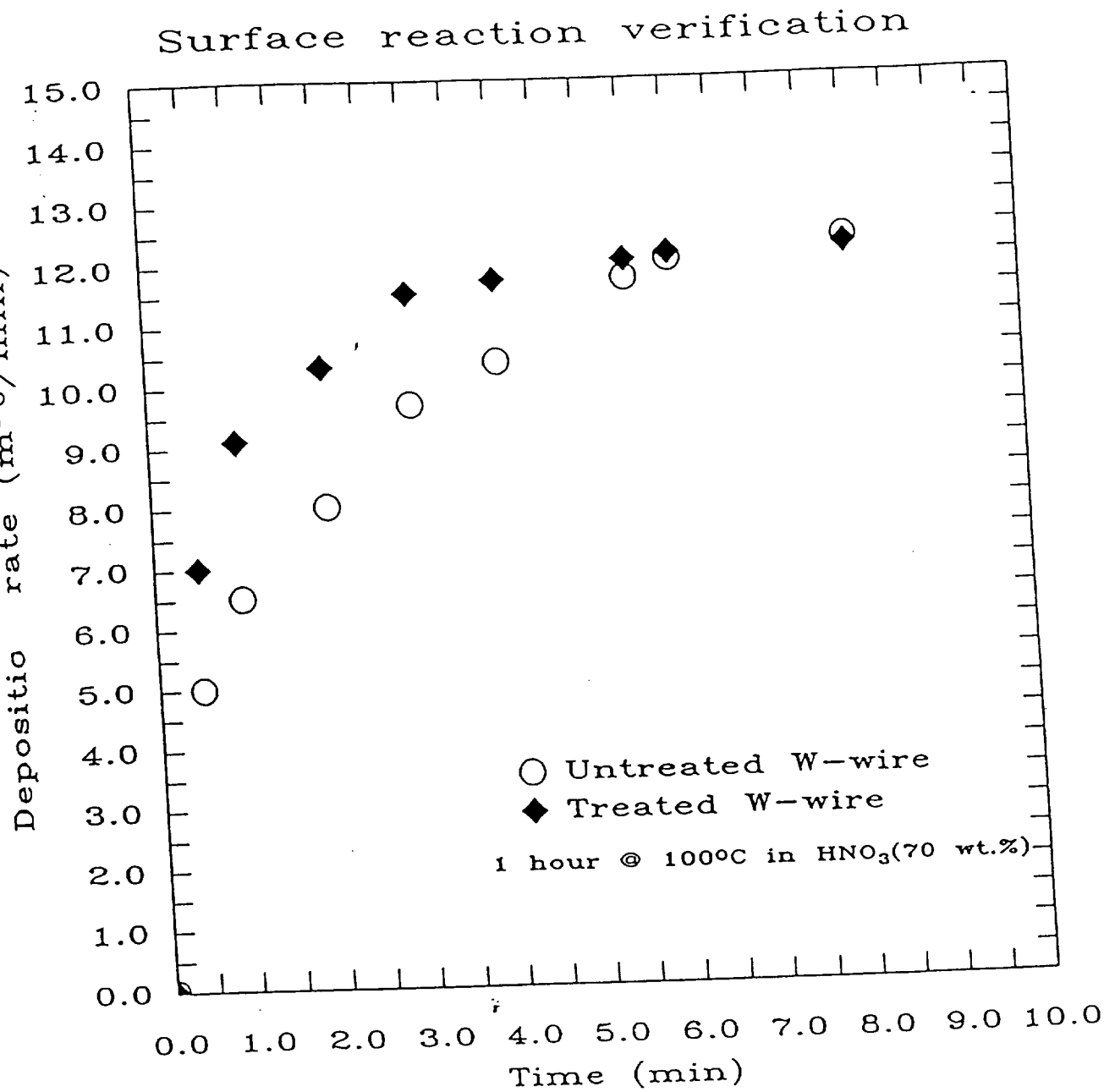

The surface reaction was verified by using different surfaces

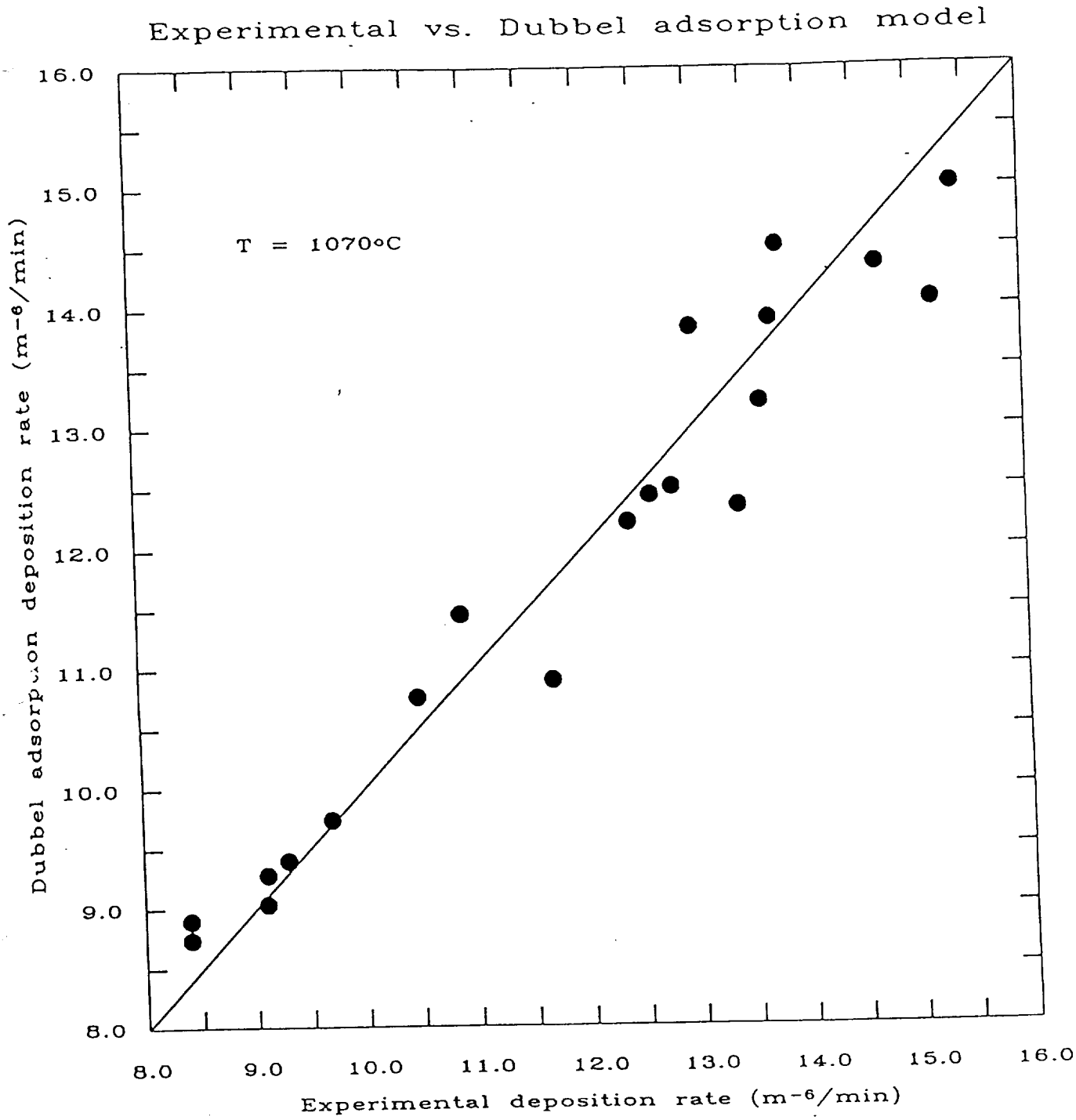

Agreement between the third model and the experimental results.